AMBIENT VIBRATION ANALYSIS OF A FULL-SCALE HYPERBOLIC COOLING TOWER

by

Michael Ray Helpingstine

B.S., Kansas State University, 1985

A MASTER'S THESIS

submitted in partial fulfillment of the

requirements of the degree

MASTER OF SCIENCE

Department of Civil Engineering

Kansas State University
Manhattan, Kansas
1987

Approved by:

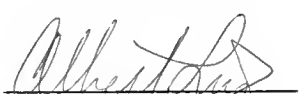

Major Professor

Table of Contents

List of Figures

List of Figures (cont.)

List of Figures (cont.) Page

List of Tables

Acknowledgements

The author wishes to express thanks to Dr. Albert N. Lin, Professor of Civil Engineering, for the guidance, instruction, and friendship rendered throughout the course of this research.

Thanks also to Dr. Robert R. Snell, Head, Department of Civil Engineering, for his support.

The financial contribution to this research, by the National Science Foundation, under Grant No. ECE-8503993, is gratefully acknowledged.

Thanks also to Brad Hull, graduate student, for his assistance in the field.

And to my wife Deb, and daughter Kimberley, without whose encouragement, patience, and love, graduate school would still be just a dream, thank you.

I. INTRODUCTION

Natural draft hyperbolic cooling towers have been used, in this country, for over two decades. They have increased in height during this time by over twenty percent to the present height of 550 feet (170 meters). Towers of 650 feet (200 meters) and more, in height, are being considered for future construction. While the typical shell thickness is approximately 15 inches (0.38 meters), the typical base diameter is 300 feet (92.3 meters).

While their unique shape is both structurally and thermally efficient, they are subject to dynamic loading, especially from wind.

A considerable amount of research has been conducted on hyperbolic cooling towers. This research includes the use of analytical (mathematical), small-scale, and full-scale prototypical models.

An analytical model consists of mathematical formulations that are used to calculate or describe various properties and responses of a structural system. There are many problems associated with the utilization of a purely theoretical model. The accuracy of such a model is dependent upon various assumptions made by the user. These may include stiffness properties, boundary conditions, and suspected foundation/soil interactions.

There are also problems associated with the utilization

of small-scale models. It is very difficult to construct a model with all of the required parameters. These may include Euler numbers, as well as mass density, Young's modulus, Poisson's ratio, and roughness coefficients.

Scale models of reinforced concrete present some special problems. For example, full-scale reinforcing steel is deformed, or roughened, to enhance the bond between the concrete and steel. The effect of this enhancement is very difficult to reproduce.

In the case of a hyperbolic cooling tower, the geometry of the structure may also present some special difficulties. The shell thickness of a scale model may preclude the use of concrete as the modeling medium.

The testing of a full-scale structure presents some unique problems. It is not economically feasible to conduct destructive tests on a full-scale structure. Most non-destructive tests are employed to determine in-situ material properties (swiss hammer, ultra-sound), or connection integrity (x-ray). The physical size of the structure may present problems with accessibility to the researcher, and often, information gained from the testing of one structure may not be applicable to other structures of the same type (13).

In general, the experimental research done on hyperbolic cooling towers has focused on defining the differential wind and pressure loadings. One exception is the

research by Abel and Billington, who compared the dynamic behavior of cracked and uncracked hyperbolic shells (4). Another is the development by Lee and Gould of a complex algorithm for the dynamic analysis of thin shell structures supported on interactive foundations (15).

Other research includes a study to collect and interpret the results of full-scale wind pressure measurements, and to determine the corresponding displacements and forces through finite element analysis, by Basu and Gould (7).

Sollenberger, et.al., established the level and distribution of design dynamic wind pressure loadings over a typical cooling tower (19), and supported their conclusions with data obtained from experimental measurements on the tower at Martin's Creek, PA. Random wind response of a cooling tower was performed by Kapania and Yang, using a Monte Carlo simulation approach (14). Results were presented in the form of a time history response, and compared to those obtained in the frequency domain.

Abu-Sitta and Hashish have presented an approach to predict dynamic wind stresses in upright shells of revolution, and compared those predictions to the measured response of an aero-elastic wind tunnel model (5).

Scale models, on the order of 1/250 and 1/500, of multiple tower groups, including surrounding structures and topography, were constructed and wind tunnel tested by

Armitt (6). A 1/40 scale micro-concrete hyperbolic tower was constructed by Swartz, et.al., and subjected to an internal vacuum to simulate external pressure (21). The tower was tested to buckling, repaired, and tested again. A second tower is presently under construction.

Other studies include a post mortem on the towers at Ferrybridge, England (17), and Ardeer, Scotland (18), as well as a study of the damage inflicted by a mobile crane, in the wake of a tornado, and the subsequent repair thereof, on the Grand Gulf cooling tower, in Mississippi (10).

A better understanding of a complex system, such as a hyperbolic cooling tower, may be enhanced by the utilization of an analytical model in conjunction with the testing of a prototype full-scale structure.

One method of full-scale structural testing is the analysis of ambient vibration data. Ambient vibration data analysis is used to determine the natural frequencies and associated mode shapes of a full-scale structure. The term 'ambient vibration' refers to culturally induced vibrations, as well as those naturally induced by wind, wave, and micro-seismic activity.

Advances in the technology required for ambient vibration data collection and analysis (accelerometers, digital computers, recorders, etc.) have increased the feasibility of this type of full-scale structural testing. It is rela-

tively inexpensive, does not result in the destruction of the structure, and yields results based on actual behavior of the structure at low levels of excitation.

Although many types of structures have been the subject of ambient vibration studies, as yet (1985), none of these tests have been performed on hyperbolic cooling towers. Several multi-story buildings have been tested, including the 24-story steel frame office tower tested by Craig, et.al., (8). Thus structure was tested at various stages of construction, and the changes in modal parameters were determined. Other tested multi-story buildings include the Imperial County Services Building (16), as well as an 18 story pre-cast building (20).

Tested structures also include the Golden Gate Bridge, both the suspended structure (1), and the pier tower structure (2), as well as a 400 ft. long, symetrical, reinforced concrete box girder bridge (9).

Other types of structures subjected to ambient vibration analysis include dams (3), inflatable structures (11), and cylindrical fluid storage tanks (12).

1.1 Research Objective

It is the aim of this research to determine the dynamic characteristics (natural frequencies and associated mode shapes) of a hyperbolic cooling tower.

Work on an analytical model (finite element analysis)

of the tower is currently in progress, at Kansas State University, and findings will be reported to the National Science Foundation.

It is hoped that the information gained from this research will be useful in calibrating such an analytical model, as well as in verifying the results of small-scale model testing in the future.

For this purpose, a series of ambient vibration tests was conducted on the hyperbolic cooling tower at Portland General Electric's Trojan Nuclear Generating Station, near Rainier, Oregon.

1.2 Description of Structure

Completed in May of 1973, the tower is an offset shell of revolution (hyperboloid of one sheet), the geometry of which is given by the following equation:

$$[(R-C)^2/a^2]-[Z^2/b^2]=1,$$

where R is the radius of revolution at height Z, and the curve parameters a and b equal 34.6 ft. (10.6 meters), and 128 ft. (39.3 meters) respectively. The offset distance between the axis of revolution and the centroidal axis,C, is equal to 81.4 ft. (24.8 meters).

The tower also has the following dimensions:

Base Diameter ..... 385.0 ft. (117.35 m.),

Lintel Diameter ..... 364.5 ft. (111.10 m.),

Throat Diameter ..... 232.0 ft. (70.72 m.),

Cornice Diameter ..... 249.8 ft. (76.14 m.),

Lintel Elevation ..... 41.0 ft. (12.50 m.),

Throat Elevation ..... 393.6 ft. (119.19 m.),

Cornice Elevation ..... 492.0 ft. (149.97 m.),

Lintel Thickness ..... 3.75 ft. (1.13 m.),

and Throat Thickness ..... 0.83 ft. (0.25 m.).

A 4.5 ft. (1.37 m.) cantilevered slab serves as a stiffening ring at the cornice elevation, and is also used as an access walkway.

Access ladders are located circumferentially along the tower, and spaced at ninety degree intervals. Three of these ladders reach the 420 ft. (128 m.) level, while the fourth provides access to the top of the tower.

Landings are located just above the lintel beam, and at approximate elevations of 150 ft. (46m.), 270 ft. (82 m.), and 390 ft. (120 m.) on all ladders. An additional landing is provided on the fourth ladder at approximately 485 ft. (148 m.). The structure has an overall height of 499 ft. (152 m.).

II. EQUIPMENT AND PROCEDURE

Ambient vibration data were collected by placing acceleration sensitive transducers at various locations on the tower, and recording the resulting acceleration time history on magnetic tape for later analysis.

Accelerometer locations were selected as part of a comprehensive testing routine to insure a sufficient quantity of data for the identification of principal mode shapes.

Both the equipment and test routine will be discussed in this chapter.

2.1 Equipment

Six basic pieces of equipment were used to collect and analyse the ambient vibration data.

Accelerometer

An accelerometer is a transducer used for the detection and/or measurement of accelerations. The transducers used in this research were FBA-11 Force Balance Accelerometers, manufactured by Kinemetrics Inc. of Pasadena, CA.

The FBA-11 is a single axis instrument with a nominal output of 2.5 volts/g., a nominal range of ± 1.0 g., and a natural frequency of 50 Hertz. They are damped to 70 percent of critical damping. Four such accelerometers were used in the data acquisition system.

A modified C-type clamp was used to attach each trans-

ducer to the tower. The clamps were modified to allow placement of the accelerometer in a level or vertical position, regardless of the position of the clamp itself. This was accomplished by utilizing two pin-type connections, the axes of which form right angles, between the transducer and the clamp. This gave the effect of a 'universal' joint.

Figure 2.1 is an exploded view of the modified clamp.

Strong Motion Accelerograph

The accelerometers were powered by the SMA-3 Strong Motion Accelerograph, also manufactured by Kinemetrics Inc. The SMA-3 also provided various functional test signals. These include an operational test, as well as a calibration test.

The SMA-3 contains two 12-volt batteries and an internal charging system. These enable it to be used in remote testing situations.

Signal Conditioner

Signal conditioning was provided by the SC-1 Signal Conditioner, manufactured by Kinemetrics Inc. The SC-1 is a portable seismic instrument with four separate data acquisition channels providing adjustable low-pass filtering and amplification. The SC-1 was designed specifically for use in data acquisition systems where adjustable filtering or amplification are desireable.

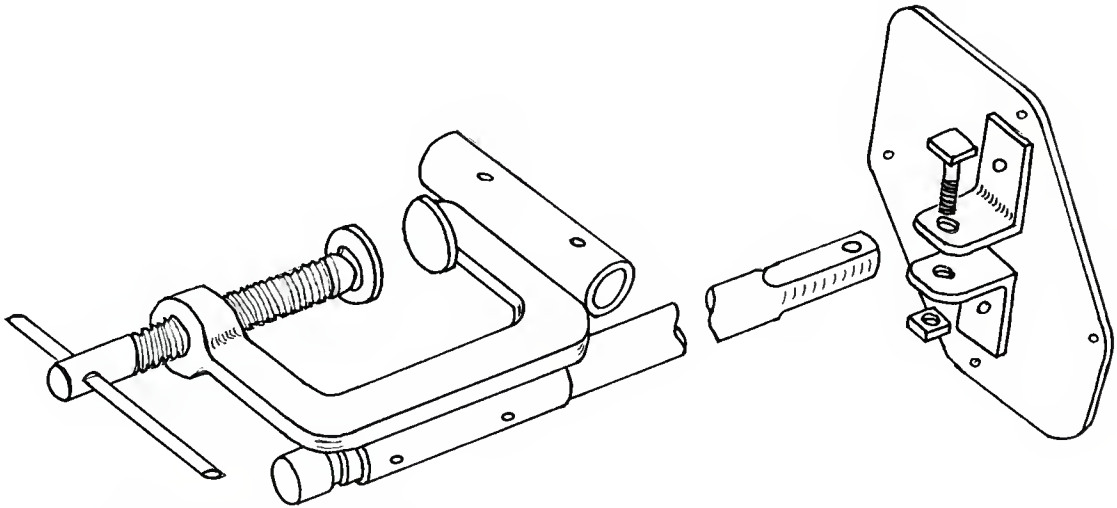

Figure2.1, Modified C-Type Clamp Used to Attach Transducer to Tower

Chart Recorder

The output from each channel of conditioned signal was recorded on a Gould Brush Model 4200 four channel strip chart recorder. This was done in an effort to provide a record for on-site visual inspection of the response data.

Magnetic Tape Recorder

The output from each channel was also recorded on a four channel Bruel & Kjaer 7006 FM recorder. This created a permanent record for future analysis.

Spectrum Analyser

The analysis of ambient vibration signals was partially accomplished through utilization of the Hewlett Packard HP-3582A real time, dual channel spectrum analyser. The analyser was used to digitize the acceleration signals, and to compute the Fast Fourier Transform, as well as to determine the coherence function and relative phase between stations. These processes will be explained further in section 2.3.

Figure 2.2 is a schematic diagram of the data acquisition and analysis system.

2.2 Test Procedure

The collection of ambient vibration data was accomplished by placing the accelerometers at various locations and orientations on the tower, and recording the resulting

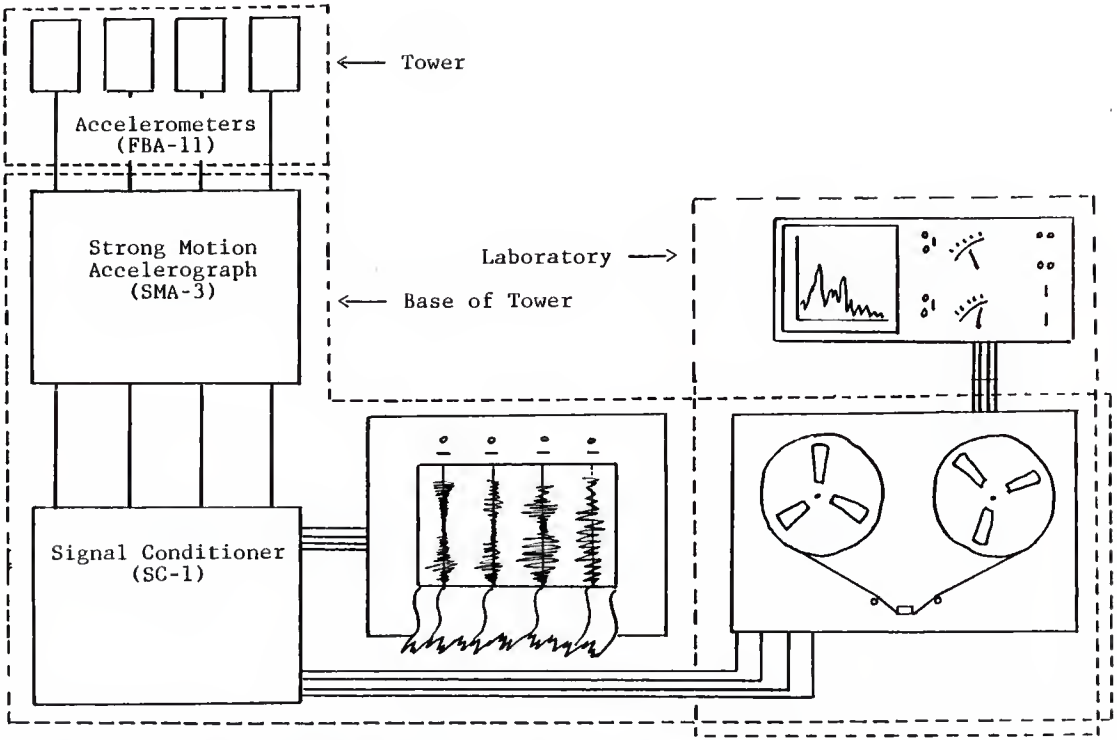

Figure 2.2, Schematic Diagram of Data Acquisition and Analysis System

acceleration time history signals for later analysis.

The axisymetry of the structure required the formulation of a coordinate system for use in locating the points of interest on the tower. The system contains three parameters. These are the elevation, position, and orientation of the accelerometer.

The base of the tower was designated as level 0, and each subsequent landing was assigned a level number.

The ladder which reached the top of the structure was designated as position 0, and each subsequent ladder, proceeding in a counter-clockwise direction, was given a position number (90, 180, or 270).

The final parameter is the orientation of the accelerometer. The accelerometer was placed in one of three orientations;

1. Vertical, pointing upward and designated V,
2. Tangential to the level circular plane of the tower, pointing counter-clockwise, and designated T, or
3. Normal to the axis of revolution, pointing inward, and designated N.

Thus the designation 5-0-N identifies the level, position, and orientation as landing number 5, ladder number 0, and oriented normal to the axis of revolution, pointing inward.

Figure 2.3 shows the designation of parameters.

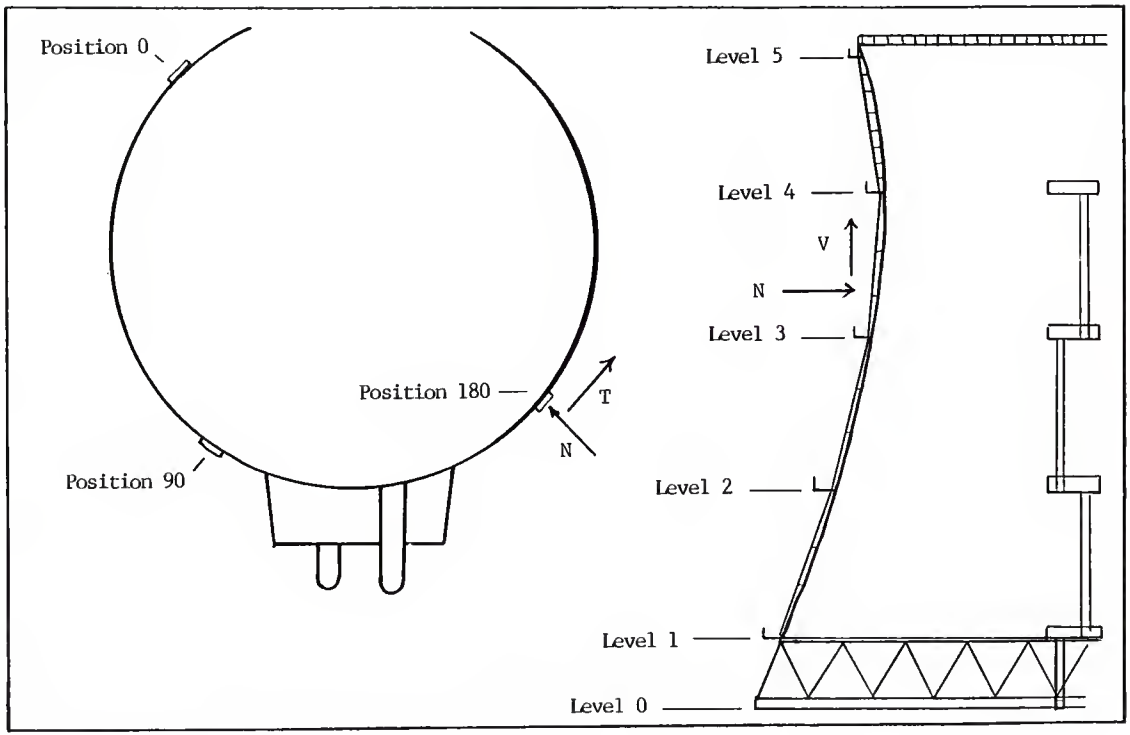

Figure 2.3, Designation of Coordinate Parameters

Because the amplitude of the tower's response is expected to change between tests, it is neccessary to normalize the response at each location to the response of a single continuously mounted accelerometer. Therefore, one accelerometer was positioned for the duration of the testing at the so called reference station. This station provides a datum, or point of reference, for the comparison of relative response of the other stations. The reference station coordinates, in this case, were 5-0-N.

The order in which the tests were carried out, the classification of each test, and the location of each transducer are listed in Table 2.1.

This sequence of testing was selected to contain the desired test configurations, and to minimize the number of times that each transducer had to be relocated. This reduced the potential for damage to the system, as well as reducing the effort required to relocate the accelerometers.

The first test was used to calibrate the accelerometers. This was accomplished by placing all of the transducers at one location and recording, simultaneously, each signal on the chart recorder. The strip chart was then observed for any discrepancies. If significant discrepancies were noted, a calibration factor would have been determined to correct for the discrepancy.

Table 2. 1 Test Routine

Test #	Ch. 1	Ch. 2	Ch. 3	Ch. 4	Class. *
0.	5-0-N	5-0-N	5-0-N	5-0-N	Calib.
1.	5-0-N	5-0-N	5-0-V	5-0-T	A
2.	5-0-N	4-0-N	4-0-V	4-0-T	A
3.	5-0-N	4-0-N	3½-0-N	3-0-N	B
4.	5-0-N	3-0-N	3-0-V	3-0-T	A
5.	5-0-N	3-0-N	2½-0-N	2-0-N	B
6.	5-0-N	2-0-N	2-0-V	2-0-T	A
7.	5-0-N	2-0-N	1½-0-N	1-0-N	B
8.	5-0-N	1-0-N	1-0-V	1-0-T	A
9.	5-0-N	0-0-N	0-0-V	0-0-T	A
10.	5-0-N	2-0-N	2-90-N	2-180-N	C
11.	5-0-N	2-0-N	2-90-T	2-180-N	C
12.	5-0-N	2-0-V	2-90-V	2-180-V	D
13.	5-0-N	1-0-N	1-90-N	1-180-N	C
14.	5-0-N	1-0-V	1-90-T	1-180-N	A
15.	5-0-N	1-0-V	1-90-V	1-180-V	D
16.	5-0-N	0-0-N	0-90-N	0-180-N	C
17.	5-0-N	0-0-V	0-90-V	0-180-V	D

* A=Triaxial Response
  B=Lateral Mode Shape
  C=Circumferential Mode Shape
  D=Vertical Responses

The accelerometers were then placed at the coordinates required for the first test. After the accelerometers were installed at the desired location and orientation, a signal was sent to the accelerometers to insure that they were functioning properly, and that all cables were attached correctly. The low pass filter was then set at the desired frequency (5, 10, or 20 Hertz). The strip chart recorder was utilized to display the accelerometer output while the attenuation/gain settings on the SC-1 were adjusted. The gain was set to maximize the output without saturating the magnetic tape. The outputs from each transducer were then recorded for up to twenty minutes. The process was repeated for low pass filter settings of twenty, ten, and five Hertz.

The recording of signals at three low pass filter settings resulted in a considerable amount of data. An on site spectrum analysis might have eliminated two of the three tests since preliminary estimates of modal frequencies could be obtained. However, a spectrum analyser was not available for use on site.

Pre-printed log sheets were used to record all filter and gain settings during each test. These were referred to during the tabulation of the response data to determine the relative magnitude of each of the Fourier spectra generated by the spectrum analyser.

Figure 2.4 is a sample of the pre-printed log sheets. Actual log sheets may be found in Appendix I.

TEST LOG

Date _____ Test No. _____

Time _____ Rec. Start _____

Rec. End _____

	Channel	1	2	3	4
	Color	Red	Green	Yellow	Blue
Acceler.	Height				
	Azimuth				
	Orientation				
Signal Cond.	Low Pass Filter				
	Attenuator Setting				
	H-P Filter I/O				
B. Rec.	Sensitivity Volts				

Notes:

Figure 2.4, Pre-printed Log Sheet Used in Ambient Vibration Study

The classification of each test is also noted in Table 2.1. Each test (excluding the calibration test) was designed specifically for the identification of the predominant structural frequencies and associated mode shapes. These include vertical modes as well as radial and lateral modes.

In addition to the 18 tests outlined in Table 2.1, free-field tests were also conducted. This was accomplished by placing the accelerometers at various locations on the ground, away from base of the tower, and recording the signals in the manner previously described. Free-field data were used to determine if any predominant site frequencies exist in the range of the predominant structural response frequencies.

Upon completion of the acquisition and recording of the data, the acceleration records were analysed at Kansas State University.

2.3 Data Reduction

The spectrum analyser was used to digitize (sample) the signals and to convert or transform them to the frequency domain. To accomplish this, the analyser made use of a numerical technique called the Fast Fourier Transform (22). The Fourier Transform of a function is defined as;

$$F(t) = \sum_{n=-\infty}^{\infty} C_n e^{in\omega t} \tag{1}$$

where

$$C_n = \frac{1}{T} \int_0^T F(t) e^{-in\omega t} dt \tag{2}$$

"The Fast Fourier Transform is an efficient technique useful for a computer determination of the response in the frequency domain. The response of a single degree of freedom system to a general force is given by;

$$y(tj) = \sum_{n=0}^{N-1} \frac{C_n e^{2\pi(nj/N)}}{k(1-r_n^2+2ir_n\xi_n)} \tag{3}$$

where N is the period, the damping ratio $\xi_n = c/\sqrt{2km}$, the frequency ratio $r_n = \omega_n/\omega$, and the coefficient

$$Cn = \frac{1}{N} \sum_{j=0}^{N-1} F(tj) e^{-2\pi i(nj/N)}, \quad n=0, 1, 2, \ldots, (N-1) \tag{4}$$

Either equation 3 or 4 may be represented, except for sign, by the exponential function

$$A(j) = \sum_{n=0}^{N-1} A^{(0)}(n) W_N^{jn}, \tag{5}$$

where

$$W_n = e^{2\pi i/N} \tag{6}$$

The evaluation of the sum will be most efficient if the number of time increments N into which the period T is divided is a power of 2, that is,

$$N = 2^M$$

where M is an integer. In this case, the integers j and n can be expressed in binary form. For the purpose of illustration, consider a very simple case where the load period is divided into only eight time increments, that is, N=8, M=3. In this case, the indices will have the binary representation

$$j = j_o + 2j_1 + 4j_2,$$

$$n = n_o + 2n_1 + 4n_2,$$

and equation (5) may be written as

$$A(j) = \sum_{n_2=0}^{1} \sum_{n_1=0}^{1} \sum_{n_0=0}^{1} A^{(0)}(n) W_8^{(j_0+2j_1+4j_2)(n_0+2n_1+4n_2)}. \tag{7}$$

The exponential factor may be written as

$$W_8^{jn} = W_8^{8(j_1n_2+2j_2n_2+j_2n_1)} W_8^{4n_2j_0} W_8^{2n_1(2j_1+j_0)} W_8^{n_0(4j_2+2j_1+j_0)} \tag{8}$$

Note that the first factor on the right side is unity,

since from equation 6

$$W_8^{8I} = e^{2\pi i(8/8)I} = \cos 2\pi I + i \sin 2\pi I = 1,$$

where $i=j_1n_2 + 2j_2n_2 + j_2n_1$ is an integer. Therefore only the remaining three factors need be considered in the summations. These summations may be performed conveniently in sequence by introducing a new notation to indicate the successive steps in the summation process. Thus the first step can be indicated by

$$A^{(1)}(j_0,n_1,n_0) = \sum_{n_2=0}^{1} A^{(0)}(n_2,n_1,n_0)W_8^{4n_2j_0},$$

where $A^{(0)}(n_2,n_1,n_0) = A^{(0)}$ in equation 5. Similarly, the second step is

$$A^{(2)}(j_0,j_1,n_0) = \sum_{n_1=0}^{1} A^{(1)}(j_0,n_1,n_0)W_8^{2n_1(2j_1+j_0)},$$

and the third step (final for M=3) is

$$A^{(3)}(j_0,j_1,j_2) = \sum_{n_0=0}^{1} A^{(2)}(j_0,j_1,n_0)W_8^{n_0(4j_2+2j_1+j_o)}.$$

The final result $A^{(3)}(j_0,j_1,j_2)$ is equal to A(j) in eq.5. This process, indicated for N=8, can readily be extended for any integer $N=2^M$. The method is particularly efficient because the results of one step are immediately used in the next step, thus reducing storage requirements."

A problem associated with the reconstruction of a continuous spectrum by discrete data is known as aliasing. This occurs when a less-than-perfect low pass filter is employed in the collection of data. In theory, the filter should remove all frequencies above the limit of the filter. In reality, however, the cut off rate is not perfect. This allows the reflection of response peaks above the cut off frequency to be displayed below the cut off frequency. As an example, consider a twenty Hertz sine wave sampled at a rate of twenty samples per second. There will be one sample per cycle, the value of which is dependent upon the time the sampling begins. Because the sampling rate and the frequency are the same, each subsequent sampling will have a value equal to the first. Figure 2.5 shows a sine wave with a sampling rate equal to its frequency. Note that the sampled data is flat and represents a zero frequency signal. Thus the process of sampling data at the same rate as the maximum expected frequency may result in erroneous reconstruction of the data into a continuous spectrum.

Prior to the analysis of the signals, several combinations of low pass filter settings and sampling rates were tested, and it was determined that aliasing would not be a problem. Therefore the signals recorded at the low pass filter setting of twenty Hertz were sampled at a rate of 40 samples per second.

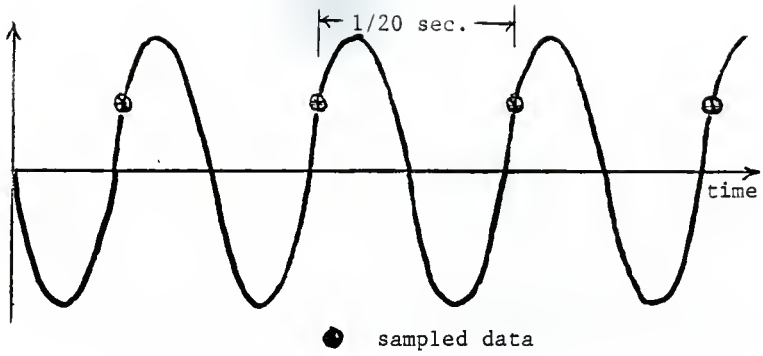

Figure 2.5, Twenty Hertz Sine Wave Sampled at 20 Samples Per Second

A total record of 1024 samples was used per reconstructed spectrum. Thus, 25 seconds of response data (1024/40) were used to calculate each spectrum. A total of 32 spectra were then averaged together to reduce the effect of noise, and to produce the Fourier amplitude plots. Figure 2.6 is a sample of the spectral amplitude, as a function of frequency, for the signals recorded at stations 5-0-N and 3-0-N.

The spectrum analyser was also used to determine the relative phase of any two responses, as a function of frequency. In addition, the coherence function was also determined and plotted. The coherence function (23) is given as

$$Kxy(f) = \frac{|Sxy(f)|^2}{Sx(f)Sy(f)}$$

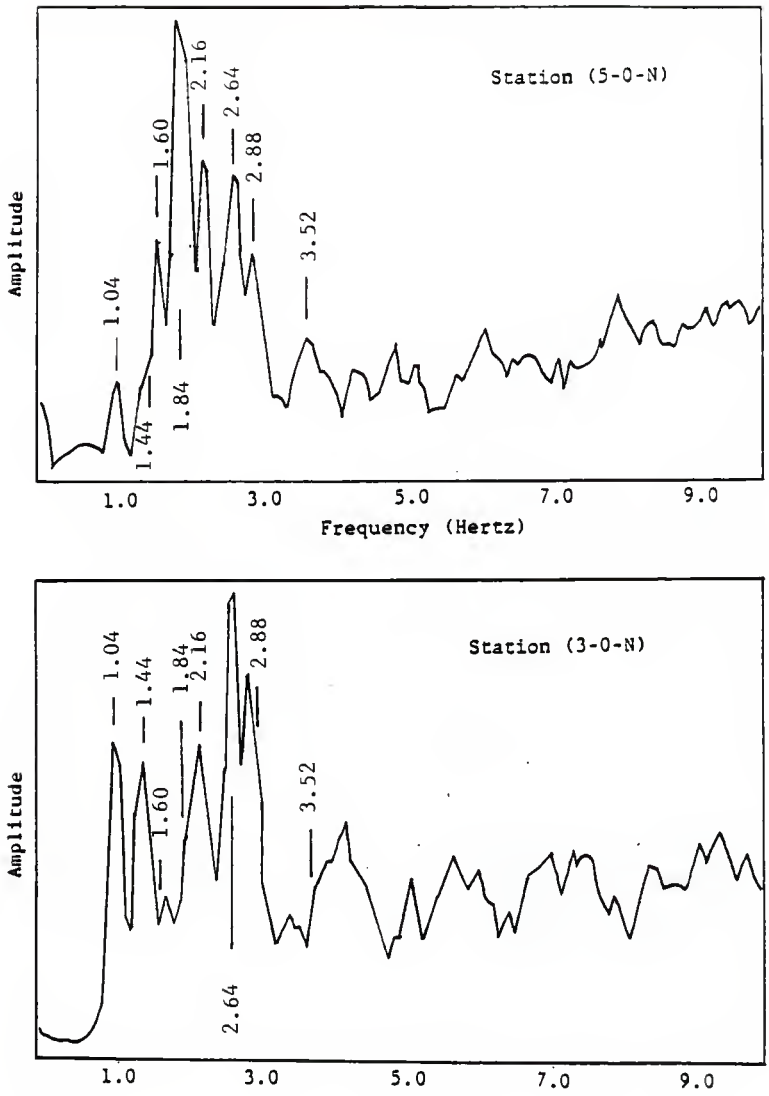

Figure 2.6, Sample Fourier Spectra From Stations 5-0-N and 3-0-N

where x and y represent two random processes,

$$Sxy(f) = \int_{-\infty}^{\infty} Rxy(\tau)e^{-i2\pi f\tau}\, d\tau,$$

$$Sx(f) = \int_{-\infty}^{\infty} Rx(\tau)e^{-i2\pi f\tau}\, d\tau,$$

$$Sy(f) = \int_{-\infty}^{\infty} Ry(\tau)e^{-i2\pi f\tau}\, d\tau.$$

The autocorrelation is given by;

$$Rx(\tau) = \lim_{T\to\infty} \frac{1}{2T} \int_{-T}^{T} x(t)x(t+\tau)dt,$$

$$Ry(\tau) = \lim_{T\to\infty} \frac{1}{2T} \int_{-T}^{T} y(t)y(t+\tau)dt,$$

and the cross-correlation is given by;

$$Rxy(\tau) = \lim_{T\to\infty} \frac{1}{2T} \int_{-T}^{T} x(t)y(t+\tau)dt.$$

If the coherence function is one at a given frequency, the signals are highly coherent, and probably related. If the function is nearly zero, the signals are highly incoherent, and probably unrelated.

Figure 2.7 is a sample of both the phase and coherence function plots from the reconstructed signals recorded at stations 5-0-N and 3-0-N.

A total of 130 Fourier amplitude plots and 65 relative phase and coherence function plots were generated by the spectrum analyser. These may be found in Appendix I.

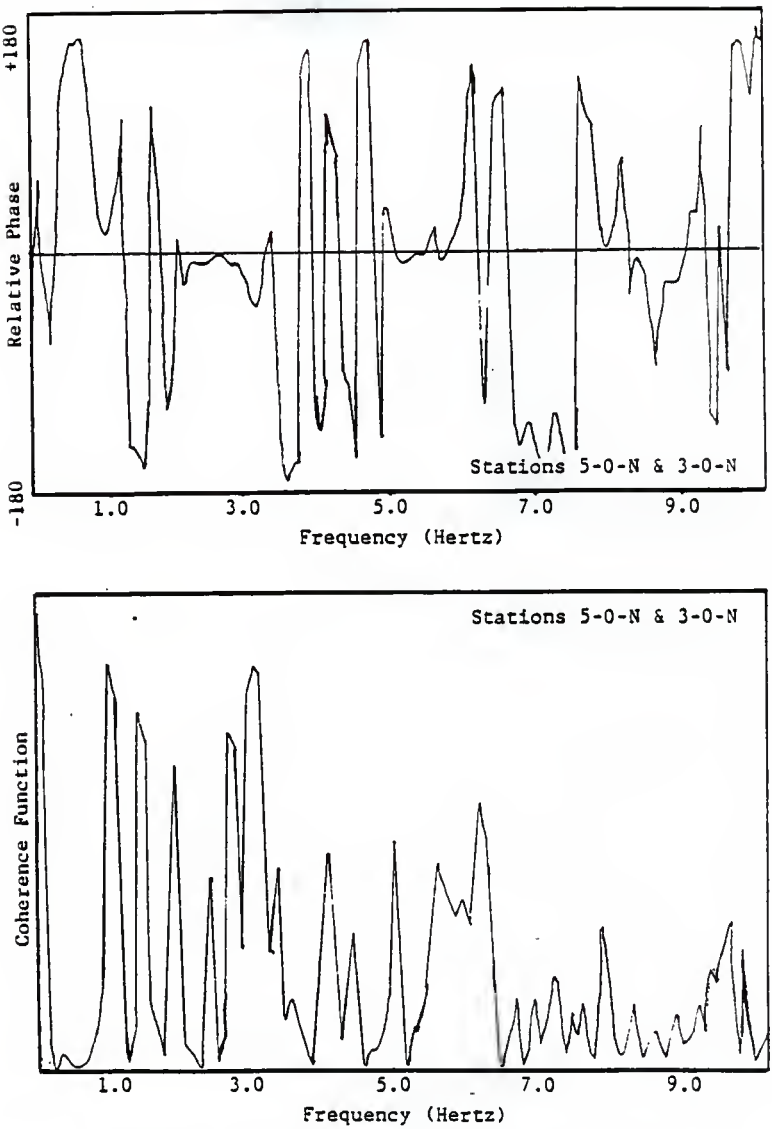

Figure 2.7, Sample Phase and Coherence Function Plots From Stations 5-0-N & 3-0-N

III. RESULTS

Inspection of the Fourier amplitude plots revealed coherent and repeatable peak responses at seven frequencies. These frequencies are 1.04, 1.44, 1.60, 1.84, 2.64, 2.88, and 3.52 Hertz. The spectral amplitude of each station, at each frequency, was measured and normalized to the spectral amplitude of the reference station at the respective frequency. These normalized values, as well as the relative phase values, were tabulated and may be found in Appendix II.

In addition, the spectral amplitude of the reference station, at each frequency, was normalized to the spectral amplitude of the reference station at 1.04 Hertz.

The tabulated information from Appendix II was also used to plot lateral, radial, and vertical mode shapes.

Free field and base rocking data were also investigated and modal damping ratios were calculated.

3.1 Normalization of Reference Spectral Amplitudes

The spectral amplitudes of the reference station, at each of the predominant frequencies, were normalized to the amplitude of the reference station at 1.04 Hertz. This provided a plotting factor, or normalization coefficient, to be applied to each mode shape plot. These coefficients may be found in Table 3.1.

Frequency (Hertz)	Measured Response (MV)	Normalization Coefficient
1.04	6.50	1.00
1.44	3.90	0.60
1.60	7.04	1.08
1.84	29.68	4.57
2.64	15.17	2.33
2.88	8.23	1.27
3.52	6.93	1.07

Table 3.1, Reference Responses & Normalization Coefficients

3.2 Mode Shapes

The tabulated response and relative phase information was used to plot lateral (m), radial (n), and vertical mode shapes, at each of the predominant frequencies.

Lateral mode shapes consist of responses (normalized spectral amplitudes) normal to the axis of revolution, at a specific position, and at varying elevations. Figure 3.2.1 shows typical lateral mode shapes of a cantilever structure.

Radial mode shapes consist of responses both normal to the axis of revolution, and tangential to the level circular plane of the structure, at varying positions, at a specific elevation. It must be noted, however, that the radial mode shape plots are defined by only three points, and therefore do not present conclusive evidence concerning the radial mode shape value of n at any level or frequency.

Figure 3.2.2 shows typical radial mode shapes for an axisymetric structure.

Vertical mode shapes were plotted and examined in an effort to determine the contribution of base rocking to the lateral response of the structure.

When more than one value is available, the mode shapes were plotted using average spectral amplitudes at each station.

The lateral, radial, and vertical mode shapes will be described in this section.

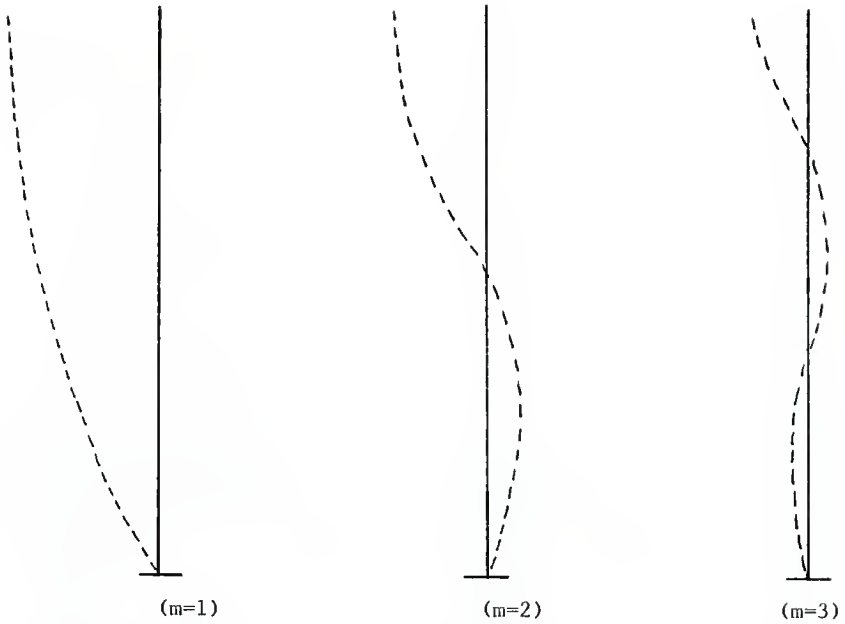

Figure 3.2.1, Typical Lateral Mode Shapes of Cantilever Structures

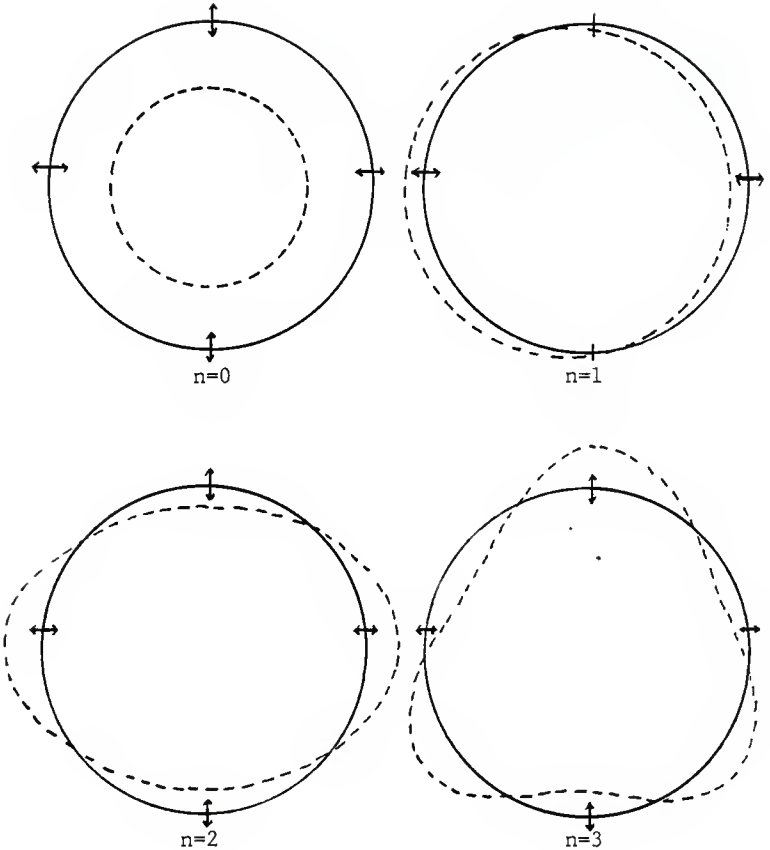

Figure 3.2.2, Typical Circumferential Mode Shapes of Axisymetric Structures (12)

1.04 Hertz

The lateral mode shape of the tower at 1.04 Hertz exhibits a maximum response at level 3. The response at level 3 is 1.50 times greater than the reference response, and is out of phase.

Levels 0 through 3.5 exhibit responses which are out of phase with respect to the reference response, while the response at level 4 is in phase.

Figure 3.2.3 is the lateral mode shape at 1.04 Hertz. The normalization coefficient is 1.00.

The radial mode shape plots at both levels 1 and 2 are indicative of an n=0 mode, however, this cannot be verified due to the limited number of data points available for analysis.

Figures 3.2.4, and 3.2.5 are the radial mode shapes at levels 1 and 2, for 1.04 Hertz.

The vertical mode shape may be found in Figure 3.2.6. Levels 1 and 4 exhibit upward responses, while levels 0,2, and 3 exhibit downward responses. The maximum vertical response may be found at level 3, and is 0.37 times greater than the reference response.

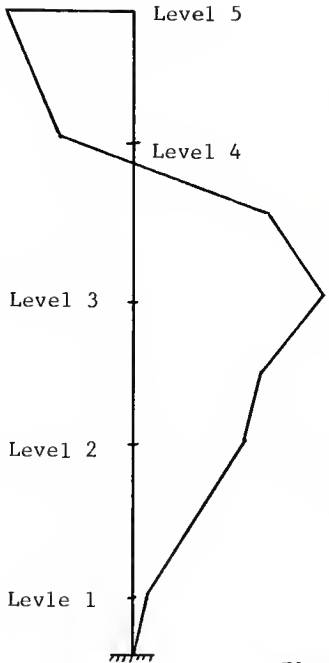

Level	Amplitudes	Ave.	Rel. Phase
1	0.20, 0.17	0.19	Out
1½	0.52	0.52	Out
2	1.12, 0.87, 0.83, 0.74	0.89	Out
2½	1.03	1.03	Out
3	1.50, 1.50	1.50	Out
3½	1.09	1.09	Out
4	0.46, 0.70	0.58	In
5	1.00	1.00	In

Figure 3.2.3, Lateral Mode Shape at 1.04 Hertz

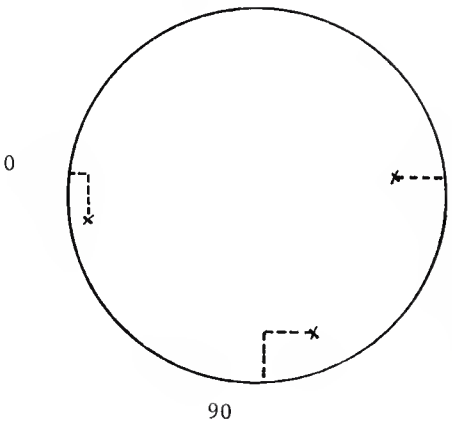

Station	Amplitude	Rel. Phase
1-0-N	0.19	Out
1-90-N	0.37	Out
1-180-N	0.35	Out
1-90-T	0.37	Out
1-0-T	0.37	Out

Figure 3.2.4, Radial Mode Shape at 1.04 Hertz (Level 1)

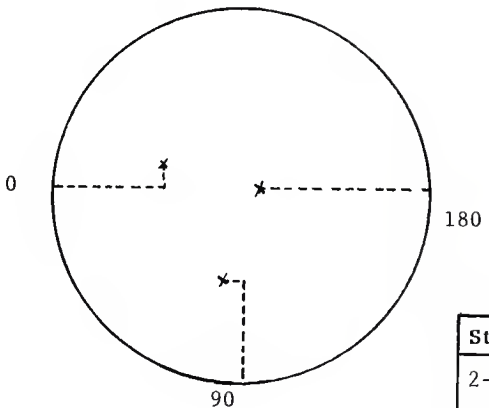

Station	Amplitude	Rel. Phase
2-0-N	0.89	Out
2-90-N	0.88	Out
2-180-N	1.26	Out
2-90-T	0.20	In
2-0-T	0.20	In

Figure 3.2.5, Radial Mode Shape at 1.04 Hertz (Level 2)

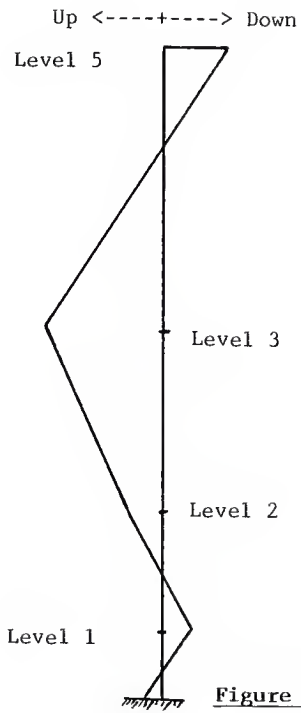

Level	Amplitude	Dir.	Test #
0	0.07	Up	9A
1	0.09	Down	8A
2	0.15	Up	6A
3	0.37	Up	4A
5	0.20	Down	1A

Figure 3.2.6, Vertical Mode Shape at 1.04 Hertz

1.44 Hertz

The lateral mode shape of the tower at 1.44 Hertz exhibits a maximum response at level 4. The response at level 4 is 1.87 times greater than the reference response, and is in phase.

The responses at all levels are in phase with the reference response.

Figure 3.2.7 is a plot of the lateral mode shape at 1.44 Hertz. The normalization coefficient is 0.60.

The radial mode shape plots at both levels 1 and 2, are indicative of an n=2 mode, however, this cannot be verified due to the limited number of data points available for analysis.

Figures 3.2.8 and 3.2.9 are the radial mode shapes at levels 1 and 2, at 1.44 Hertz.

The vertical mode shape may be found in Figure 3.2.10. Levels 0, 2, 3, and 5 exhibit upward responses, while level 1 exhibits a downward response. The maximum vertical response is found at the top of the tower.

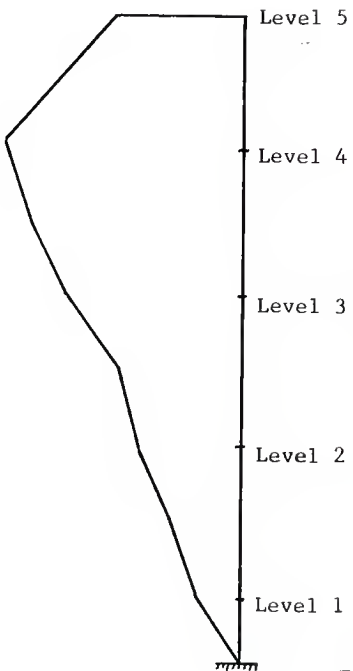

Level	Amplitudes	Ave.	Rel. Phase
1	0.29, 0.36	0.33	In
1½	0.50	0.50	In
2	0.58, 0.86, 0.72, 0.75	0.73	In
2½	0.92	0.92	In
3	1.35, 1.31	1.33	In
3½	1.64	1.64	In
4	1.73, 2.00	1.87	In
5	1.00	1.00	In

Figure 3.2.7, Lateral Mode Shape at 1.44 Hertz

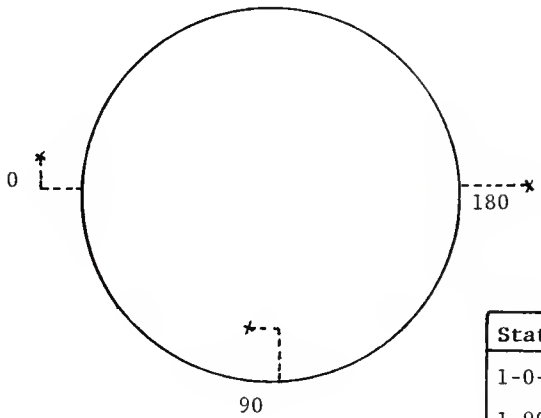

Station	Amplitude	Rel. Phase
1-0-N	0.33	In
1-90-N	0.42	Out
1-180-N	0.55	In
1-90-T	0.26	In
1-0-T	0.28	In

Figure 3.2.8, Radial Mode Shape at 1.44 Hertz (Level 1)

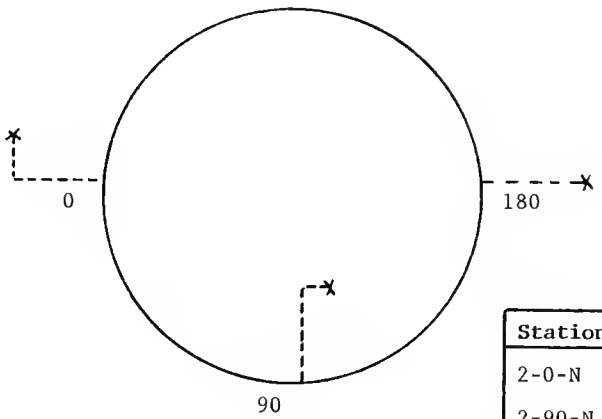

Station	Amplitude	Rel. Phase
2-0-N	0.73	In
2-90-N	0.79	Out
2-180-N	0.80	In
2-90-T	0.19	Out
2-0-T	0.34	In

Figure 3.2.9, Radial Mode Shape at 1.44 Hertz (Level 2)

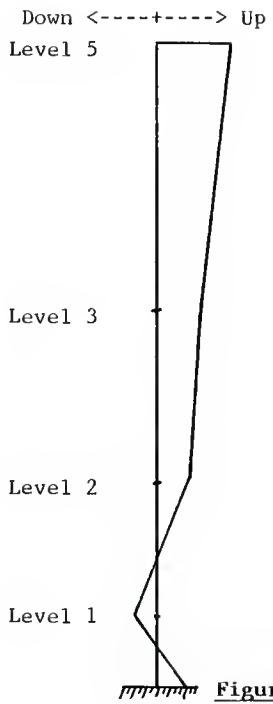

Level	Amplitude	Dir.	Test #
0	0.10	Up	9A
1	0.07	Up	8A
2	0.10	Down	6A
3	0.13	Down	4A
5	0.22	Down	1A

Figure 3.2.10, Vertical Mode Shape at 1.44 Hertz

1.60 Hertz

The lateral mode shape of the tower at 1.69 Hertz exhibits a maximum response at level 4. The response at level 4 is 1.50 times greater than the reference response, and is in phase.

Levels 0 through 3 exhibit responses which are out of phase with respect to the reference response, while the response at levels 3.5 and 4 are in phase.

Figure 3.2.11 is a plot of the lateral mode shape of the tower at 1.60 Hertz. The normalization coefficient is 1.08.

The radial mode shape plot at level 1 is indicative of an n=0 mode while the plot at level 2 indicates that n=1. This cannot be verified due to the limited number of data points available for analysis.

Figures 3.2.12 and 3.2.13 are the radial mode shape plots at levels 1 and 2, at 1.60 Hertz.

The vertical mode shape may be found in Figure 3.2.14. With the exception of level 5, all of the responses are in a downward direction, and from levels 1 through 3, seem to increase linearly. The maximum vertical response occurs at level 3.

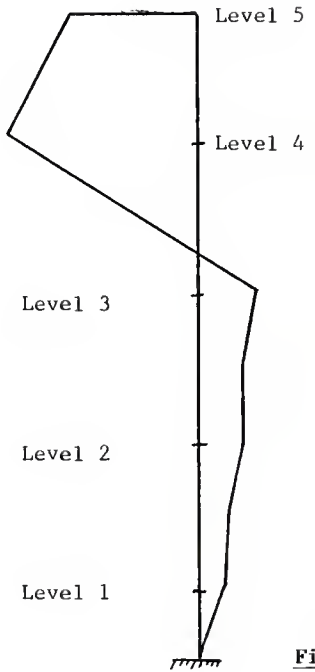

Level	Amplitudes	Ave.	Rel. Phase
1	0.14, 0.18	0.16	Out
1½	0.21	0.21	Out
2	0.42, 0.29, 0.34, 0.35	0.35	Out
2½	0.34	0.34	Out
3	0.28, 0.54	0.41	Out
3½	o.48	0.48	In
4	1.50, 1.49	1.50	In
5	1.00	1.00	In

Figure 3.2.11, Lateral Mode Shape at 1.60 Hertz

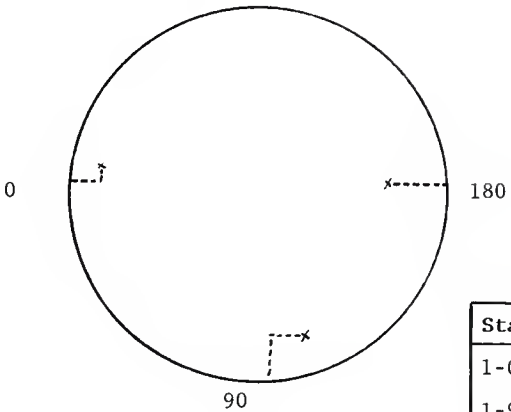

Station	Amplitude	Rel. Phase
1-0-N	0.21	Out
1-90-N	0.35	Out
1-180-N	0.49	Out
1-90-T	0.26	Out
1-0-T	0.09	In

Figure 3.2.12, Radial Mode Shape at 1.60 Hertz (Level 1)

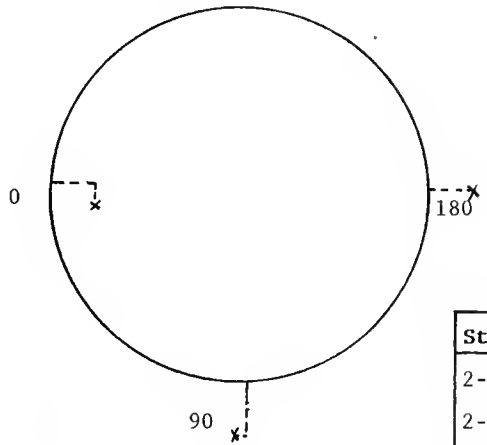

Station	Amplitude	Rel. Phase
2-0-N	0.35	Out
2-90-N	0.45	In
2-180-N	0.35	In
2-90-T	0.10	In
2-0-T	0.20	Out

Figure 3.2.13, Radial Mode Shape at 1.60 Hertz (Level 2)

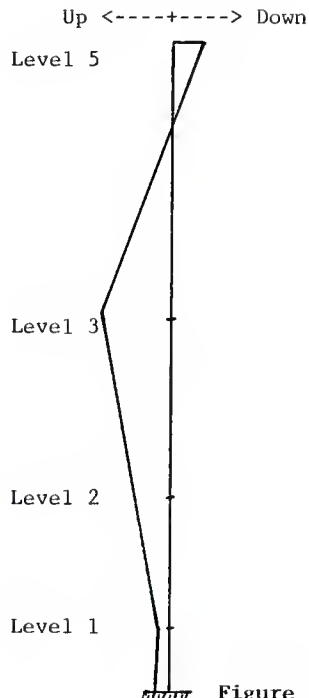

Level	Amplitude	Dir.	Test #
0	0.04	Up	9A
1	0.03	Up	8A
2	0.11	Up	6A
3	0.21	Up	4A
5	0.10	Down	1A

Figure 3.2.14, Vertical Mode Shape at 1.60 Hertz

1.84 Hertz

The lateral mode shape of the tower at 1.84 Hertz exhibits a maximum response at level 5 (reference station).

Levels 3 and 3.5 exhibit responses which are out of phase with respect to the reference response, while the responses at levels 1, 1.5, 2, 2.5, and 4 are in phase.

Figure 3.2.15 is a plot of the lateral mode shape of the tower at 1.84 Hertz. The normalization coefficient is 4.57.

The radial mode shape plots at both levels 1 and 2 are indicative of an n=0 mode, however, this cannot be verified due to the limited number of data points available for analysis.

Figures 3.2.16 and 3.2.17 are the radial mode shapes at levels 1 and 2, at 1.84 Hertz.

The vertical mode shape may be found in Figure 3.2.18. With the exception of level 3, all of the responses are in an upward direction.

The maximum vertical response may be found to occur at the top of the tower.

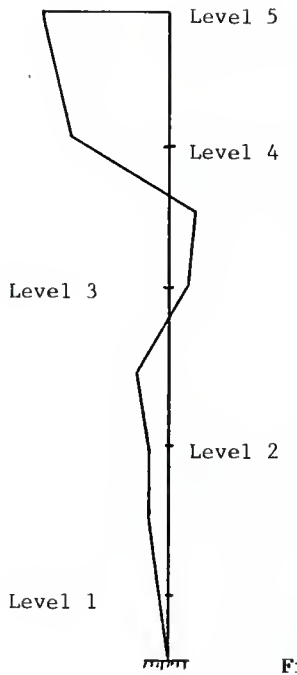

Level	Amplitudes	Ave.	Rel. Phase
1	0.09, 0.07	0.08	In
1½	0.15	0.15	In
2	0.15, 0.20, 0.11, 0.11	0.14	In
2½	0.23	0.23	In
3	0.16, 0.11	0.14	Out
3½	0.20	0.20	Out
4	0.70, 0.79	0.75	In
5	1.00	1.00	In

Figure 3.2.15, Lateral Mode Shape at 1.84 Hertz

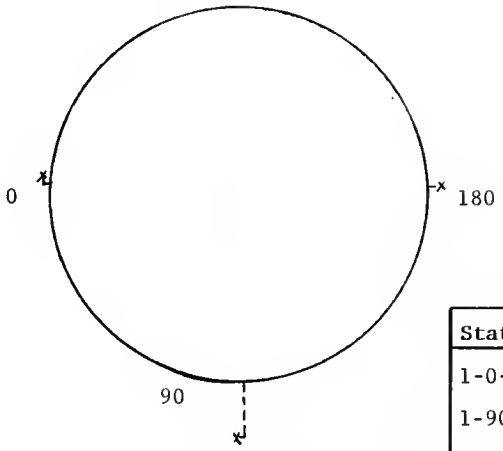

Station	Amplitude	Rel. Phase
1-0-N	0.09	In
1-90-N	0.43	In
1-180-N	0.10	In
1-90-T	0.06	In
1-0-T	0.08	In

Figure 3.2.16, Radial Mode Shape at 1.84 Hertz (Level 1)

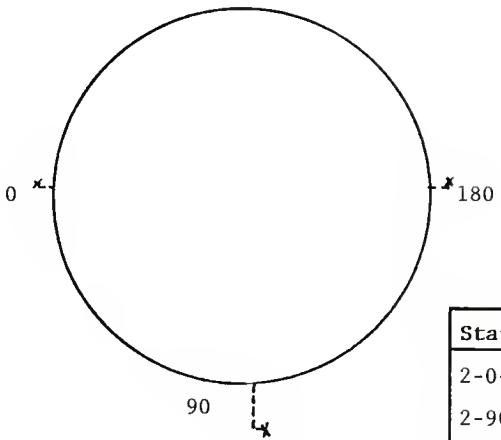

Station	Amplitude	Rel. Phase
2-0-N	0.14	In
2-90-N	0.34	In
2-180-N	0.16	In
2-90-T	0.07	Out
2-0-T	0.03	In

Figure 3.2.17, Radial Mode Shape at 1.84 Hertz (Level 2)

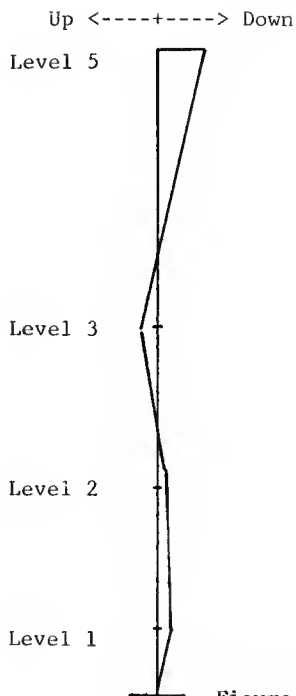

Level	Amplitude	Dir.	Test #
0	0.01	Down	9A
1	0.03	Down	8A
2	0.14	Down	6A
3	0.04	Up	4A
5	0.15	Down	1A

Figure 3.2.18, Vertical Mode Shape at 1.84 Hertz

2.64 Hertz

The lateral mode shape of the tower at 2.64 Hertz exhibits a maximum response at level 5 (reference station).

Levels 1.5, 3.5, and 4 exhibit responses which are out of phase with respect to the reference response, while the responses at levels 2, 2.5, 3 and 5 are in phase.

Figure 3.2.19 is the lateral mode shape at 2.64 Hertz. The normalization coefficient is 2.33.

The radial mode shape plots at both levels 1 and 2 are indicative of an n=0 mode, however, this is also not verifiable.

Figures 3.2.20 and 3.2.21 are the radial mode shapes at 2.64 Hertz.

The vertical mode shape may be found in Figure 3.2.22. Levels 2 through 5 exhibit upward responses, while level 1 exhibits a downward response.

The maximum vertical response may be found to occur at the top of the tower.

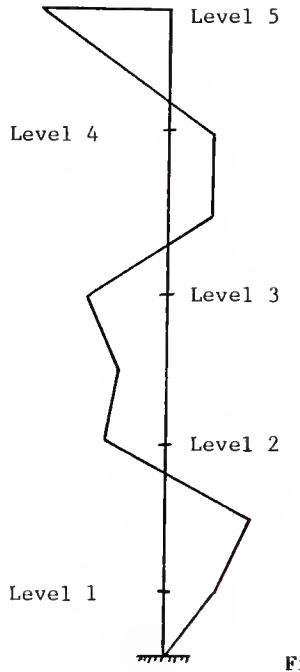

Level	Amplitudes	Ave.	Rel. Phase
1	0.47, 0.35	0.41	Out
1½	0.66	0.66	Out
2	0.44, 0.74, 0.39, 0.33	0.48	In
2½	0.37	0.37	In
3	0.75, 0.54	0.65	In
3½	0.39	0.39	Out
4	0.39, 0.36	0.38	Out
5	1.00	1.00	In

Figure 3.2.19, Latera; Mode Shape at 2.64 Hertz

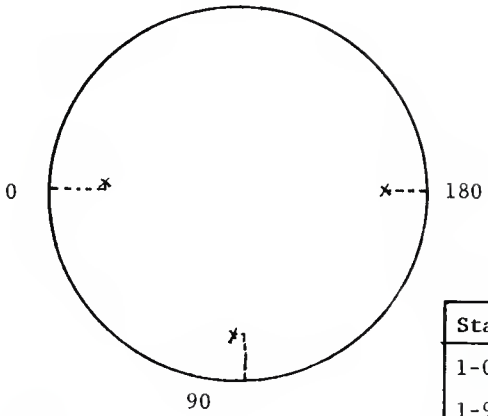

Station	Amplitude	Rel. Phase
1-0-N	0.44	Out
1-90-N	0.36	Out
1-180-N	0.37	Out
1-90-T	0.15	In
1-0-T	0.08	In

Figure 3.2.20, Radial Mode Shape at 2.64 Hertz (Level 1)

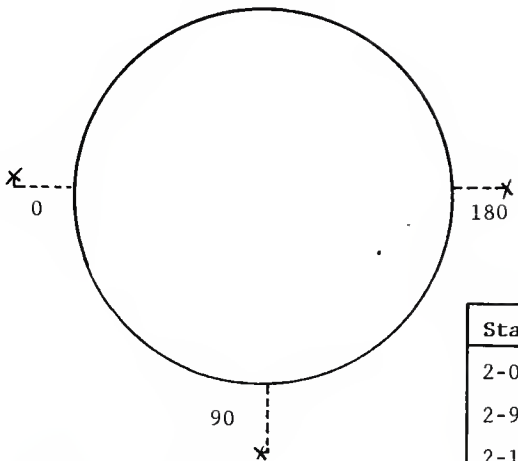

Station	Amplitude	Rel. Phase
2-0-N	0.48	In
2-90-N	0.54	In
2-180-N	0.46	In
2-90-T	0.05	In
2-0-T	0.07	In

Figure 3.2.21, Radial Mode Shape at 2.64 Hertz (Level 2)

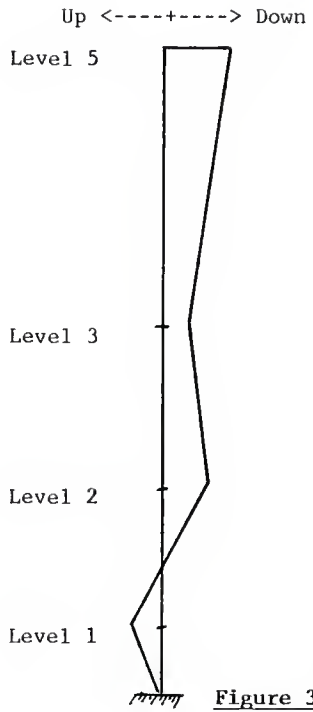

Level	Amplitude	Dir.	Test #
0	0.03	Up	9A
1	0.10	Up	8A
2	0.14	Down	6A
3	0.08	Down	4A
5	0.21	Down	1A

Figure 3.2.22, Vertical Mode Shape at 2.64 Hertz

2.88 Hertz

The lateral mode shape of the tower at 2.88 Hertz exhibits a maximum response at level 5 (reference station).

Levels 1, 1.5, 2, and 4 exhibit responses which are out of phase with respect to the reference response, while the responses at levels 3 and 5 are in phase. The dashed line on the lateral mode shape plot represents the uncertainty concerning the relative phase at level 2.5.

Figure 3.2.21 is a plot of the lateral mode shape of the tower at 2.88 Hertz. The normalization coefficient is 1.27.

The radial mode shape plot at level 1 is indicative of an n=0 mode, while the plot at level 2 seems to indicate that n=3 or more.

Figures 3.2.22 and 3.2.23 are the radial mode shapes at levels 1 and 2, at 2.88 Hertz.

The vertical mode shape may be found in Figure 3.2.24. Levels 3 and 5 exhibit downward responses.

The maximum vertical response may be found to occur at the top of the tower.

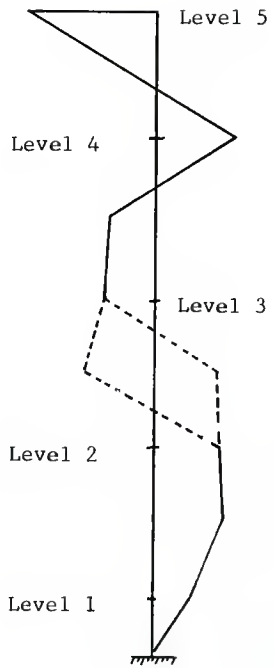

Level	Amplitudes	Ave.	Rel. Phase
1	0.37, 0.29	0.33	Out
1½	0.57	0.57	Out
2	0.57, 0.49, 0.48, 0.52	0.52	Out
2½	0.51 (Ø=90°)	0.51	???
3	0.89, 0.96	0.93	In
3½	0.38	0.38	In
4	0.68, 0.56	0.62	Out
5	1.00	1.00	In

Figure 3.2.23, Lateral Mode Shape at 2.88 Hertz

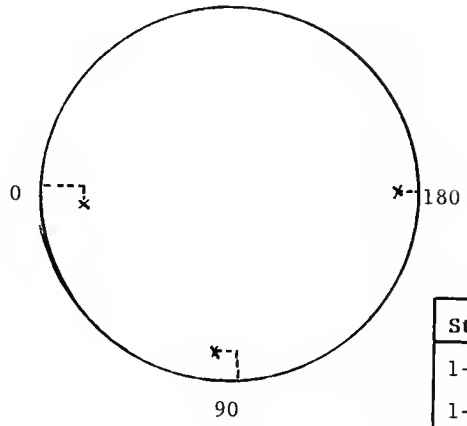

Station	Amplitude	Rel. Phase
1-0-N	0.31	Out
1-90-N	0.22	Out
1-180-N	0.17	Out
1-90-T	0.19	Out
1-0-T	0.18	Out

Figure 3.2.24, Radial Mode Shape at 2.88 Hertz (Level 1)

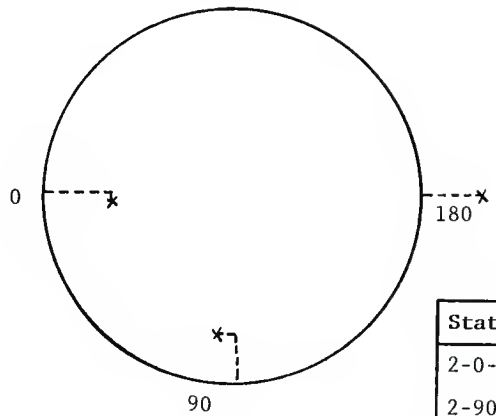

Station	Amplitude	Rel. Phase
2-0-N	0.52	Out
2-90-N	0.44	Out
2-180-N	0.47	In
2-90-T	0.16	In
2-0-T	0.10	Out

Figure 3.2.25, Radial Mode Shape at 2.88 Hertz (Level 2)

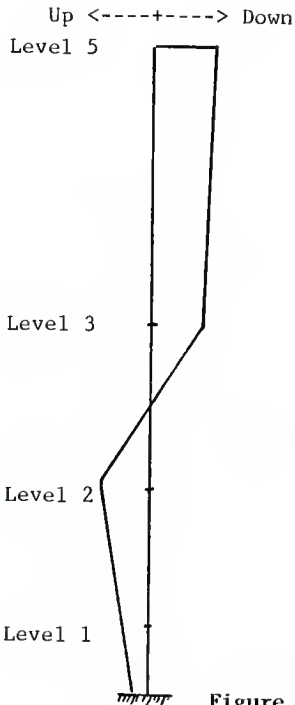

Level	Amplitude	Dir.	Test #
0	0.06	Up	9A
1	0.10	Up	8A
2	0.16	Up	6A
3	0.15	Down	4A
5	0.19	Down	1A

Figure 3.2.26, Vertical Mode shape at 2.88 Hertz

3.52 Hertz

The lateral mode shape of the tower at 3.52 Hertz exhibits a maximum response at level 5 (reference station).

Levels 2.5, 3, and 4 exhibit responses which are out of phase with respect to the reference response, while the response of levels 1, 1.5, 2, 3.5, and 5 are in phase.

Figure 3.2.27 is a plot of the lateral mode shape of the tower at 3.52 Hertz. The normalization coefficient is 1.07.

The radial mode shape of the tower at level 1 is indicative of an n=1 mode, while the radial mode shape at level 2 seems to indicate an n=0 mode.

Figures 3.2.28 and 3.2.29 are the radial mode shape plots at levels 1 and 2, for frequency 3.52 Hertz.

The vertical mode shape may be found in Figure 3.2.30. Levels 1 and 5 exhibit upward responses, while levels 0, 2, and 3 exhibit downward responses.

The maximum vertical response may be found to occur at level 3.

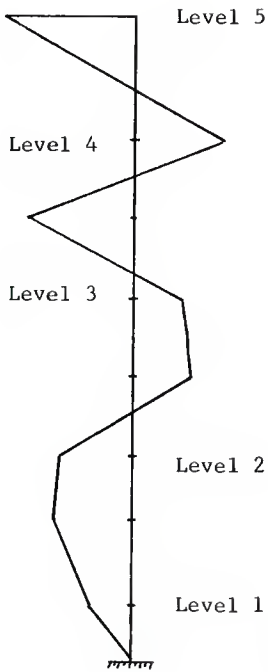

Level	Amplitudes	Ave.	Rel. Phase
1	0.33, 0.42	0.38	In
1½	0.56	0.56	In
2	0.64, 0.47, 0.59, 0.43	0.51	In
2½	0.47	0.47	Out
3	0.42, 0.31	0.37	Out
3½	0.81	0.81	In
4	0.67, 0.75	0.71	Out
5	1.00	1.00	In

Figure 3.2.27, Lateral Mode Shape at 3.52 Hertz

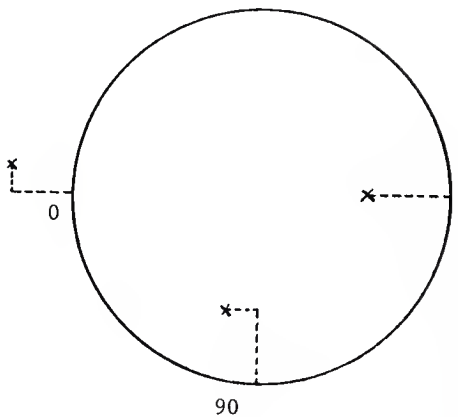

Station	Amplitude	Rel. Phase
1-0-N	0.50	In
1-90-N	0.57	Out
1-180-N	0.66	Out
1-90-T	0.25	In
1-0-T	0.26	In

Figure 3.2.28, Radial Mode Shape at 3.52 Hertz (Level 1)

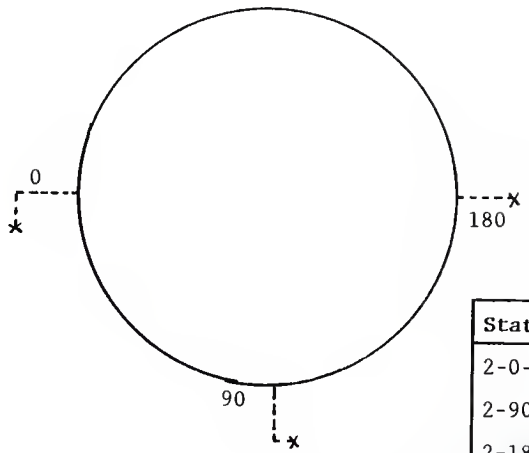

Station	Amplitude	Rel. Phase
2-0-N	0.53	In
2-90-N	0.44	In
2-180-N	0.41	In
2-90-T	0.16	Out
2-0-T	0.25	Out

Figure 3.2.29, Radial Mode Shape at 3.52 Hertz (Level 2)

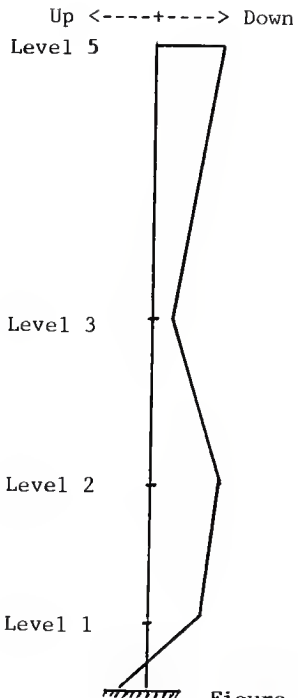

Level	Amplitude	Dir.	Test #
0	0.08	Up	9A
1	0.16	Down	8A
.2	0.21	Down	6A
3	0.06	Down	4A
5	0.20	Down	1A

Figure 3.2.30, Vertical Mode Shape at 3.52 Hertz

3.3 Free-Field Tests

Free-field tests were conducted at various locations away from the base of the tower. These locations are shown in Figure 3.3.

Figures 3.4, 3.5, and 3.6 are response plots generated from the three free-field tests. Note that no predominant frequencies exist in the range of the predominant structural response frequencies. This precludes the possibility that the predominant structural response peaks were artificially induced through low levels of seismic activity.

3.3 Base Rocking

Vertical responses at the base of the structure were examined to determine if any base rocking occured at any of the predominant frequencies.

Table 3.4 summarizes the response and relative phase information from test 17, coordinates 0-0-V, 0-90-V, and 0-180-V. Examination of Table 3.4 reveals responses at 0-0-V and 0-180-V which are nearly equal in magnitude at all frequencies. With the exception of 3.52 Hertz, the relative phase is also the same at each frequency. This is not indicative of a significant contribution to the lateral response by base rocking about the 90-270 axis.

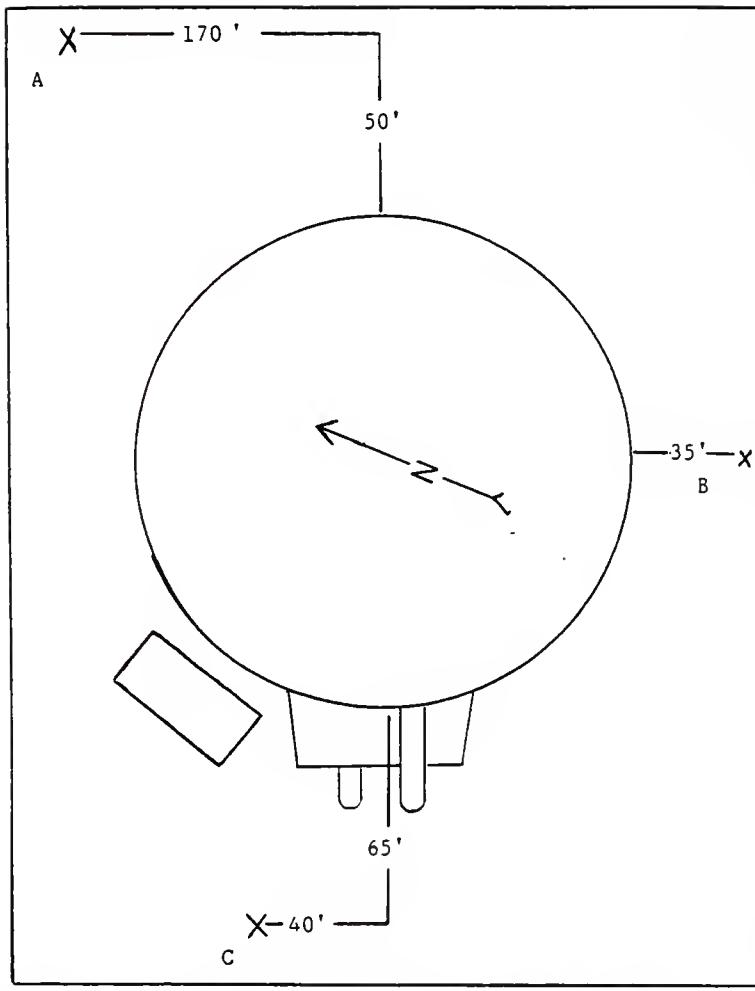

Figure 3.3, Approximate Free-Field Test Locations

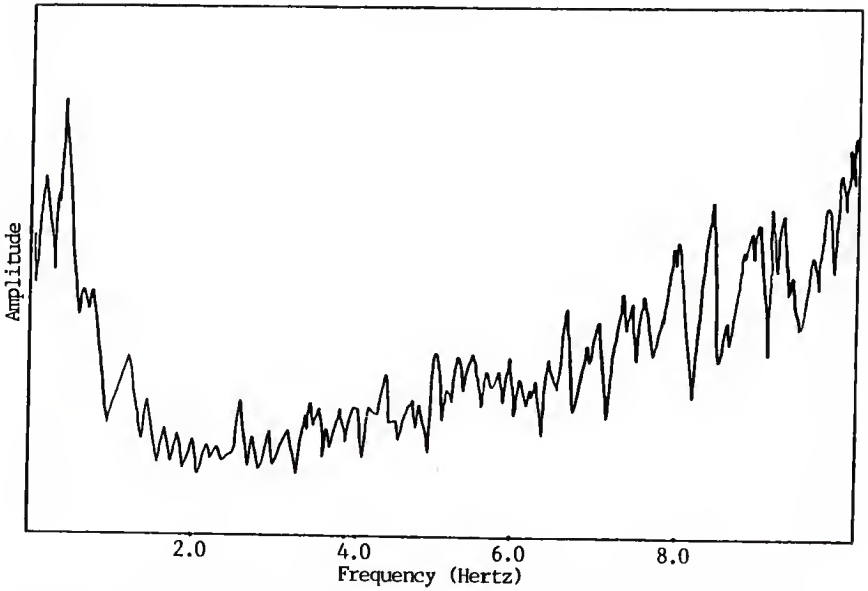

Figure 3.4, Response Plot from Free-Field Test Location 'A' (Accelerometer Oriented Upward)

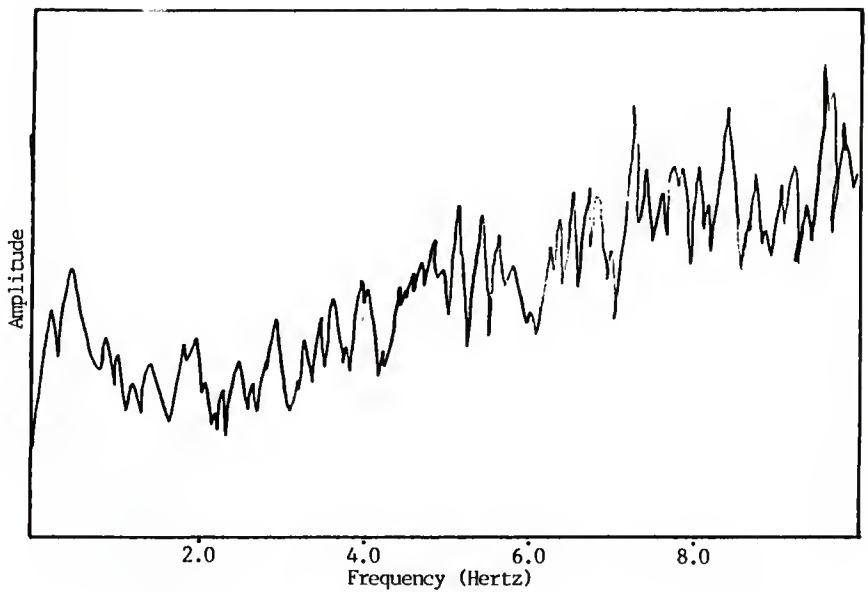

Figure 3.5, Response Plot from Free-Field Test Location 'B' (Accelerometer Oriented Along N/S Axis)

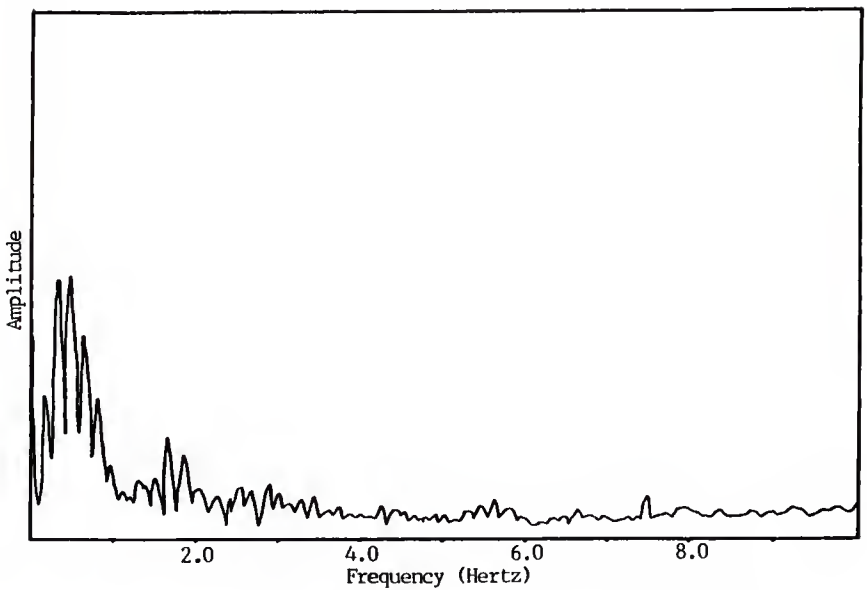

Figure 3.6, Response Plot from Free-Field Test Location 'C' (Accelerometer Oriented Along E/W Axis)

Station	Frequency	Response	Phase
0-0-V		0.11	In
0-90-V	1.04	0.26	In
0-180-V		0.11	In
0-0-V		0.09	In
0-90-V	1.44	0.19	In
0-180-V		0.09	In
0-0-V		0.05	In
0-90-V	1.60	0.19	In
0-180-V		0.05	In
0-0-V		0.02	In
0-90-V	1.84	0.05	In
0-180-V		0.02	In
0-0-V		0.02	In
0-90-V	2.64	0.06	Out
0-180-V		0.03	In
0-0-V		0.05	Out
0-90-V	2.88	0.10	Out
0-180-V		0.04	Out
0-0-V		0.07	In
0-90-V	3.52	0.11	Out
0-180-V		0.06	Out

Table 3.4, Summary of Response & Relative Phase Information from Test 17A

3.5 Modal Damping Ratios

The damping ratio may be computed at each of the predominant frequencies, provided the peaks on the response spectra may be isolated. This is accomplished by the half-power band width method. The method states that:

$$\xi = \Delta\omega / \omega_n$$

where $\Delta\omega$ = the band width at $1/\sqrt{2}$ of the peak response at an isolated frequency (ω_n).

Figure 3.7 shows a typical response plot, complete with half-power measurements and calculations.

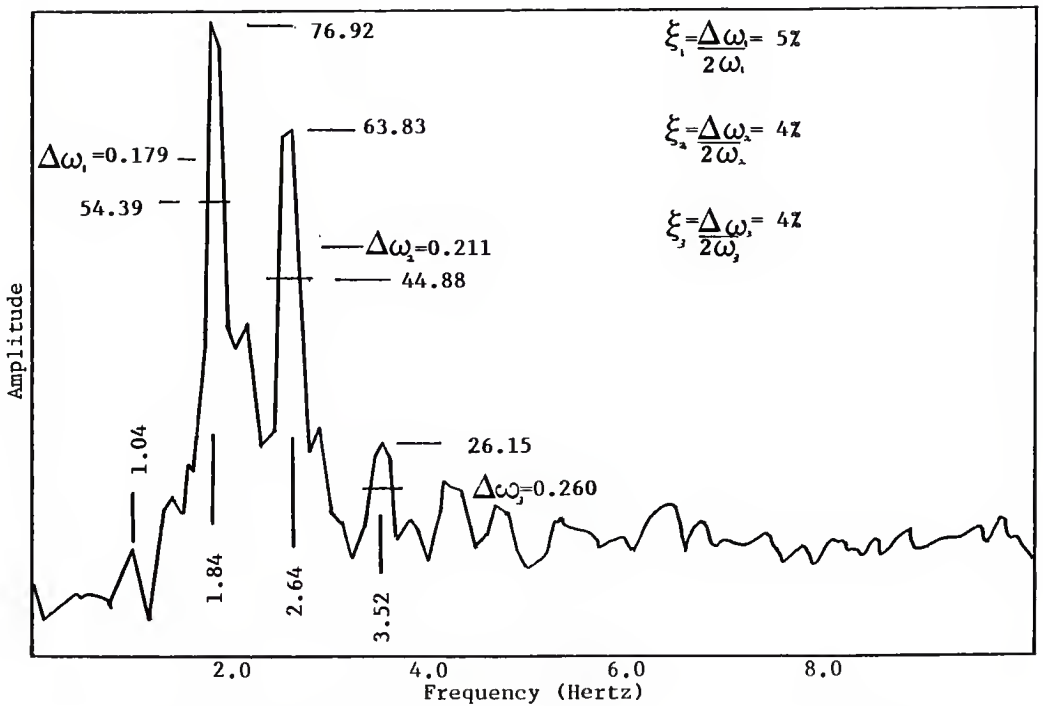

Figure 3.7, Half-Power Band Width Measurements & Calculations (5-0-N)

IV. CONCLUSIONS

An ambient vibration study was conducted on the hyperbolic cooling tower at Portland General Electric's Trojan Nuclear Generating Station, near Rainier, Oregon.

The purpose of this study was to determine the dynamic characteristics (natural frequencies and associated mode shapes) of the tower. The mode shapes include vertical and radial, as well as lateral responses.

It is hoped that the results will be useful in the calibration and/or verification of results obtained from a mathematical model (finite element analysis) currently under study at Kansas State University.

Seven predominant frequencies were identified. These are 1.04, 1.44, 1.60, 1.84, 2.64, 2.88, and 3.52 Hertz. The mode shapes associated with the predominant frequencies were plotted.

At the outset of this research, it was believed that the structure would be found to behave more like a cantilevered beam, and would display predominant lateral modes. Instead, it is now thought that the predominant modes are circumferential waves, n=0, 1, 2, 3, etc., each with a set of lateral mode shapes unique to itself.

In as much as there are insufficient data for the isolation of n, no clear conclusions may be drawn concerning the relationship of m to n, for this structure.

Examination of the vertical response data led to the conclusion that there was no significant contribution to the lateral response by base rocking.

Free-field data indicated that no predominant site frequencies exist in the range of the predominant structural response frequencies. This precludes the possibility that the structural response peaks were artificially induced by low level seismic, or man made disturbances.

The principal problem encountered with the testing of a structure of this type was the lack of accessibility to the various areas of the structure. This resulted in a lack of sufficient data for the identification and plotting of radial mode shapes.

Possible remedies include the construction of scaffolding to increase the accessibility, the use of optical methods in obtaining data (interferometry), or the instrumenting of a tower with permanent transducers, during the construction of the tower. This would supply a continuing record for analysis, and would enable the researcher to study the effects of aging on the dynamic characteristics of the structure.

References

1. Abdel-Ghaffar, A.M., Scanlan, R.H., "Ambient Vibration Studies of the Golden Gate Bridge: I. Suspended Structure," A.S.C.E. Journal of Engineering Mechanics, Vol. 111, No. 4, April, 1985.

2. Abdel-Ghaffar, A.M., Scanlan, R.H., "Ambient Vibration Studies of the Golden Gate Bridge: II. Pier Tower Structure," A.S.C.E. Journal of Engineering Mechanics, Vol. 111, No. 4, April, 1985.

3. Abdel-Ghaffar, A.M., "Dynamic Longitudinal Response of an Earth Dam," Proceedings of the Conference on Dynamic Response of Structures, by A.S.C.E., Jan. 15-16, 1981.

4. Abel, J.F., Billington, D.P., "Effect of Shell Cracking on Dynamic Response of Cooling Towers," I.A.S.S. World Congress on Space Enclosures, Concordia University, Montreal, July, 1976.

5. Abu-Sitta, S.H., Hashish, M.G., "Dynamic Wind Stresses in Hyperbolic Cooling Towers," A.S.C.E. Journal of the Structural Division, Vol. 99, No. ST9, Sept. 1973.

6. Armitt, J., "Wind Loading on Cooling Towers," A.S.C.E. Journal of the Structural Division, Vol. 106, No. ST3, March, 1980.

7. Basu, P.K., Gould, P.L., "Cooling Towers Using Measured Wind Data," A.S.C.E. Journal of the Structural Division, Vol. 106, No. ST3, March, 1980.

8. Craig, J.I., et.al., "Modal Parameter Estimation for a High Rise Building Using Ambient Vibration Data Taken During Construction," Proceedings of the Conference on Dynamic Response of Structures, by A.S.C.E., Jan. 15-16, 1981.

9. Douglas, B.M., "Experimental Dynamics of Highway Bridges," Proceedings of the Conference on Dynamic Response of Structures, by A.S.C.E., Jan. 15-16, 1981.

References (Cont.)

10. Fujita, T.T., "Tornado Wind Effects on the Grand Gulf Cooling Tower," Proceedings of the Conference on Dynamic Response of Structures, by A.S.C.E., Jan. 15-16, 1981

11. Glockner, P.G., et.al., "Dynamic Response of Cable Reinforced Structures Under Wind Loading," Proceedings of the Conference on Dynamic Response of Structures, by A.S.C.E., Jan. 15-16, 1981.

12. Haroun, M.A., "Dynamic Analysis of Liquid Storage Tanks," Earthquake Engineering Research Lab., California Institute of Technology, Pasadena, CA. 1980.

13. Hudson, D.E., "Dynamic properties of Full-Scale Structures Determined from Natural Excitations," California Institute of Technology, Pasadena, CA.

14. Kapania, r.k., Yang, T.Y., "Time Domain Random Wind Response of Cooling Tower," A.S.C.E. Journal of Engineering Mechanics, Vol. 110, No. 10, Oct. 1984.

15. Lee, b.j., Gould, P.L., "Complex Response Analysis of Shells of Revolution Including Uniform Base Translation and Rocking," Earthquake Engineering and Structural Dynamics, Vol. 12, 1984.

16. Pardoen, G.C., et.al., "Earthquake and Ambient Response of the El Centro County Services Building," Proceedings of the Conference on Dynamic Response of Structures, by A.S.C.E., Jan. 15-16, 1981.

17. "Report of the Committee of Inquiry Into the Colapse of the Cooling Tower at Ferrybridge, Mon., November 1, 1965," Central Electricity Generating Board, H.M.'s Stationary Office, London, 1966.

18. "Report of the Committee of Inquiry Into the Colapse of the Cooling Tower at Ardeer Nylon Works, Thursday, September 27, 1973," Imperial Chemical Industries Ltd., Millbanf, London.

References (Cont.)

19. Sollenberger, N.J., Scanlan, R.H., "Wind Loading and Response of Cooling Towers," A.S.C.E. Journal of the Structural Division, Vol. 106, No. ST3, March, 1980.

20. Sparks, P.R., et.al., "A Study of the Use of Ambient Vibration Measurements to Detect Changes in the Structural Characteristics of a Building," Proceedings of the Conference on Dynamic Response of Structures, by A.S.C.E., Jan. 15-16, 1981.

21. Swartz, S.E., et.al., "On the Validity of Reinforced Concrete Models of Cooling Tower Shells," Proceedings of the Second International Symposium on Natural Draft Cooling Towers, Ruhr-University, Bochum, Germany, Sept., 1984.

22. Paz, Mario, "Structural Dynamics, Theory & Computation," Second Edition, Van Nostrad-Reinhold Co., NY. 1985.

23. Thomson, W.T., "Vibration Theory and Application," Prentice Hall Inc., Englewood Cliffs, NJ. 1965.

APPENDIX I.

TEST LOG

DATE 6/15

TIME 3:45

TEST NO. 1 A

RECORDER START 120

RECORDER END 140

Pointed down

CHANNEL	1	2	3	4
COLOR	RED	GREEN	YELLOW	BLUE
HEIGHT	5	4	5	5
AZIMUTH	0	0	0	0
ORIENTATION	N	N	- V	T
LOW PASS FILTER	20			
ATTENUATOR SETTING	42	30	36	42
H-P FILTER I/O	✓	✓	✓	✓
SENSITIVITY VOLTS	30 dB atten			→

ACCEL. SIGNAL GRND BRUEL

B-K.

NOTES:

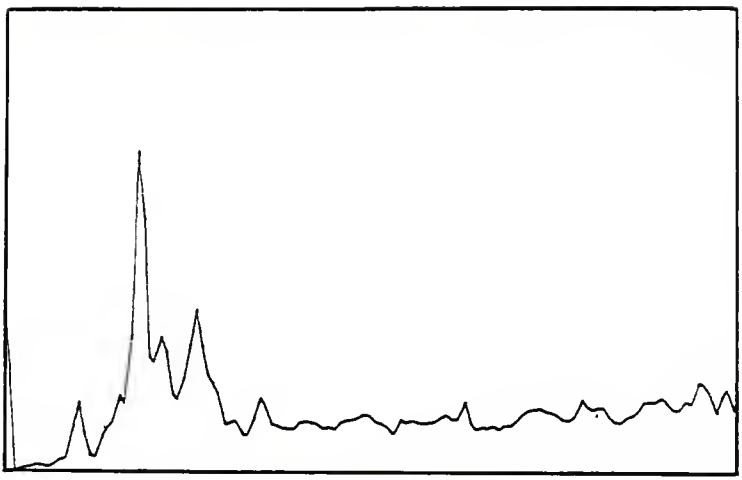

Response vs. Frequency, Channel A (5-0-N), 40 mv. F.S., Test # 1A

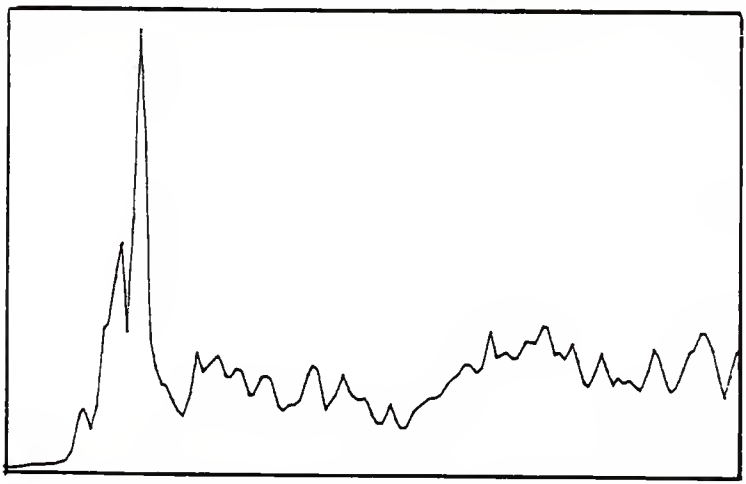

Response vs. Frequency, Channel B (4-0-N), 80 mv. F.S., Test # 1A

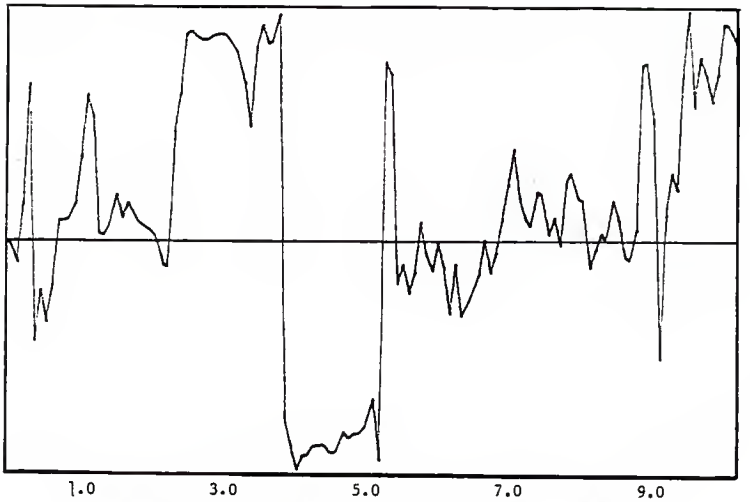

Transfer Function (Phase Angle), 5-0-N & 4-0-N, Test # 1A

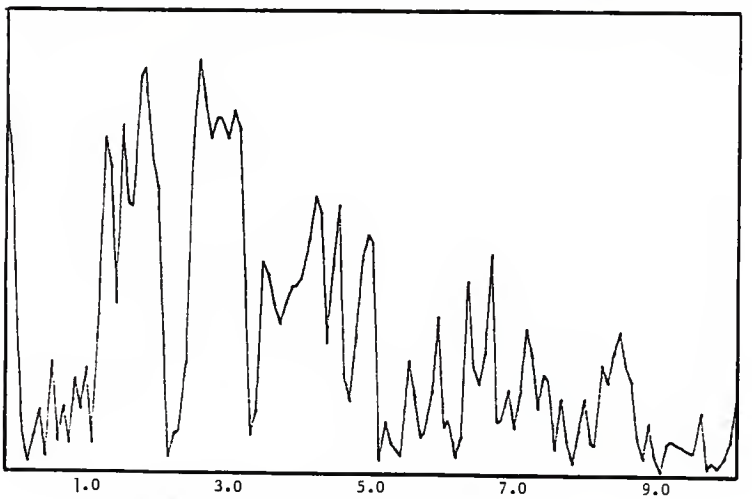

Coherence Function, 5-0-N & 4-0-N, Test # 1A

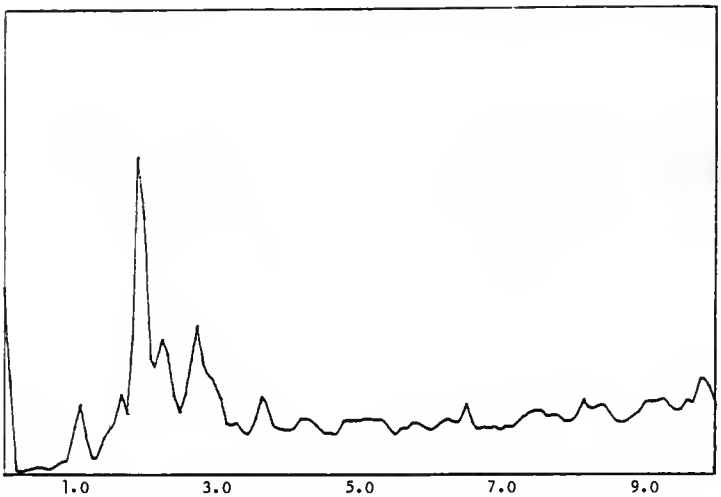

Response vs. Frequency, Channel A (5-0-N), 40 mv. F.S., Test # 1A

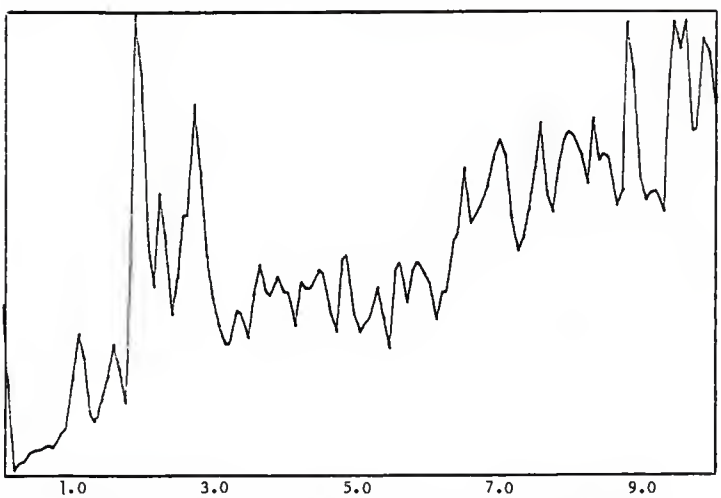

Response vs. Frequency, Channel B (5-0—V), 8 mv. F.S., Test # 1A

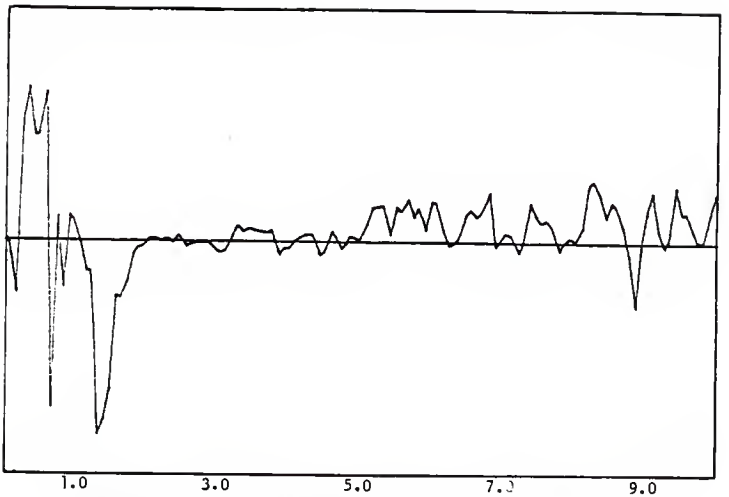

Transfer Function (Phase Angle), 5-0-N & 5-0--V, Test # 1A

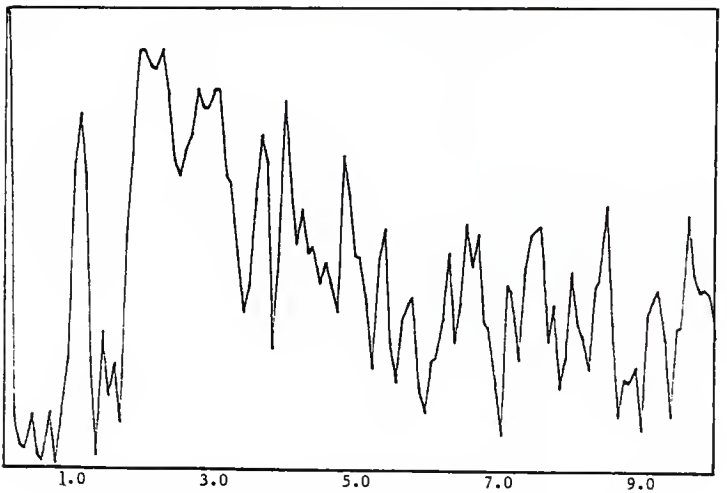

Coherence Function, 5-0-N & 5-0--V, Test # 1A

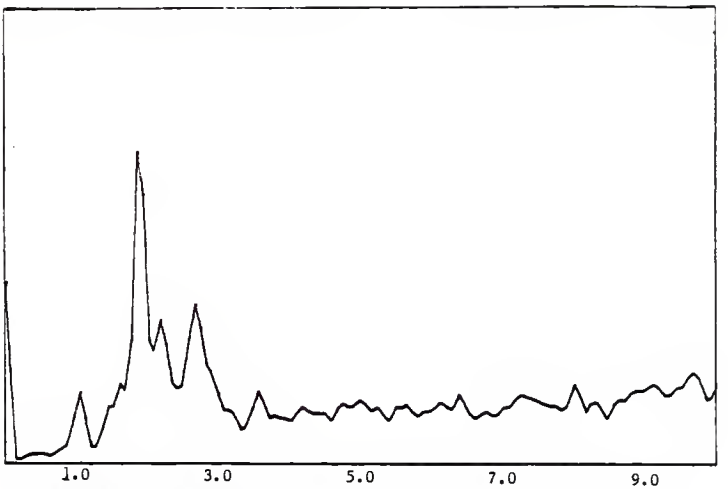

Response vs. Frequency, Channel A (5-0-N), 40 mv. F.S., Test # 1A

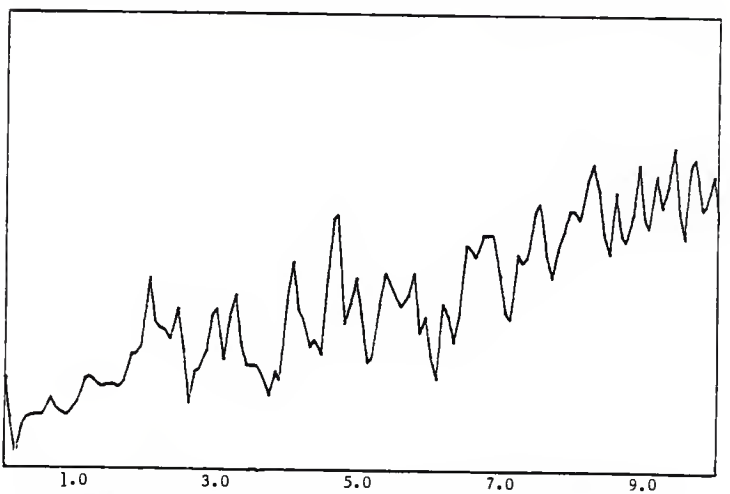

Response vs. Frequency, Channel B (5-0-T), 16 mv. F.S., Test # 1A

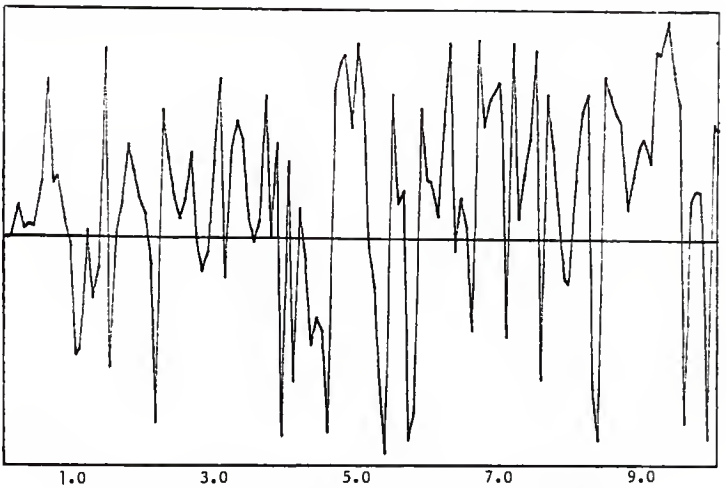

Transfer Function (Phase Angle), 5-0-N & 5-0-T, Test # 1A

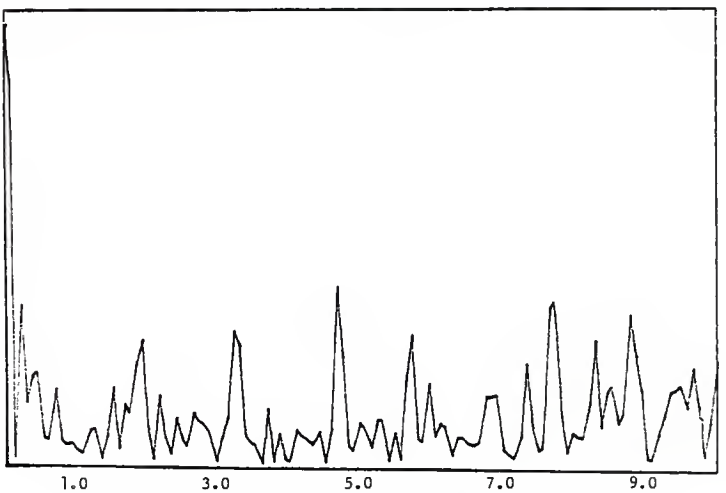

Coherence Function, 5-0-N & 5-0-T, Test # 1A

TEST LOG

DATE 6/15

TIME 5:45 5:40

TEST NO. 3 A

RECORDER START 285

RECORDER END 295

CHANNEL	1	2	3	4
COLOR	RED	GREEN	YELLOW	BLUE
HEIGHT	5	4	2.5	3.0
AZIMUTH	0	0	0	0
ORIENTATION	N	N	N	N
LOW PASS FILTER	10	10	10	10
ATTENUATOR SETTING	30	30	30	30
H-P FILTER I/O				
SENSITIVITY VOLTS				

ACCEL. SIGNAL GRND BRNK

NOTES:

All input atten at 30 dB.

$$\frac{V_1}{V_2} = 10^{dB/20}$$

$$\frac{P}{P_0} = 10^{dB/10}$$

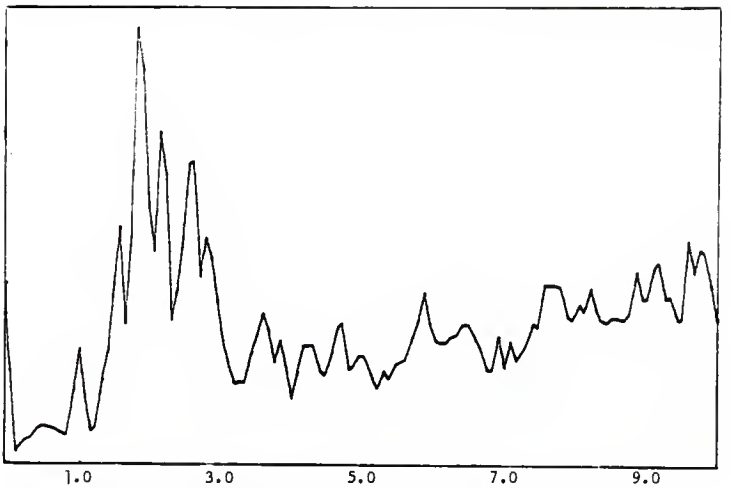

Response vs. Frequency, Channel A (5-0-N), 40 mv. F.S., Test # 3A

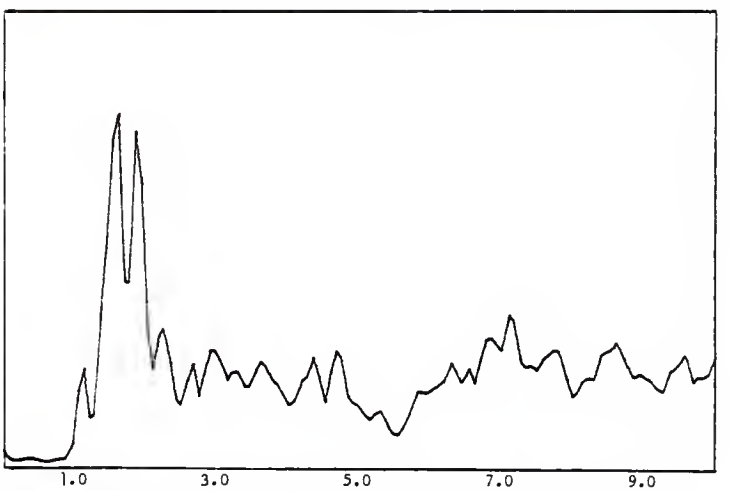

Response vs. Frequency, Channel B (4-0-N), 80 mv. F.S., Test # 3A

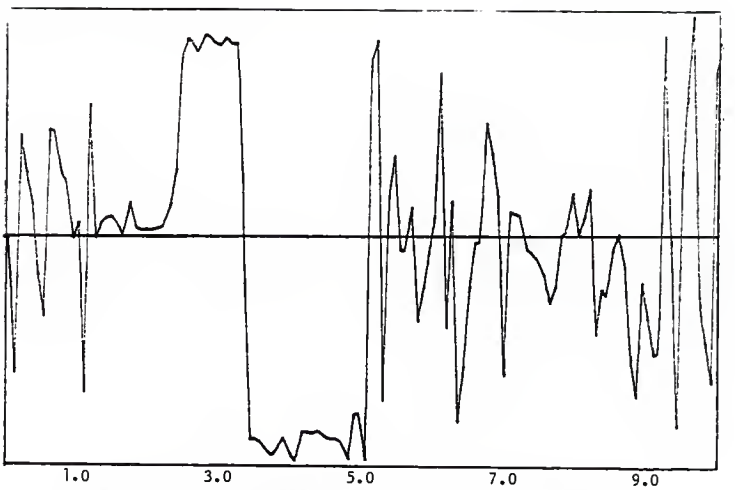

Transfer Function (Phase Angle), 5-0-N & 4-0-N, Test # 3A

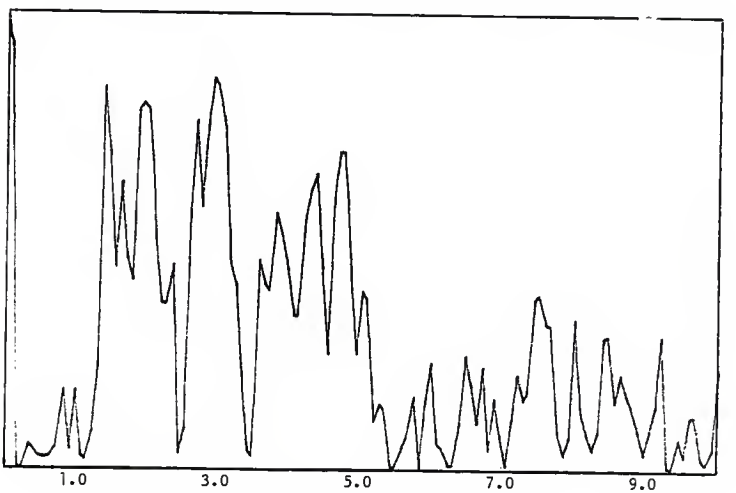

Coherence Function, 5-0-N & 4-0-N, Test # 3A

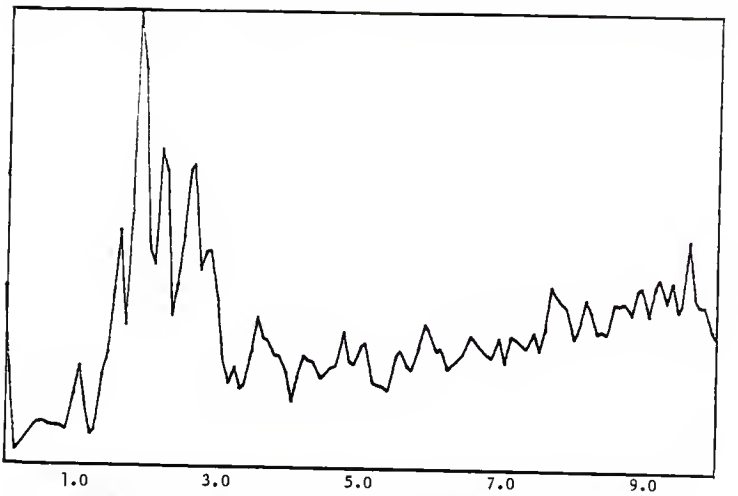

Response vs. Frequency, Channel A (5-0-N), 40 mv. F.S., Test # 3A

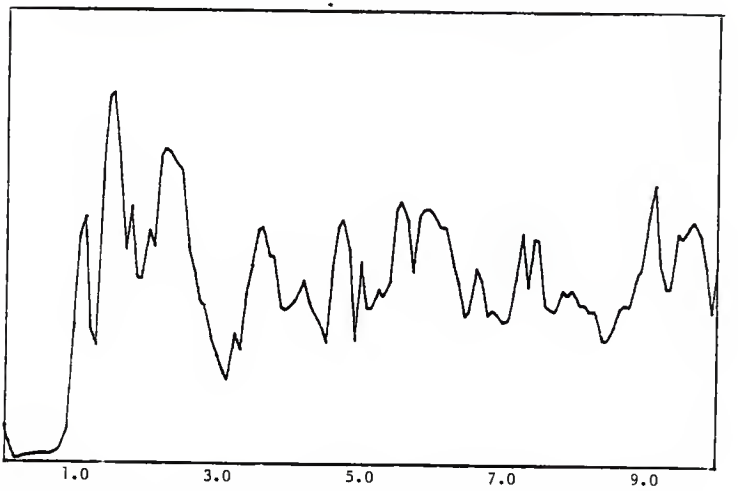

Response vs. Frequency, Channel B (3.5-0-N), 40 mv. F.S., Test # 3A

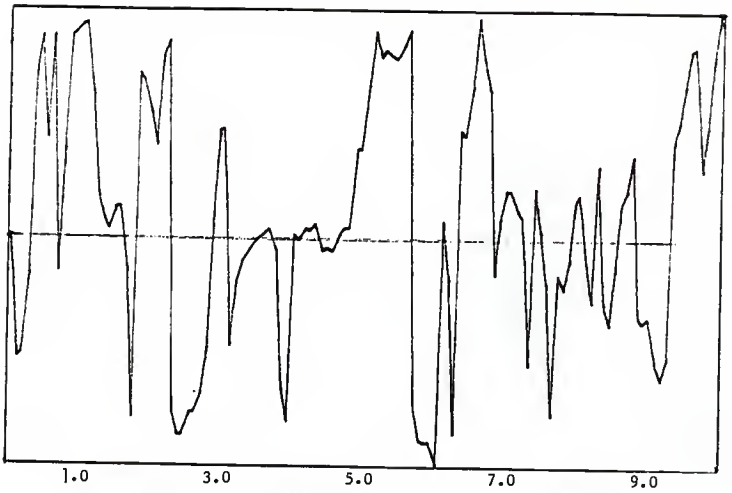

Transfer Function (Phase Angle), 5-0-N & 3.5-0-N, Test # 3A

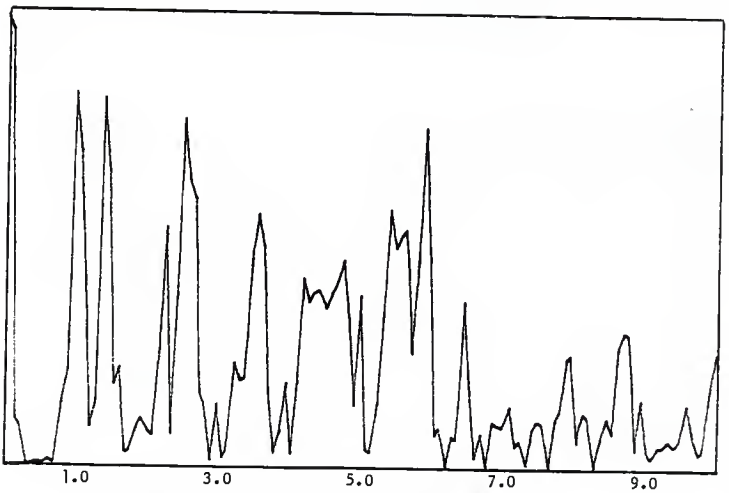

Coherence Function, 5-0-N & 3.5-0-N, Test # 3A

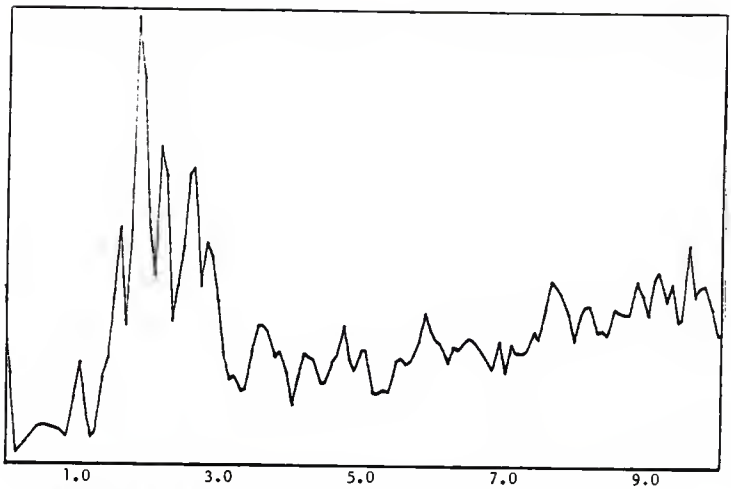

Response vs. Frequency, Channel A (5-0-N), 40 mv. F.S., Test # 3A

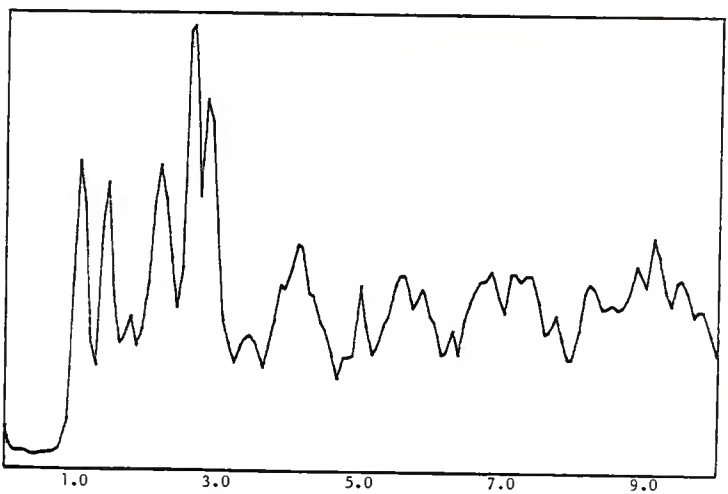

Response vs. Frequency, Channel B (3-0-N), 40 mv. F.S., Test # 3A

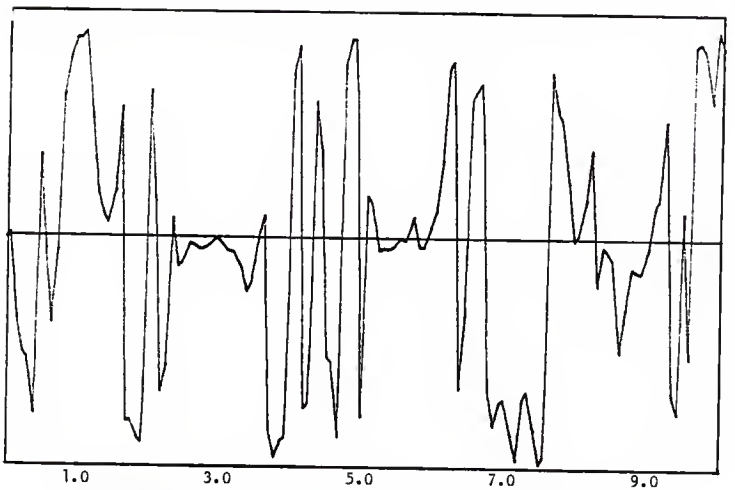

Transfer Function (Phase Angle), 5-0-N & 3-0-N, Test # 3A

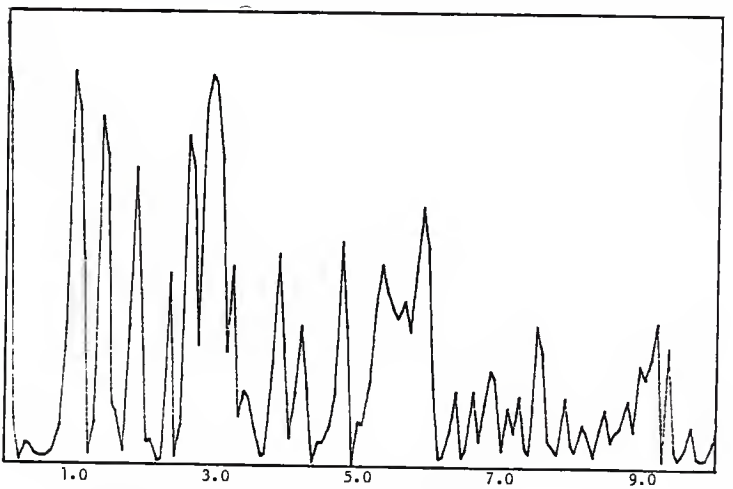

Coherence Function, 5-0-N & 3-0-N, Test #3 A

TEST LOG

DATE 8/17

TIME 8:55

TEST NO. 4 A

RECORDER START 330

RECORDER END 350

CHANNEL	1	2	3	4
COLOR	RED	GREEN	YELLOW	BLUE
HEIGHT	5	3	3	3
AZIMUTH	0	0	0	0
ORIENTATION	N	N	V	T
LOW PASS FILTER	20	20	20	20
ATTENUATOR SETTING	30	30	30	30
H-P FILTER I/O	✓	✓	✓	✓
SENSITIVITY VOLTS				

ACWA. SIGNAL GRND BRIDGE

NOTES:

Input attenuator at 30 dB

Fog, moderately still.

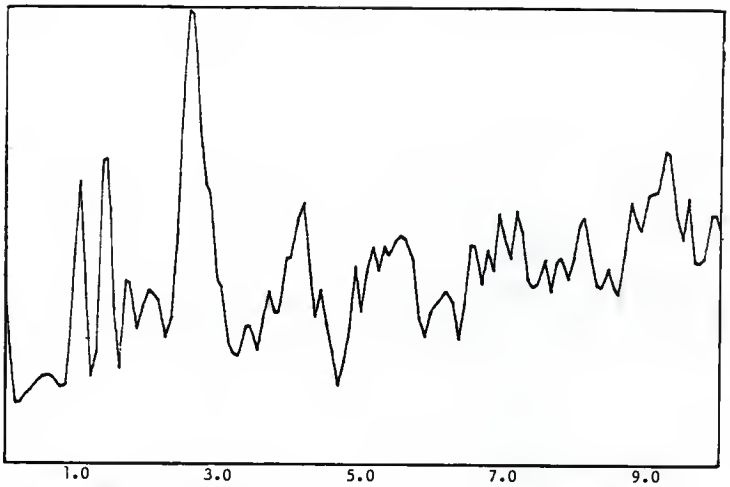

Response vs. Frequency, Channel A (3-0-N), 40 mv. F.S., Test # 4A

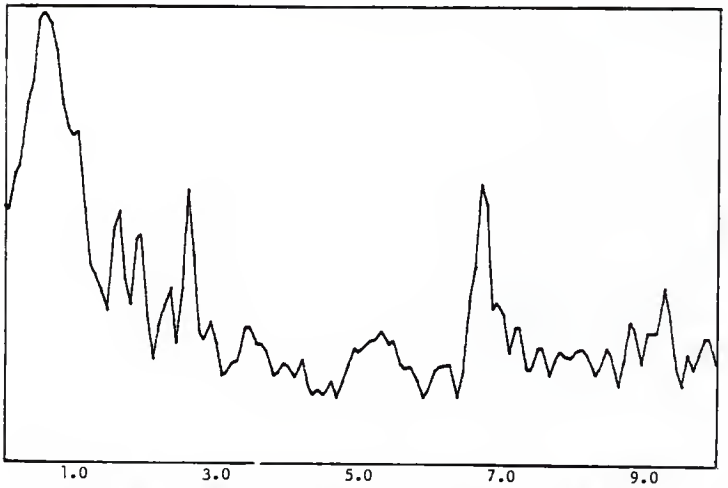

Response vs. Frequency, Channel B (3-0-V), 8 mv. F.S., Test # 4A

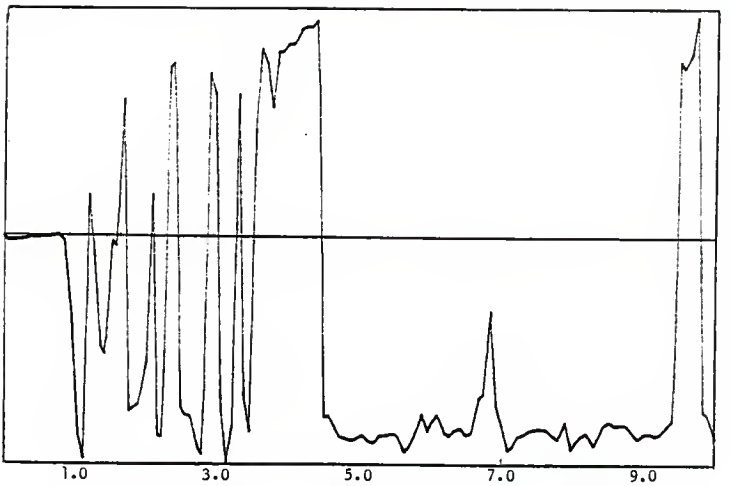

Transfer Function (Phase Angle), 3-0-N & 3-0-V, Test # 4A

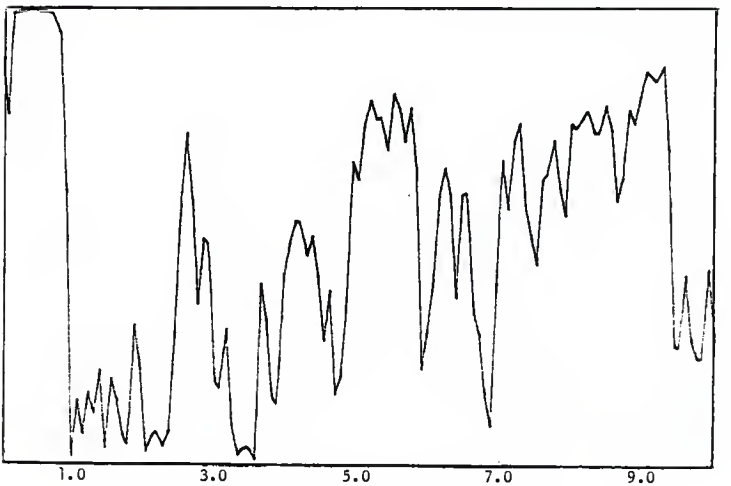

Coherence Function, 3-0-N & 3-0-V, Test # 4A

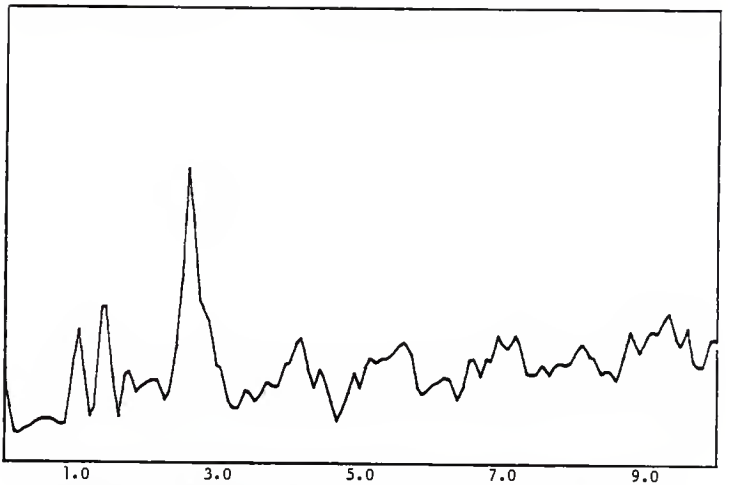

Response vs. Frequency, Channel A (3-0-N) 80 mv. F.S., Test # 4A

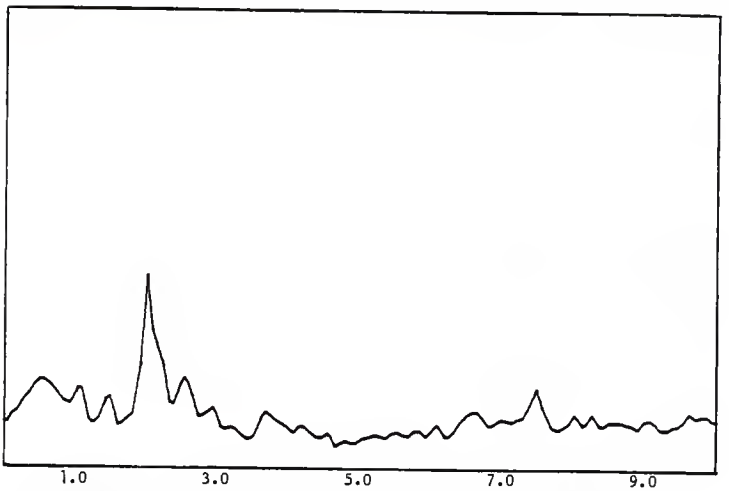

Response vs. Frequency, Channel B (3-0-T) 40 mv. F.S., Test # 4A

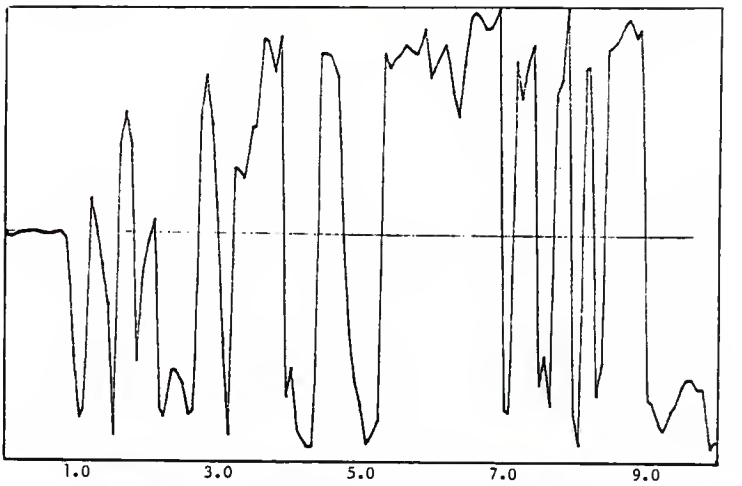

Transfer Function (Phase Angle), 3-0-N & 3-0-T, Test # 4A

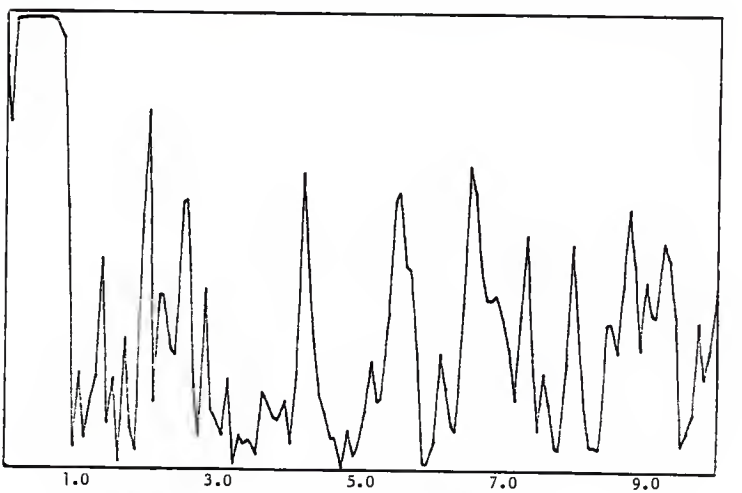

Coherence Function, 3-0-N & 3-0-T, Test # 4A

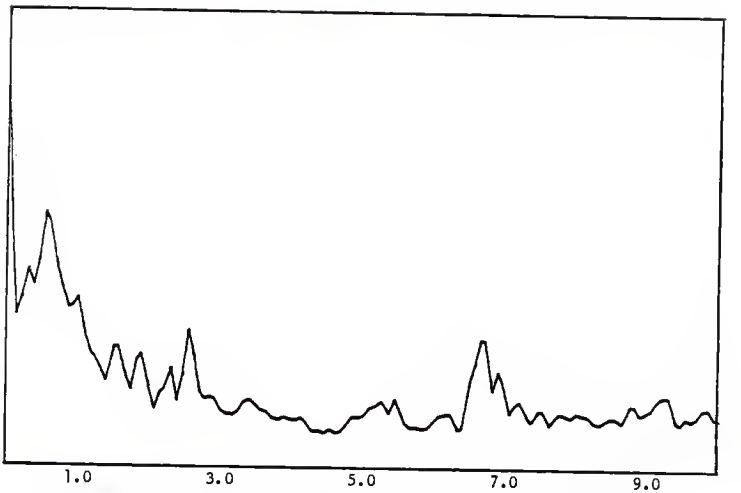

Response vs. Frequency, Channel A (3-0-V) 16 mv. F.S., Test # 4A

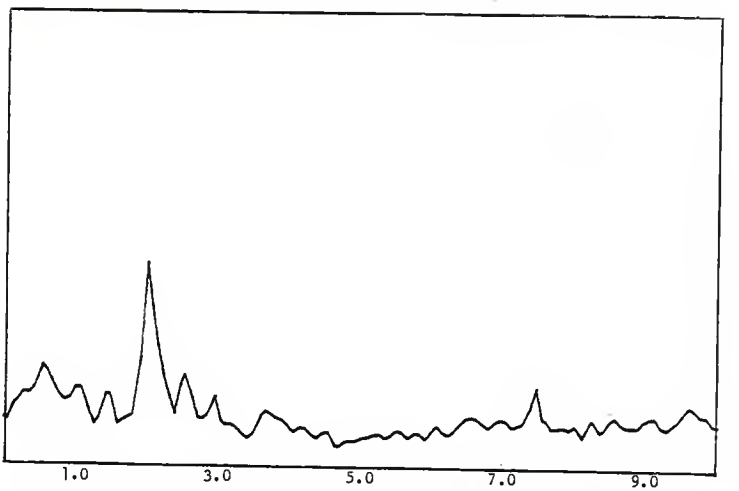

Response vs. Frequency, Channel B (3-0-T) 40 mv. F.S., Test # 4A

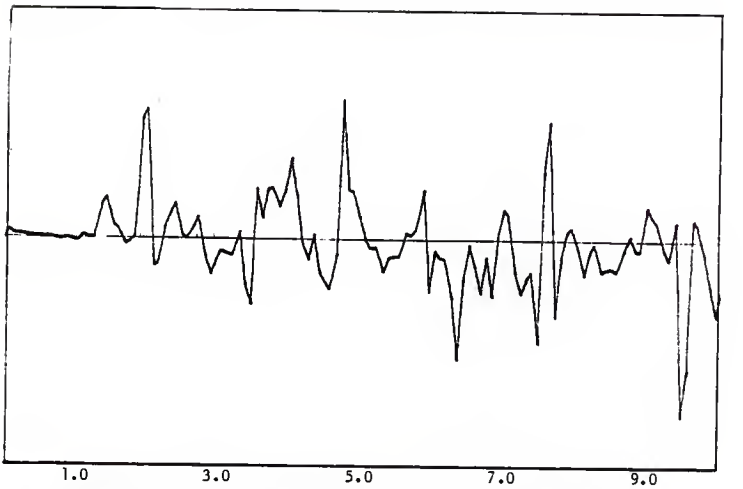

Transfer Function (Phase Angle), 3-0-V & 3-0-T, Test # 4A

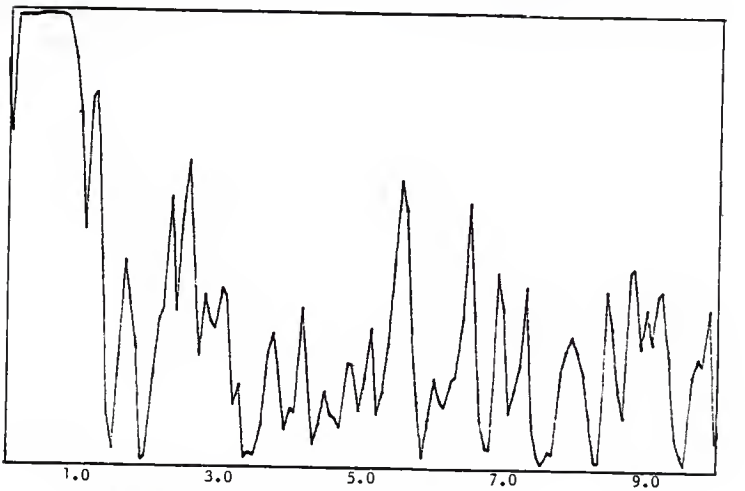

Coherence Function, 3-0-V & 3-0-T, Test # 4A

TEST LOG

DATE 8/17

TIME 10:05

TEST NO. 5A

RECORDER START 420

RECORDER END 435

CHANNEL	1	2	3	4
COLOR	RED	GREEN	YELLOW	BLUE
HEIGHT	5	3	2.5	2
AZIMUTH	0	0	0	0
ORIENTATION	N	N	N	N
LOW PASS FILTER	20	20	20	20
ATTENUATOR SETTING	30	30	30	30
H-P FILTER I/O				
SENSITIVITY VOLTS				

ACCEL. SIGNAL COND BRKR

NOTES:

.25

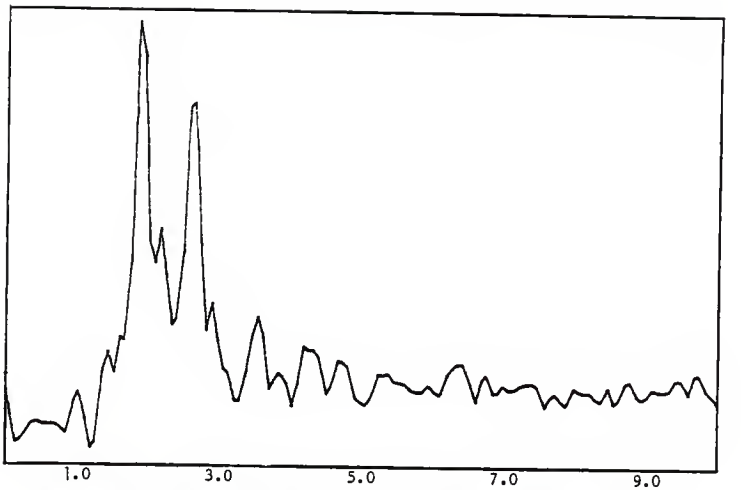

Response vs. Frequency, Channel A (5-0-N), 80 mv. F.S., Test # 5A

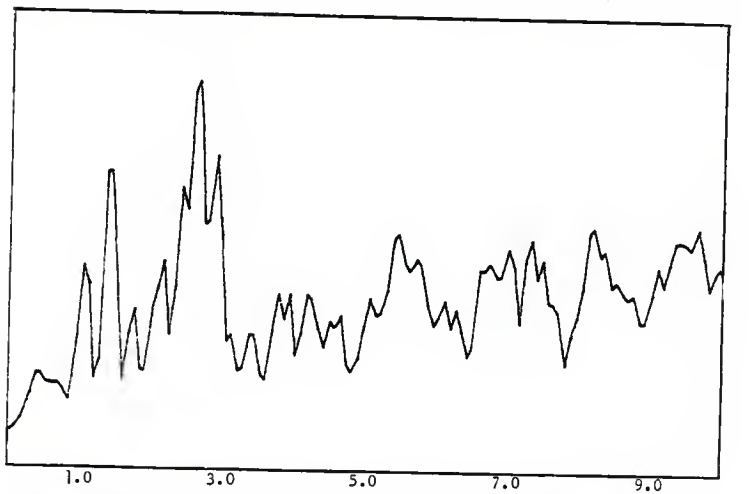

Response vs, Frequency, Channel B (3-0-N), 40 mv. F.S., Test # 5A

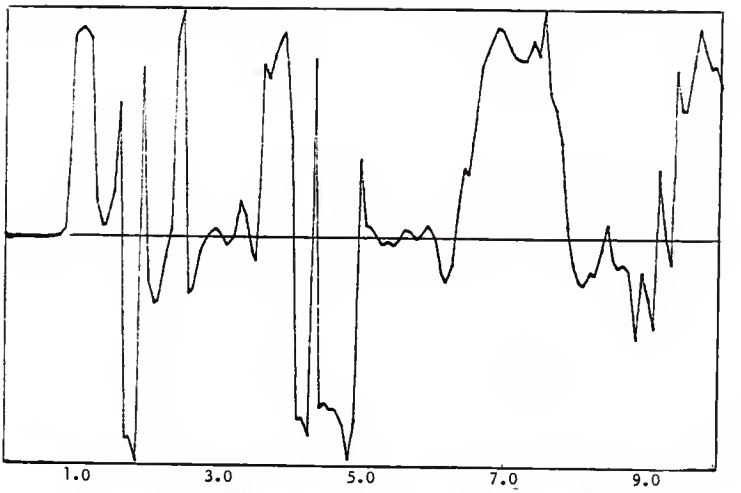

Transfer Function (Phase Angle), 5-0-N & 3-0-N, Test # 5A

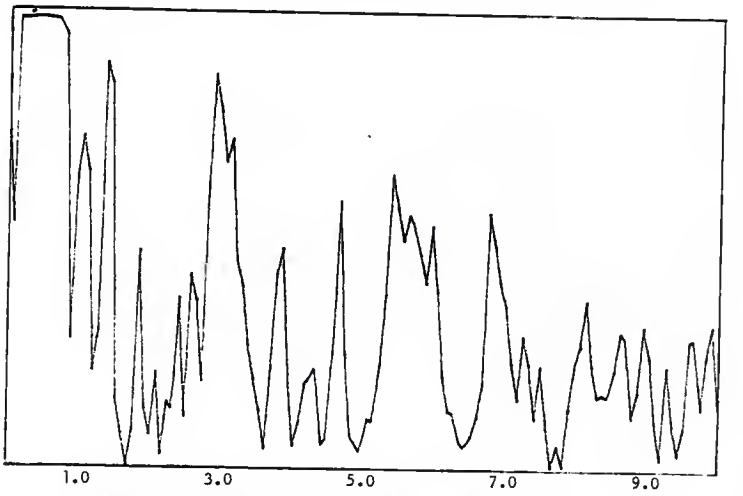

Coherence Function, 5-0-N & 3-0-N, Test # 5A

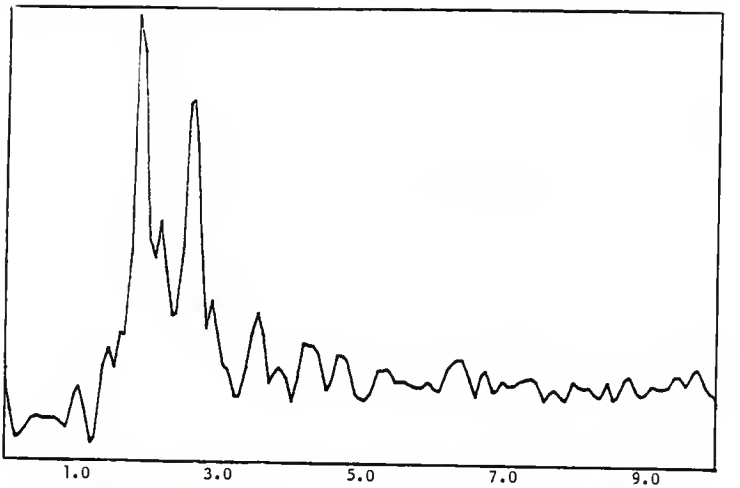

Response vs. Frequency, Channel A (5-0-N), 80 mv. F.S., Test # 5A

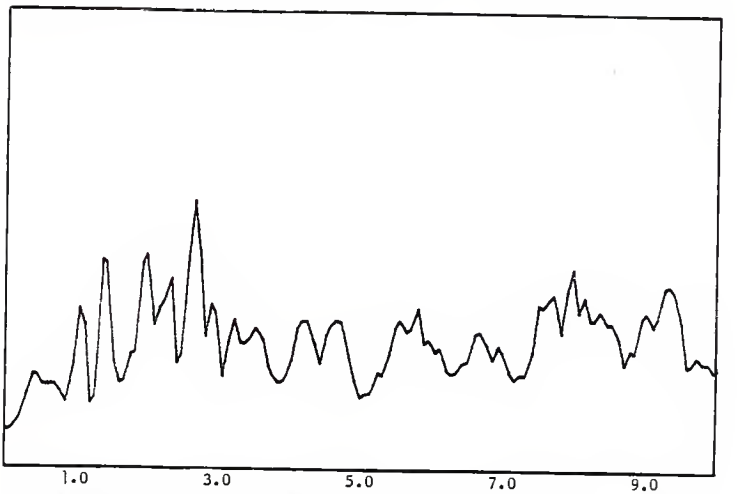

Response vs. Frequency, Channel B (2.5-0-N), 40 mv. F.S., Test # 5A

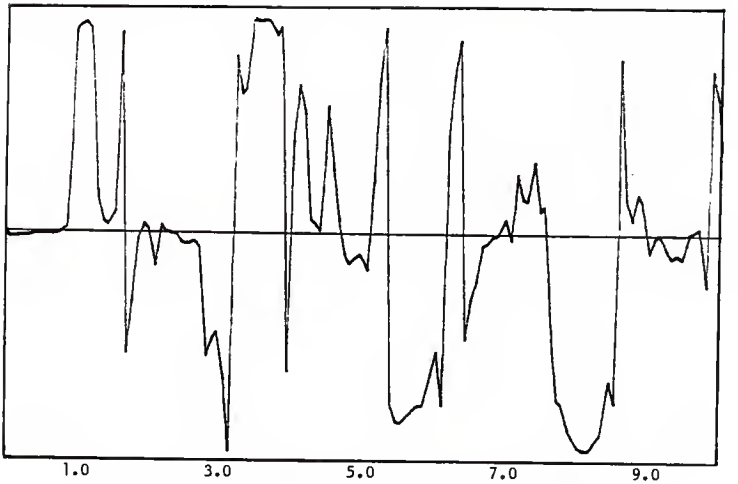

Transfer Function (Phase Angle), 5-0-N & 2.5-0-N, Test # 5A

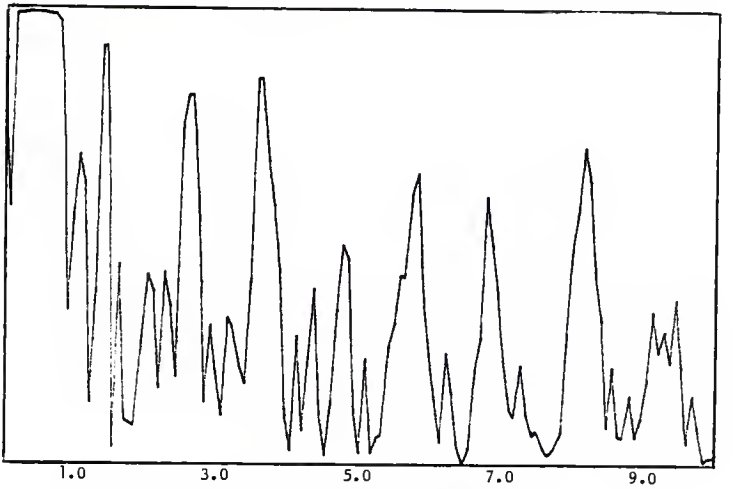

Coherence Function, 5-0-N & 2.5-0-N, Test # 5A

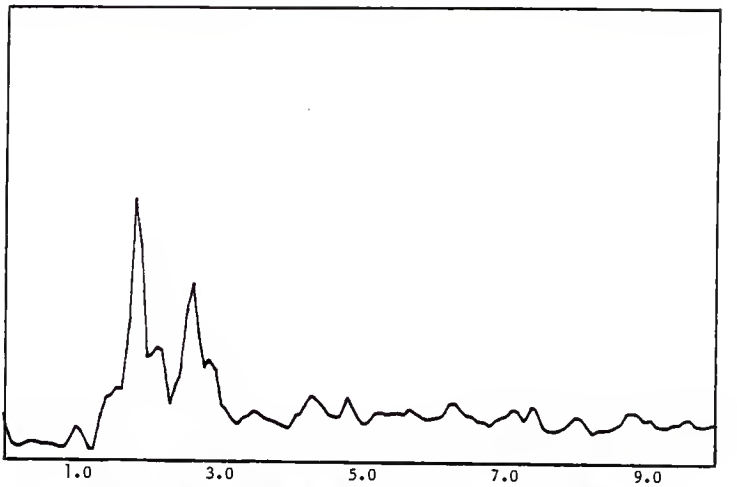

Response vs. Frequency, Channel A (5-0-N), 160 mv. F.S., Test # 5A

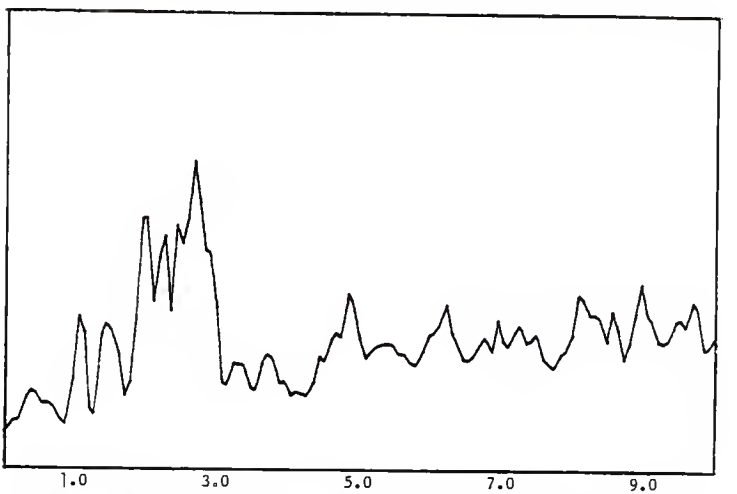

Response vs. Frequency, Channel B (2-0-N), 40 mv. F.S., Test # 5A

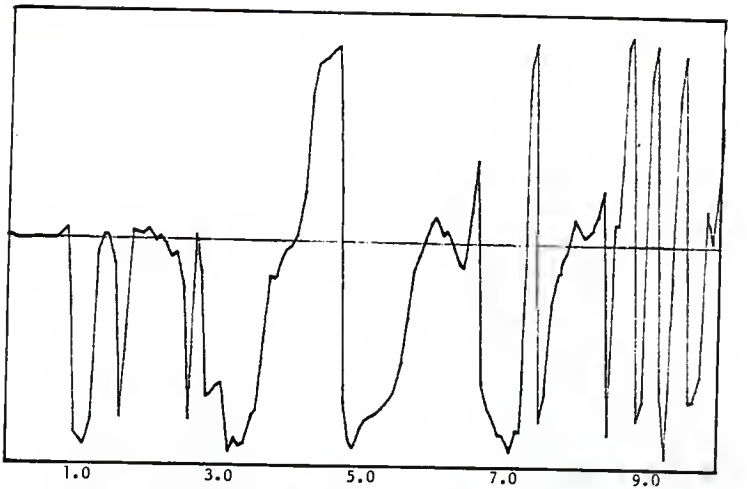

Transfer Function (Phase Angle), 5-0-N & 2-0-N, Test # 5A

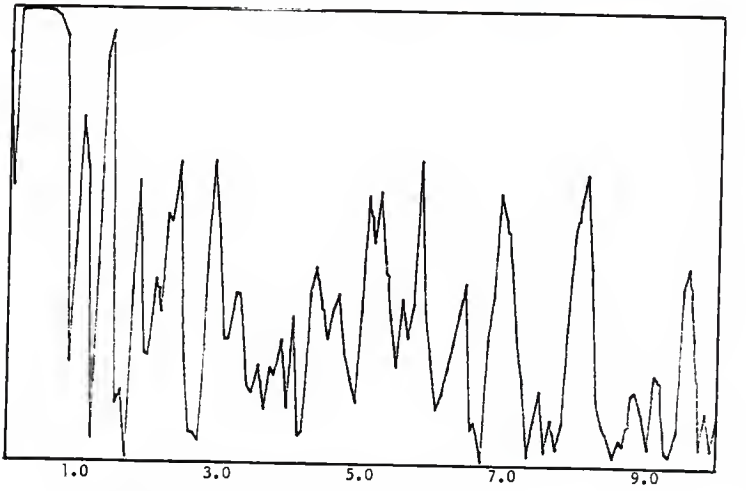

Coherence Function, 5-0-N & 2-0-N, Test # 5A

TEST LOG

DATE 8/17

TIME 11:15

TEST NO. 6A

RECORDER START 500

RECORDER END 520

CHANNEL	1	2	3	4
COLOR	RED	GREEN	YELLOW	BLUE
HEIGHT	5	2	2	2
AZIMUTH	0	0	0	0
ORIENTATION	N	N	V	T
LOW PASS FILTER	20	20	20	20.
ATTENUATOR SETTING	30	24	30	42
H-P FILTER I/O				
SENSITIVITY VOLTS				

ACOUS. SIGNAL SOND BRUIT

NOTES:

Input atten 30 dB

Wind gusts increasing

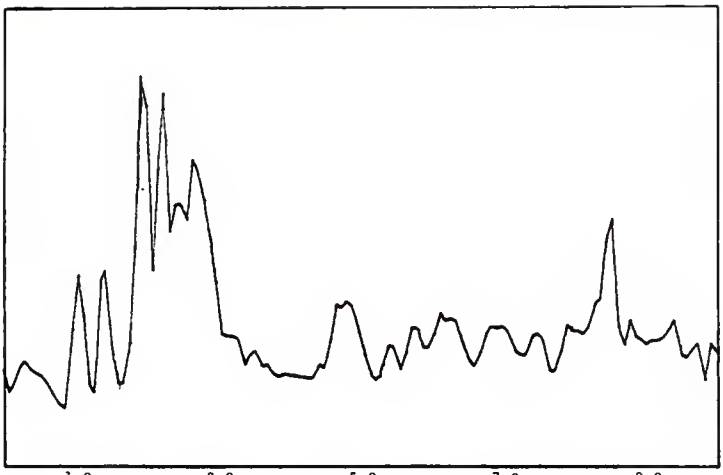

Response vs. Frequency, Channel A (2-0-N), 80 mv. F.S., Test # 6A

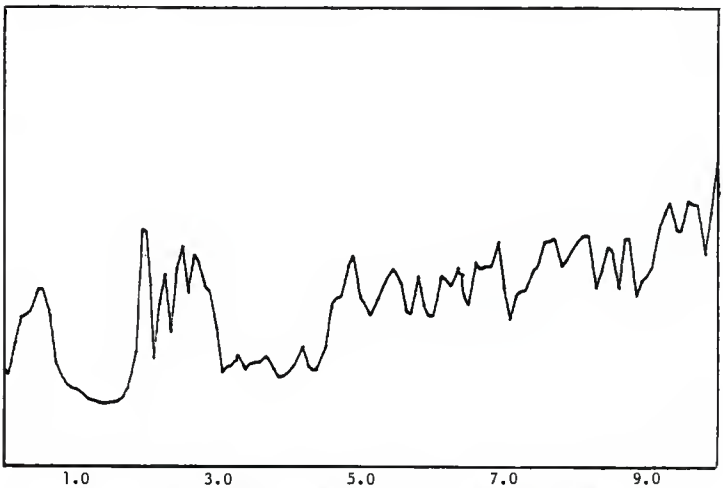

Response vs. Frequency, Channel B (2-0-V), 16 mv. F.S., Test # 6A

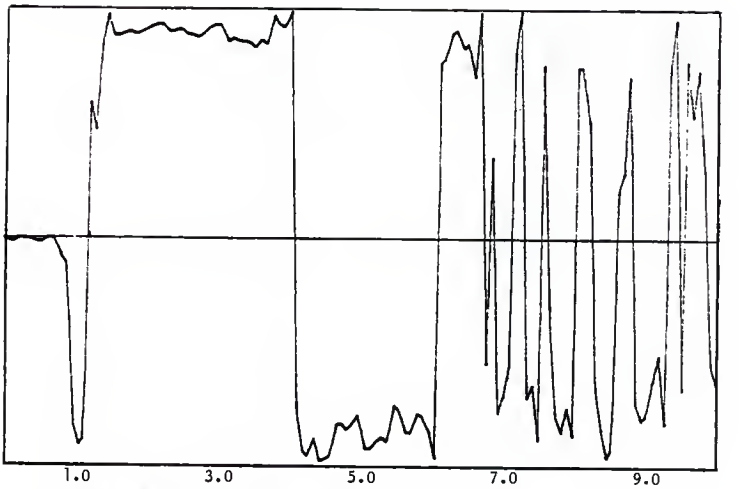

Transfer Function (Phase Angle), 2-0-N & 2-0-V, Test # 6A

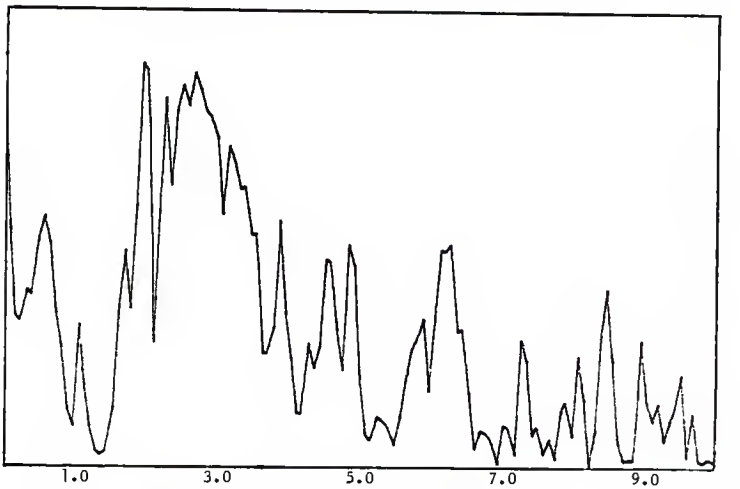

Coherence Function, 2-0-N & 2-0-V, Test # 6A

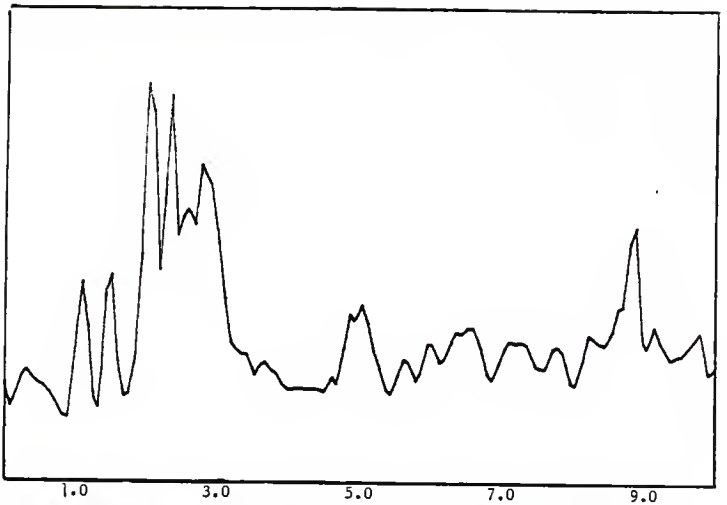

Response vs. Frequency, Channel A (2-0-N), 80 mv. F.S., Test # 6A

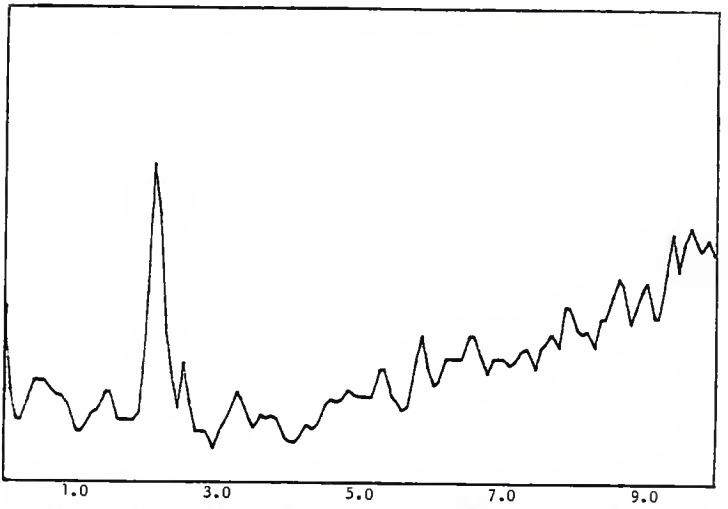

Response vs. Frequency, Channel B (2-0-T), 8 mv. F.S., Test # 6A

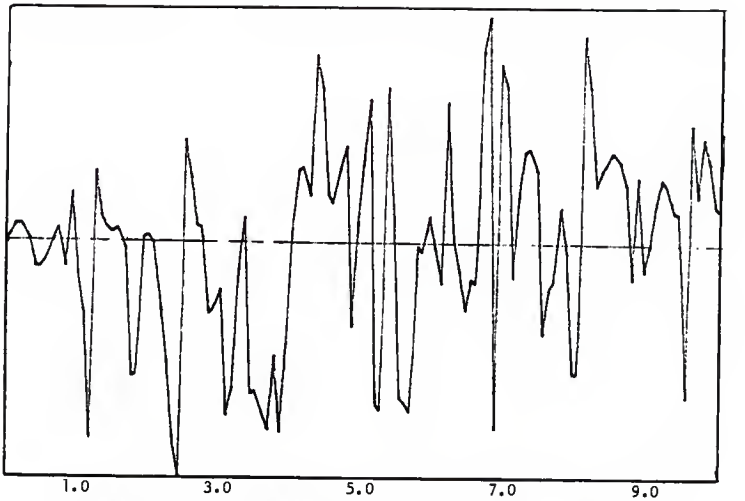

Transfer Function (Phase Angle), 2-0-N & 2-0-T, Test # 6A

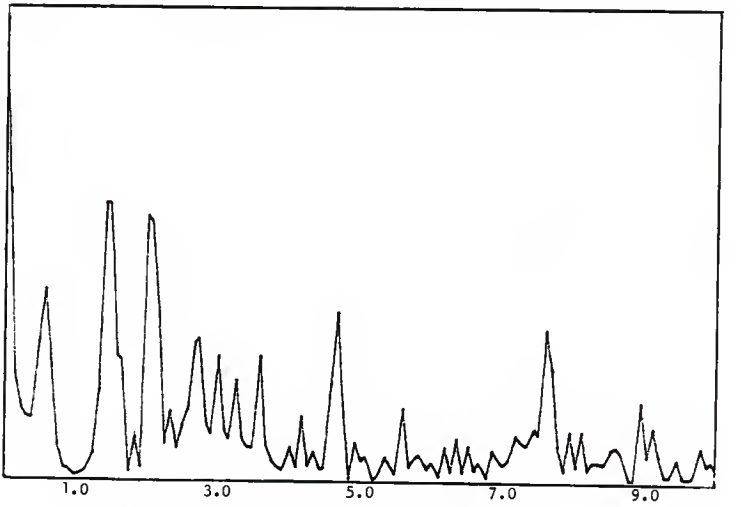

Coherence Function, 2-0-N & 2-0-T, Test # 6A

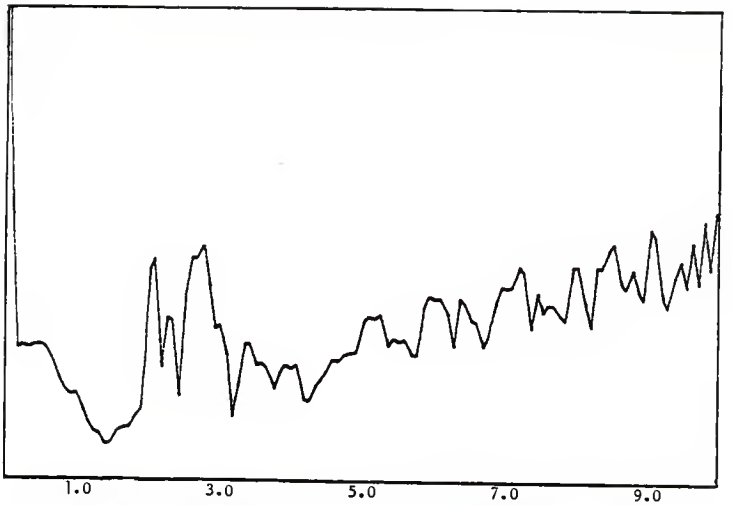

Response vs. Frequency, Channel A (2-0-V), 16 mv. F.S., Test # 6A

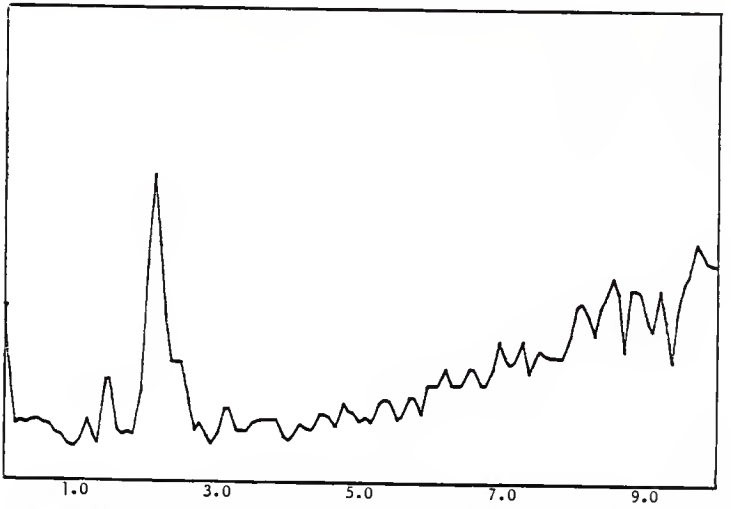

Response vs. Frequency, Channel B (2-0-T), 8 mv. F.S., Test # 6A

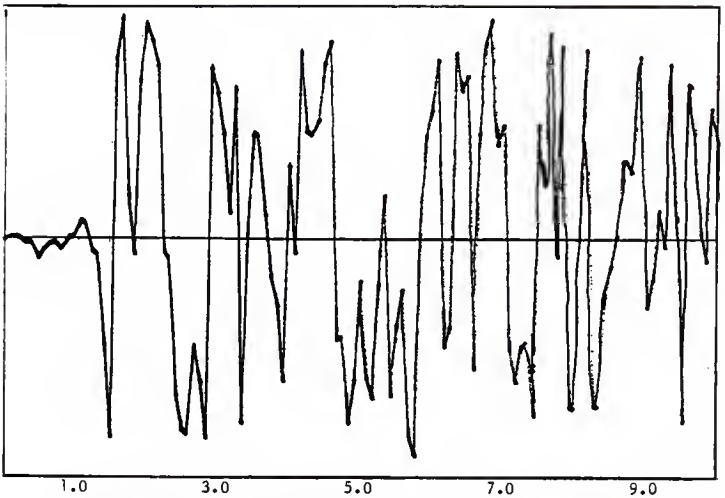

Transfer Function (Phase Angle), 2-0-V & 2-0-T, Test # 6A

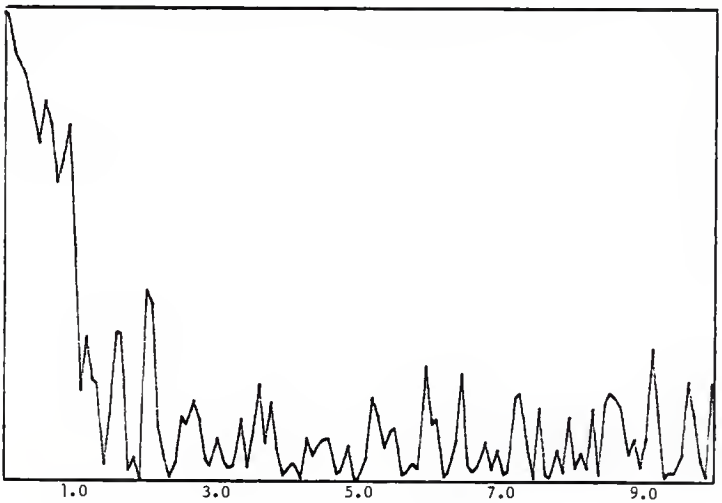

Coherence Function, 2-0-V & 2-0-T, Test # 6A

TEST LOG

DATE 8/17

TIME 12:55

TEST NO. 7A

RECORDER START 0600

RECORDER END 0615

CHANNEL	1	2	3	4
COLOR	RED	GREEN	YELLOW	BLUE
HEIGHT	5	2	1.5	1
AZIMUTH	0	0	0	0
ORIENTATION	N	N	N	N
LOW PASS FILTER	20	20	20	20
ATTENUATOR SETTING	30	30	30	30
H-P FILTER I/O	—	—	—	—
SENSITIVITY VOLTS				

ACCEL. SIGNAL GOES BLUE

NOTES: 30 dB input attenuator

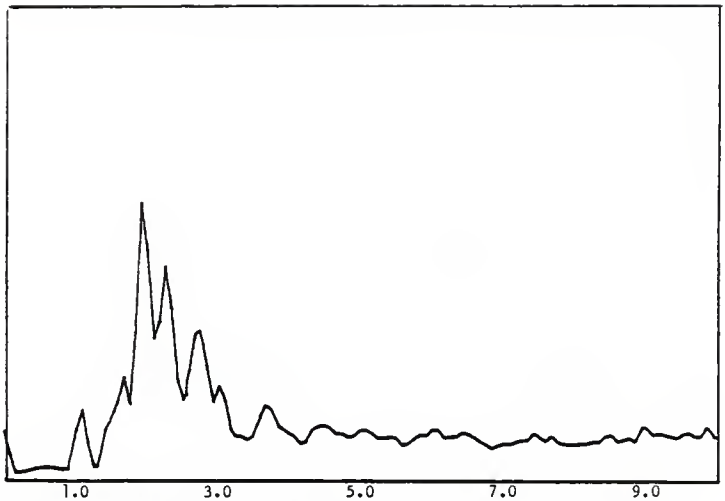

Response vs. Frequency, Channel A (5-0-N), 160 mv. F.S., Test # 7A

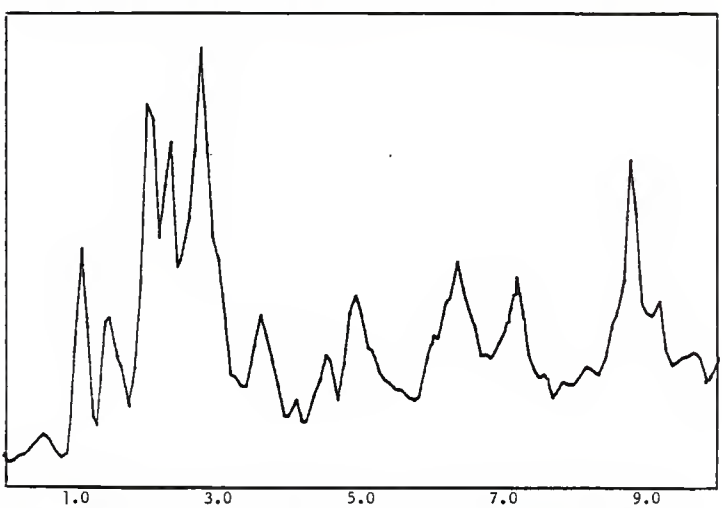

Response vs. Frequency, Channel B (2-0-N), 40 mv. F.S., Test # 7A

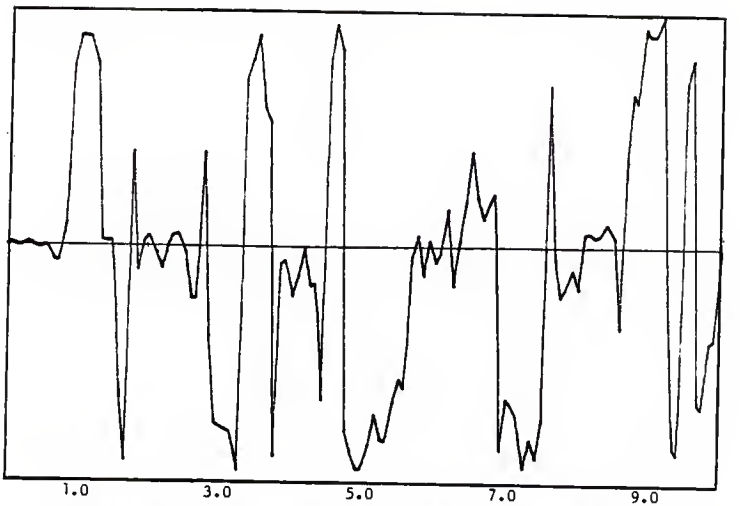

Transfer Function (Phase Angle), 5-0-N & 2-0-N, Test # 7A

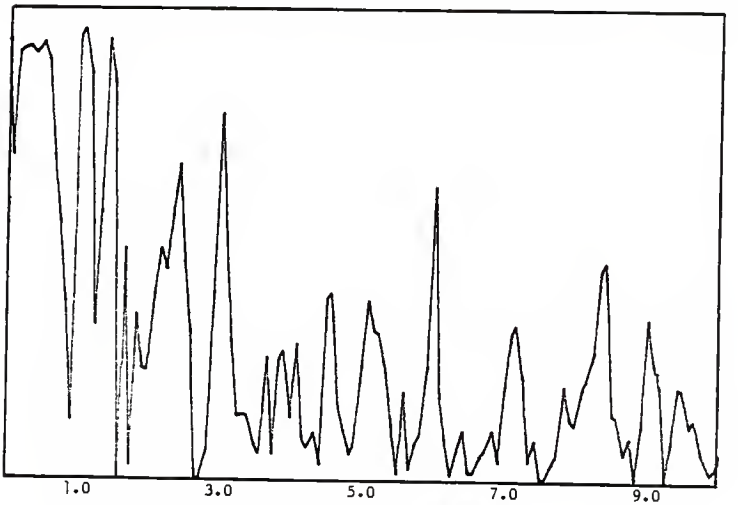

Coherence Function, 5-0-N & 2-0-N, Test # 7A

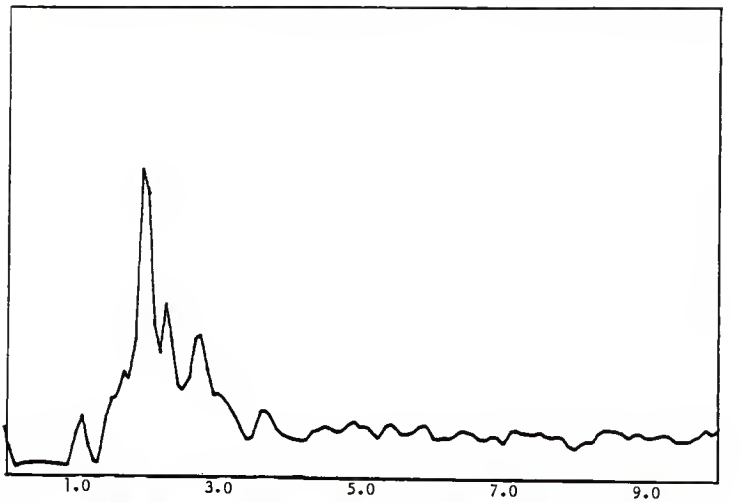

Response vs. Frequency, Channel A (5-O-N), 160 mv. F.S., Test # 7A

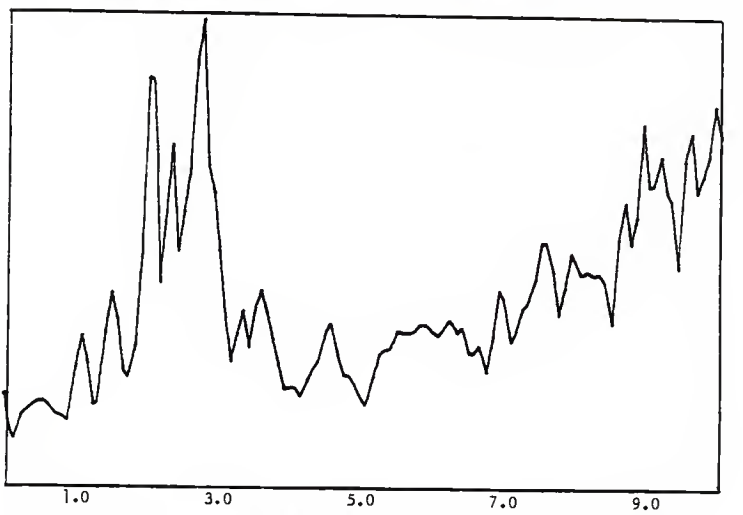

Response vs. Frequency, Channel B (1.5-O-N), 16 mv. F.S., Test # 7A

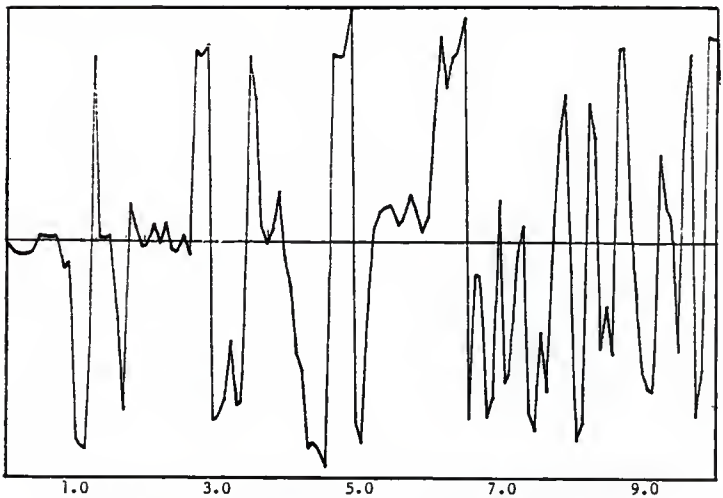

Transfer Function (Phase Angle), 5-0-N & 1.5-0-N, Test # 7A

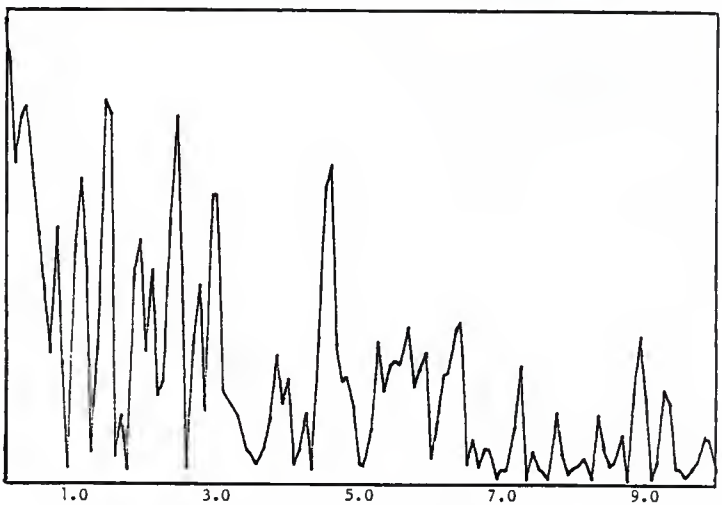

Coherence Function, 5-0-N & 1.5-0-N, Test # 7A

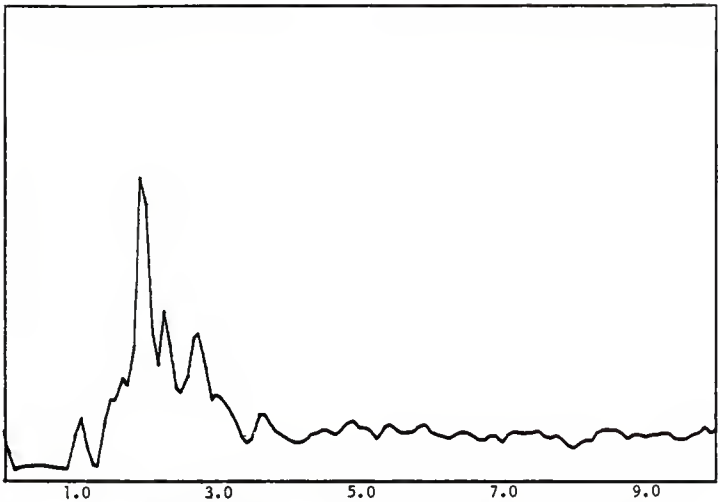

Response vs. Frequency, Channel A (5-0-N), 160 mv. F.S., Test # 7A

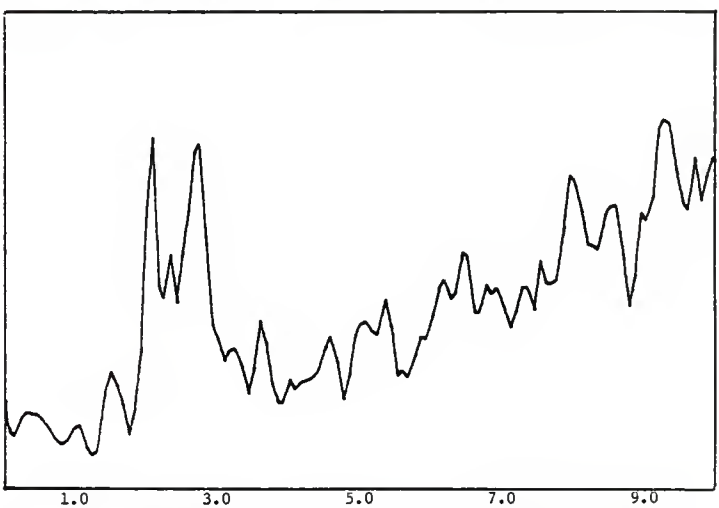

Response vs. Frequency, Channel B (1-0-N), 16 mv. F.S., Test # 7A

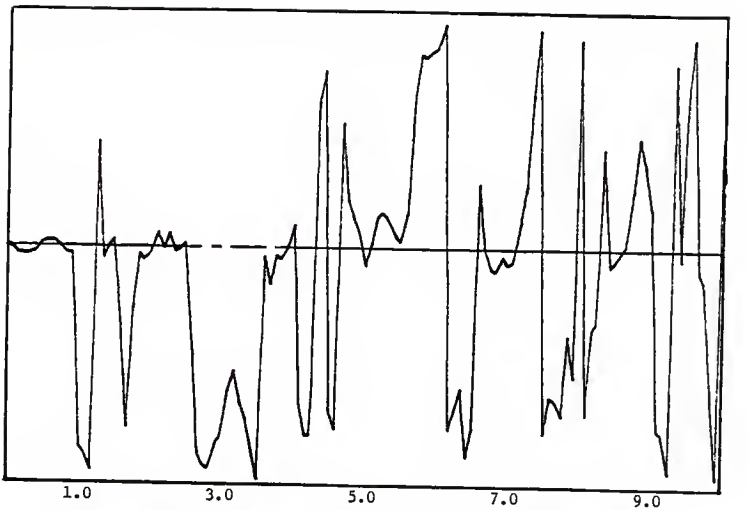

Transfer Function (Phase Angle), 5-0-N & 1-0-N, Test # 7A

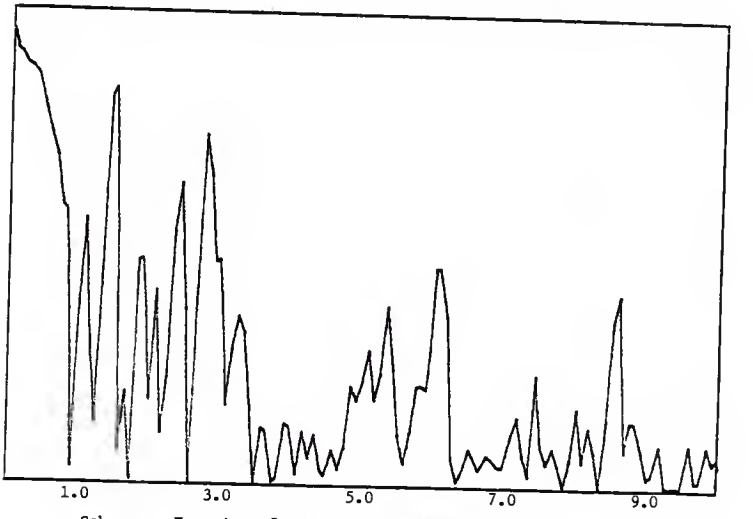

Coherence Function, 5-0-N & 1-0-N, Test # 7A

TAPE 2

TEST LOG

DATE 8/17

TIME 2:00

TEST NO. 8A

RECORDER START 000

RECORDER END 020

CHANNEL	1	2	3	4
COLOR	RED	GREEN	YELLOW	BLUE
HEIGHT	5	1	1	1
AZIMUTH	0	0	0	0
ORIENTATION	N	N	V	T
LOW PASS FILTER	20	20	20	20
ATTENUATOR SETTING	42	30	24	30
H-P FILTER I/O	V	✓	✓	✓
SENSITIVITY VOLTS				

ACSAT SIGNAL SEND BRUSH

NOTES:

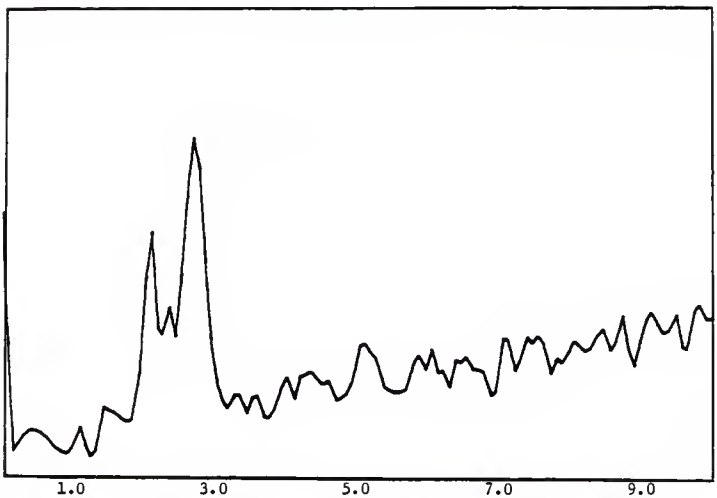

Response vs. Frequency, Channel A (1-0-N), 40 mv. F.S., Test # 8A

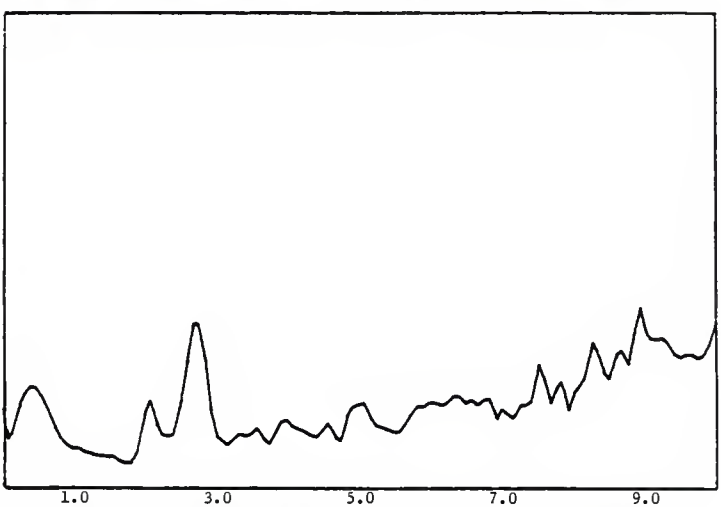

Response vs. Frequency, Channel B (1-0-V), 40 mv. F.S., Test # 8A

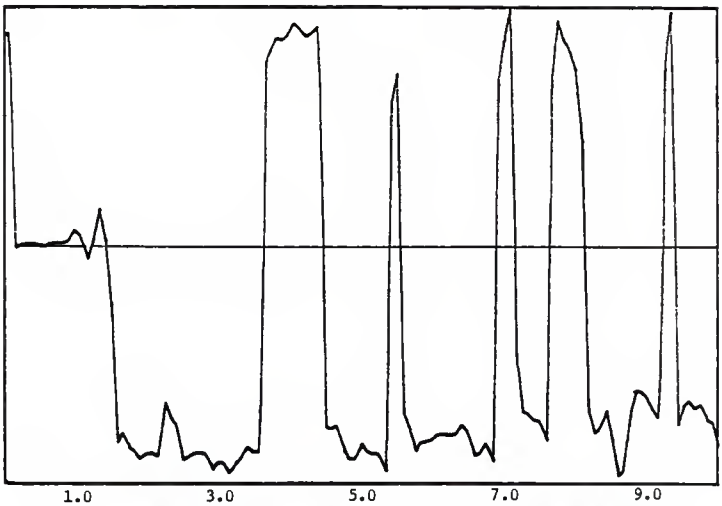

Transfer Function (Phase Angle), 1-0-N & 1-0-V, Test # 8A

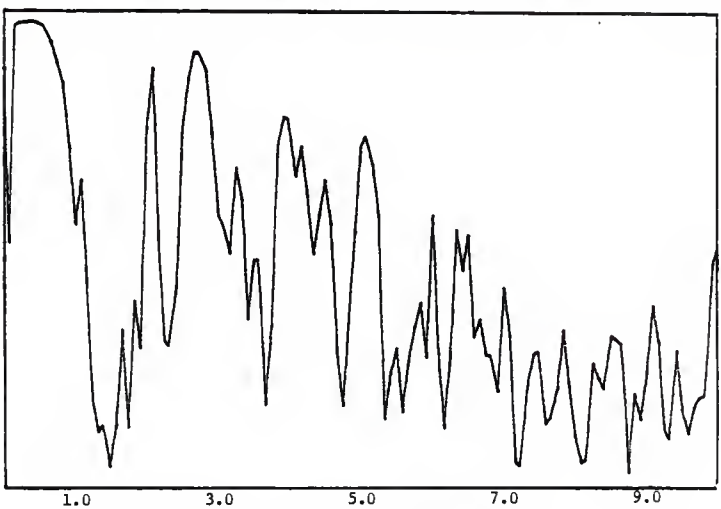

Coherence Function, 1-0-N & 1-0-V, Test # 8A

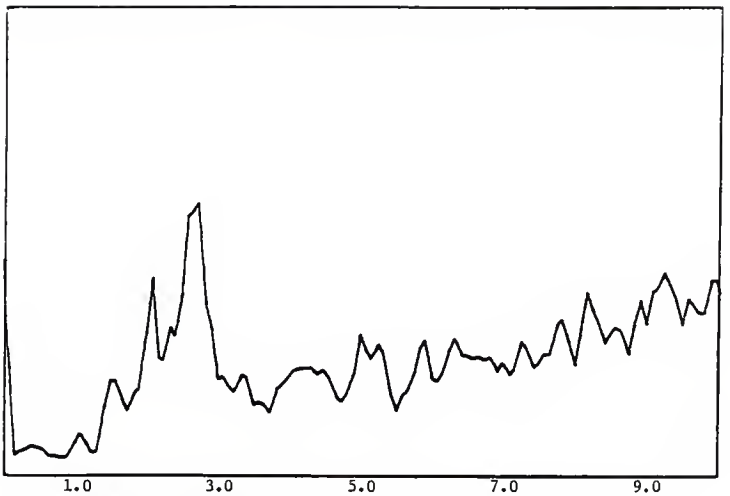

Response vs. Frequency, Channel A (1-0-N), 40 mv. F.S., Test # 8A

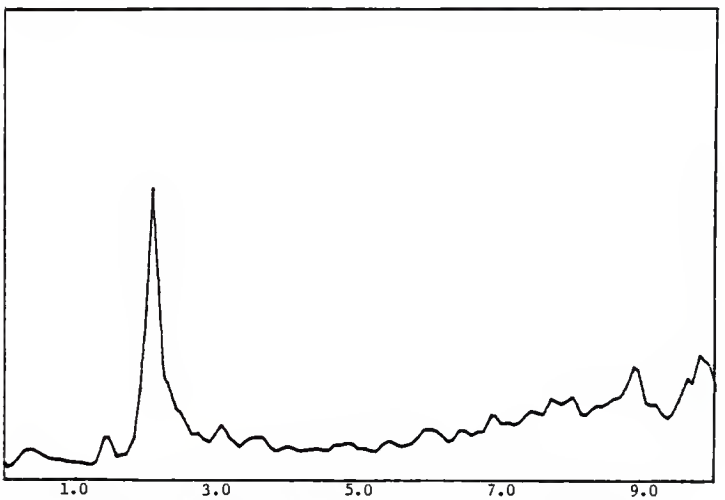

Response vs. Frequency, Channel B (1-0-T), 40 mv. F.S., Test # 8A

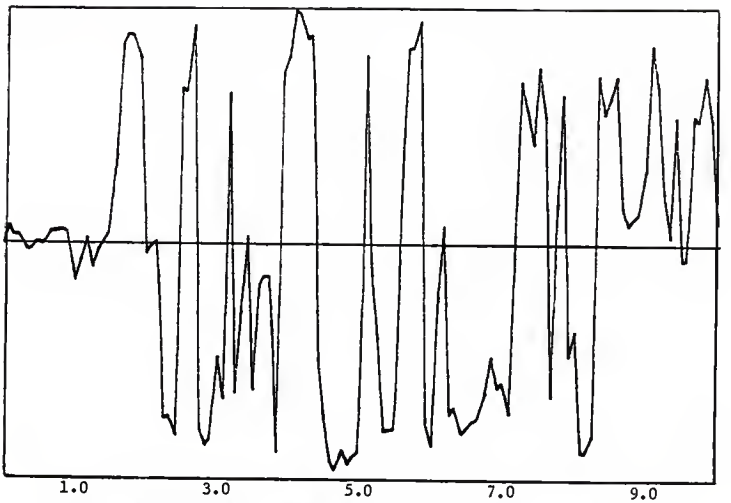

Transfer Function (Phase Angle), 1-0-N & 1-0-T, Test # 8A

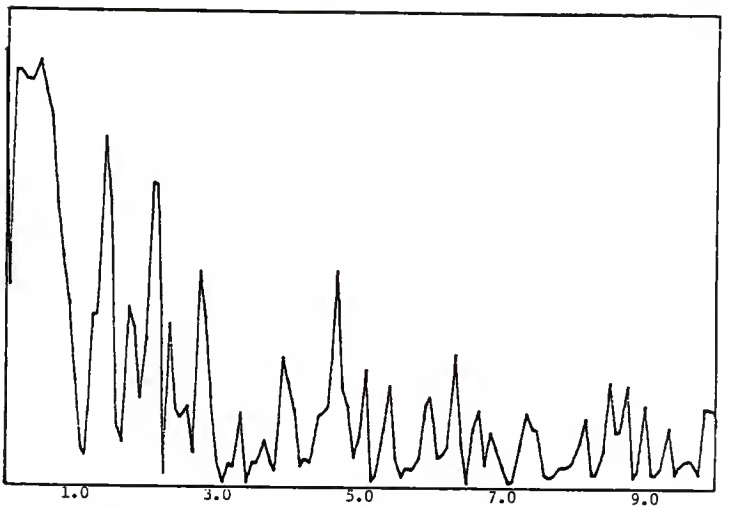

Coherence Function, 1-0-N & 1-0-T, Test # 8A

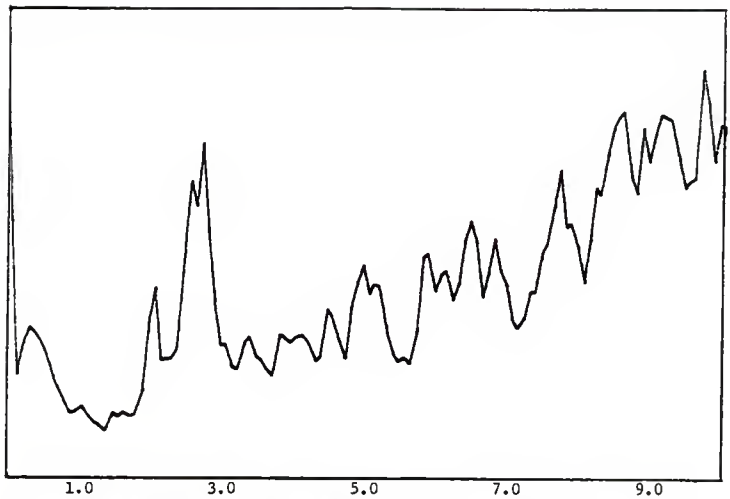

Response vs. Frequency, Channel A (1-0-V), 16 mv. F.S., Test # 8A

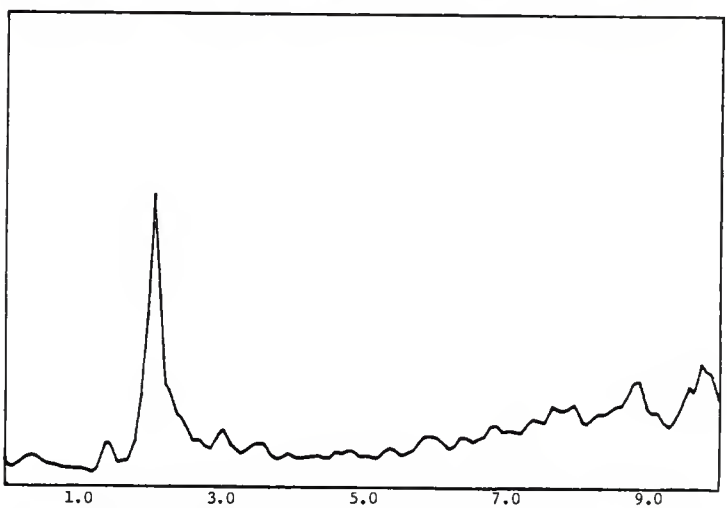

Response vs. Frequency, Channel B (1-0-T), 40 mv. F.S., Test # 8A

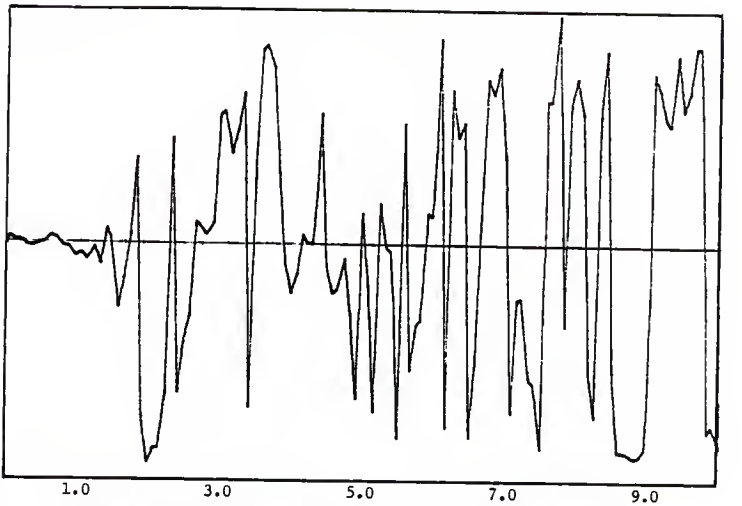

Transfer Function (Phase Angle), 1-0-V & 1-0-T, Test # 8A

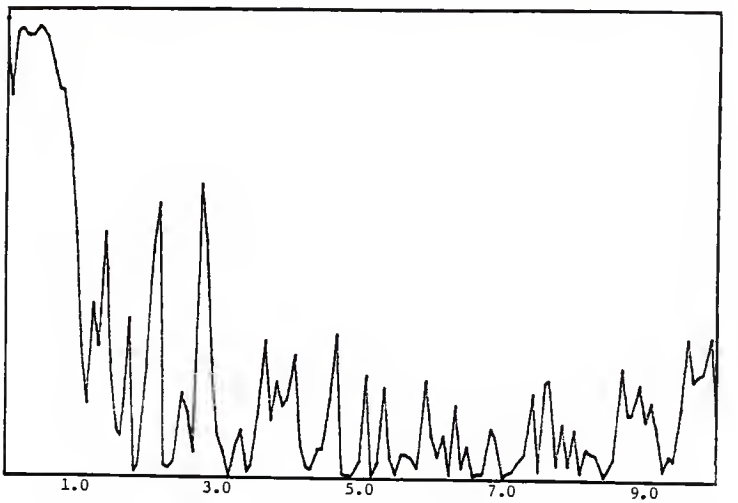

Coherence Function, 1-0-V & 1-0-T, Test # 8A

TEST LOG

DATE 9/17

TIME 3:15

TEST NO. 9A

RECORDER START 100

RECORDER END 120

ACCEL. SIGNAL COND DRWR

CHANNEL	1	2	3	4
COLOR	RED	GREEN	YELLOW	BLUE
HEIGHT	5	0	0	0
AZIMUTH	0	0	0	0
ORIENTATION	N	N	V	T
LOW PASS FILTER	20	20	20	20
ATTENUATOR SETTING	42	12	12	18
H-P FILTER I/O	✓	✓	✓	✓
SENSITIVITY VOLTS				

NOTES:

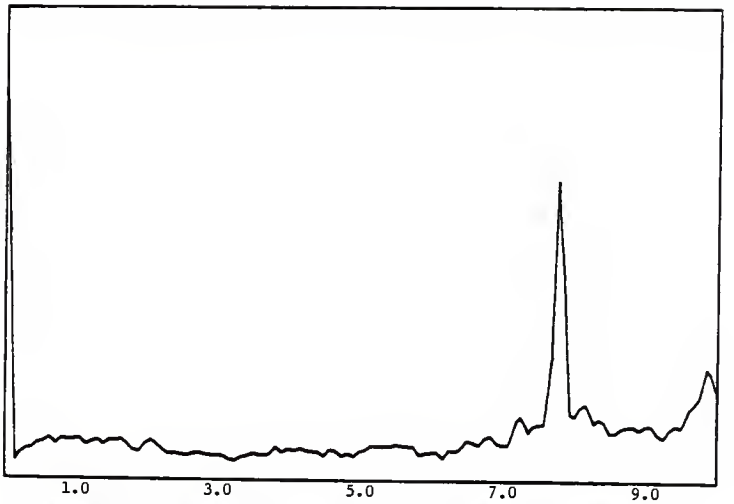

Response vs. Frequency, Channel A (0-0-N), 16 mv. F.S., Test # 9A

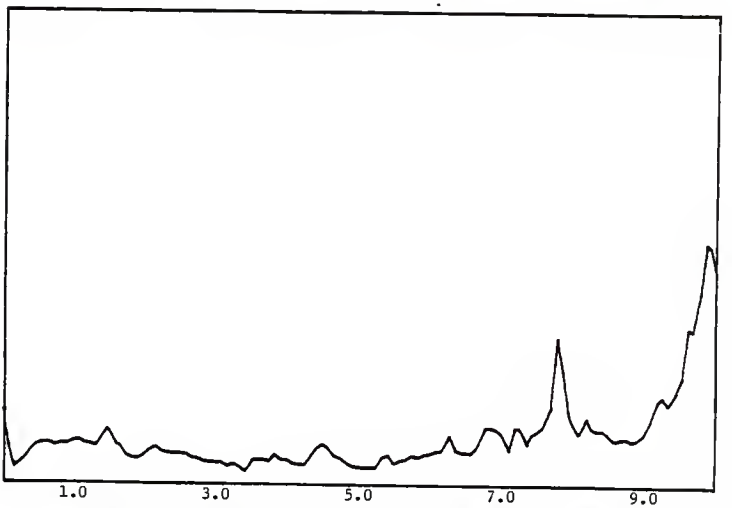

Response vs. Frequency, Channel B (0-0-V), 16 mv. F.S., Test # 9A

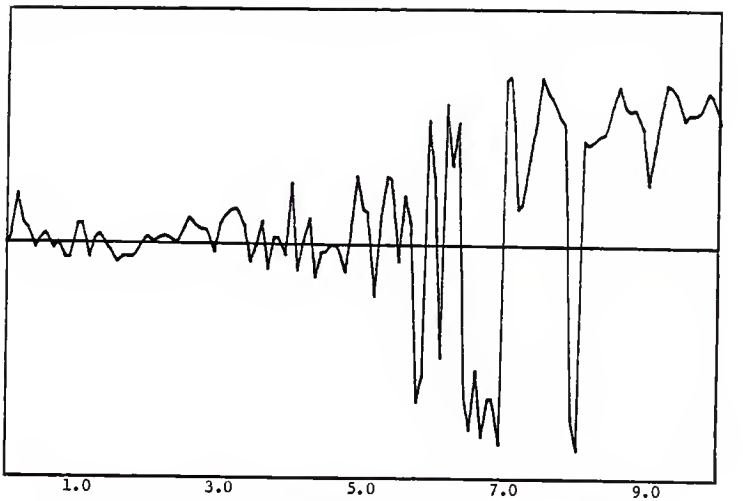

Transfer Function (Phase Angle), 0-0-N & 0-0-V, Test # 9A

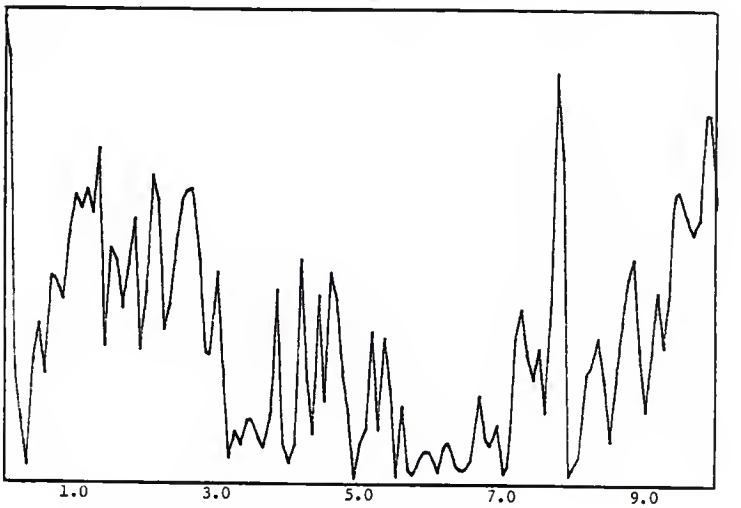

Coherence Function, 0-0-N & 0-0-V, Test # 9A

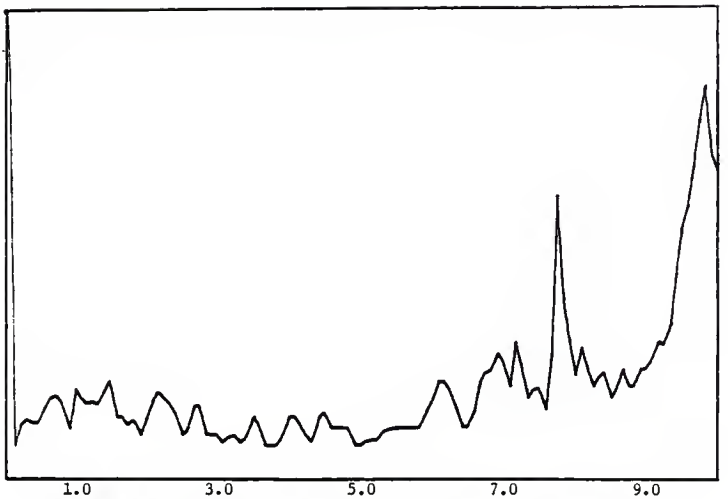

Response vs. Frequency, Channel A (0-0-V), 8 mv. F.S., Test # 9A

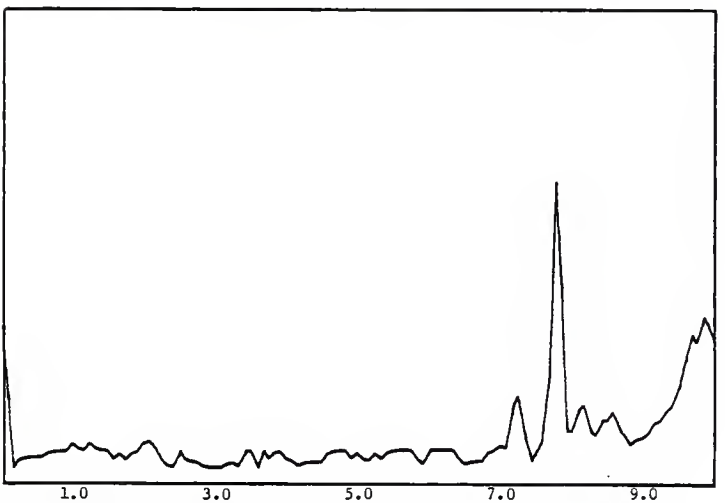

Response vs. Frequency, Channel B (0-0-T), 8 mv. F.S., Test # 9A

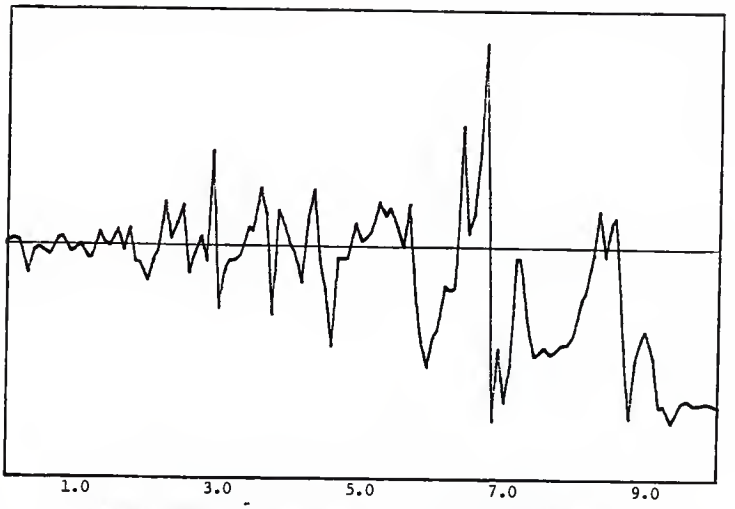

Transfer Function (Phase Angle), 0-0-V & 0-0-T, Test # 9A

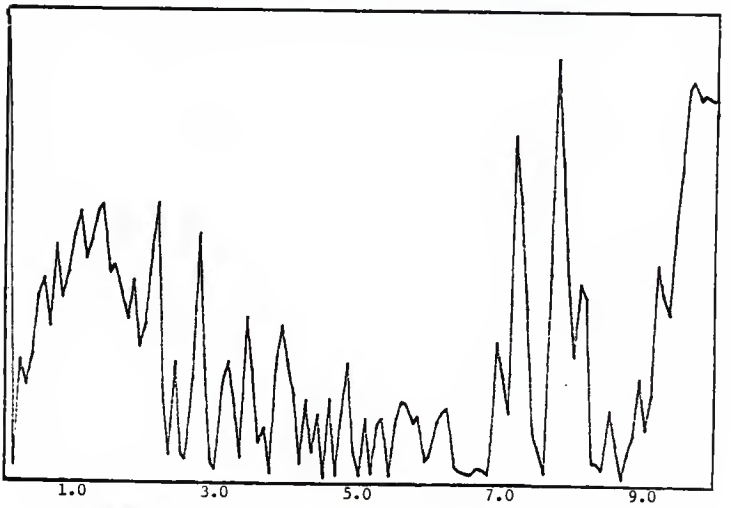

Coherence Function, 0-0-V & 0-0-T, Test # 9A

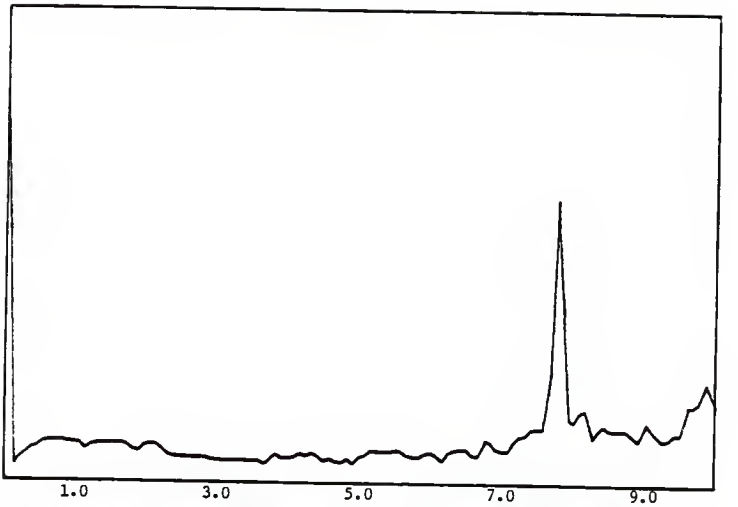

Response vs. Frequency, Channel A (0-0-N), 16 mv. F.S., Test # 9A

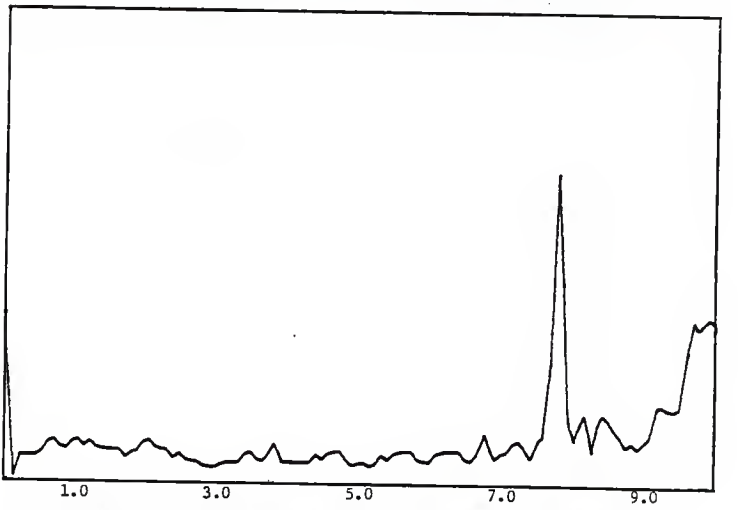

Response vs. Frequency, Channel B (0-0-T), 8 mv. F.S., Test # 9A

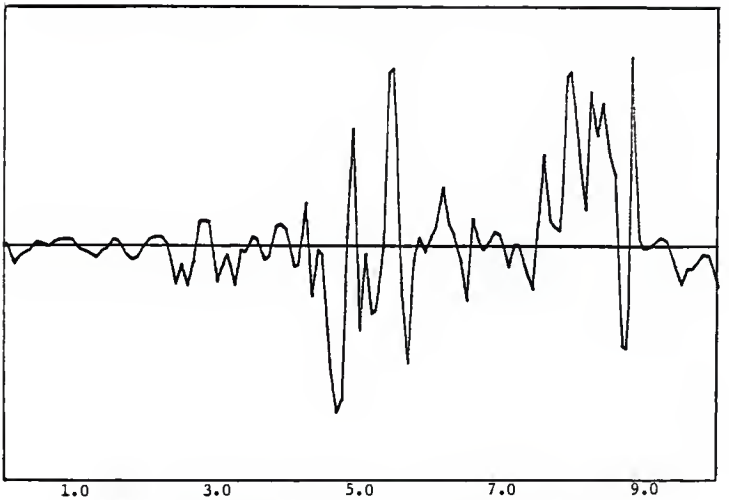

Transfer Function (Phase Angle), 0-0-N & 0-0-T, Test # 9A

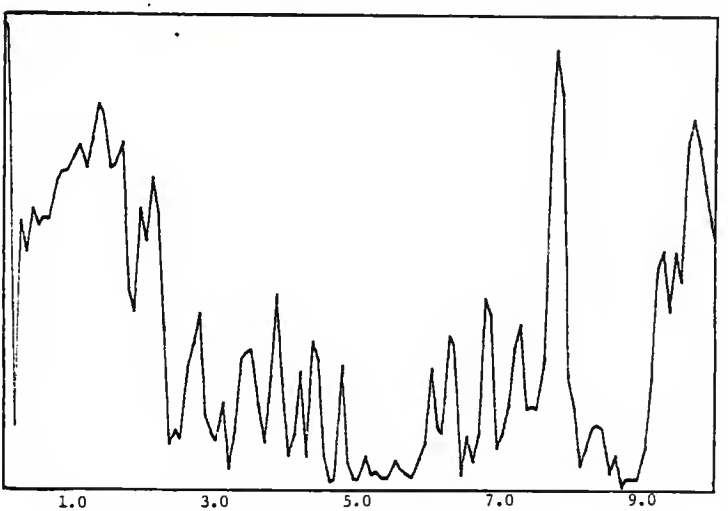

Coherence Function, 0-0-N & 0-0-T, Test # 9A

TEST LOG

DATE 8/19/85

TIME 10:05

TEST NO. 10 A

RECORDER START 200

RECORDER END 230

CHANNEL	1	2	3	4
COLOR	RED	GREEN	YELLOW	BLUE
HEIGHT	5	2	2	2
AZIMUTH	0	0	90	180
ORIENTATION	N	N	N	N
LOW PASS FILTER	20	20	20	20
ATTENUATOR SETTING	30	30	30	30
H-P FILTER I/O	✓	✓	✓	✓
SENSITIVITY VOLTS				

ACCEL. SIGNAL GRND BRUSH

NOTES: Recorder input atten at 30 dB

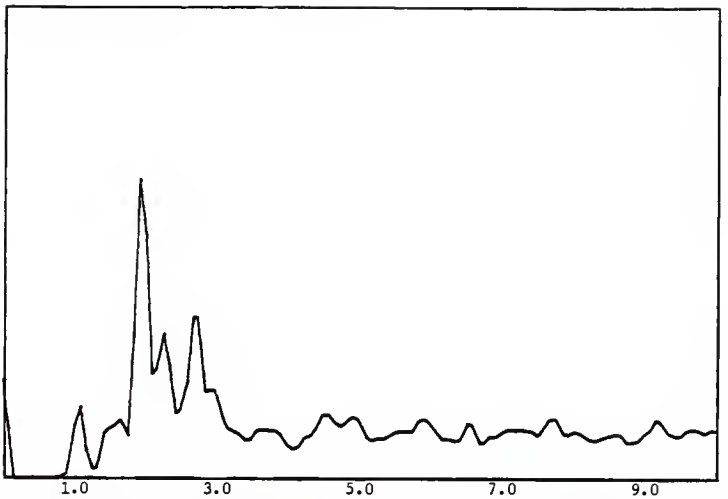

Response vs. Frequency, Channel A (5-O-N), 80 mv. F.S., Test # 10A

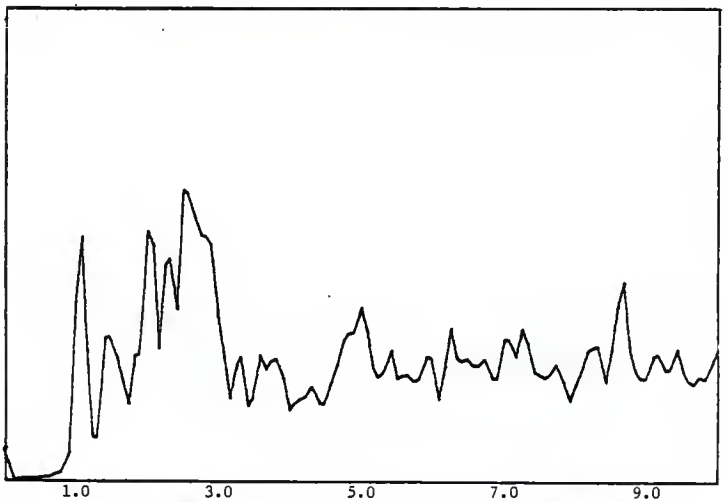

Response vs. Frequency, Channel B (2-O-N), 40 mv. F.S., Test # 10A

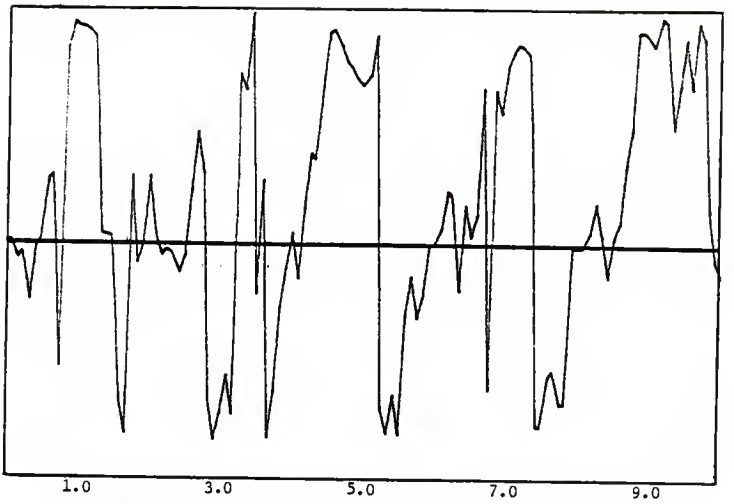

Transfer Function (Phase Angle), 5-0-N & 2-0-N, Test # 10A

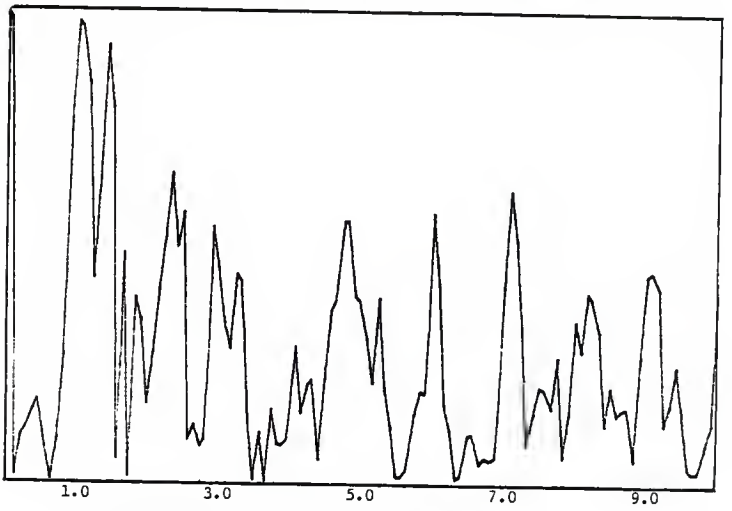

Coherence Function, 5-0-N & 2-0-N, Test # 10A

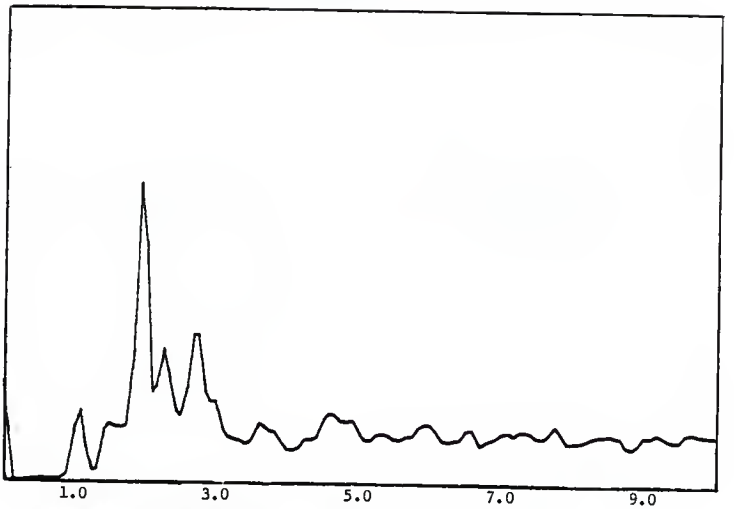

Response vs. Frequency, Channel A (5-0-N), 80 mv. F.S., Test # 10A

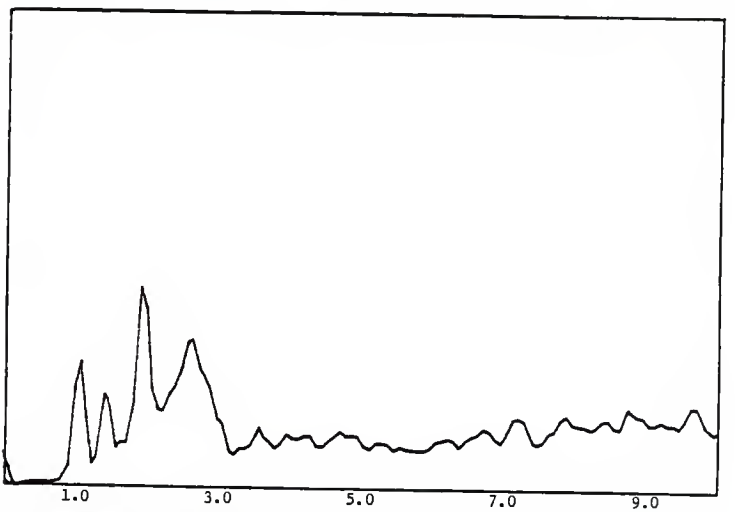

Response vs. Frequency, Channel B (2-90-N), 40 mv. F.S., Test # 10A

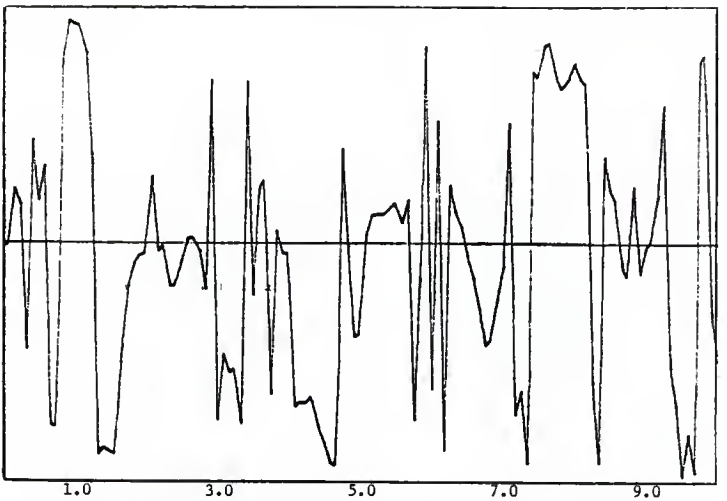

Transfer Function (Phase Angle), 5-0-N & 2-90-N, Test # 10A

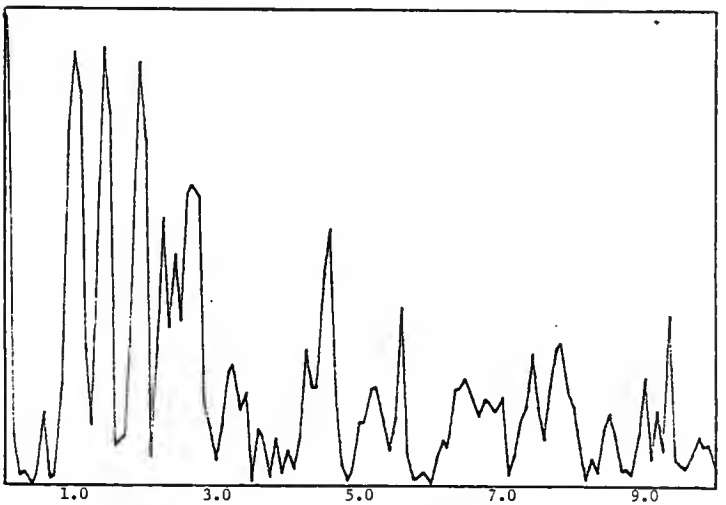

Coherence Function, 5-0-N & 2-90-N, Test # 10A

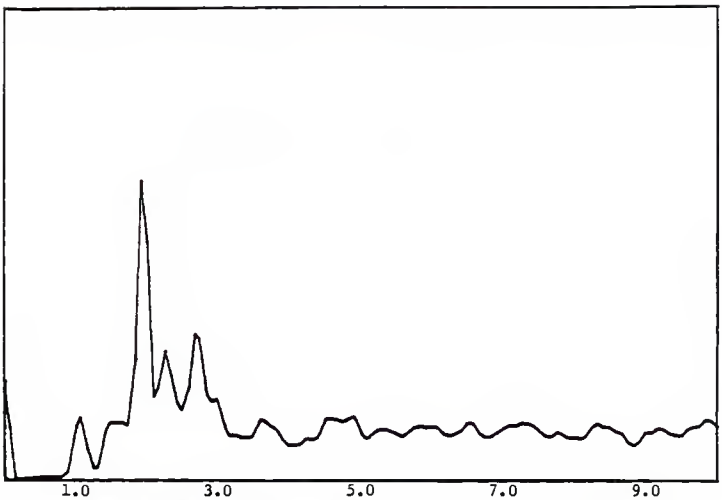

Response vs. Frequency, Channel A (5-0-N), 80 mv. F.S., Test # 10A

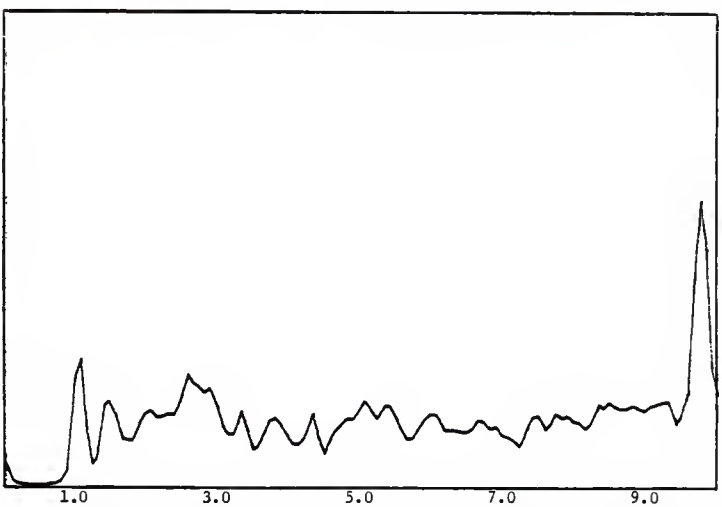

Response vs. Frequency, Channel B (2-180-N), 40 mv. F.S., Test # 10A

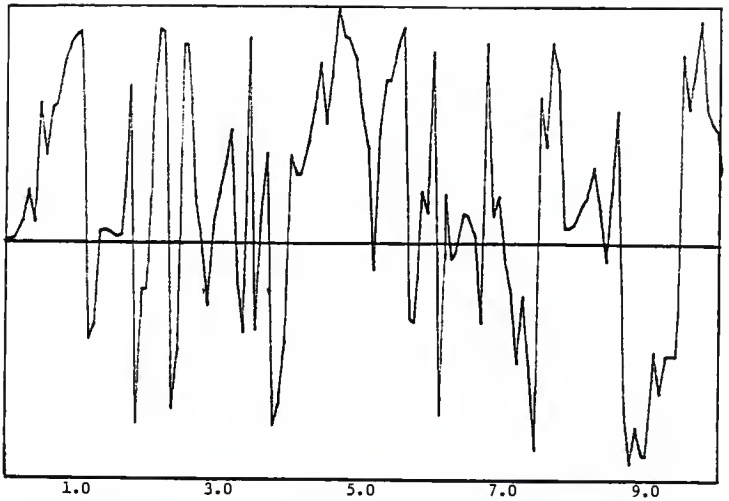

Transfer Function (Phase Angle), 5-0-N & 2-180-N, Test # 10A

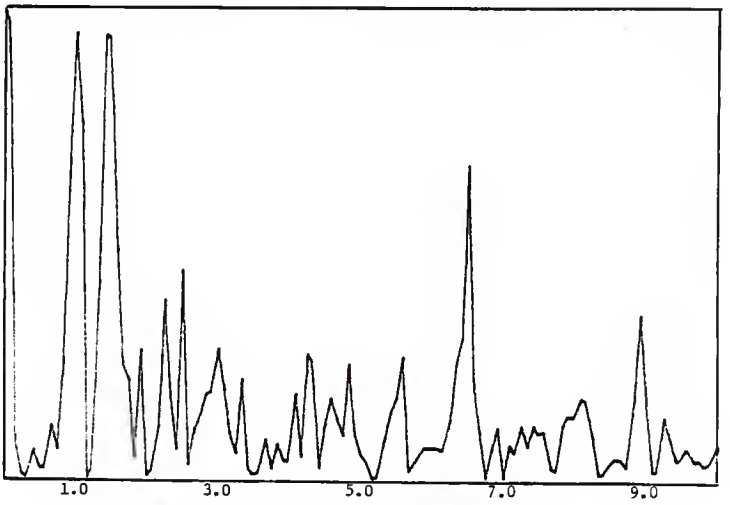

Coherence Function, 5-0-N & 2-180-N, Test # 10A

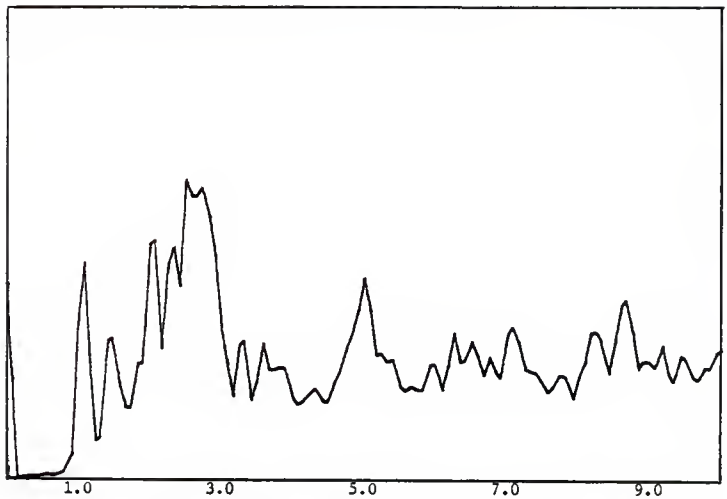

Response vs. Frequency, Channel A (2-0-N), 40 mv. F.S., Test # 10A

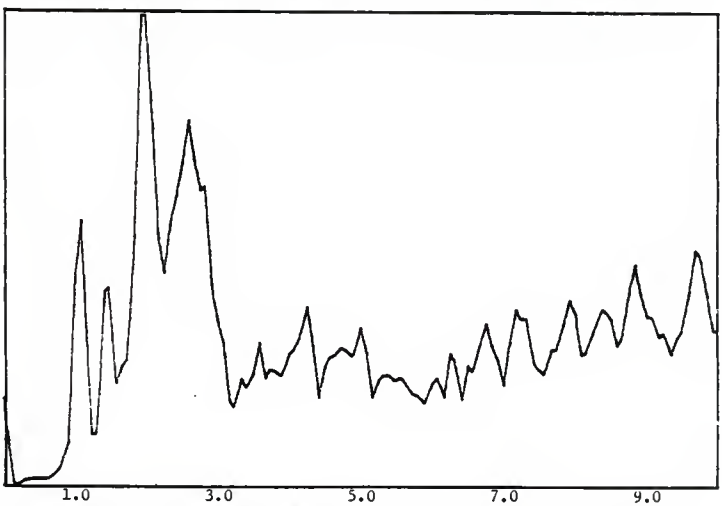

Response vs. Frequency, Channel B (2-90-N), 16 mv. F.S., Test # 10A

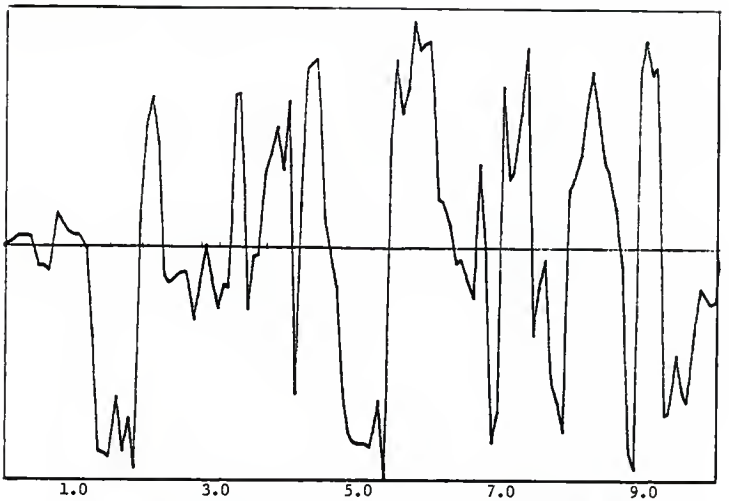

Transfer Function (Phase Angle), 2-0-N & 2-90-N, Test # 10A

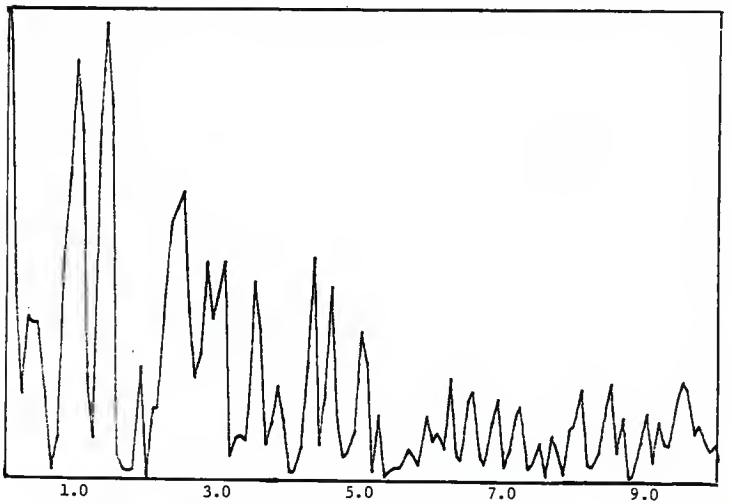

Coherence Function, 2-0-N & 2-90-N, Test # 10A

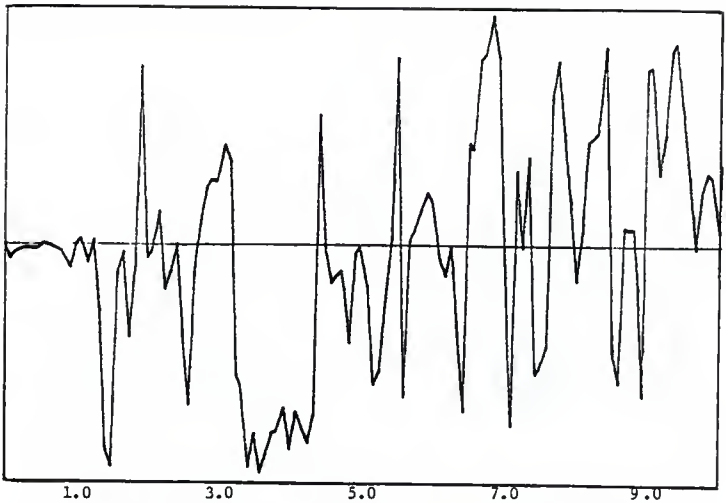

Transfer Function (Phase Angle), 5-0-N & 2-90-T, Test # 11A

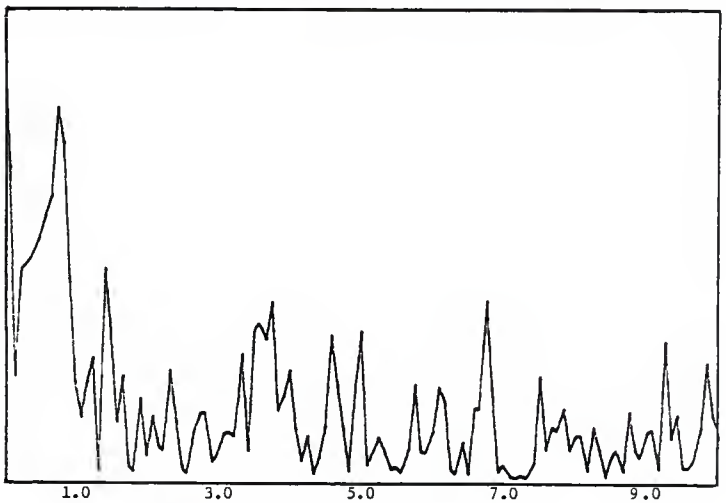

Coherence Function, 5-0-N & 2-90-T, Test # 11A

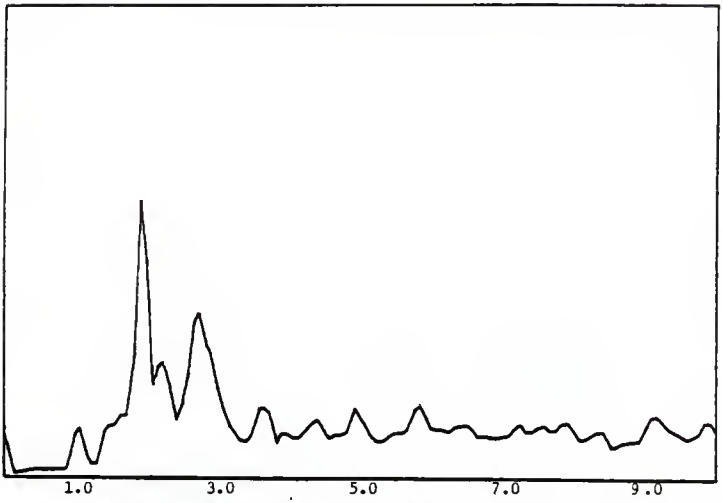

Response vs. Frequency, Channel A (5-0-N), 160 mv. F.S., Test # 11A

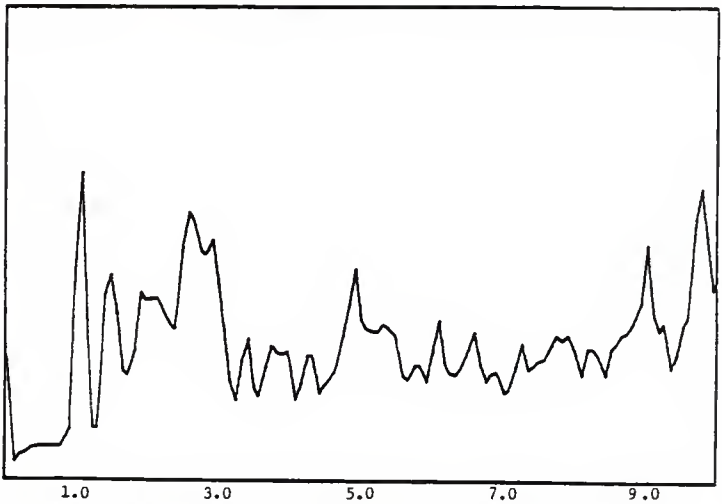

Response vs, Frequency, Channel B (2-180-N), 8 mv. F.S., Test # 11A

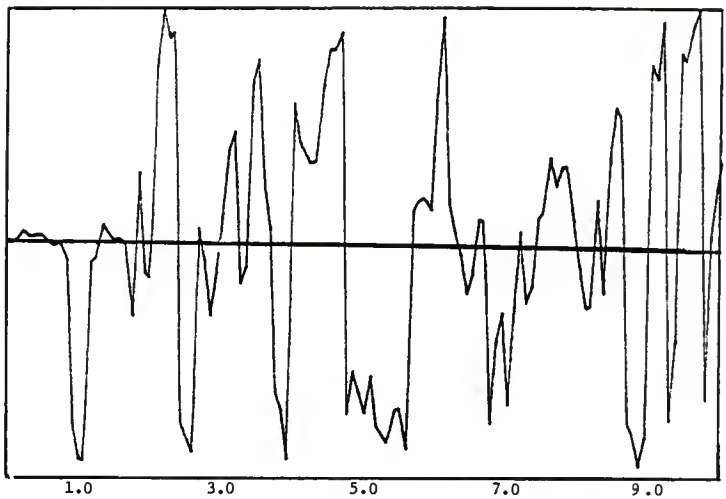

Transfer Function (Phase Angle), 5-0-N & 2-180-N, Test # 11A

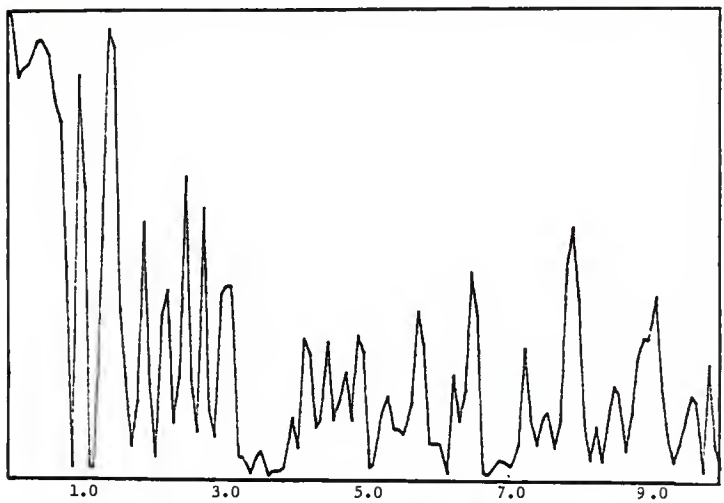

Coherence Function, 5-0-N & 2-180-N, Test # 11A

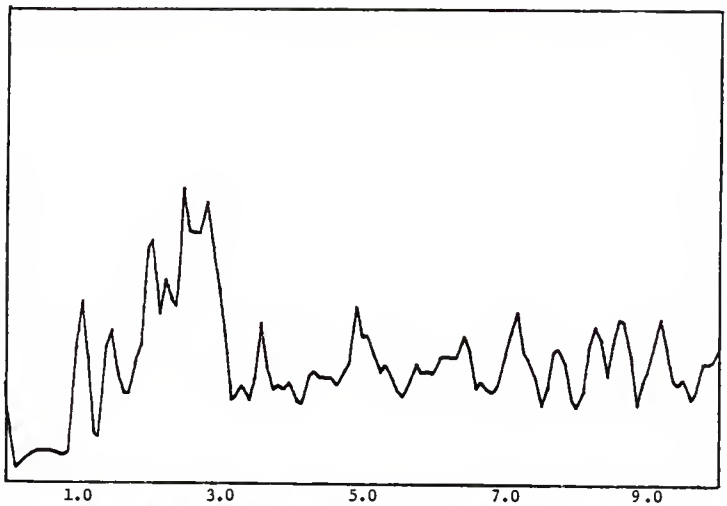

Response vs. Frequency, Channel A (2-0-N), 80 mv. F.S., Test # 11A

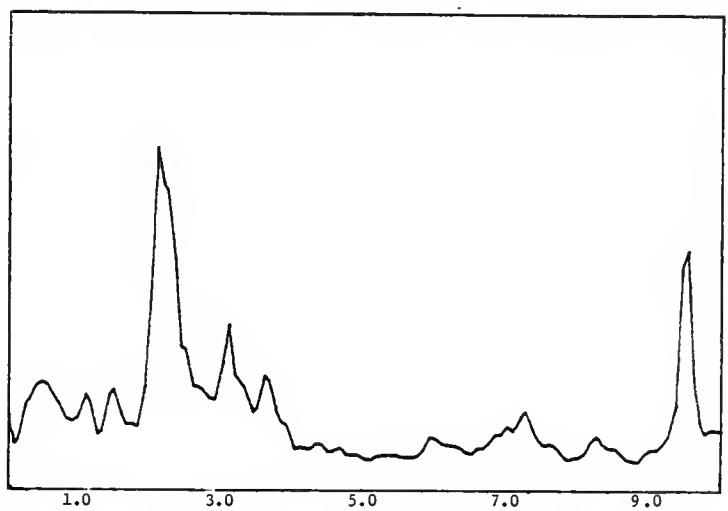

Response vs. Frequency, Channel B (2-90-T), 16 mv. F.S., Test # 11A

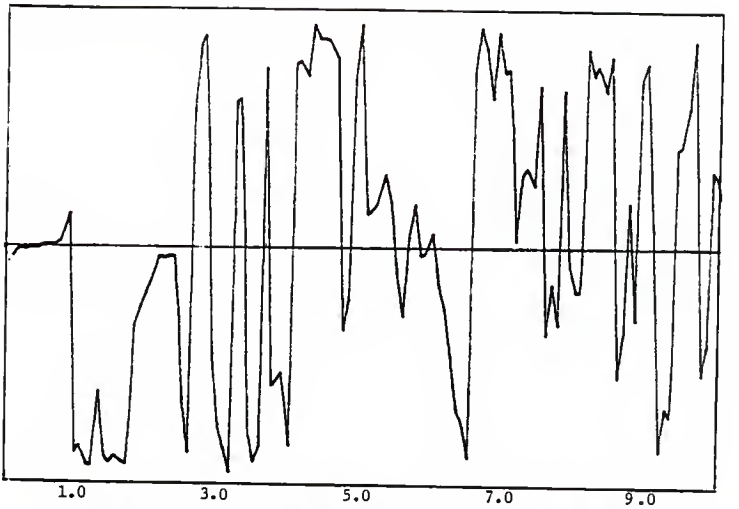

Transfer Function (Phase Angle), 2-0-N & 2-90-T, Test # 11A

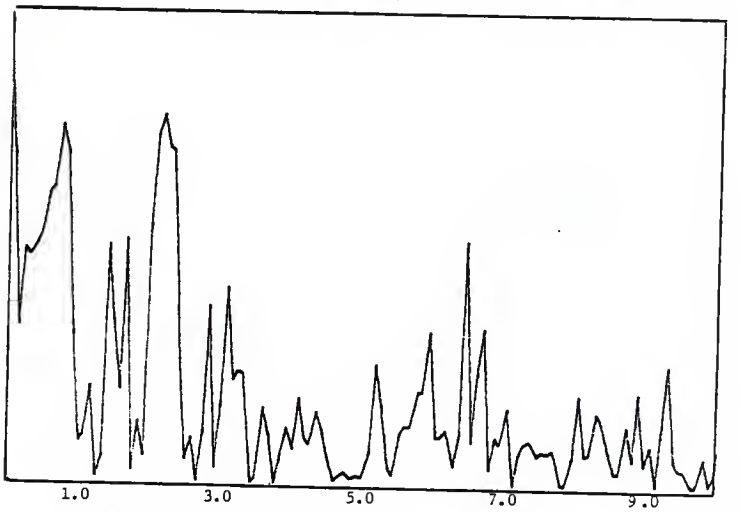

Coherence Function, 2-0-N & 2-90-T, Test # 11A

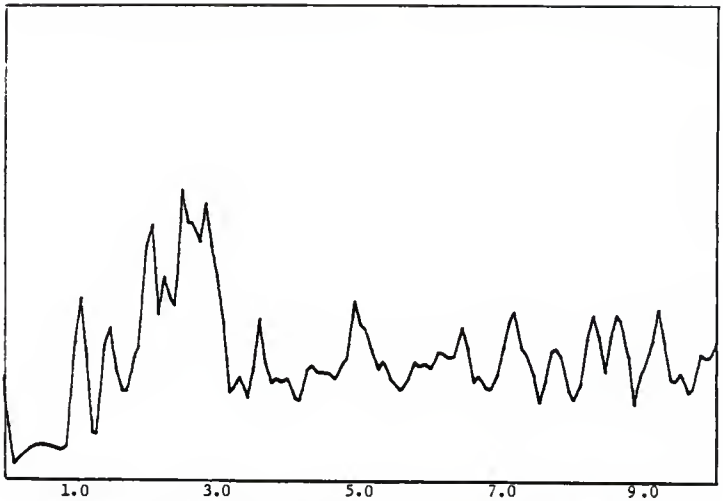

Response vs. Frequency, Channel A (2-0-N), 80 mv. F.S., Test # 11A

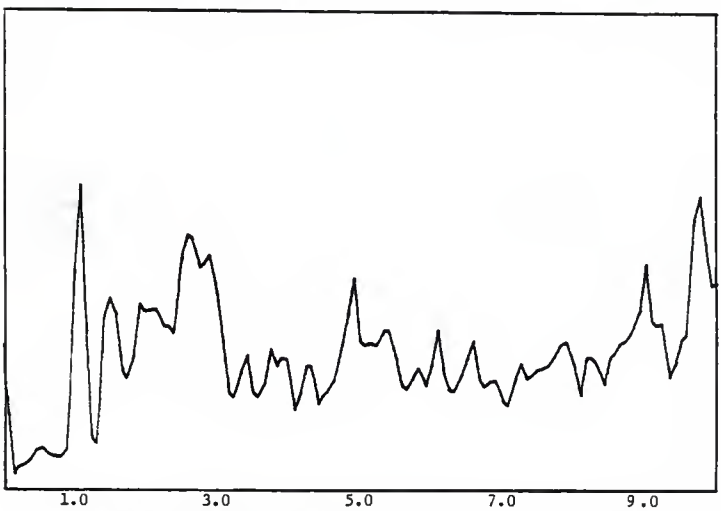

Response vs. Frequency, Chsnnel B (2-180-N), 8 mv. F.S., Test # 11A

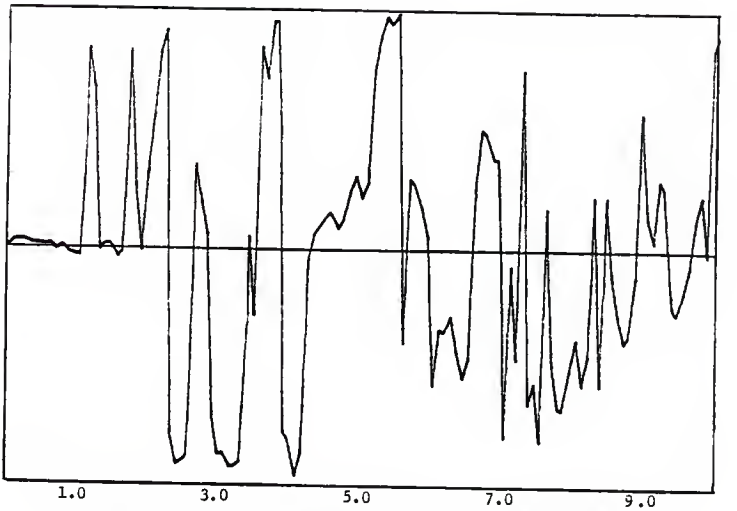

Transfer Function (Phase Angle), 2-0-N & 2-180-N, Test # 11A

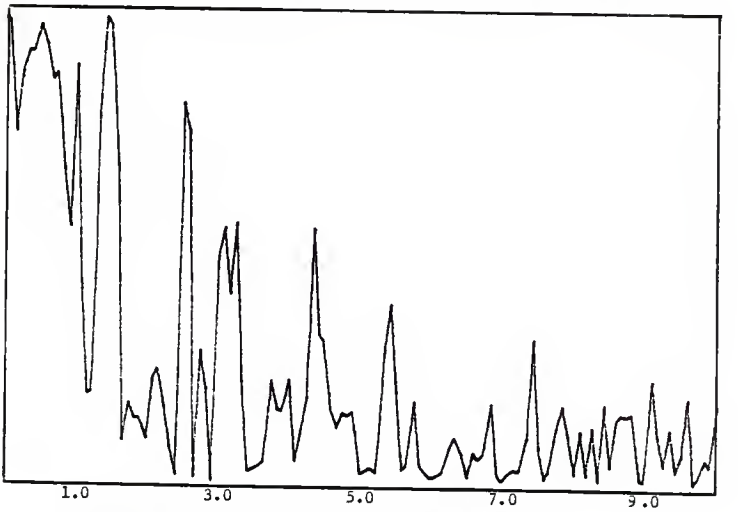

Coherence Function, 2-0-N & 2-180-N, Test # 11A

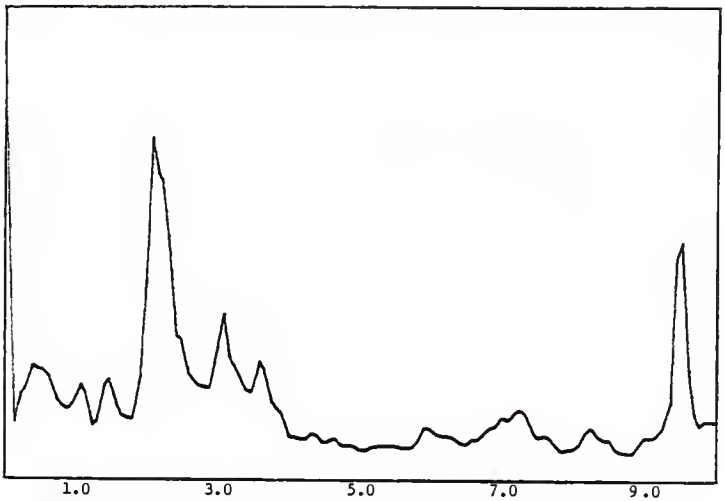

Response vs. Frequency, Channel A (2-90-T), 16 mv. F.S., Test # 11A

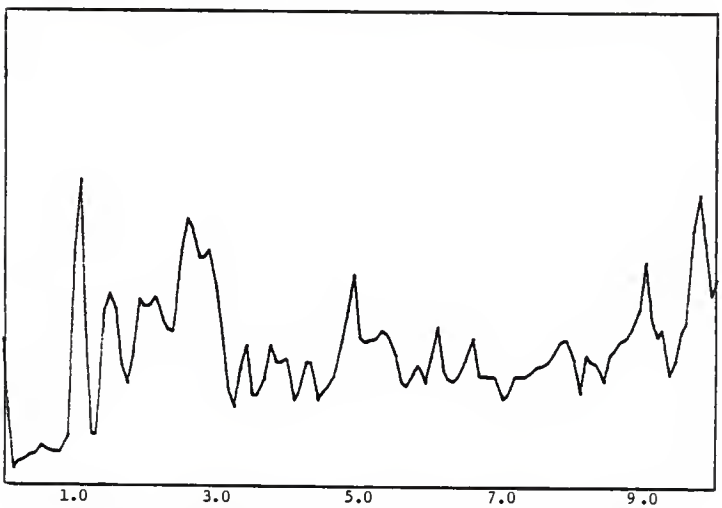

Response vs. Frequency, Channel B (2-180-N), 8 mv. F.S., Test # 11A

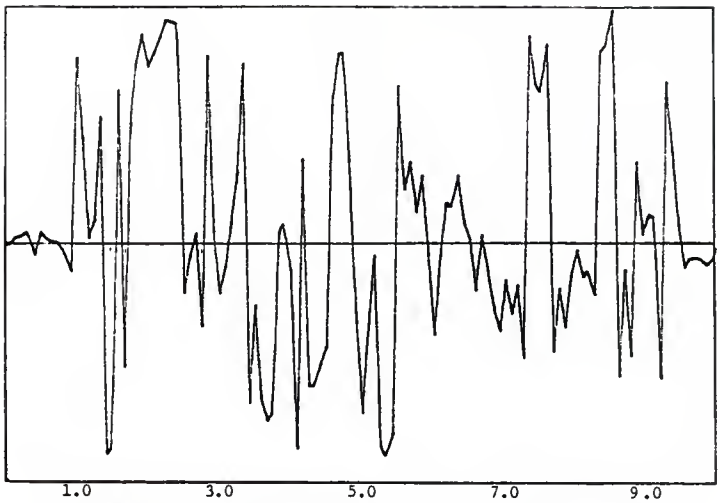

Transfer Function (Phase Angle), 2-90-T & 2-180-N, Test # 11A

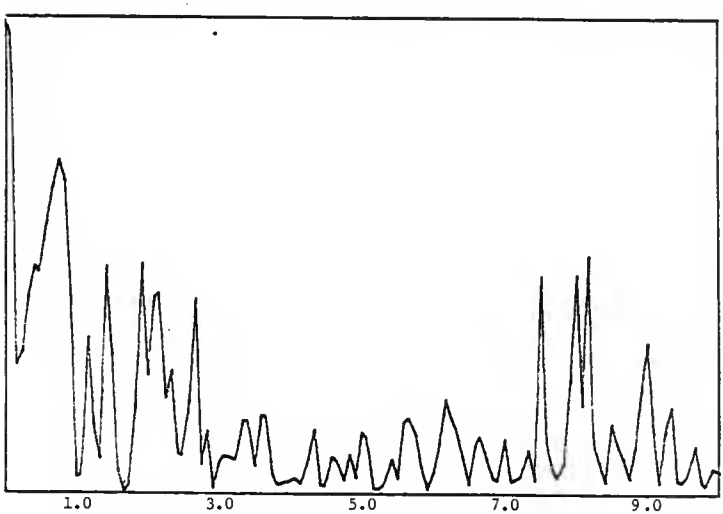

Coherence Function, 2-90-T & 2-180-N, Test # 11A

TEST LOG

DATE 8/19

TIME 12:15

TEST NO. 12A

RECORDER START 460

RECORDER END 480

CHANNEL	1	2	3	4
COLOR	RED	GREEN	YELLOW	BLUE
HEIGHT	5	2	2	2
AZIMUTH	0	0	90	180
ORIENTATION	N	V	V	V
LOW PASS FILTER	20	20	20	20
ATTENUATOR SETTING	30	24	30	30
H-P FILTER I/O				
SENSITIVITY VOLTS				

ACCEL. SIGNAL GRND BRIDGE

NOTES:

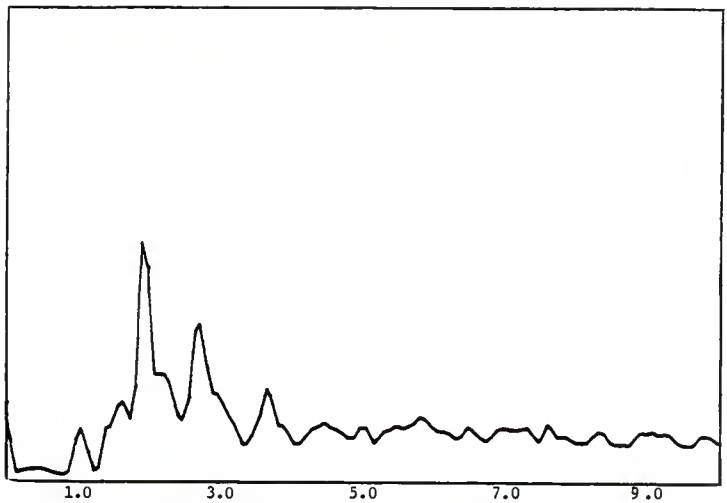

Response vs. Frequency, Channel A (5-0-N), 160 mv. F.S., Test # 12A

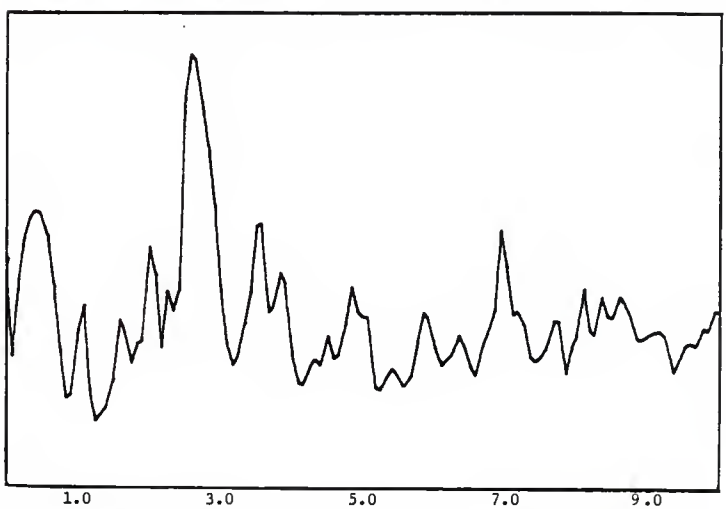

Response vs. Frequency, Channel B (2-0-V), 16 mv. F.S., Test # 12A

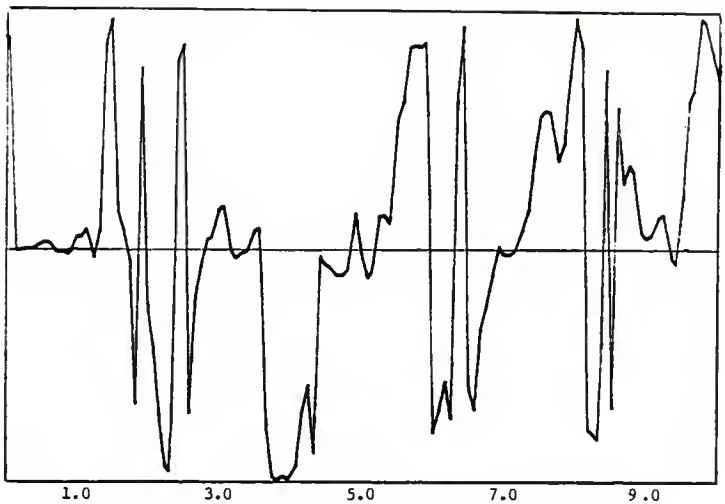

Transfer Function (Phase Angle), 5-0-N & 2-0-V, Test # 12A

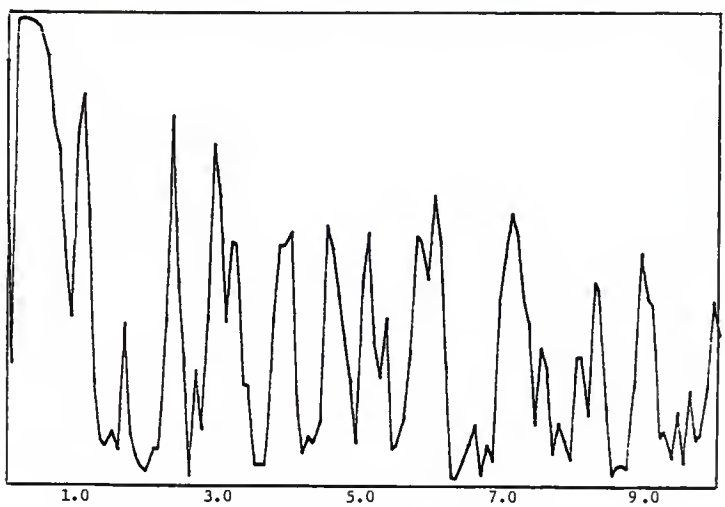

Coherence Function, 5-0-N & 2-0-V, Test # 12A

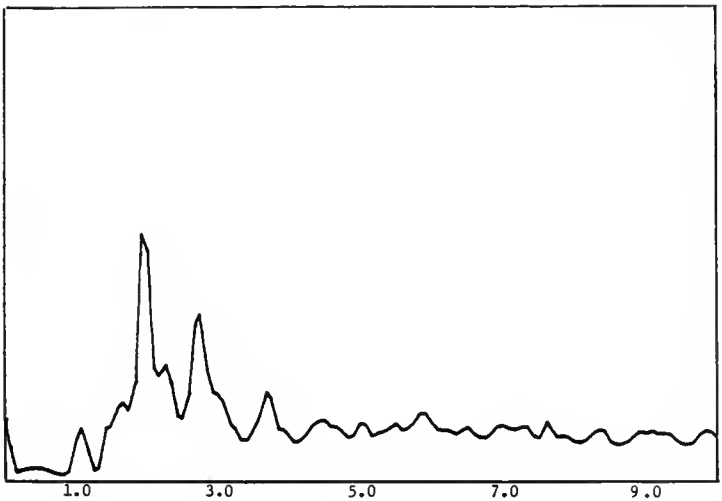

Response vs. Frequency, Channel A (5-0-N), 160 mv. F.S., Test # 12A

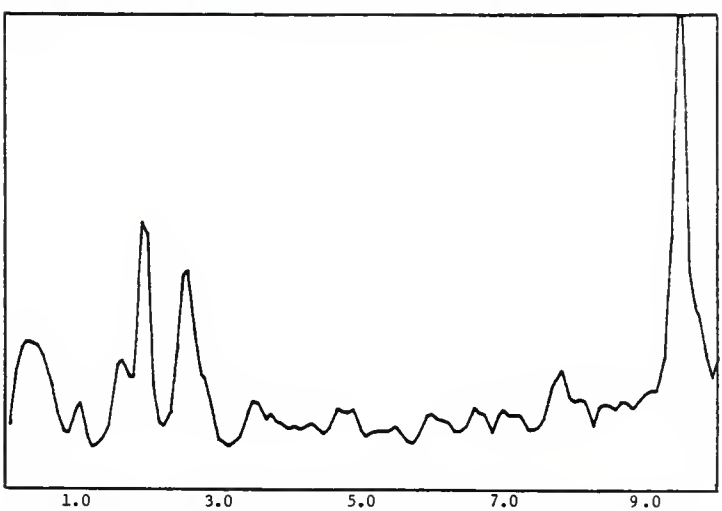

Response vs. Frequency, Channel B (2-90-V), 16 mv. F.S., Test # 12A

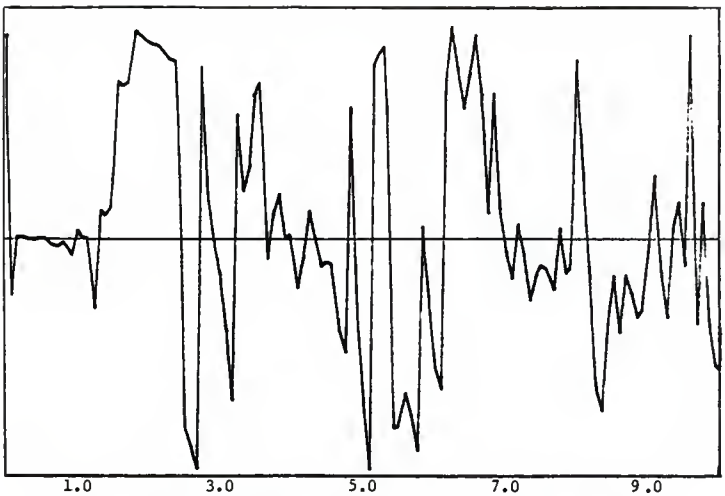

Transfer Function (Phase Angle), 5-0-N & 2-90-V, Test # 12A

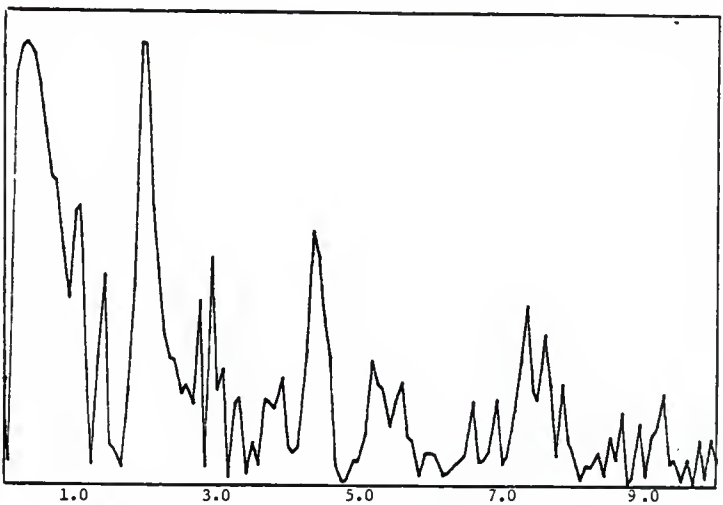

Coherence Function, 5-0-N & 2-90-V, Test # 12A

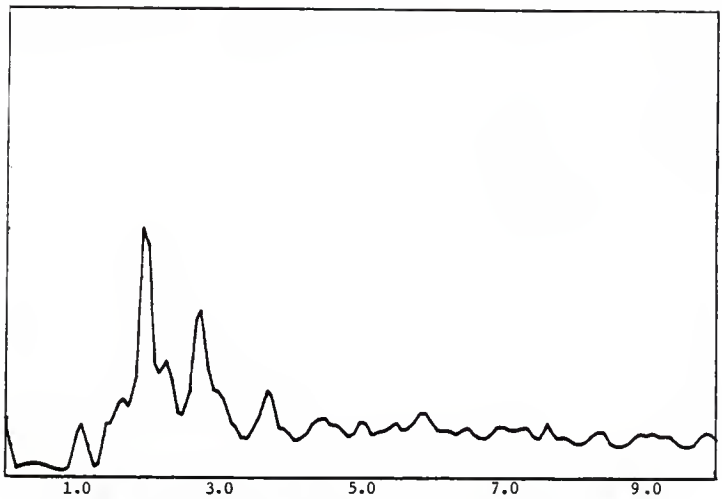

Response vs. Frequency, Channel A (5-0-N), 160 mv. F.S., Test # 12A

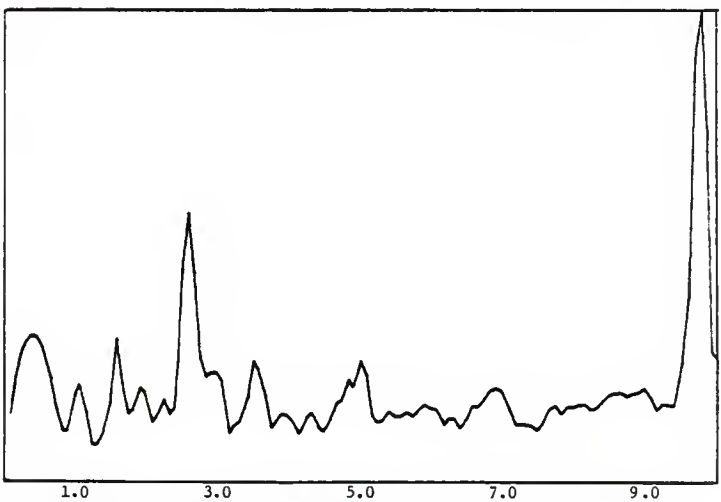

Response vs. Frequency, Channel B (2-180-V), 16 mv. F.S., Test # 12A

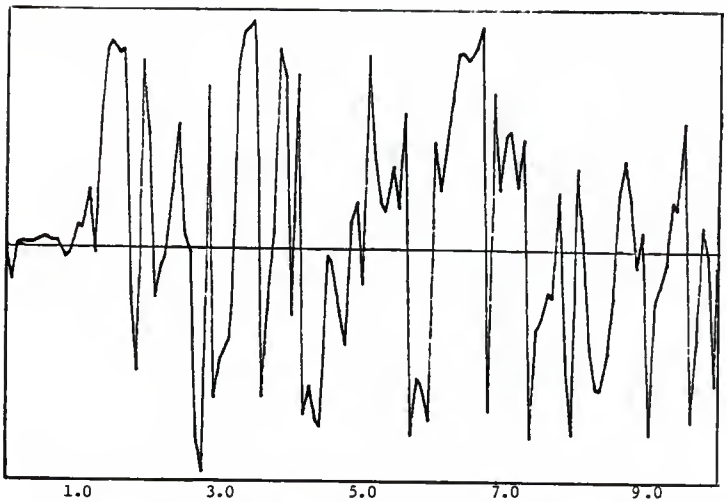

Transfer Function (Phase Angle), 5-0-N & 2-180-V, Test # 12A

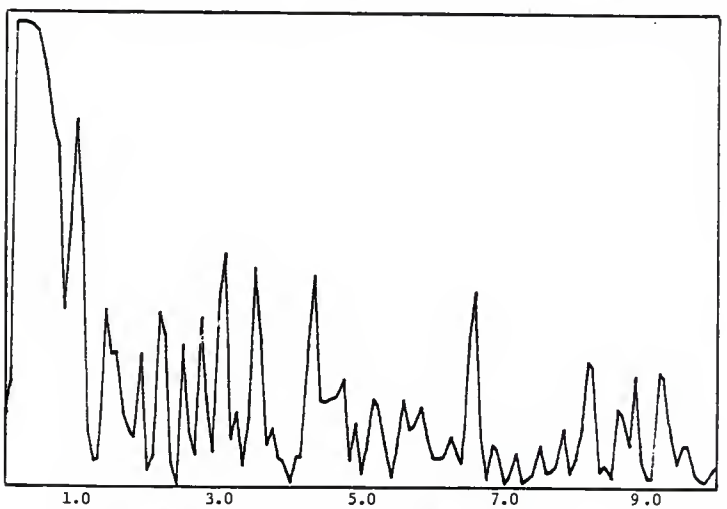

Coherence Function, 5-0-N & 2-180-V, Test # 12A

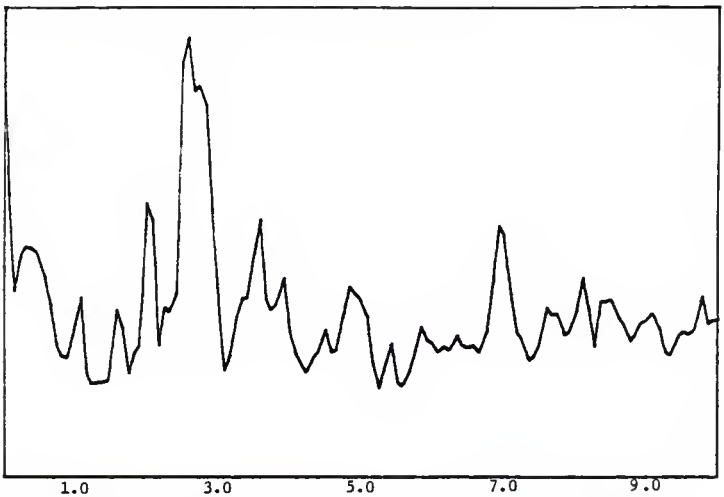

Response vs. Frequency, Channel A (2-0-V), 16 mv. F.S., Test # 12A

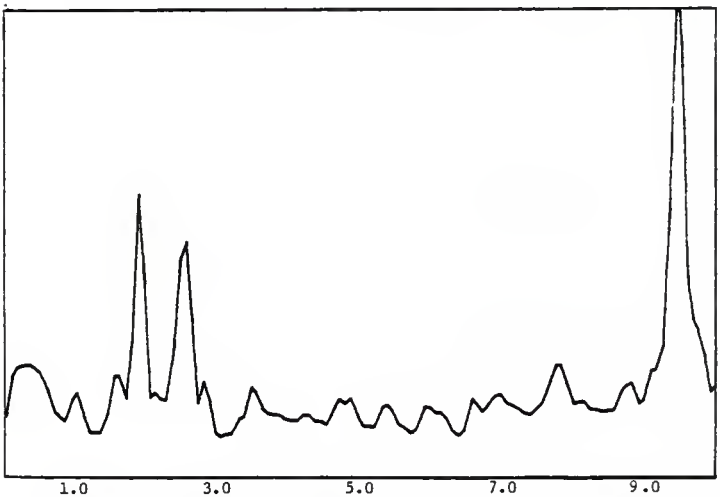

Response vs. Frequency, Channel B (2-90-V), 16 mv. F.S., Test # 12A

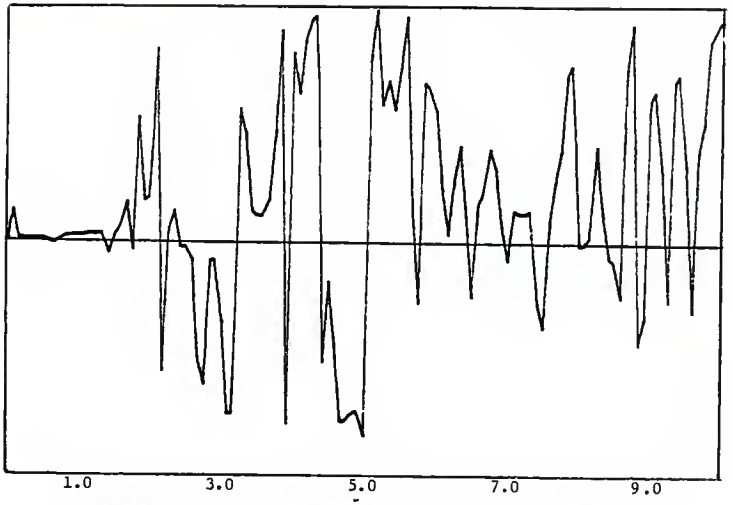

Transfer Function (Phase Angle), 2-0-V & 2-90-V, Test # 12A

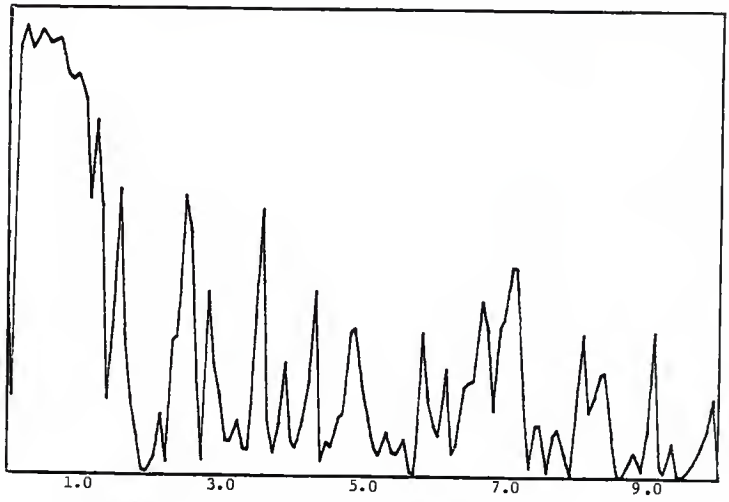

Coherence Function, 2-0-V & 2-90-V, Test # 12A

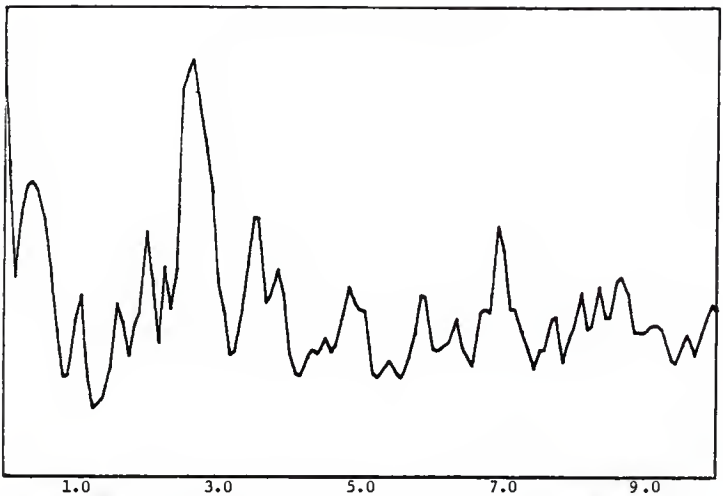

Response vs. Frequency, Channel A (2-0-V), 16 mv. F.S., Test # 12A

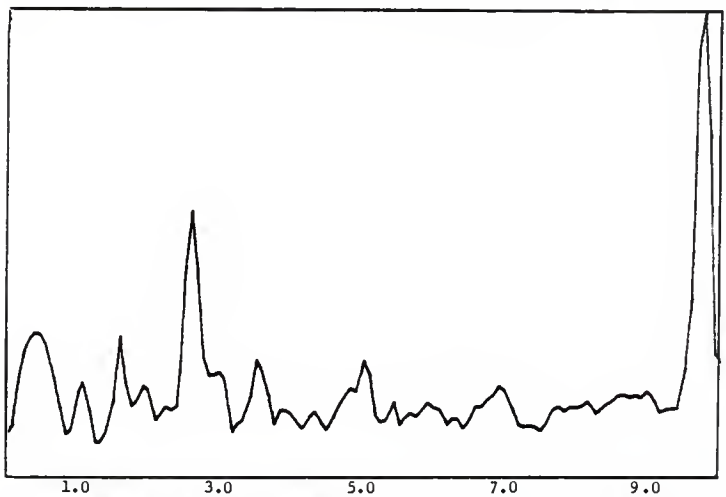

Response vs. Frequency, Channel B (2-180-V), 16 mv. F.S., Test # 12A

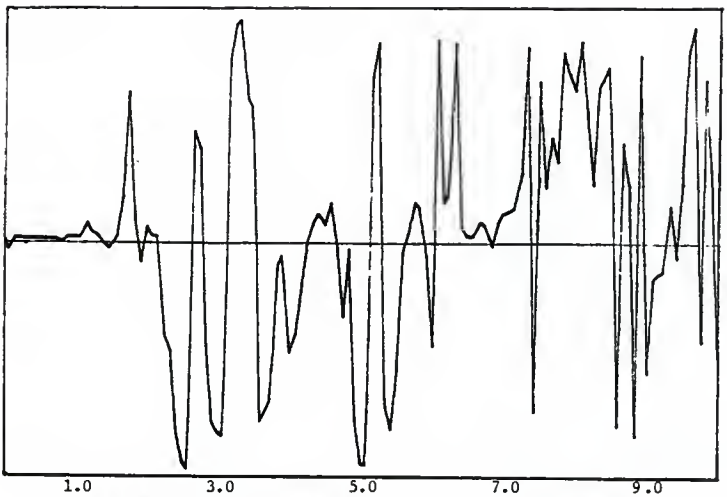

Transfer Function (Phase Angle), 2-0-V & 2-180-V, Test # 12A

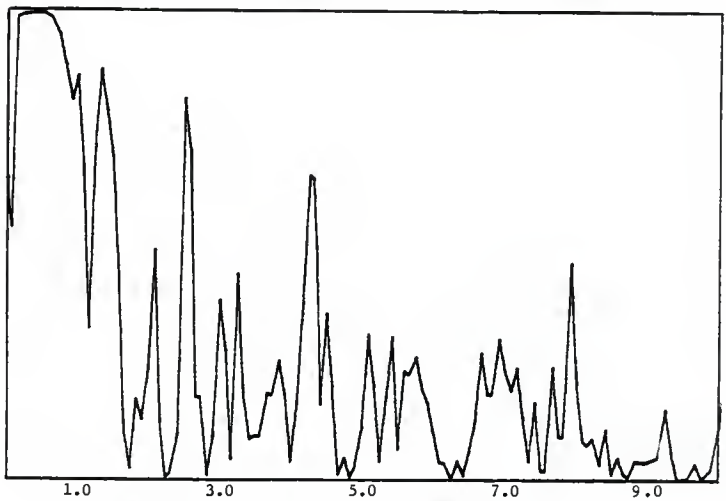

Coherence Function, 2-0-V & 2-180-V, Test # 12A

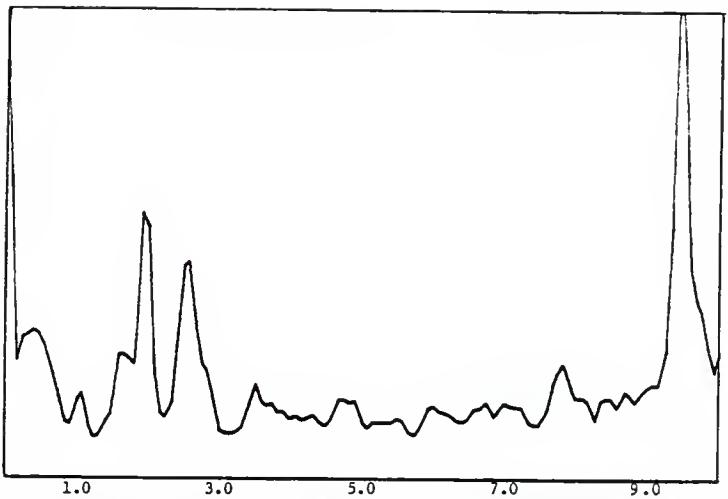

Response vs. Frequency, Channel A (2-90-V), 16 mv. F.S., Test # 12A

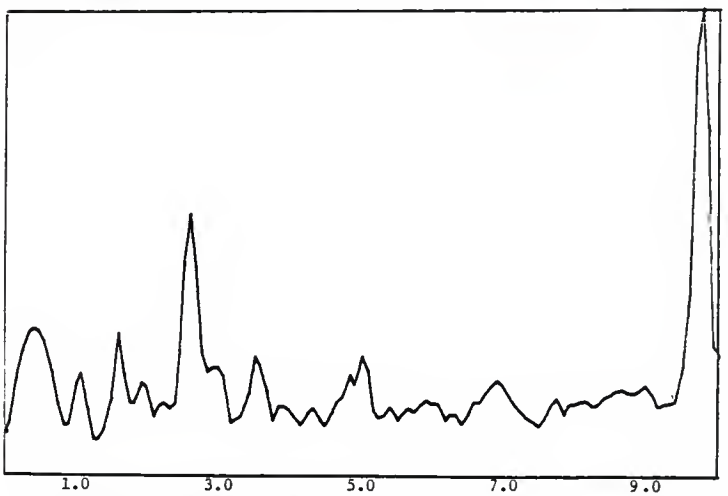

Response vs. Frequency, Channel B (2-180-V), 16 mv. F.S., Test # 12A

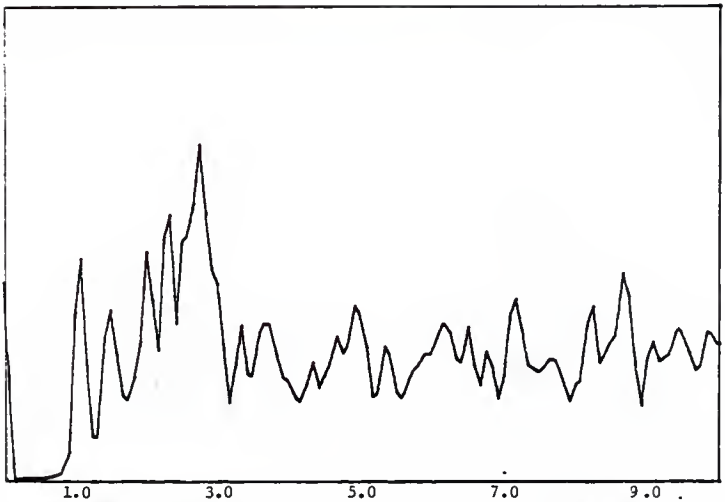

Response vs. Frequency, Channel A (2-0-N), 40 mv. F.S., Test # 10A

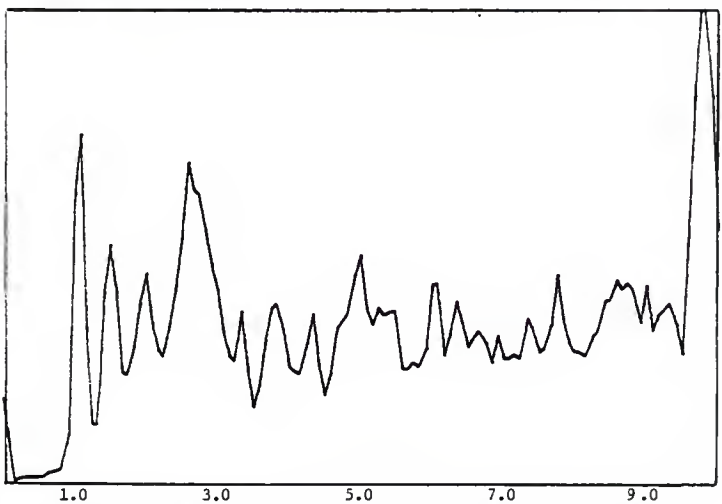

Response vs. Frequency, Channel B (2-180-N),16 mv. F.S., Test # 10A

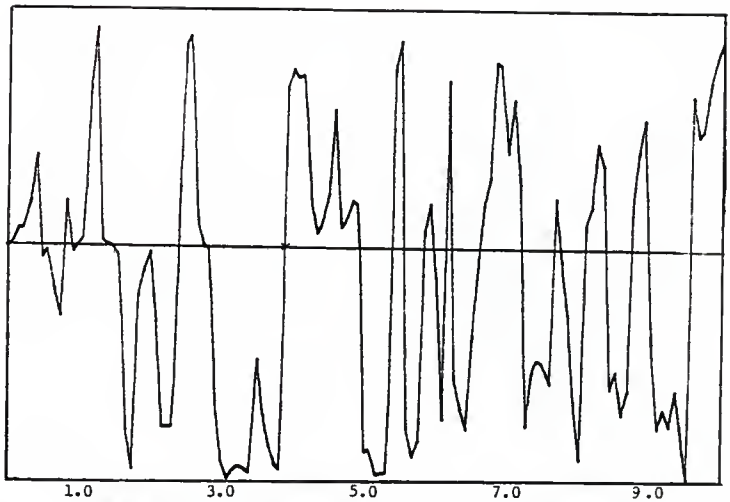

Transfer Function (Phase Angle), 2-0-N & 2-180-N, Test # 10A

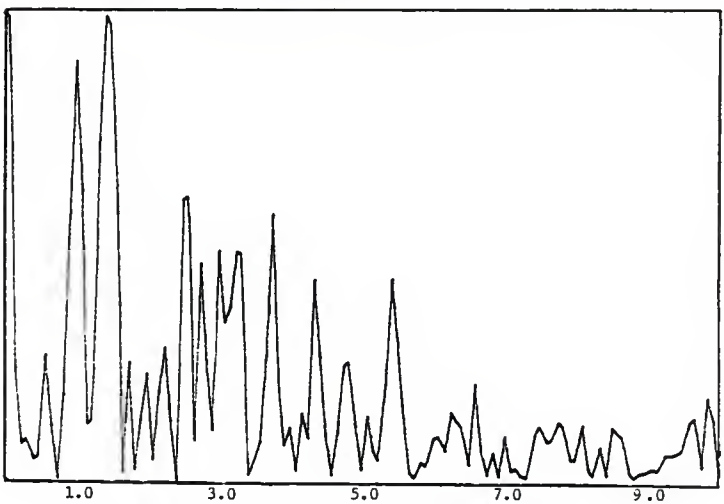

Coherence Function, 2-0-N & 2-180-N, Test # 10A

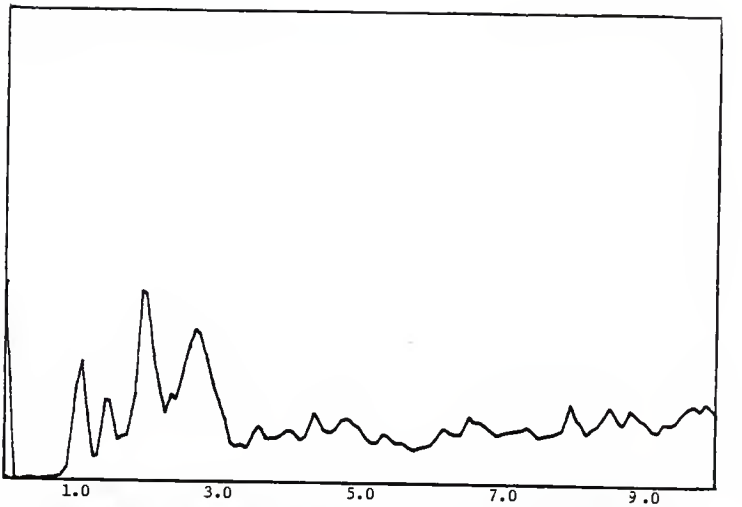

Response vs. Frequency, Channel A (2-90-N), 40 mv. F.S., Test # 10A

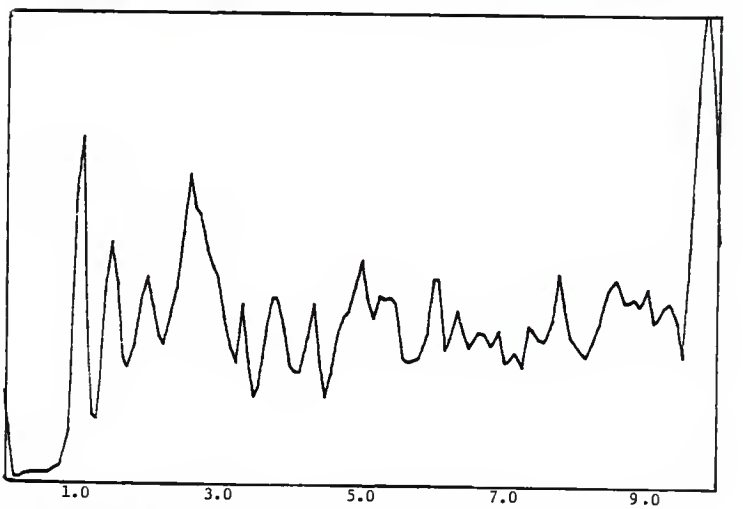

Response vs. Frequency, Channel B (2-180-N),16 mv. F.S., Test # 10A

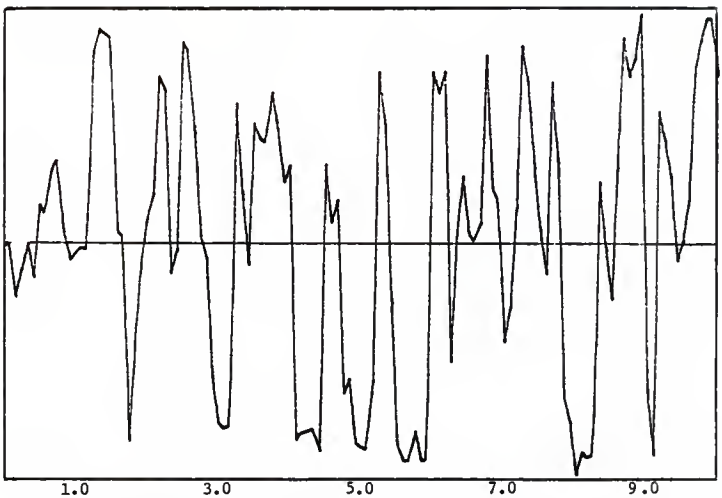

Transfer Function (phase Angle), 2-90-N & 2-180-N, Test # 10A

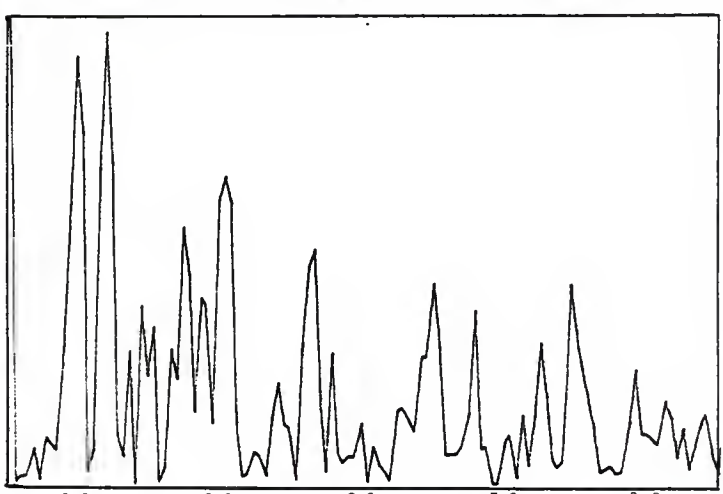

Coherence Function, 2-90-N & 2-180-N, Test # 10A

TEST LOG

DATE _____

TIME 11:00

TEST NO. 11A

RECORDER START 330

RECORDER END 360

CHANNEL	1	2	3	4
COLOR	RED	GREEN	YELLOW	BLUE
HEIGHT	5	2	2	2
AZIMUTH	0	0	90	F80
ORIENTATION	N	N	T	N
LOW PASS FILTER	20	20	20	20
ATTENUATOR SETTING	30	24	30	42
H-P FILTER I/O				
SENSITIVITY VOLTS				

NOTES:

ACWAL SIGNAL GOND BRUSH

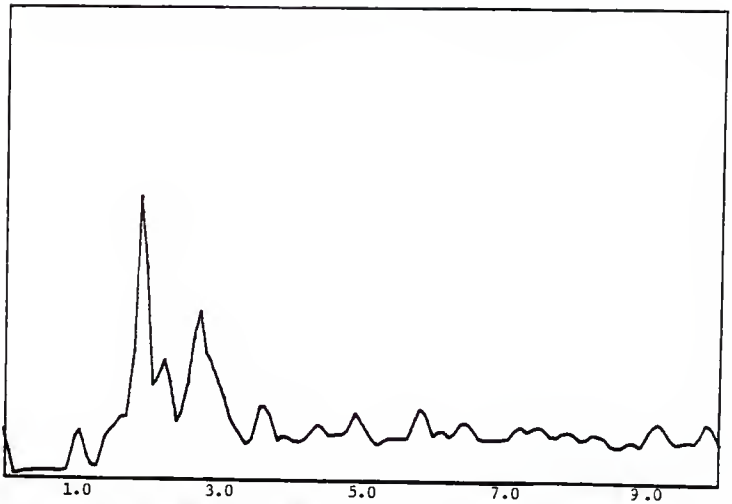

Response vs. Frequency, Channel A (5-0-N), 160 mv. F.S., Test # 11A

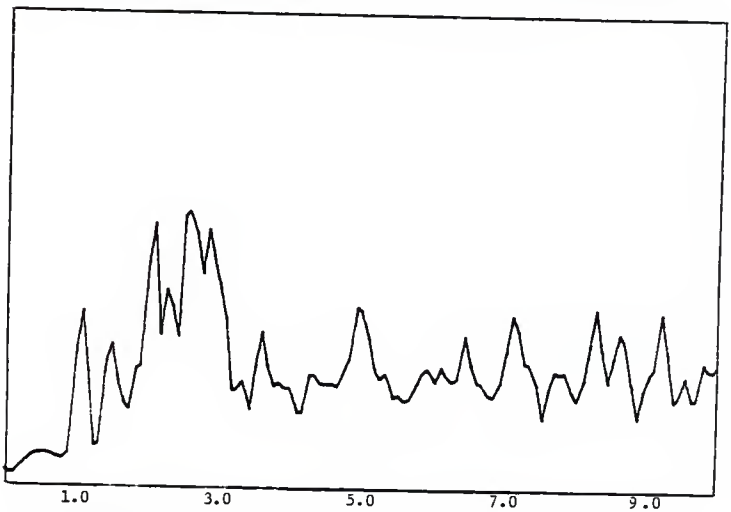

Response vs. Frequency, Channel B (2-0-N), 80 mv. F.S., Test # 11A

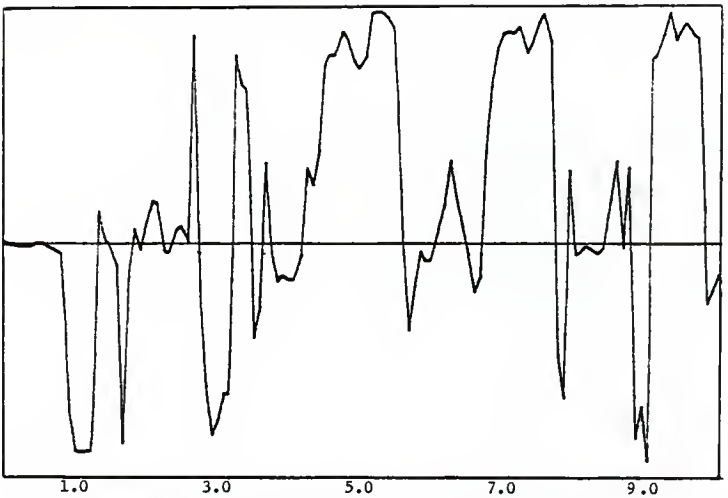

Transfer Function (Phase Angle), 5-0-N & 2-0-N, Test # 11A

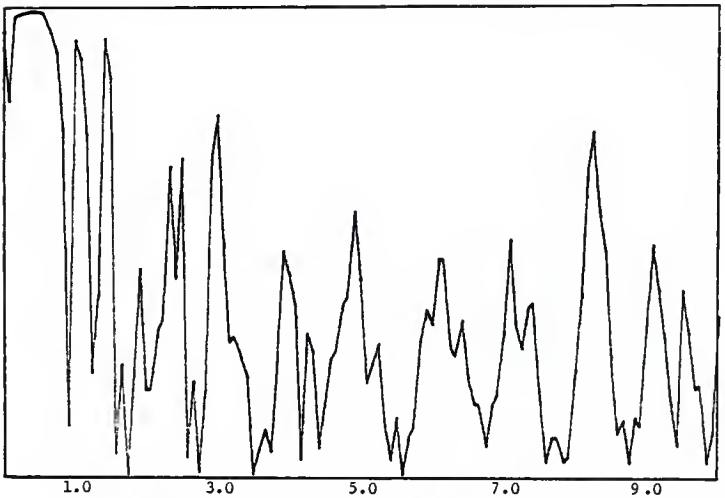

Coherence Function, 5-0-N & 2-0-N, Test # 11A

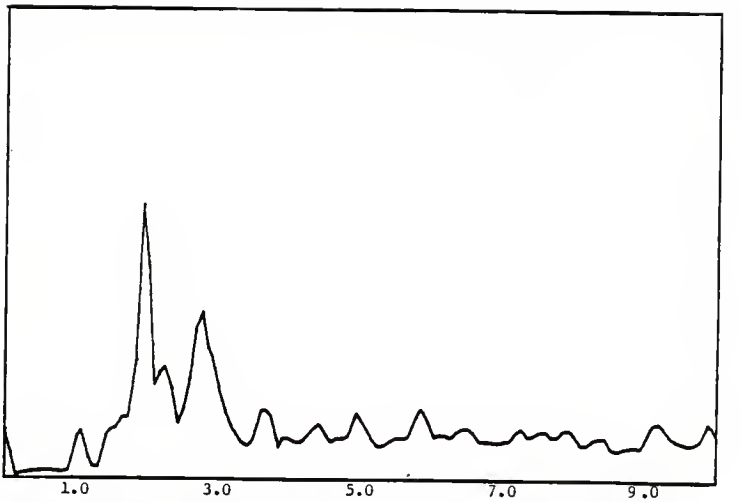

Response vs. Frequency, Channel A (5-0-N), 160 mv. F.S., Test # 11A

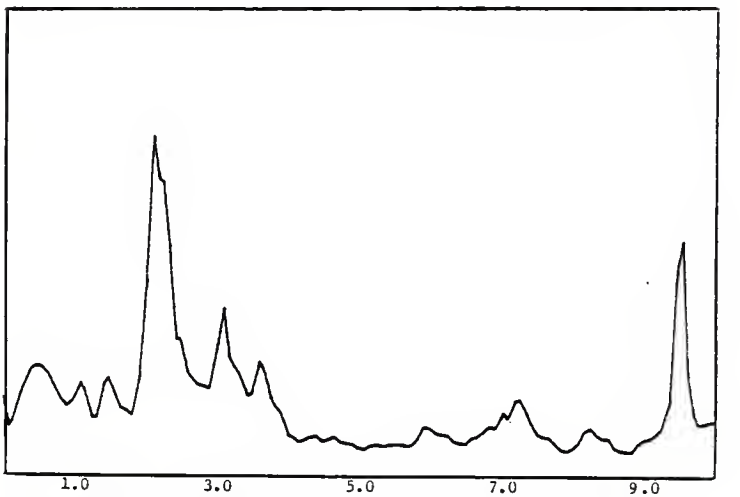

Response vs. Frequency, Channel B (2-90-T), 16 mv. F.S., Test # 11A

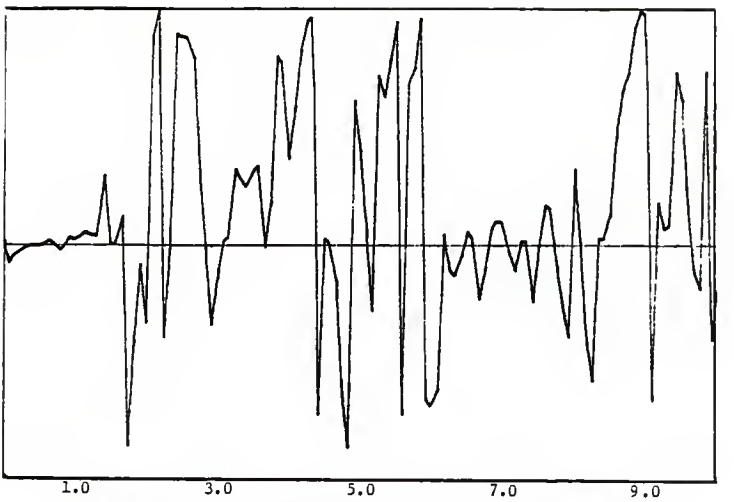

Transfer Function (Phase Angle), 2-90-V & 2-180-V, Test # 12A

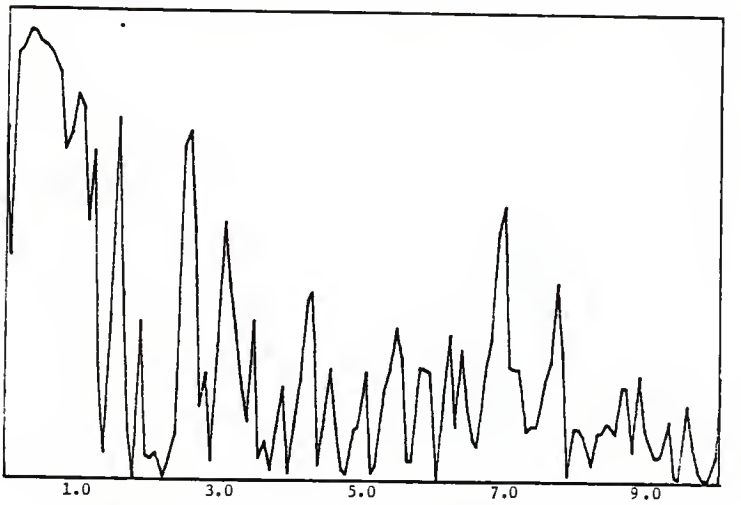

Coherence Function, 2-90-V & 2-180-V, Test # 12A

TEST LOG

DATE 8/19

TIME 1:45

TEST NO. 13A

RECORDER START 550

RECORDER END 580

CHANNEL	1	2	3	4
COLOR	RED	GREEN	YELLOW	BLUE
HEIGHT	5	1	1	1
AZIMUTH	0	0	90	180
ORIENTATION	N	N	N	N
LOW PASS FILTER	20	20	20	20
ATTENUATOR SETTING	30	24	30	30
H-P FILTER I/O	✓	✓	✓	-
SENSITIVITY VOLTS				

ACCEL. SIGNAL COND BRKR

NOTES:

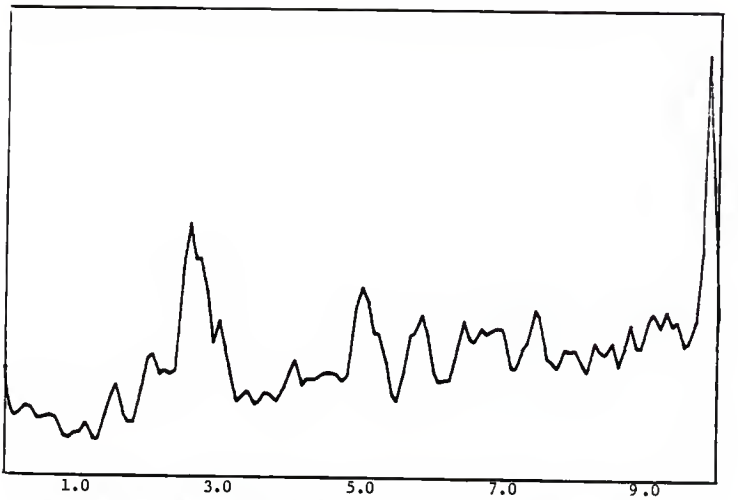

Response vs. Frequency, Channel A (1-0-N), 80 mv. F.S., Test # 13A

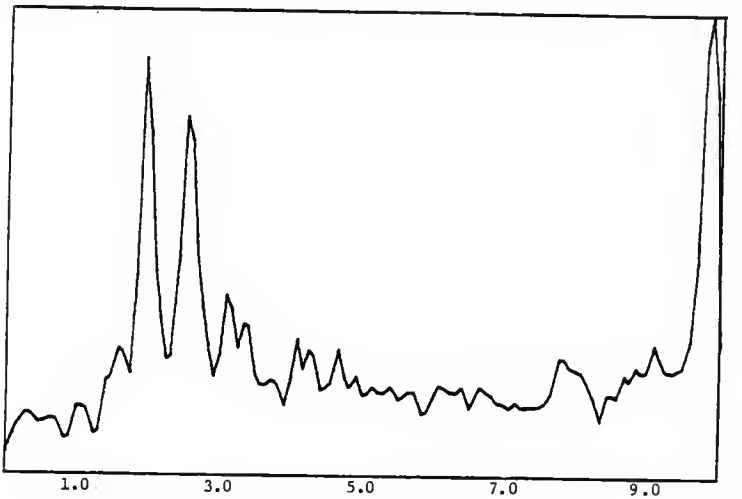

Response vs. Frequency, Channel B (1-90-N), 40 mv. F.S., Test #13A

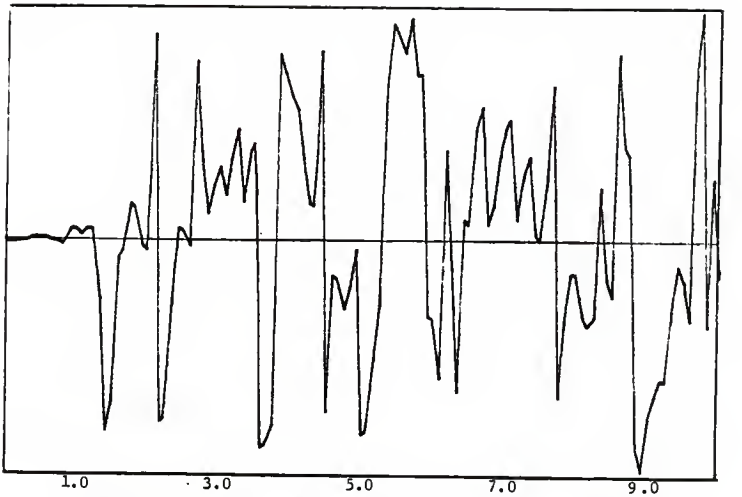

Transfer Function (Phase Angle), 1-0-N & 1-90-N, Test # 13A

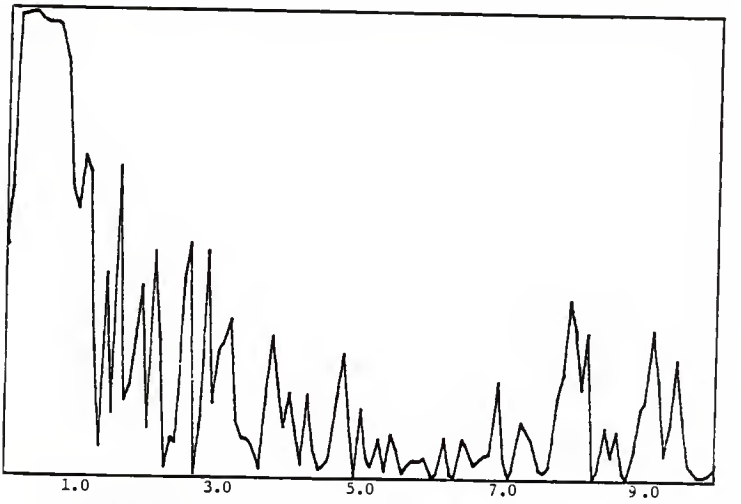

Coherence Function, 1-0-N & 1-90-N, Test # 13A

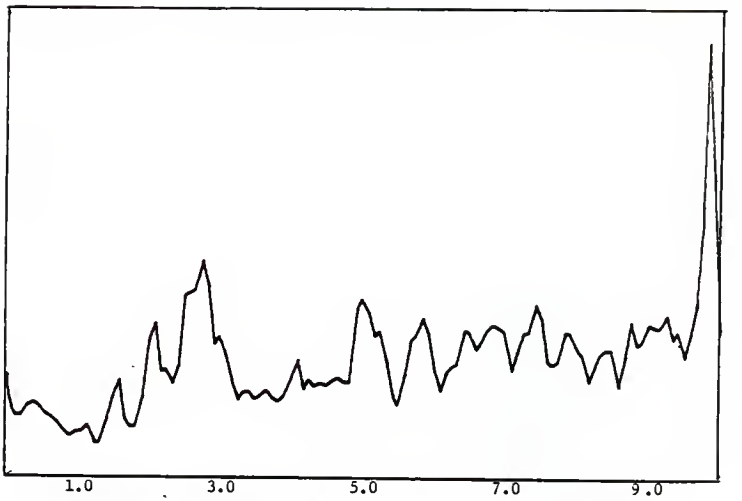

Response vs. Frequency, Channel A (1-0-N), 80 mv. F.S., Test # 13A

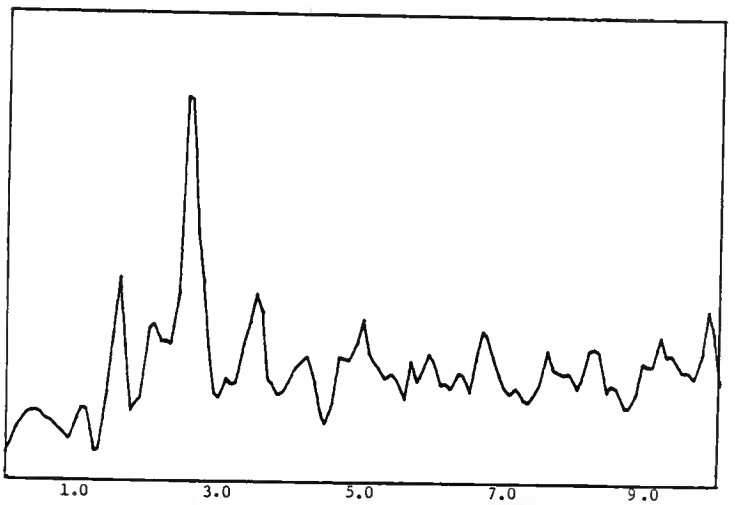

Response vs. Frequency, Channel B (1-180-N), 40 mv. F.S., Test # 13A

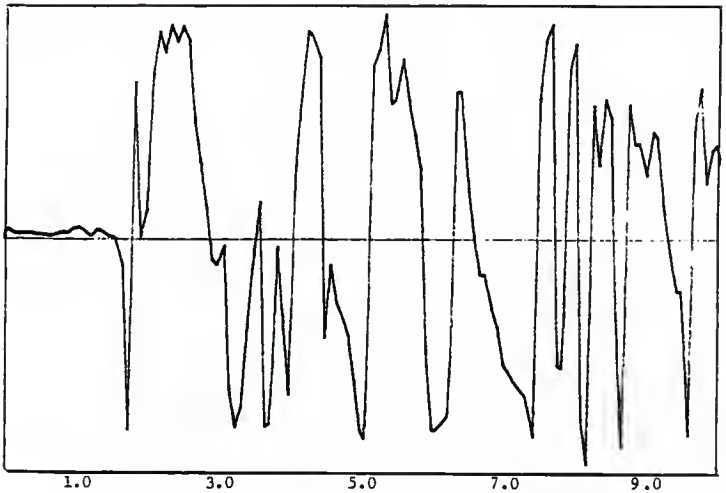

Transfer Function (Phase Angle), 1-0-N & 1-180-N, Test # 13A

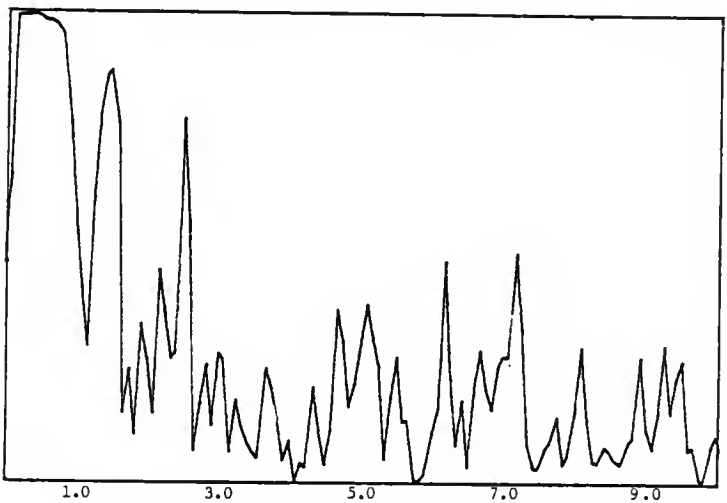

Coherence Function, 1-0-N & 1-180-N, Test # 13A

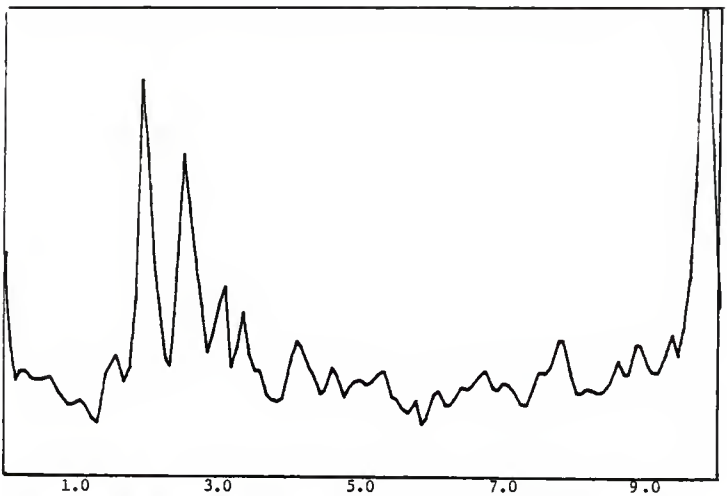

Response vs. Frequency, Channel A (1-90-N), 40 mv. F.S., Test # 13A

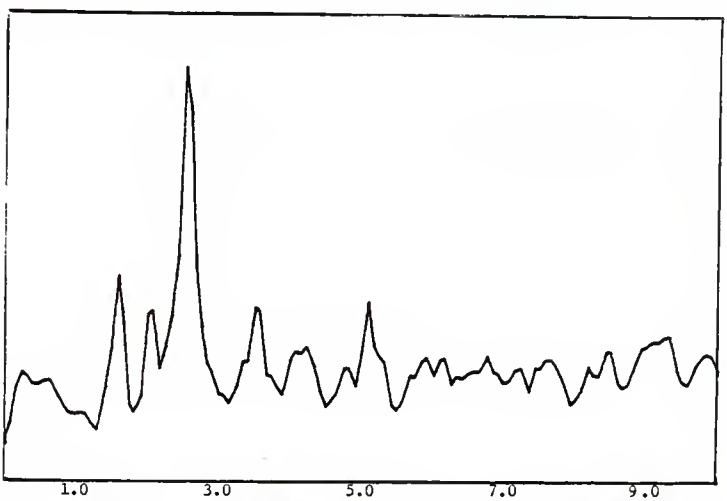

Response vs. Frequency, Channel B (1-180-N), 40 mv. F.S., Test # 13A

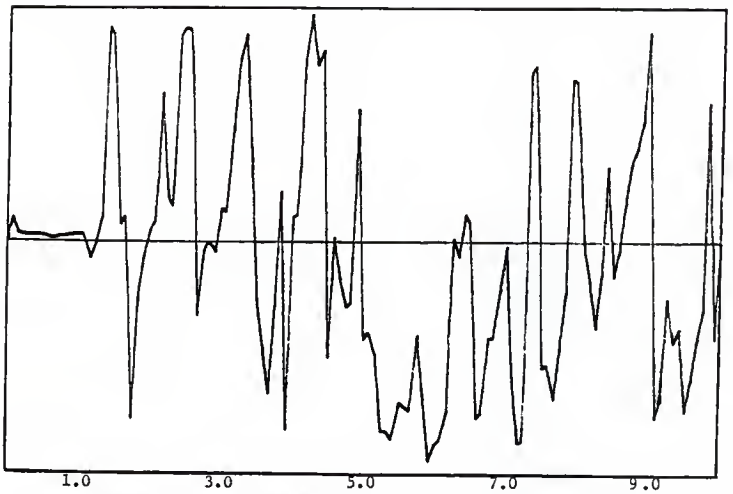

Transfer Function (Phase Angle), 1-90-N & 1-180-N, Test # 13A

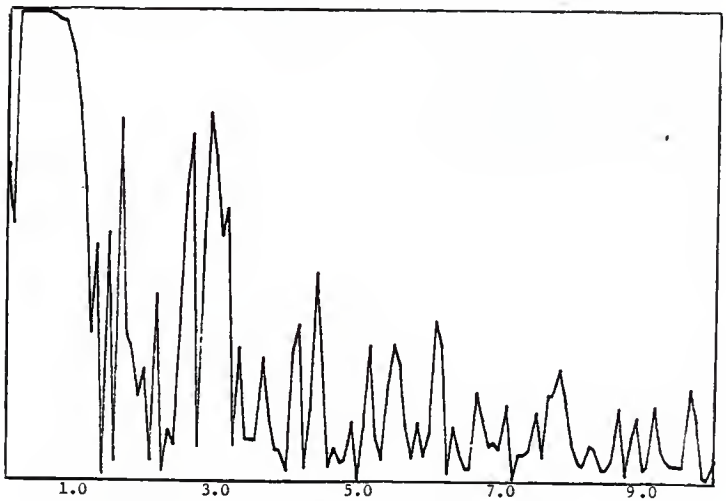

Coherence Function, 1-90-N & 1-180-N, Test # 13A

TEST LOG

DATE _____ TEST NO. 14A

TIME 2:45 RECORDER START 000

RECORDER END 030

CHANNEL	1	2	3	4
COLOR	RED	GREEN	YELLOW	BLUE
HEIGHT	5	1	1	1
AZIMUTH	0	0	90	180
ORIENTATION	N	N	T	N
LOW PASS FILTER	20	20	20	20
ATTENUATOR SETTING	30	30	30	30
H-P FILTER I/O				
SENSITIVITY VOLTS				

ACCEL. SIGNAL COND BRUSH

NOTES:

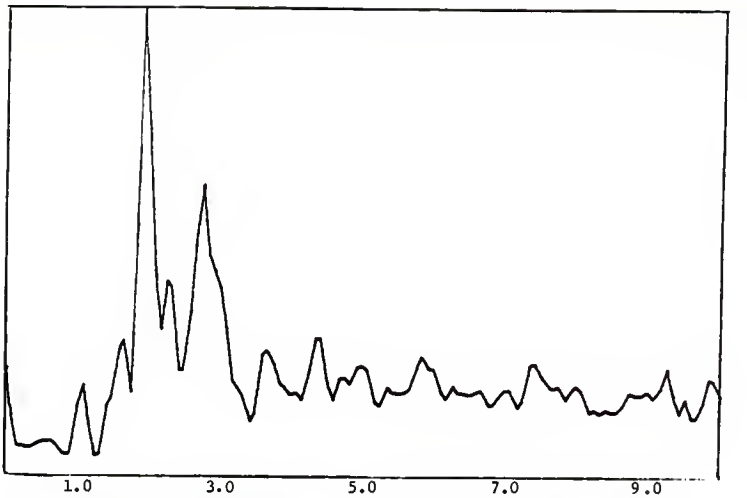

Response vs. Frequency, Channel A (5-0-N), 80 mv. F.S., Test # 14A

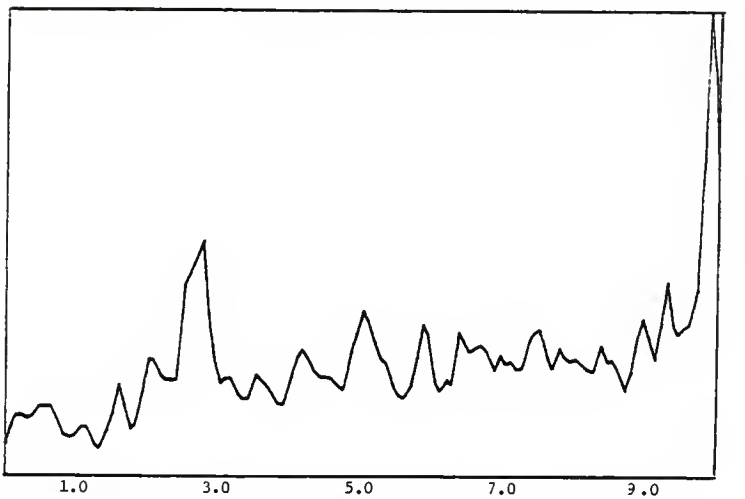

Response vs. Frequency, Channel B (1-0-N), 40 mv. F.S., Test # 14A

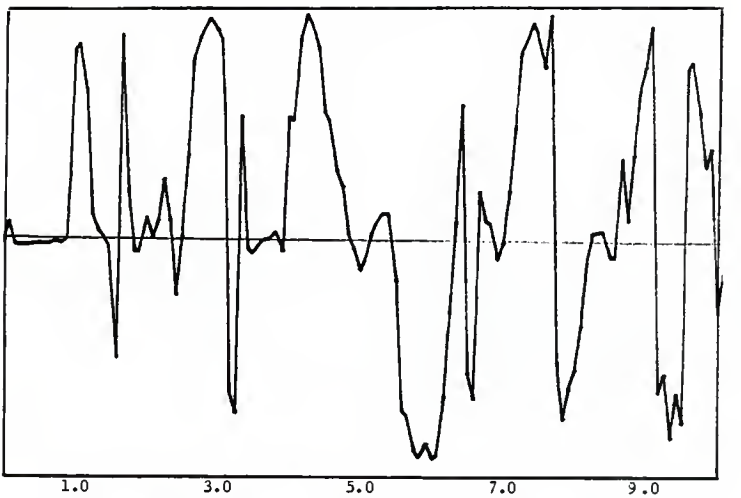

Transfer Function (Phase Angle), 5-0-N & 1-0-N, Test # 14A

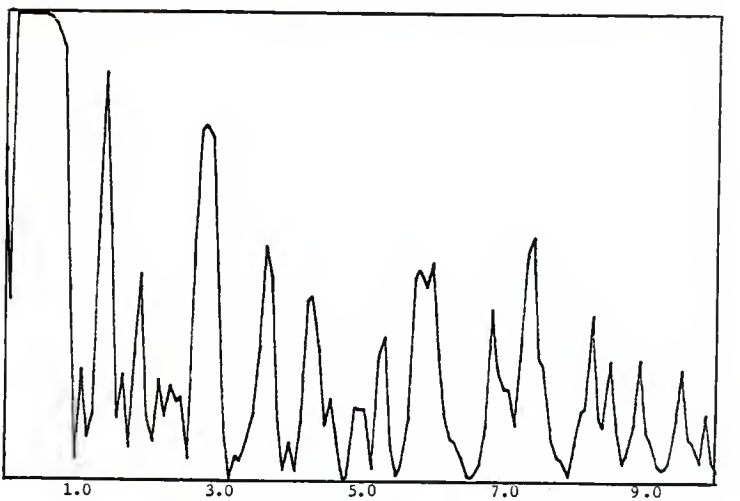

Coherence Function, 5-0-N & 1-0-N, Test # 14A

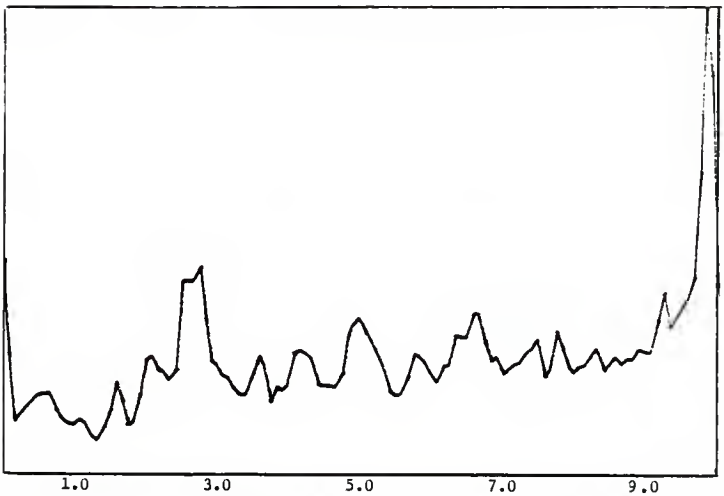

Response vs. Frequency, Channel A (1-0-N), 40 mv. F.S., Test # 14A

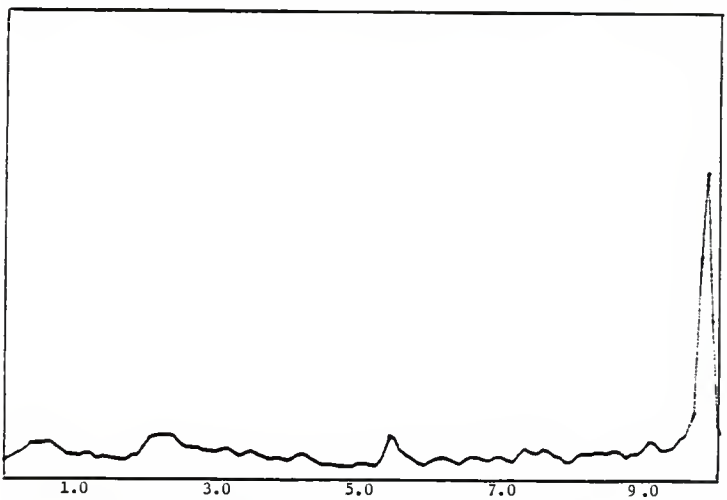

Response vs. Frequency, Channel B (1-90-T), 80 mv. F.S., Test # 14A

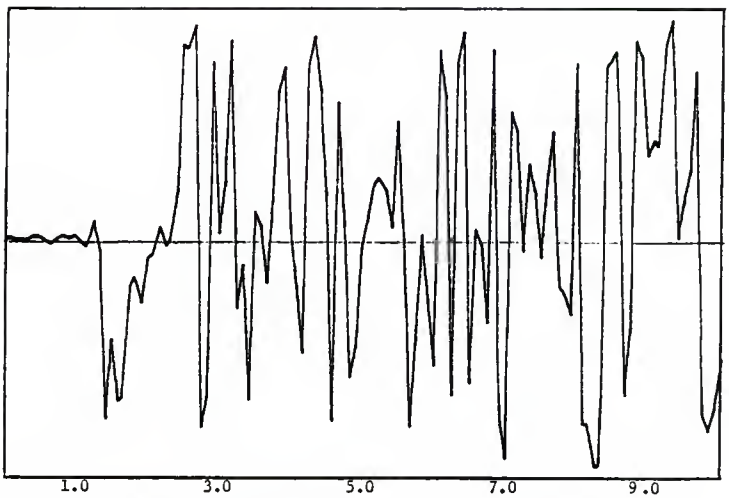

Transfer Function (Phase Angle), 1-0-N & 1-90-T, Test # 14A

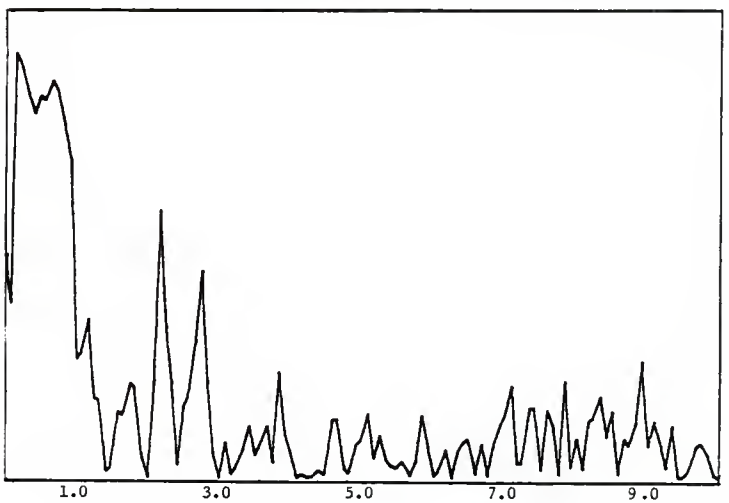

Coherence Function, 1-0-N & 1-90-T, Test # 14A

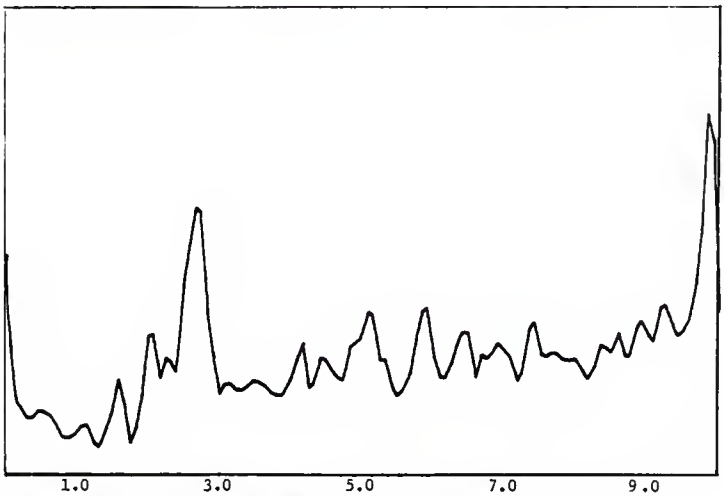

Response vs. Frequency, Channel A (1-0-N), 40 mv. F.S., Test # 14A

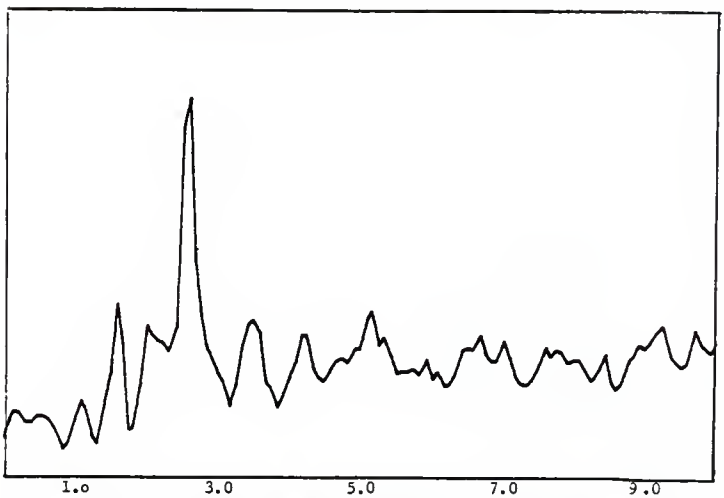

Response vs. Frequency, Channel B (1-180-N), 40 mv. F.S., Test # 14A

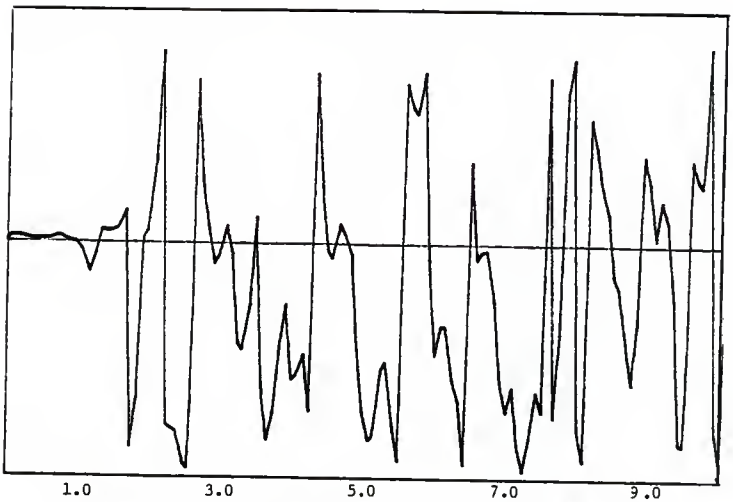

Transfer Function (Phase Angle), 1-0-N & 1-180-N, Test # 14A

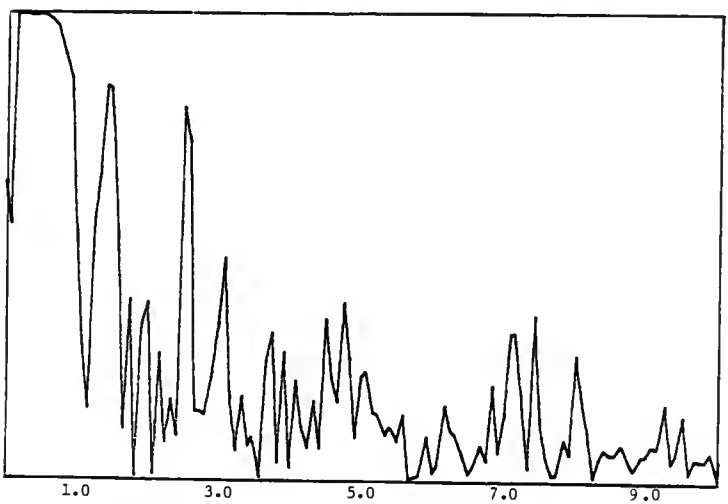

Coherence Function, 1-0-N & 1-180-N, Test # 14A

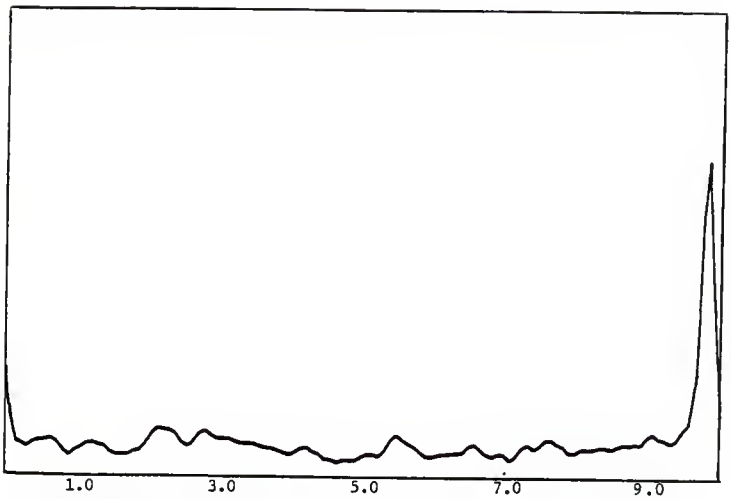

Response vs. Frequency, Channel A (1-90-T), 80 mv. F.S., Test #14A

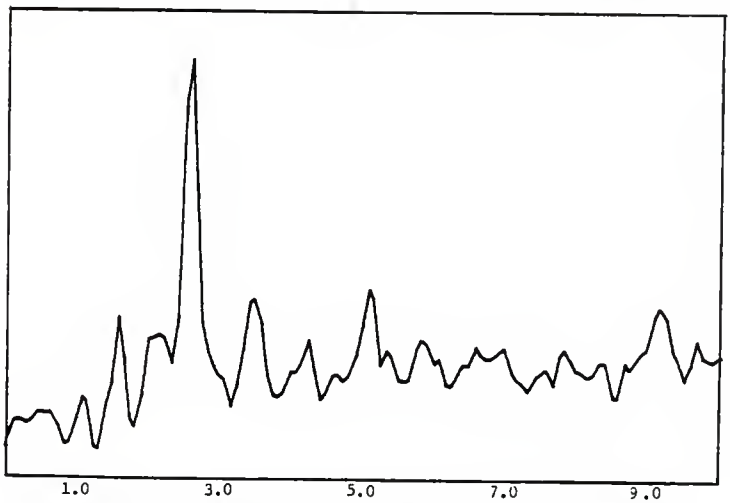

Response vs. Frequency, Channel B (1-180-N), 40 mv. F.S., Test # 14A

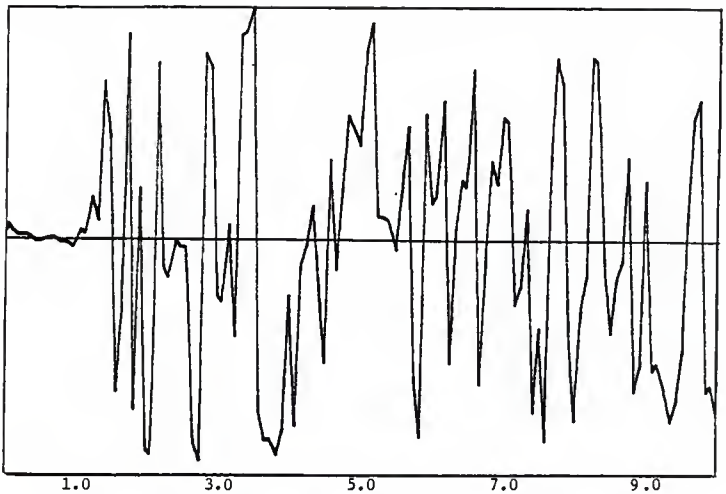

Transfer Function (Phase Angle), 1-90-T & 1-180-N, Test # 14A

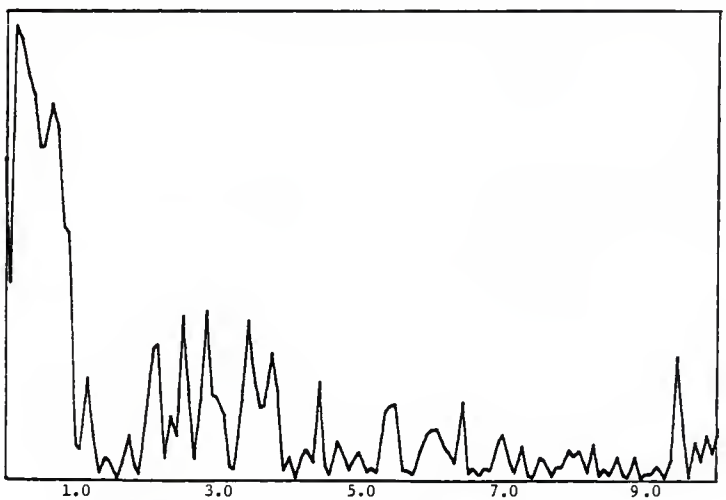

Coherence Function, 1-90-T & 1-180-N, Test # 14A

TEST LOG

DATE 6/20

TIME 9:30

TEST NO. 15A

RECORDER START 130

RECORDER END 150

CHANNEL	1	2	3	4
COLOR	RED	GREEN	YELLOW	BLUE
HEIGHT	5	1	1	1
AZIMUTH	0	0	90	180
ORIENTATION	N	V	V	V
LOW PASS FILTER	20	20	20	20
ATTENUATOR SETTING	30	24	30	24
H-P FILTER I/O				
SENSITIVITY VOLTS				

ACSAL SIGNAL GEND BRSNK

NOTES:

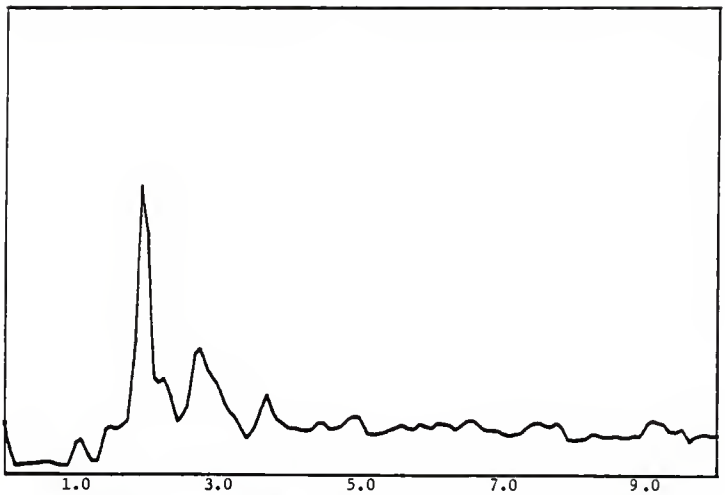

Response vs. Frequency, Channel A (5-0-N), 160 mv. F.S., Test # 15A

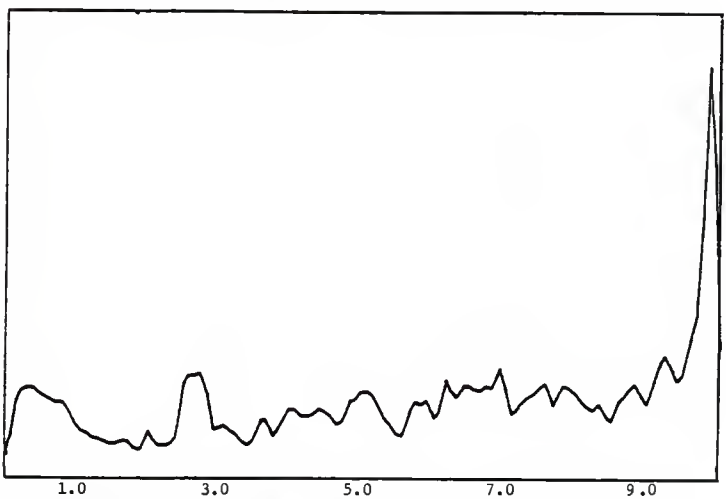

Response vs. Frequency, Channel B (1-0-V), 40 mv. F.S., Test # 15A

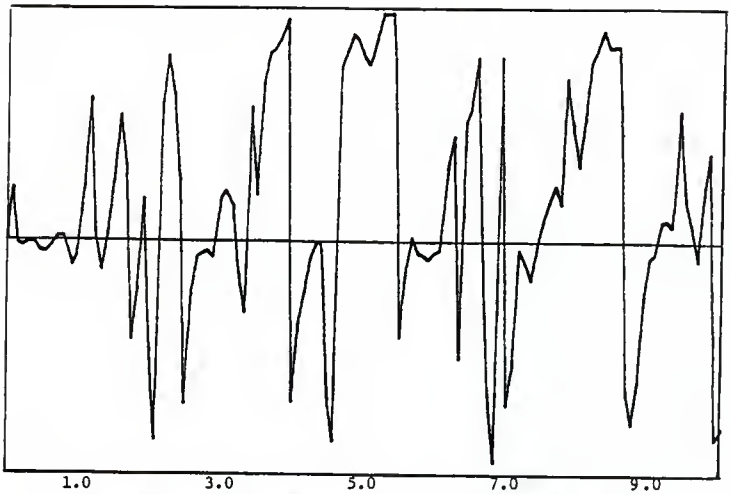

Transfer Function (Phase Angle), 5-0-N & 1-0-V, Test # 15A

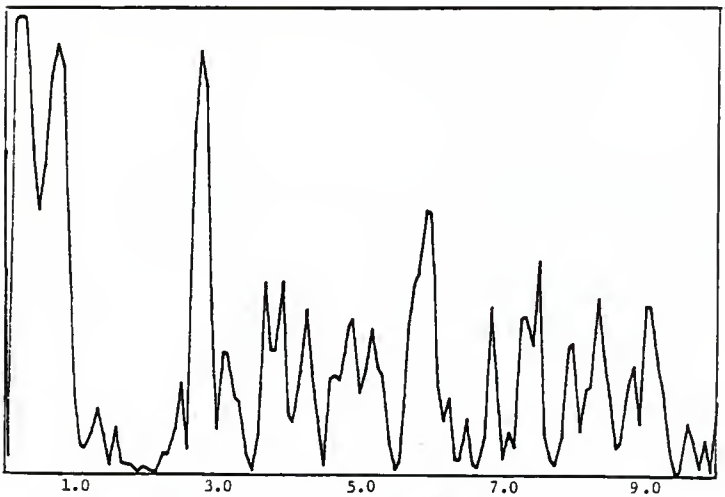

Coherence Function, 5-0-N & 1-0-V, Test # 15A

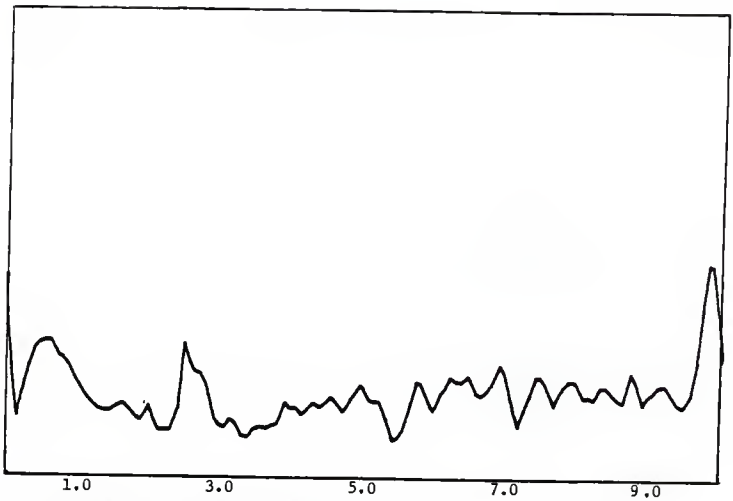

Response vs. Frequency, Channel A (1-0-V), 40 mv. F.S., Test # 15A

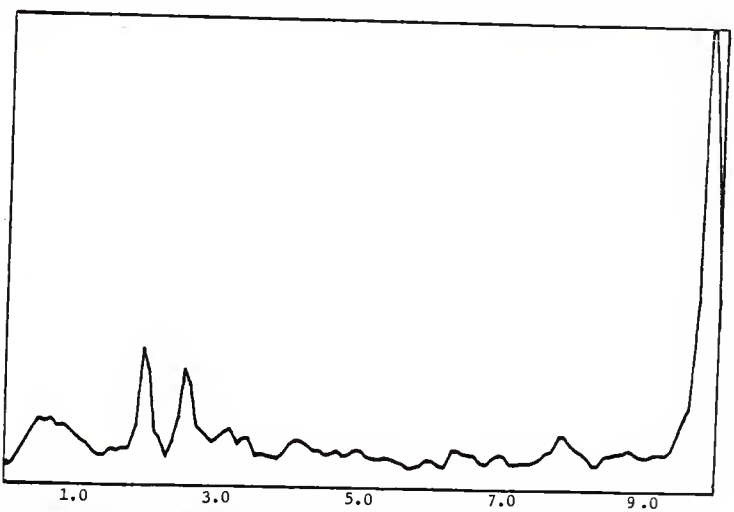

Response vs. Frequency, Channel B (1-90-V), 40 mv. F.S., Test # 15A

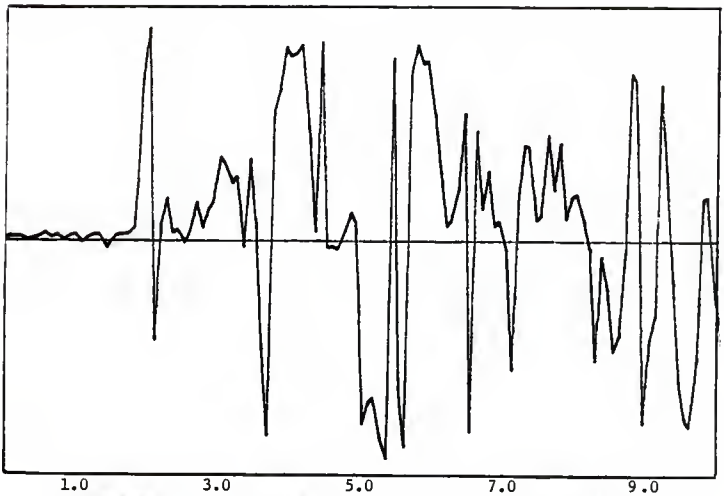

Transfer Function (Phase Angle), 1-0-V & 1-90-V, Test # 15A

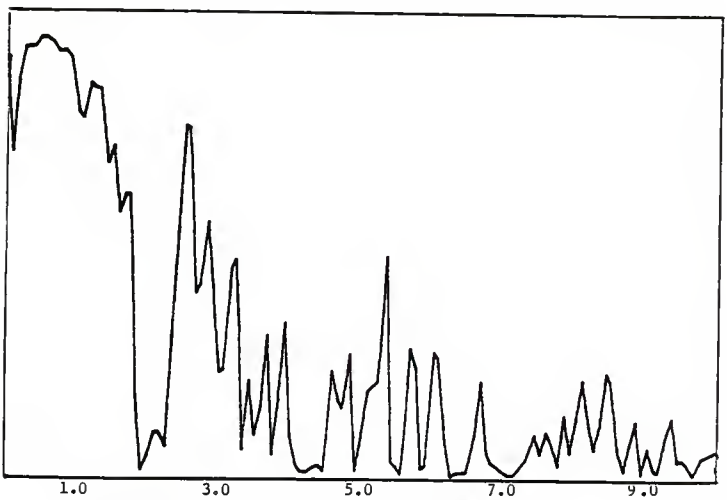

Coherence Function, 1-0-V & 1-90-V, Test # 15A

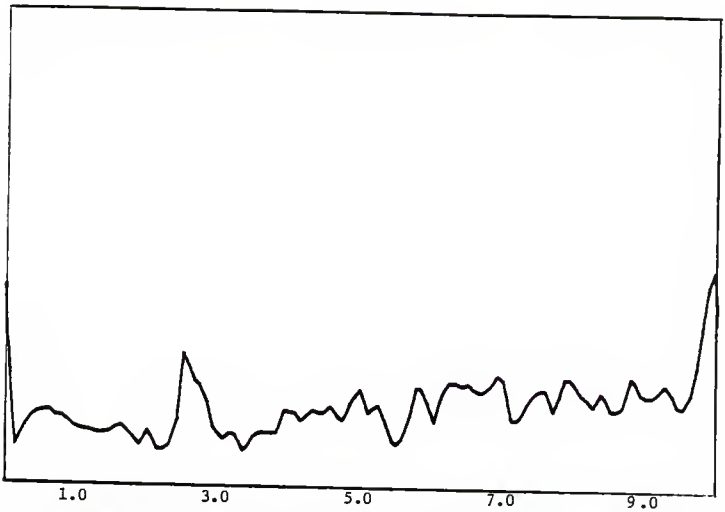

Response vs. Frequency, Channel A (1-0-V), 40 mv. F.S., Test # 15A

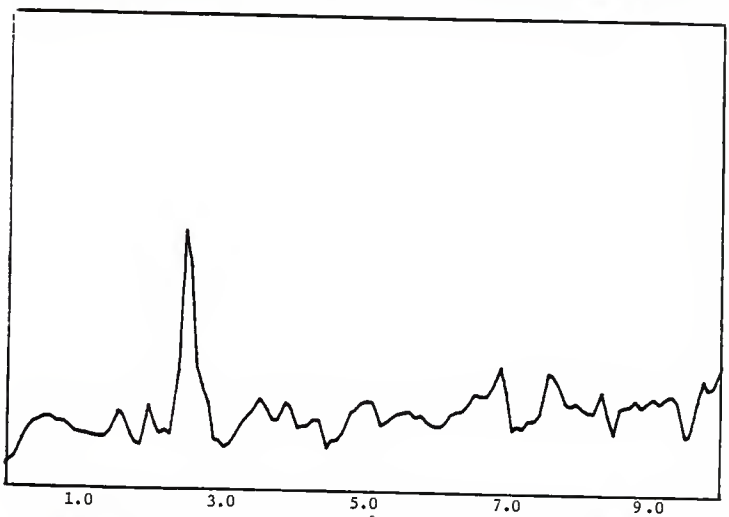

Response vs. Frequency, Channel B (1-180-V), 40 mv. F.S., Test # 15A

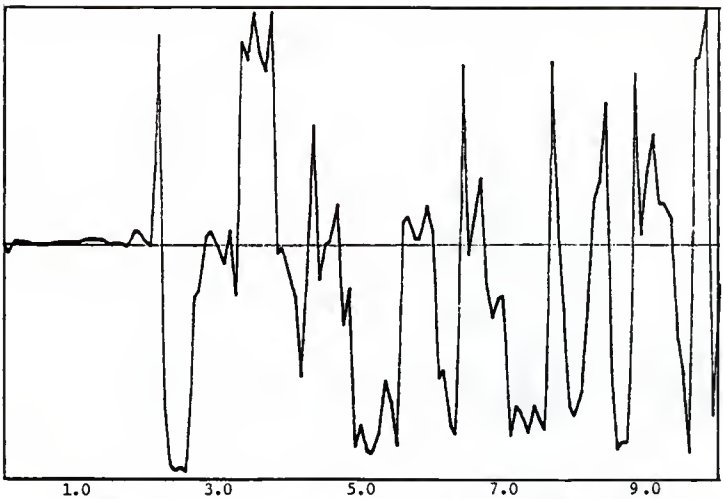

Transfer Function (Phase Angle), 1-0-V & 1-180-V, Test # 15A

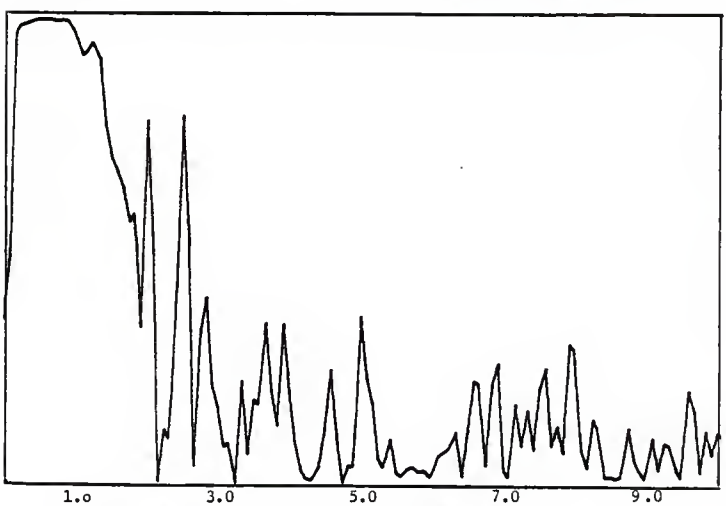

Coherence Function, 1-o-V & 1-180-V, Test # 15A

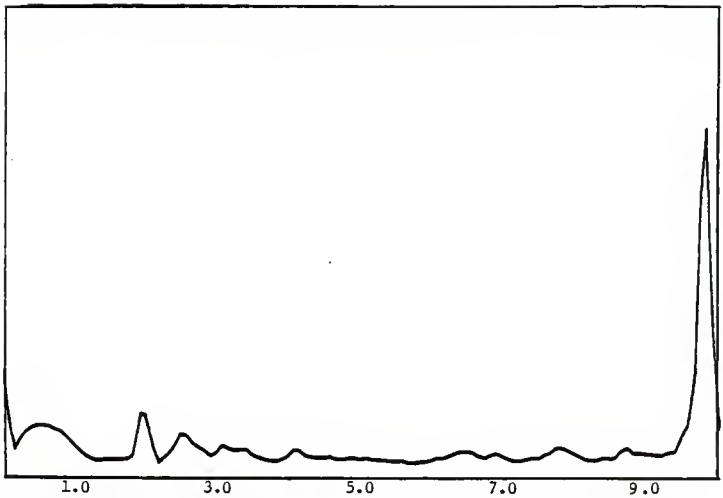

Response vs. Frequency, Channel A (1-90-V), 80 mv. F.S., Test # 15A

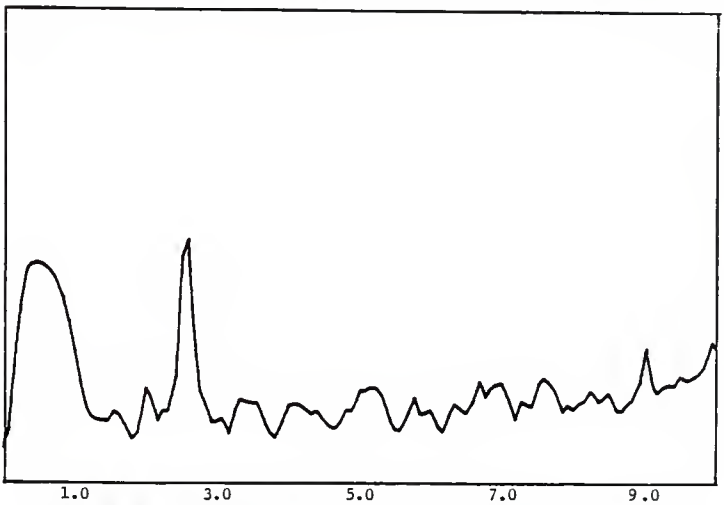

Response vs. Frequency, Channel B (1-180-V), 40 mv. F.S., Test # 15A

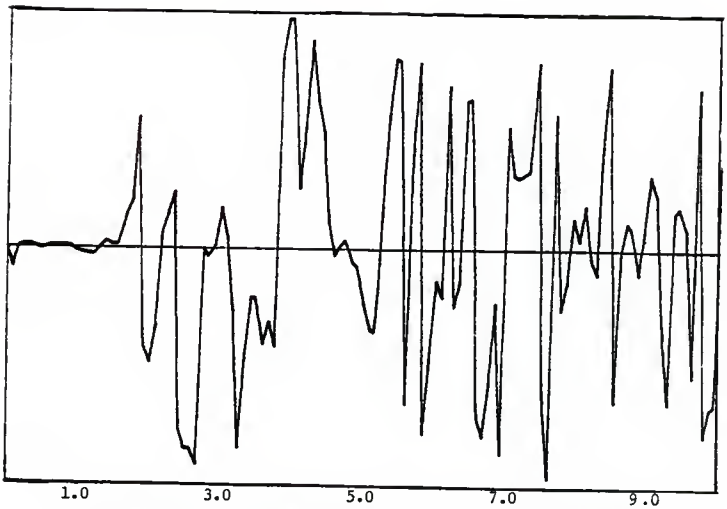

Transfer Function (Phase Angle), 1-90-V & 1-180-V, Test # 15A

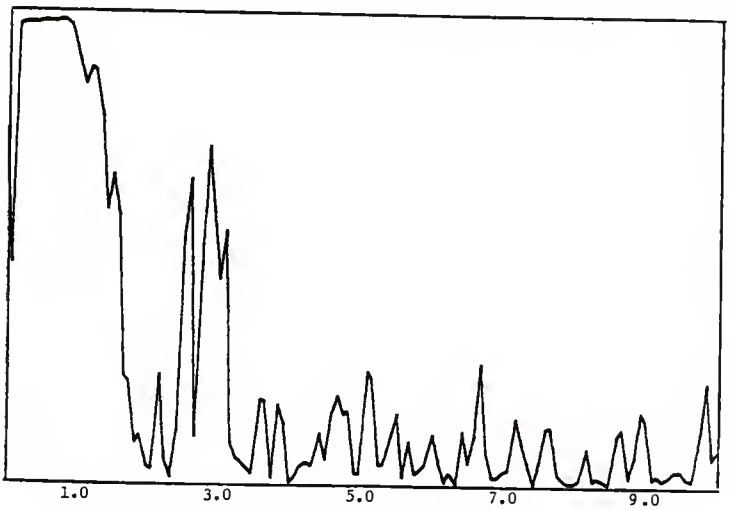

Coherence Function, 1-90-V &1-180-V, Test # 15A

TEST LOG

DATE 8/20

TIME 10:40

TEST NO. 10A

RECORDER START 220

RECORDER END 250

CHANNEL	1	2	3	4
COLOR	RED	GREEN	YELLOW	BLUE
HEIGHT	5	0	0	0
AZIMUTH	0	0	90	180
ORIENTATION	N	N	N	N
LOW PASS FILTER	20	20	20	20
ATTENUATOR SETTING	30	18	18	24
H-P FILTER I/O	✓	✓	✓	✓
SENSITIVITY VOLTS				

ACWA. SIGNAL GRND BRIDGE

NOTES:

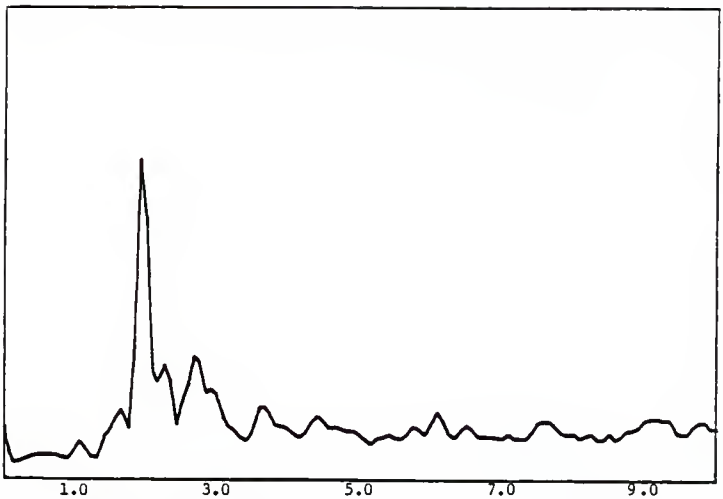

Response vs. Frequency, Channel A (5-0-N), 160 mv. F.S., Test # 16A

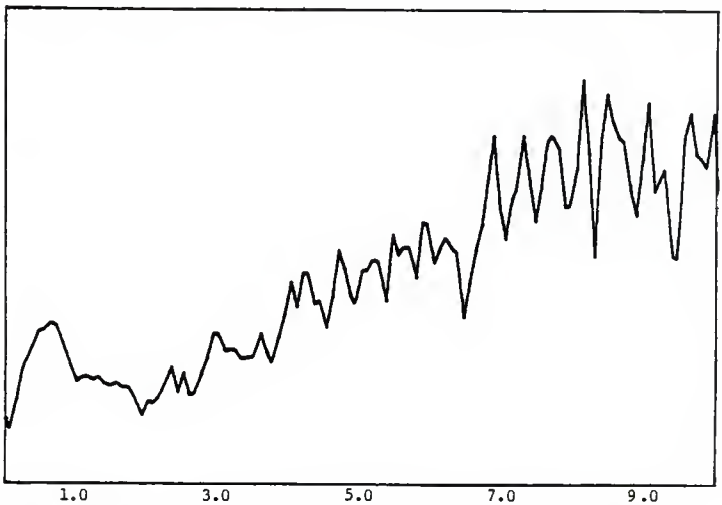

Response vs. Frequency, Channel B (0-0-N), 16 mv. F.S., Test # 16A

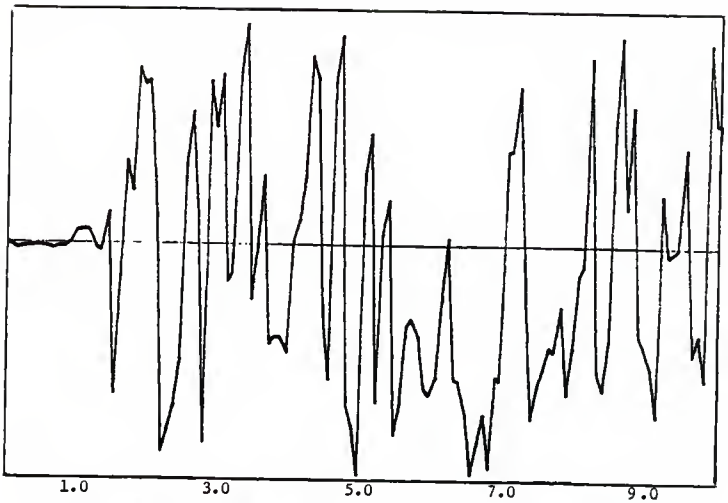

Transfer Function (Phase Angle), 5-0-N & 0-0-N, Test # 16A

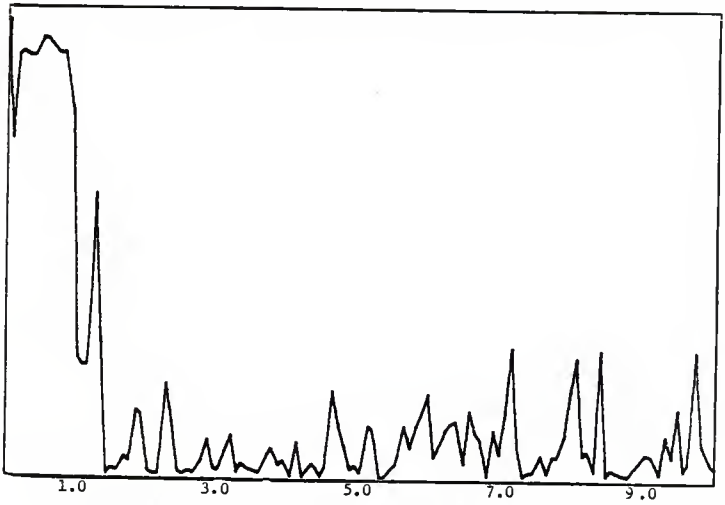

Coherence Function, 5-0-N & 0-0-N, Test # 16A

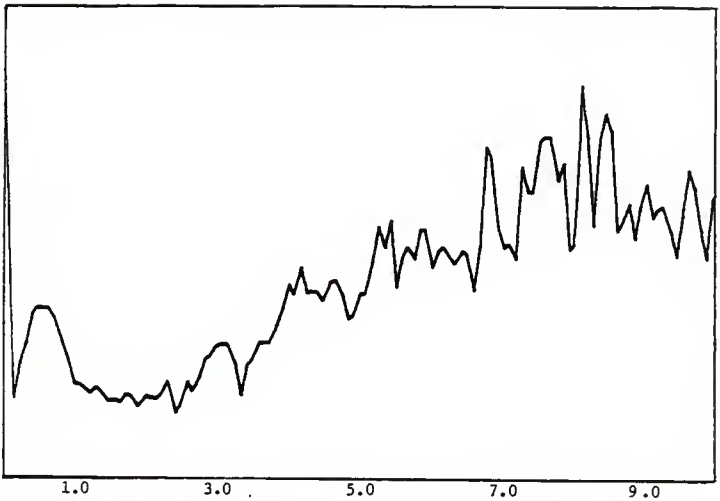

Response vs. Frequency, Channel A (0-0-N), 16 mv. F.S., Test # 16A

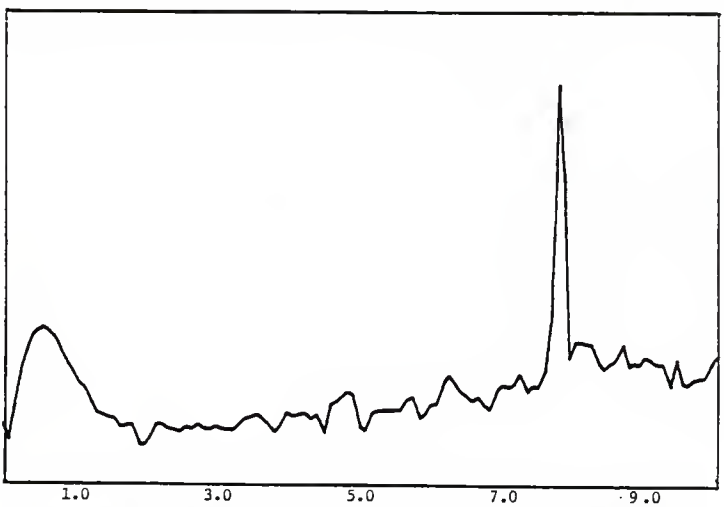

Response vs. Frequency, Channel B (0-90-N), 16 mv. F.S., Test # 16A

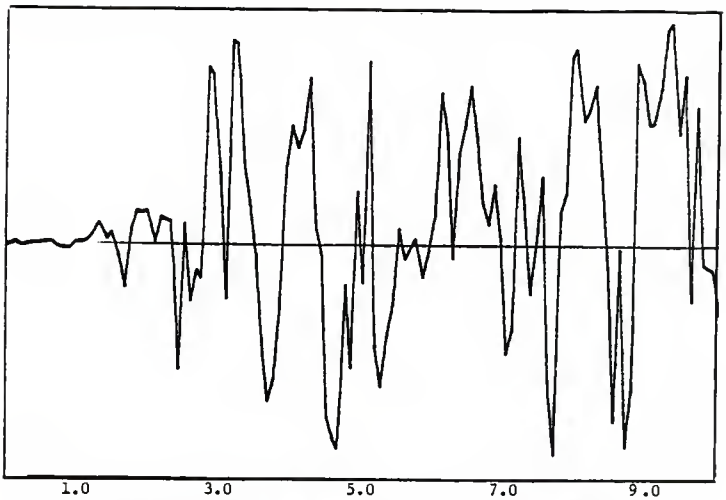

Transfer Function (Phase Angle), 0-0-N & 0-90-N, Test # 16A

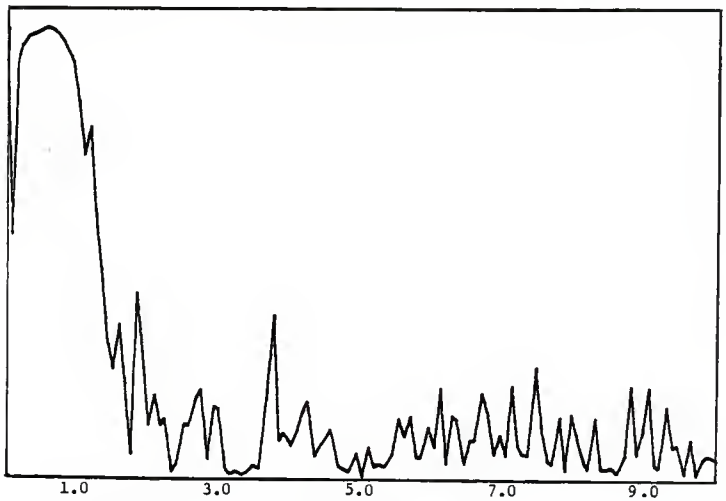

Coherence Function, 0-0-N & 0-90-N, Test # 16A

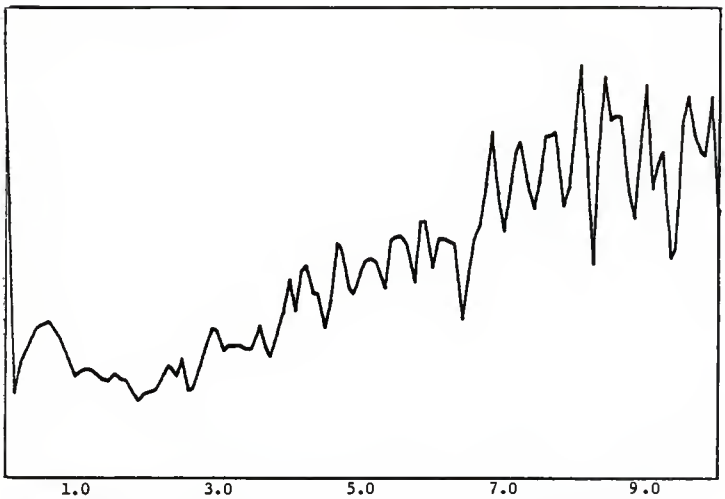

Response vs. Frequency, Channel A (0-0-N), 16 mv. F.S., Test # 16A

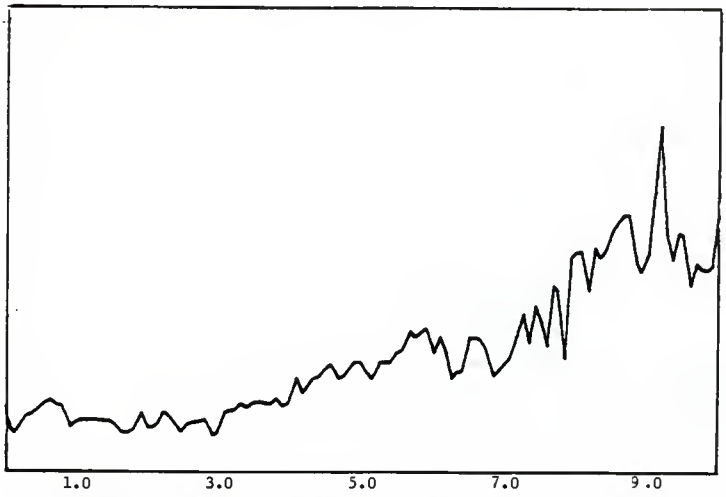

Response vs. Frequency, Channel B (0-180-N), 16 mv. F.S., Test # 16A

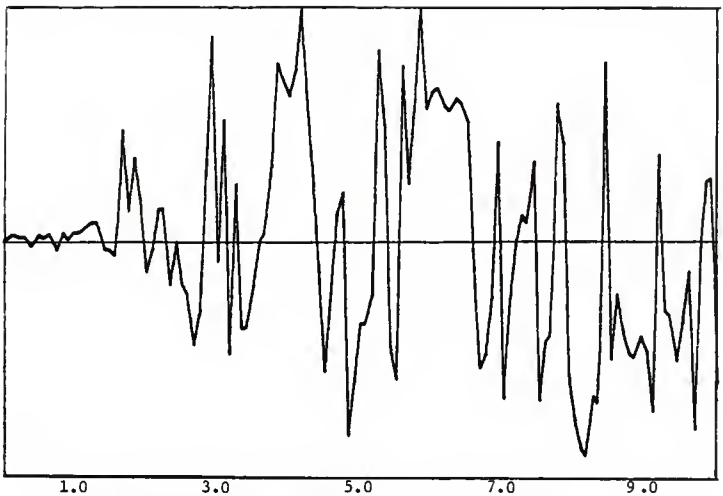

Transfer Function (Phase Angle), 0-0-N & 0-180-N, Test # 16A

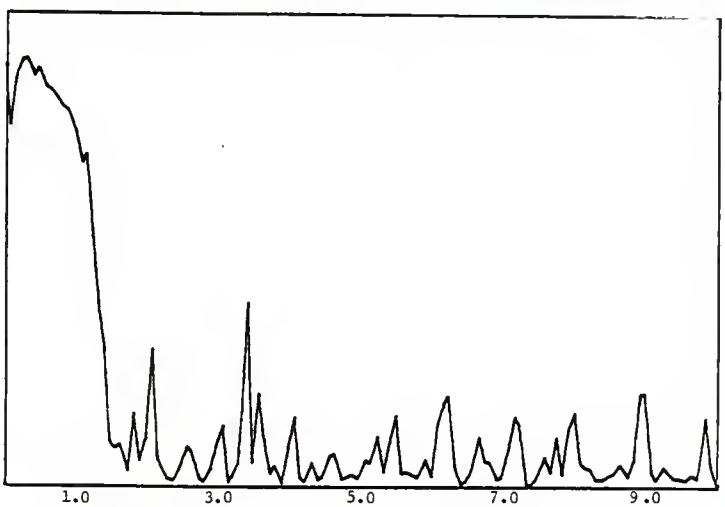

Coherence Function, 0-0-N & 0-180-N, Test # 16A

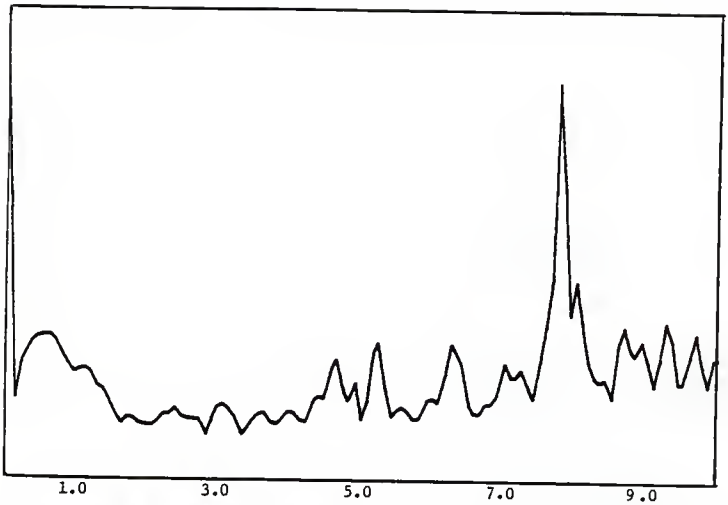

Response vs. Frequency, Chsnnel A (0-90-N), 16 mv. F.S., Test # 16A

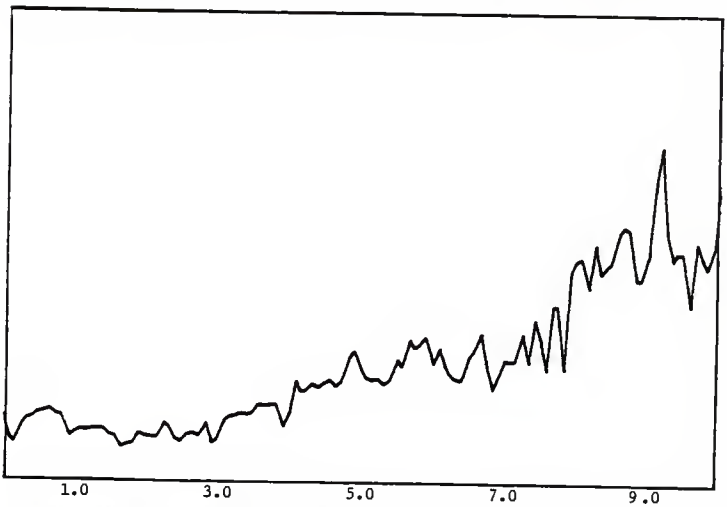

Response vs. Frequency, Channel B (0-180-N), 16 mv. F.S., Test # 16A

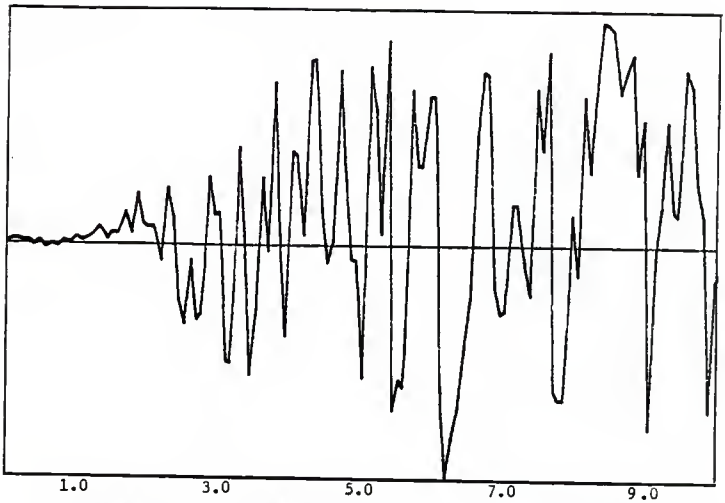

Transfer Function (Phase Angle), 0-90-N & 0-180-N, Test # 16A

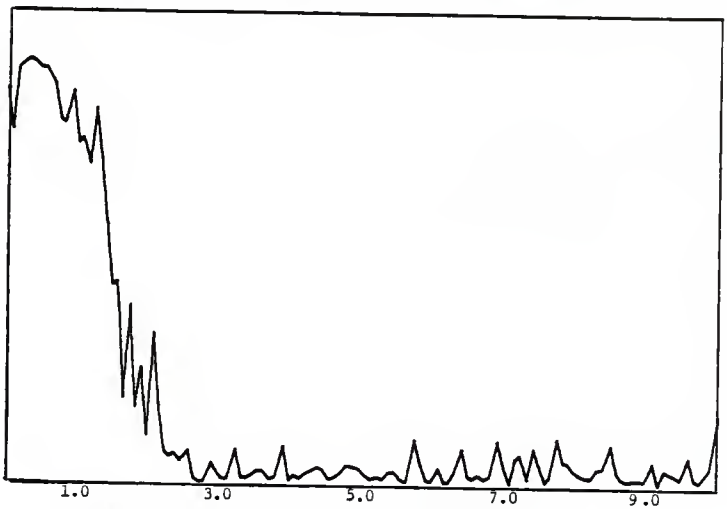

Coherence Function, 0-90-N & 0-180-N, Test # 16A

TEST LOG

DATE 8/20

TIME 11:45

TEST NO. 17A

RECORDER START 330

RECORDER END 350

CHANNEL	1	2	3	4
COLOR	RED	GREEN	YELLOW	BLUE
HEIGHT	5	D	D	D
AZIMUTH	0	0	90	180
ORIENTATION	N	V	V	V
LOW PASS FILTER	20	20	20	20.
ATTENUATOR SETTING	30	12	12	18
H-P FILTER I/O				
SENSITIVITY VOLTS				

ACCEL. SIGNAL GRND BRUSH

NOTES:

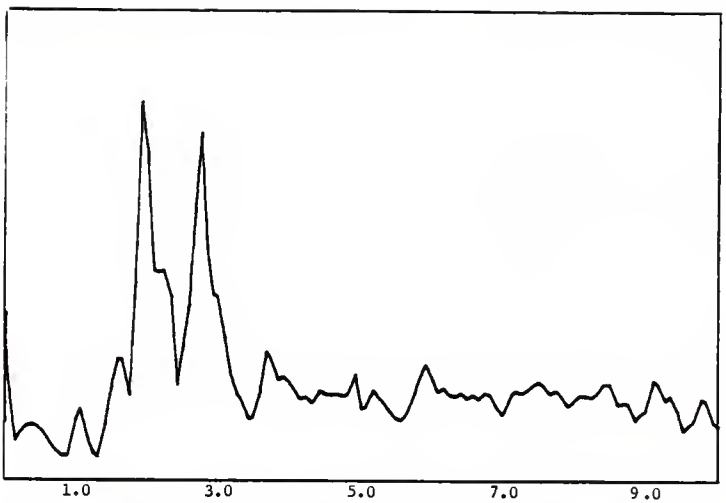

Response vs. Frequency, Channel A (5-0-N), 80 mv. F.S., Test # 17A

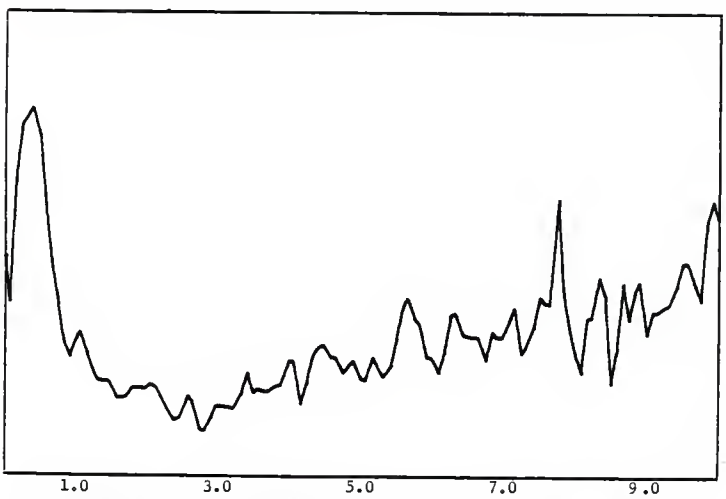

Response vs. Frequency, Channel B (0-0-V), 16 mv. F.S., Test # 17A

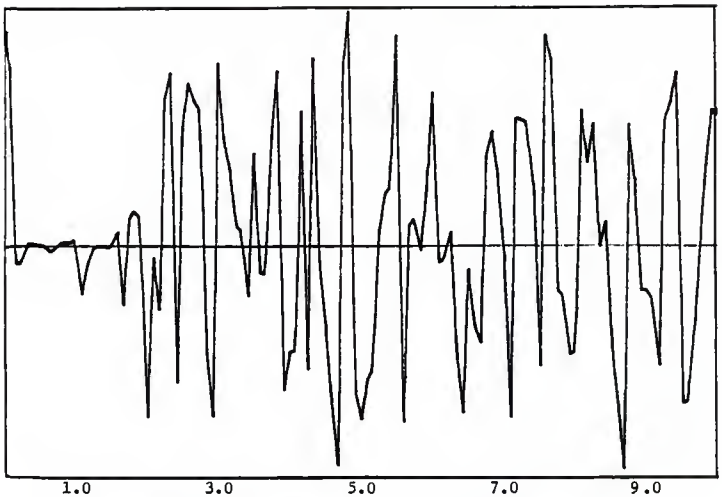

Transfer Function (Phase Angle), 5-0-N & 0-0-V, Test # 17A

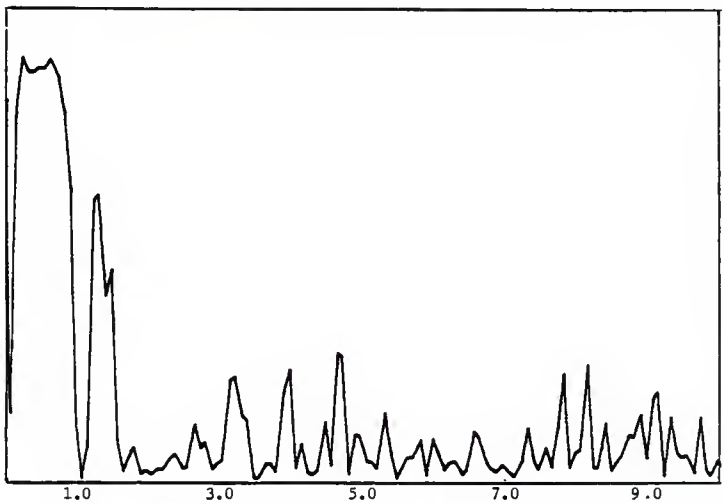

Coherence Function, 5-0-N & 0-0-V, Test # 17A

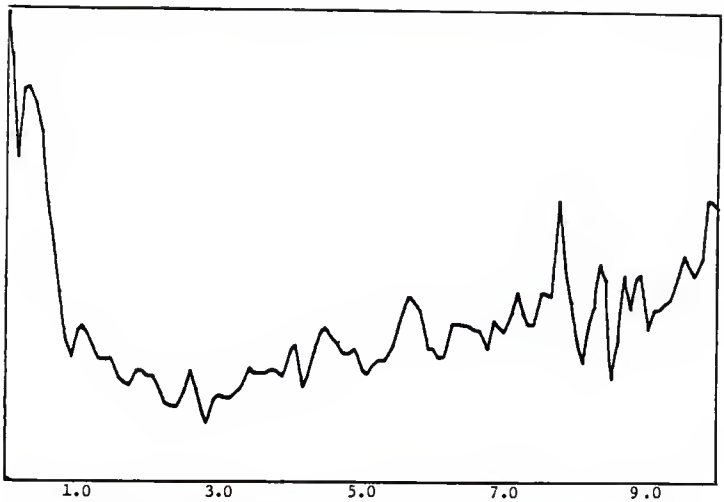

Response vs. Frequency, Channel A (0-0-V), 16 mv. F.S., Test # 17A

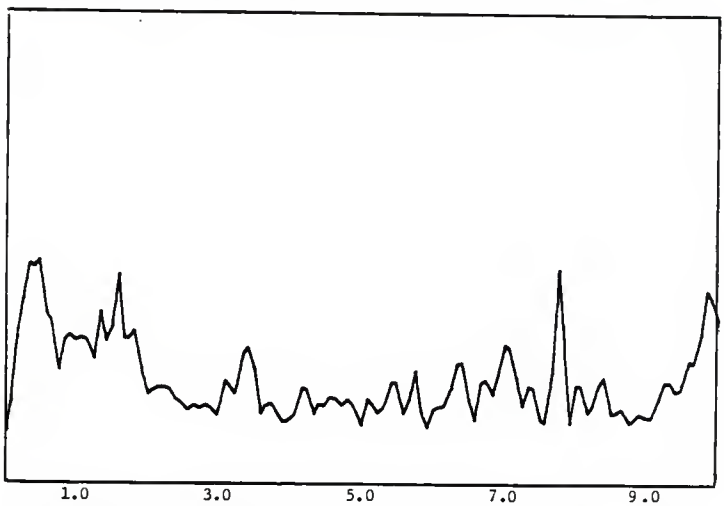

Response vs. Frequency, Channel B (0-90-V), 40 mv. F.S., Test # 17A

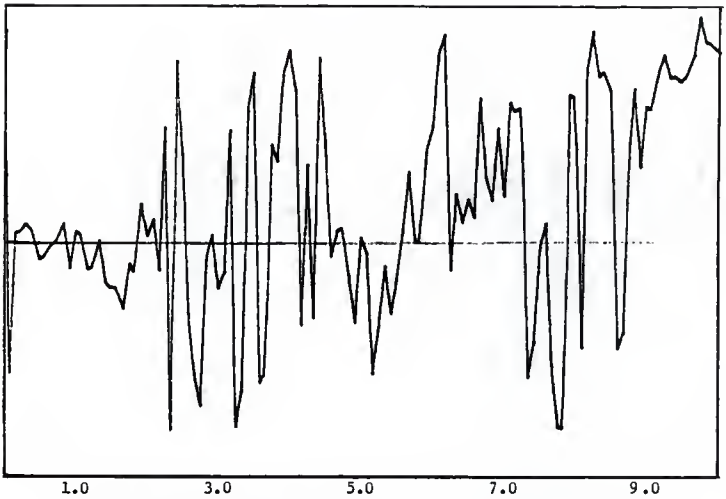

Transfer Function (Phase Angle), 0-0-V & 0-90-V, Test # 17A

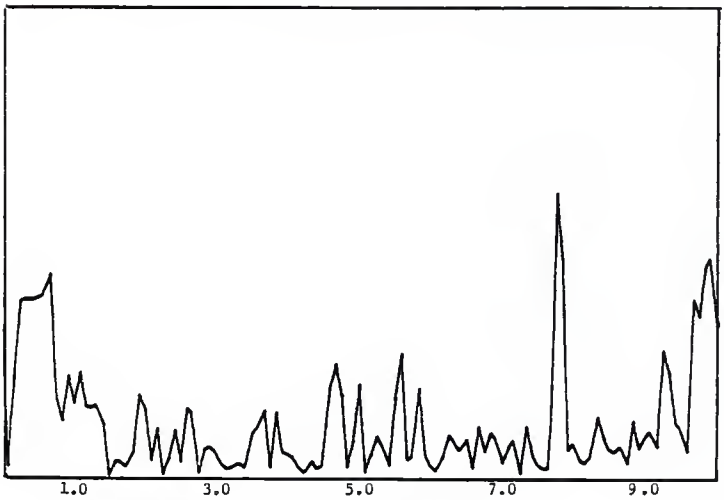

Coherence Function, 0-0-V & 0-90-V, Test # 17A

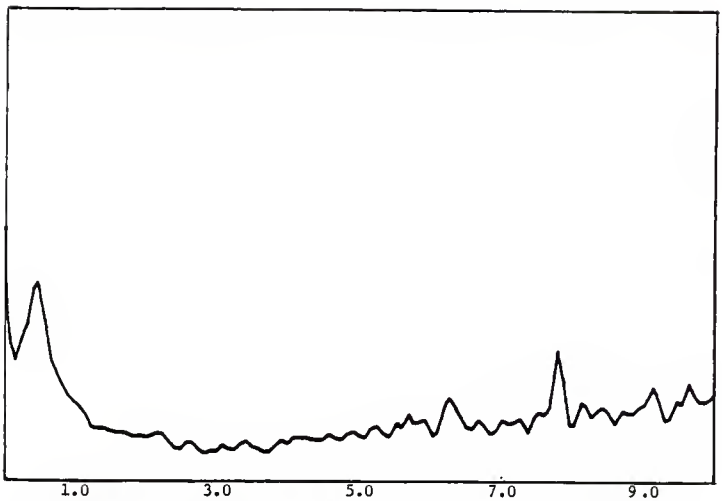

Response vs. Frequency, Channel A (0-0-V), 40 mv. F.S., Test # 17A

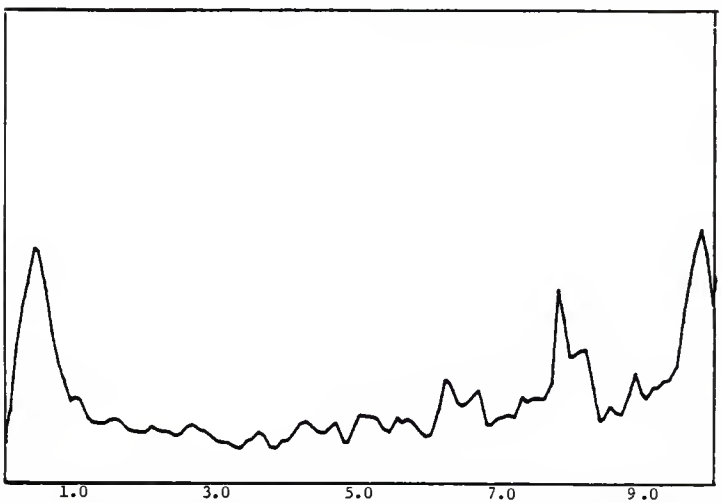

Response vs. Frequency, Channel B (0-180-V), 16 mv. F.S., Test # 17A

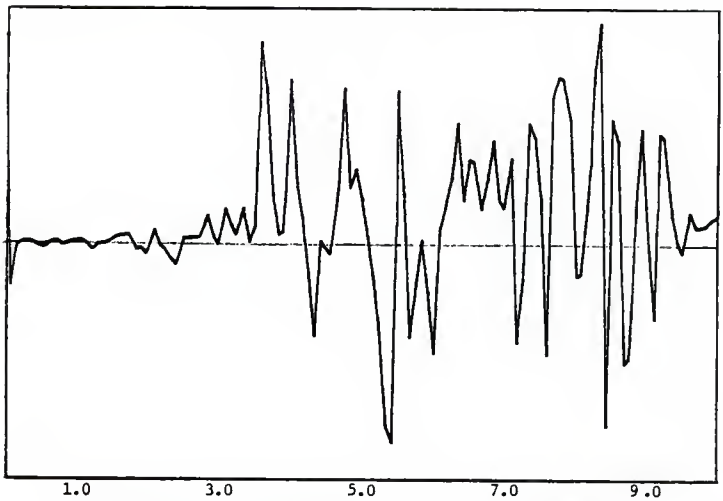

Transfer Function (Phase Angle), 0-0-V & 0-180-V, Test # 17A

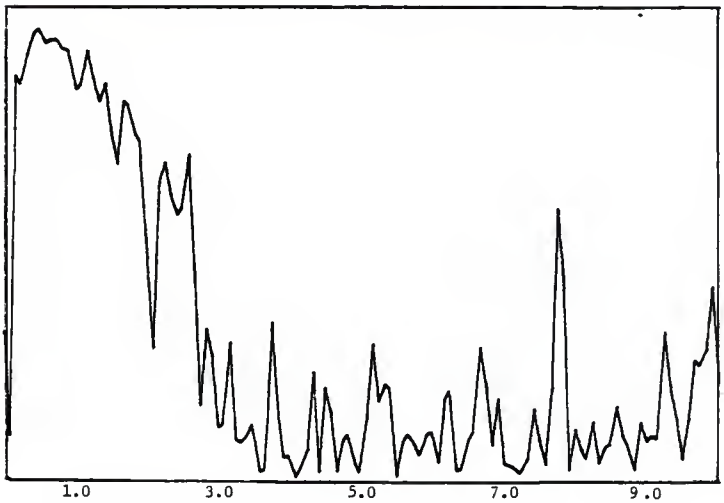

Coherence Function, 0-0-V & 0-180-V, Test # 17A

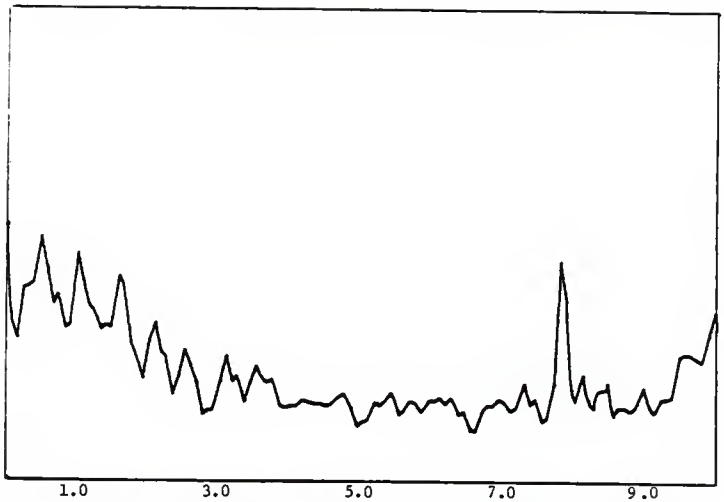

Response vs. Frequency, Channel A (0-90-V), 40 mv. F.S., Test # 17A

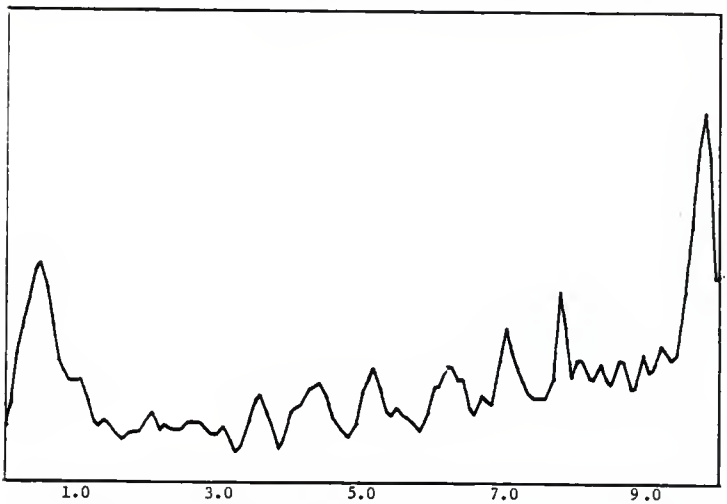

Response vs. Frequency, Channel B (0-180-V), 16 mv. F.S., Test # 17A

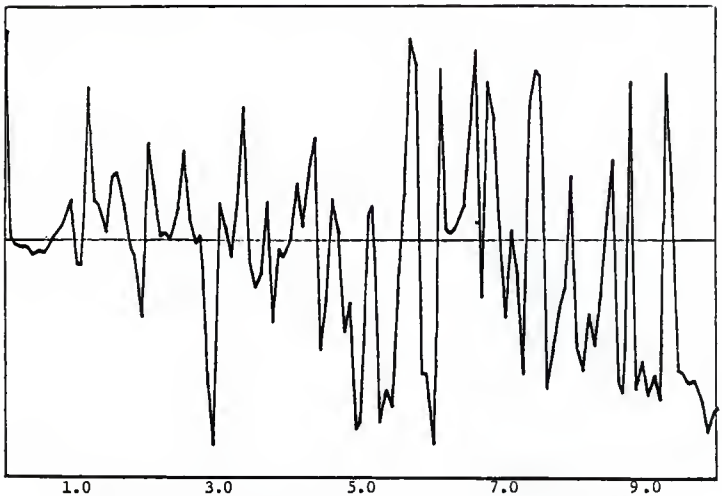

Transfer Function (Phase Angle), 0-90-V & 0-180-V, Test # 17A

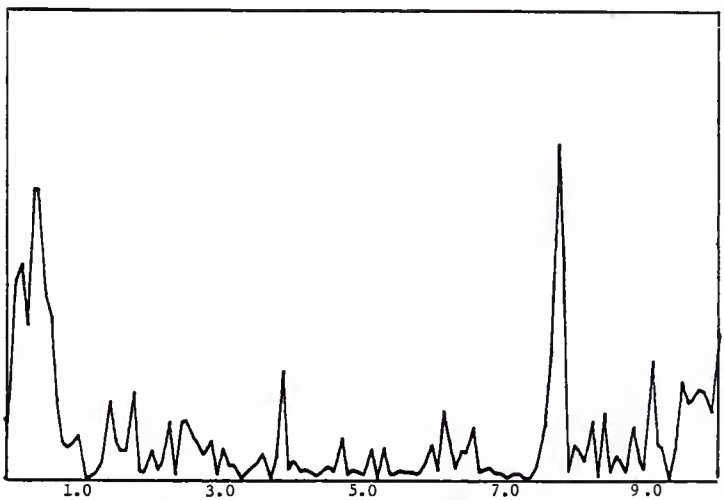

Coherence Function, 0-90-V & 0-180-V, Test # 17A

TEST LOG

DATE _____

TIME 1:25

TEST NO. 19A

RECORDER START 515

RECORDER END 535

CHANNEL	1	2	3	4
COLOR	RED	GREEN	YELLOW	BLUE
HEIGHT	5	1	0.1 *	0
AZIMUTH	0	0	0	0
ORIENTATION	N	N	N	N
LOW PASS FILTER	20	20	20	20
ATTENUATOR SETTING	30	24	24	24
H-P FILTER I/O				
SENSITIVITY VOLTS				

ACCEL. SIGNAL COND BRUNK

NOTES:

Accelerometer at top of pier footing

1 — L

0.1 — L

0 —

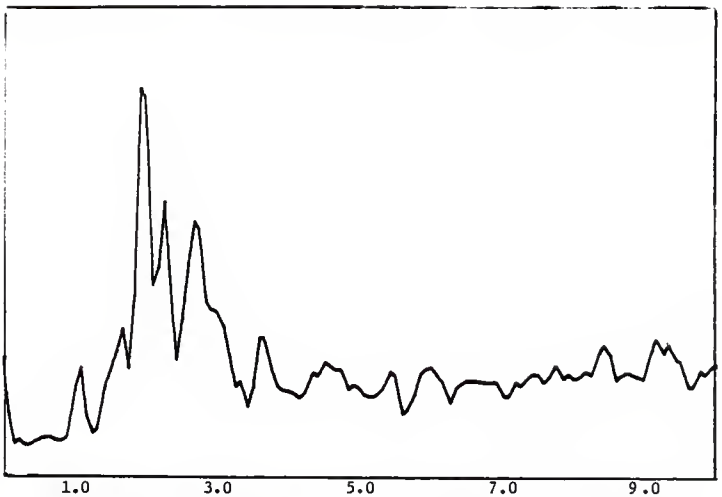

Response vs. Frequency, Channel A (5-0-N), 80 mv. F.S., Test # 19A

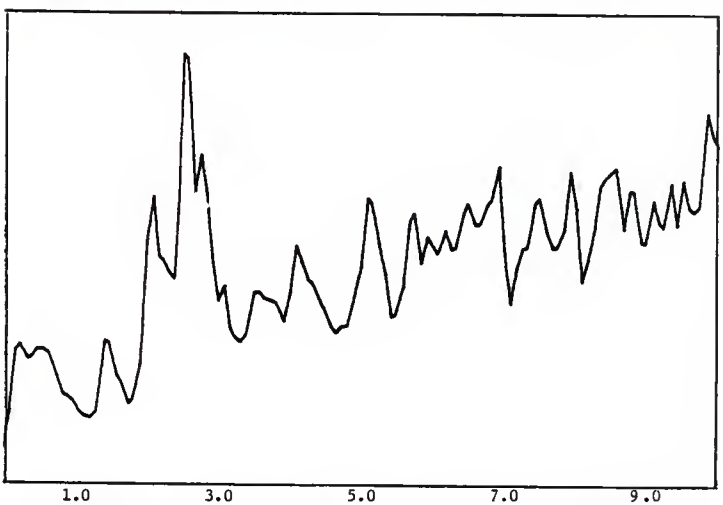

Response vs. Frequency, Channel B (1-0-N), 40 mv. F.S., Test # 19A

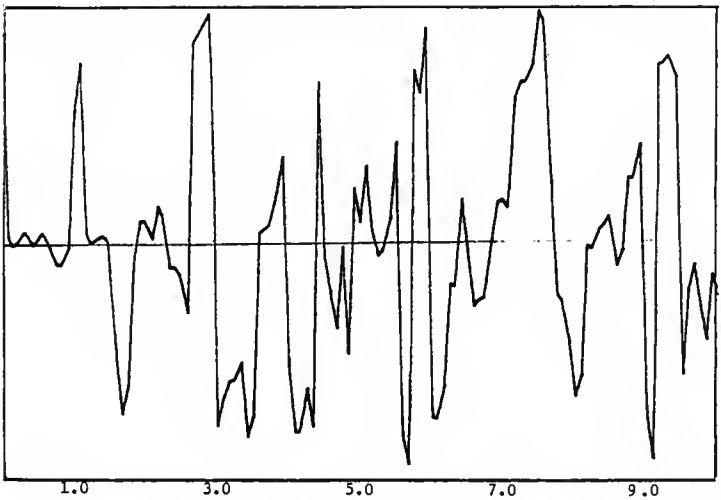

Transfer Function (Phase Angle), 5-0-N & 1-0-N, Test # 19A

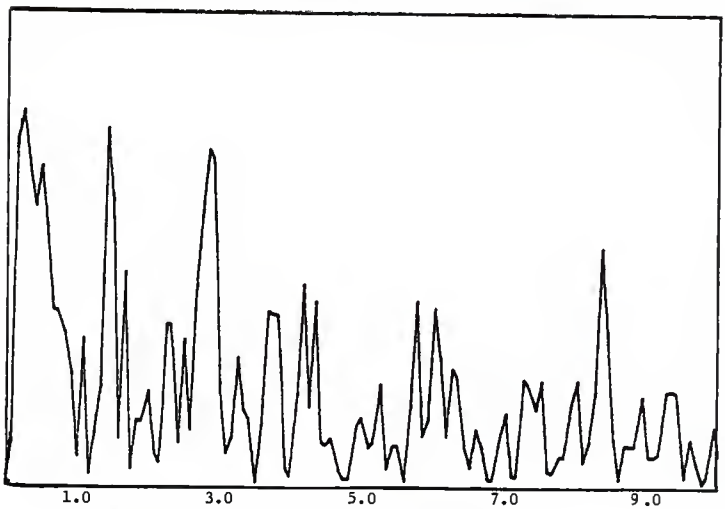

Coherence Function, 5-0-N & 1-0-N, Test # 19A

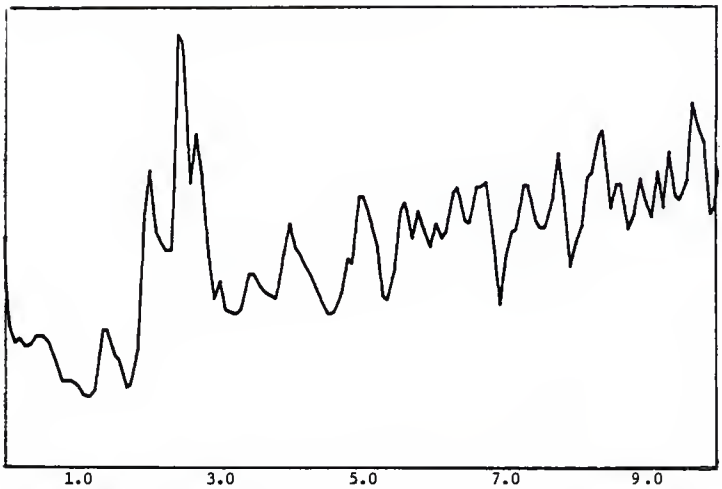

Response vs. Frequency, Channel A (1-0-N), 40 mv. F.S., Test # 19A

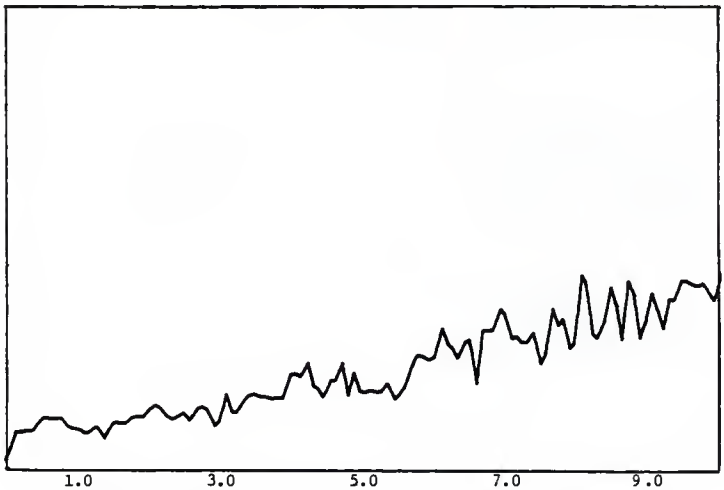

Response vs. Frequency, Channel B (0.1-0-N), 40 mv. F.S., Test # 19A

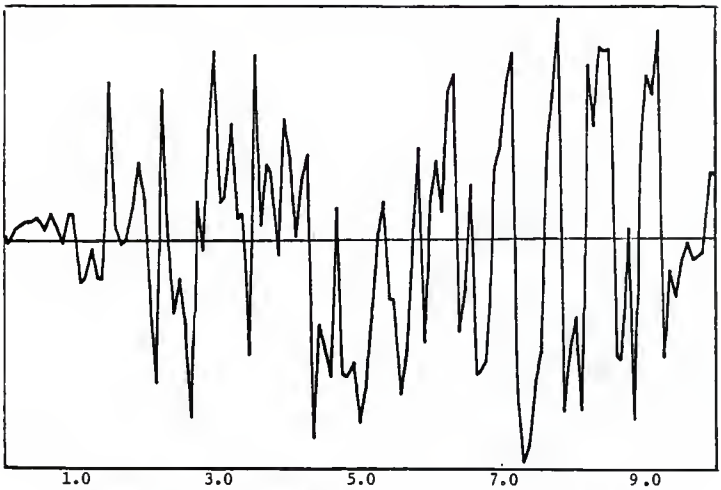

Transfer Function (Phase Angle), 1-0-N & 0.1-0-N, Test # 19A

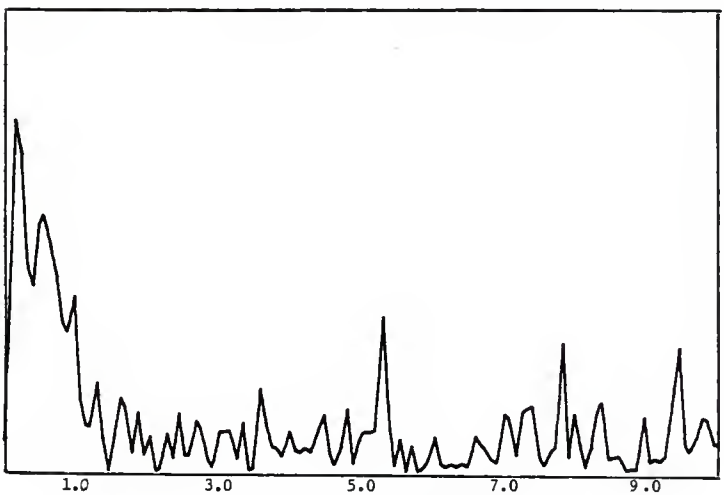

Coherence Function, 1-0-N & 0.1-0-N, Test # 19A

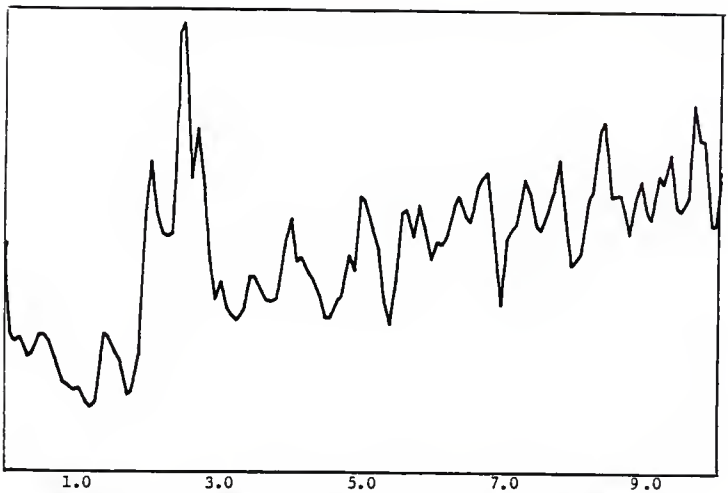

Response vs. Frequency, Channel A (1-0-N), 40 mv. F.S., Test # 19

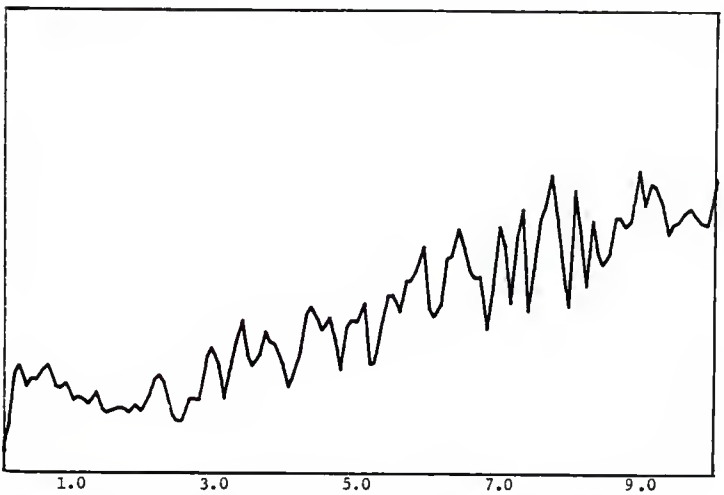

Response vs. Frequency, Channel B (0-0-N), 16 mv. F.S., Test # 19A

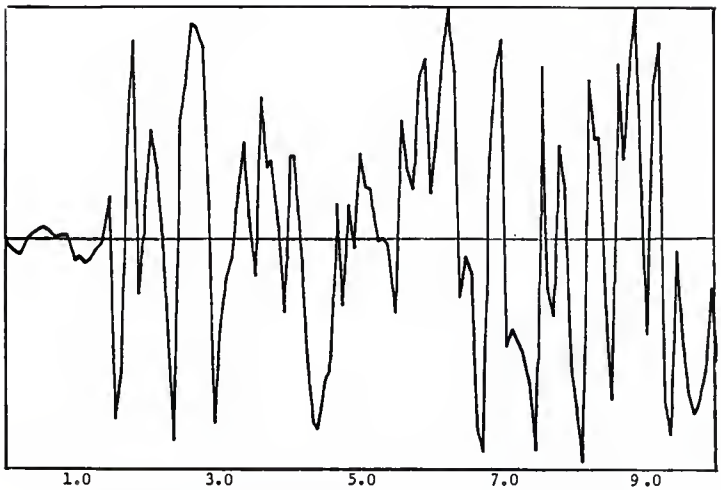

Transfer Function (Phase Angle), 1-0-N & 0-0-N, Test # 19A

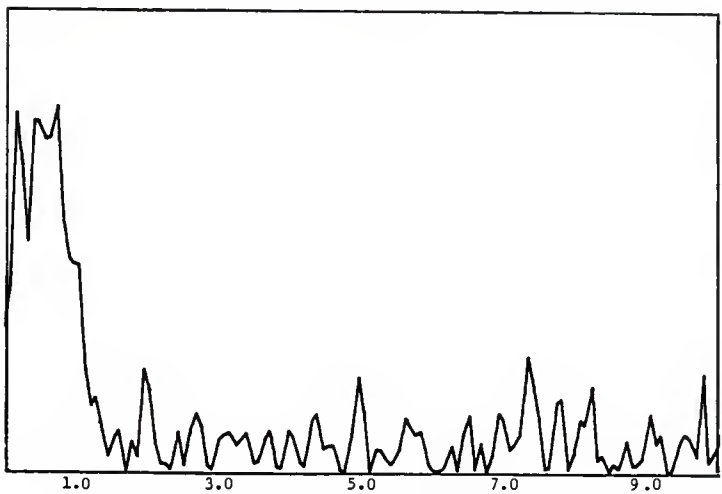

Coherence Function, 1-0-N & 0-0-N, Test # 19A

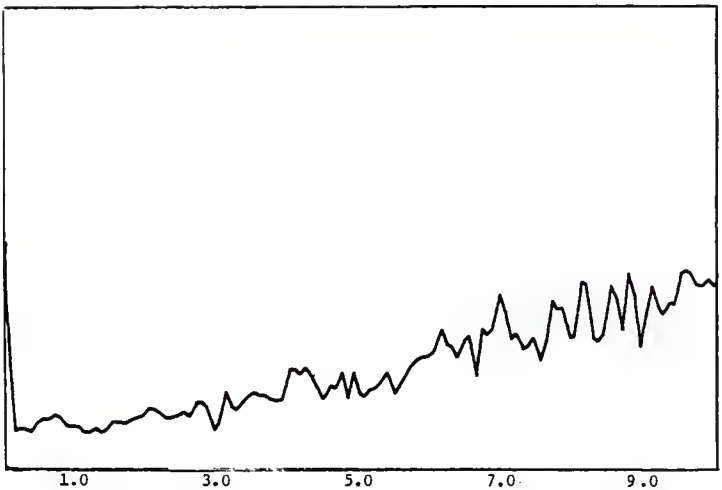

Response vs. Frequency, Channel A (0.1-0-N), 40 mv. F.S., Test # 19A

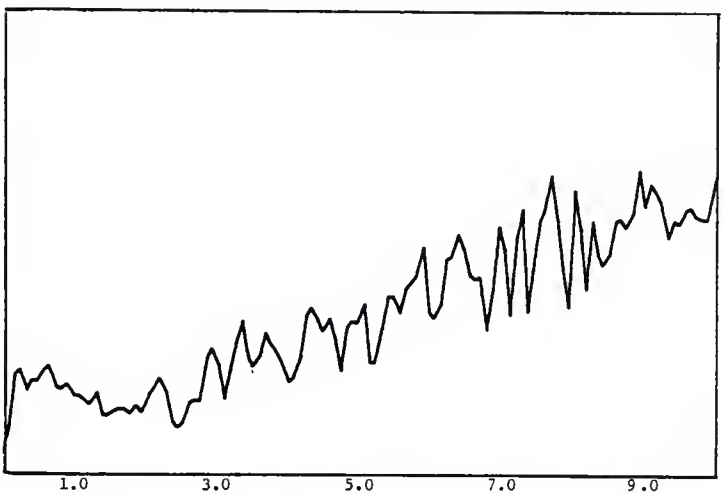

Response vs. Frequency, Channel B (0-0-N), 16 mv. F.S., Test # 19A

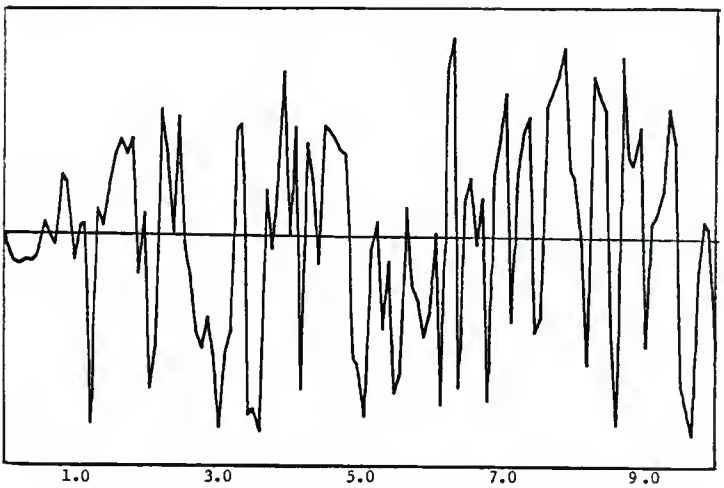

Transfer Function (Phase Angle), 0.1-0-N & 0-0-N, Test # 19A

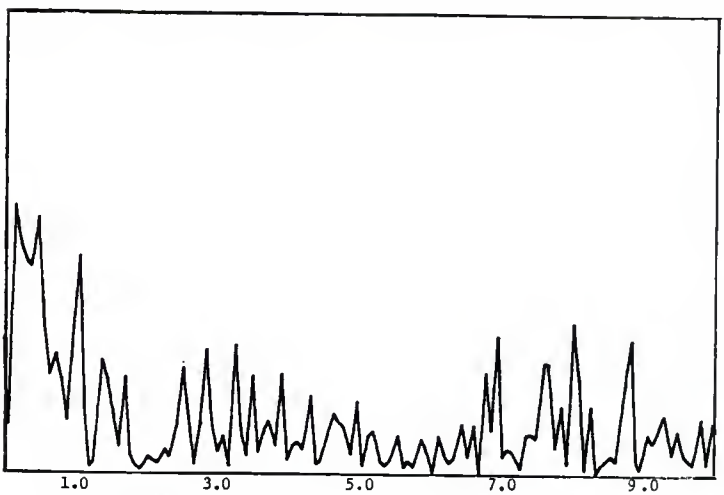

Coherence Function, 0.1-0-N & 0-0-N, Test # 19A

APPENDIX II.

RESPONSE NORMALIZED TO REFERENCE ACCELEROMETER (5-0-N)

PHASE ANGLES BETWEEN LISTED STATIONS

Atten	Station	1.04 hz	0	1.44 hz	0	1.60 hz	0	1.84 hz	0	2.64 hz	0	2.88 hz	0	3.52 hz	0	Test #
42	5-0-N	1.00	+70°	1.00	+20°	1.00	+18°	1.00	+12°	1.00	+174°	1.00	+176°	1.00	+188°	1A
30	4-0-N	0.46		1.73		1.50		0.70		0.39		0.68		0.69		
42	5-0-N	1.00	-27°	1.00	-47°	1.00	-33°	1.00	-6°	1.00	0°	1.00	-8°	1.00	+6°	1A
36	5-0-V	0.20		0.22		0.10		0.15		0.21		0.19		0.20		
42	5-0-N	1.00	0°	1.00	0°	1.00	+30°	1.00	+34°	1.00	0°	1.00	0°	1.00	+124°	1A
42	5-0-T	0.40		0.60		0.47		0.15		0.25		0.86		0.59		
36	5-0-N	1.00	+10°	1.00	+16°	1.00	+2°	1.00	+10°	1.00	+160°	1.00	+176°	1.00	-180°	3A
30	4-0-N	0.70		2.00		1.49		0.79		0.36		0.56		0.75		
36	5-0-N	1.00	+190°	1.00	+28°	1.00	+2°	1.00	+106°	1.00	-110°	1.00	+12°	1.00	+4°	3A
30	3½-0-N	1.09		1.64		0.48		0.20		0.39		0.38		0.81		
36	5-0-N	1.00	+180°	1.00	+40°	1.00	+116°	1.00	-178°	1.00	-9°	1.00	0°	1.00	-170°	3A
30	3-0-N	1.50		1.35		0.28		0.16		0.75		0.89		0.42		

* Average Values

Appendix II.

RESPONSE NORMALIZED TO REFERENCE ACCELEROMETER (5-0-N)

PHASE ANGLES BETWEEN LISTED STATIONS

Atten	Station	1.04 hz	0	1.44 hz	0	1.60 hz	0	1.84 hz	0	2.64 hz	0	2.88 hz	0	3.52 hz	0	Test #
30	3-0-N	1.50 *	-160°	1.33 *	-102°	0.41 *	+154°	0.14 *	-150°	0.65 *	-162°	0.93 *	+114°	0.37 *	+174°	4A
30	3-0-V	0.37		0.13		0.21		0.04		0.08		0.15		0.06		
30	3-0-N	1.50 *	-160°	1.33 *	-62°	0.41 *	+84°	0.14 *	-112°	0.65 *	+140°	0.93 *	+110°	0.37 *	+17°	4A
30	3-0-T	0.45		0.29		0.08		0.10		0.10		0.27		0.14		
30	3-0-V	0.37 *	+2°	0.13 *	+20°	0.21 *	0°	0.04 *	+119°	0.08 *	+19°	0.15 *	-30°	0.06 *	+41°	4A
30	3-0-T	0.86		0.37		0.40		0.20		0.26		0.78		0.28		
30	5-0-N	1.00	+184°	1.00	+40°	1.00	-176°	1.00	-194°	1.00	-10°	1.00	+4°	1.00	?????	5A
30	3-0-N	1.50		1.31		0.54		0.11		0.54		0.96		0.31		
30	5-0-N	1.00	+184°	1.00	+6°	1.00	+176°	1.00	-4°	1.00	-6°	1.00	-90°	1.00	+168°	5A
30	2½-0-N	1.03		0.92		0.34		0,23		0.37		0.51		0.47		
30	5-0-N	1.00	-184°	1.00	0°	1.00	-160°	1.00	+8°	1.00	0°	1.00	-126°	1.00	-80°	5A
30	2-0-N	1.12		0.58		0.40		0.15		0.44		0.57		0.64		

* Average Values

Appendix II.

RESPONSE NORMALIZED TO REFERENCE ACCELEROMETER (5-0-N)

PHASE ANGLES BETWEEN LISTED STATIONS

Atten	Station	1.04 hz	0	1.44 hz	0	1.60 hz	0	1.84 hz	0	2.64 hz	0	2.88 hz	0	3.52 hz	0	Test #
24	2-0-N	0.89 *	+174°	0.73 *	+198°	0.35 *	+176°	0.14 *	+180°	0.48 *	+178°	0.52 *	+168°	0.53 *	+170°	6A
30	2-0-V	0.15		0.10		0.11		0.02		0.14		0.16		0.21		
24	2-0-N	0.89 *	-62°	0.73 *	+10°	0.35 *	-6°	0.14 *	+2°	0.48 *	0°	0.52 *	-38°	0.53 *	-154°	6A
42	2-0-T	0.18		0.26		0.20		0.02		0.06		0.08		0.23		
30	2-0-V	0.15	+14°	0.10	-160°	0.11	+180°	0.02	+134°	0.14	-120°	0.16	+120°	0.21	0°	6A
42	2-0-T	0.20		0.42		0.20		0.03		0.07		0.11		0.26		
30	5-0-N	1.00	+178°	1.00	-6°	1.00	0°	1.00	+10°	1.00	0°	1.00	-154°	1.00	0°	7A
30	2-0-N	0.87		0.86		0.29		0.20		0.74		0.49		0.47		
30	5-0-N	1.00	-178°	1.00	+4°	1.00	-140°	1.00	-4°	1.00	+160°	1.00	-134°	1.00	0°	7A
36	1½-0-N	0.52		0.50		0.21		0.15		0.66		0.57		0.56		
30	5-0-N	1.00	-180°	1.00	+4°	1.00	-148°	1.00	-10°	1.00	-188°	1.00	-140°	1.00	-30°	7A
36	1-0-N	0.20		0.29		0.14		0.09		0.47		0.37		0.42		

* Average Values

Appendix II.

RESPONSE NORMALIZED TO REFERENCE ACCELEROMETER (5-0-N)

PHASE ANGLES BETWEEN LISTED STATIONS

Atten	Station	1.04 hz	0	1.44 hz	0	1.60 hz	0	1.84 hz	0	2.64 hz	0	2.88 hz	0	3.52 hz	0	Test #
30	1-0-N	0.20	0°	0.29	-50°	0.14	-168°	0.09	-178°	0.47	-180°	0.37	-184°	0.42	+168°	8A
24	1-0-V	0.08		0.07		0.03		0.03		0.10		0.10		0.16		
30	1-0-N	0.20 *	-20°	0.29 *	+6°	0.14 *	+176°	0.09 *	+138°	0.47 *	-160°	0.37 *	-94°	0.42 *	-28°	8A
30	1-0-T	0.09		0.13		0.04		0.06		0.08		0.19		0.26·		
24	1-0-V	0.13 *	-10°	0.13 *	0°	0.07 *	-39°	0.02 *	-150°	0.09 *	+10°	0.09 *	+110°	0.13 *	+170°	8A
30	1-0-T	0.15		0.44		0.14		0.11		0.06		0.17		0.25		
12	0-0-N	0.07 *	+18°	0.07 *	-10°	0.04 *	-10°	0.01 *	+4°	0.03 *	+10°	0.06 *	+20°	0.08 *	-20°	9A
12	0-0-V	0.07		0.10		0.04		0.01		0.03		0.06		0.08		
12	0-0-N	0.07 *	-2°	0.07 *	0°	0.04 *	-4°	0.01 *	0°	0.03 *	+20°	0.06 *	-30°	0.08 *	-10°	9A
18	0-0-T	0.08		0.06		0.03		0.01		0.03		0.04		0.10		
12	0-0-V	0.11	0°	0.09	0°	0.05	0°	0.02	-24°	0.02	-10°	0.05	-30°	0.07	0°	9A
18	0-0-T	0.10		0.06		0.04		0.02		0.01		0.08		0.07		

* Average Values

RESPONSE NORMALIZED TO REFERENCE ACCELEROMETER (5-0-N)

PHASE ANGLES BETWEEN LISTED STATIONS

Atten	Station	1.04 hz	0	1.44 hz	0	1.60 hz	0	1.84 hz	0	2.64 hz	0	2.88 hz	0	3.52 hz	0	Test #
36	5-0-N	1.00	+182°	1.00	0°	1.00	-160°	1.00	0°	1.00	+60°	1.00	-144°	1.00	-162°	10A
30	2-0-N	0.83		0.72		0.34		0.11		0.39		0.48		0.59		
36	5-0-N	1.00	+180°	1.00	-176°	1.00	-46°	1.00	0°	1.00	-24°	1.00	-142°	1.00	-38°	10A
36	2-90-N	0.88		0.74		0.39		0.35		0.67		0.43		0.45		
36	5-0-N	1.00	+178°	1.00	+6°	1.00	+128°	1.00	-38°	1.00	-15°	1.00	+54°	1.00	0°	10A
36	2-180-N	1.04		0.75		0.43		0.12		0.58		0.53		0.52		
30	2-0-N	0.89 *	+8°	0.73 *	-178°	0.35 *	-170°	0.14 *	+32°	0.48 *	-18°	0.52 *	-42°	0.53 *	+64°	10A
36	2-90-N	0.87		0.84		0.50		0.33		0.40		0.45		0.42		
30	2-0-N	0.89 *	+4°	0.73 *	0°	0.35 *	-166°	0.14 *	-10°	0.48 *	0°	0.52 *	-190°	0.53 *	-160°	10A
36	2-180-N	1.15		0.86		0.37		0.15		0.33		0.41		0.40		

* Average Values

Appendix II.

RESPONSE NORMALIZED TO REFERENCE ACCELEROMETER (5-0-N)

PHASE ANGLES BETWEEN LISTED STATIONS

Atten	Station	1.04 hz	0	1.44 hz	0	1.60 hz	0	1.84 hz	0	2.64 hz	0	2.88 hz	0	3.52 hz	0	Test #
30	5-0-N	1.00	-174°	1.00	0°	1.00	-170°	1.00	-4°	1.00	0°	1.00	-144°	1.00	+64°	11A
24	2-0-N	0.74		0.75		0.35		0.11		0.33		0.52		0.43		
30	5-0-N	1.00	+4°	1.00	-188°	1.00	-14°	1.00	+140°	1.00	+20°	1.00	+60°	1.00	-170°	11A
30	2-90-T	0.20		0.19		0.10		0.08		0.04		0.15		0.13		
30	5-0-N	1.00	-184°	1.00	0°	1.00	-28°	1.00	-28°	1.00	-20°	1.00	+60°	1.00	0°	11A
42	2-180-N	1.30		0.80		0.35		0.14		0.30		0.43		0.37		
24	2-0-N	0.89 *	-170°	0.73 *	-182°	0.35 *	-184°	0.14 *	-45°	0.48 *	+160°	0.52 *	-152°	0.53 *	+146°	11A
30	2-90-T	0.19		0.19		0.09		0.05		0.07		0.18		0.18		
24	2-0-N	0.89 *	+30°	0.73 *	0°	0.35 *	+164°	0.14 *	+45°	0.48 *	+20°	0.52 *	-172°	0.53 *	+180°	11A
42	2-180-N	1.22		0.74		0.34		0.09		0.31		0.53		0.42		
30	2-90-T	0.20 *	+160°	0.19 *	-176°	0.10 *	-100°	0.07 *	+180°	0.06 *	-70°	0.16 *	-40°	0.16 *	-150°	11A
42	2-180-N	1.32		0.77		0.33		0.25		0.30		0.47		0.33		

* Average Values

Appendix II.

RESPONSE NORMALIZED TO REFERENCE ACCELEROMETER (5-0-N)

PHASE ANGLES BETWEEN LISTED STATIONS

Atten	Station	1.04 hz	0	1.44 hz	0	1.60 hz	0	1.84 hz	0	2.64 hz	0	2.88 hz	0	3.52 hz	0	Test #
30	5-0-N	1.00	+20°	1.00	+192°	1.00	+15°	1.00	+148°	1.00	-6°	1.00	+38°	1.00	-150°	12A
24	2-0-V	0.17		0.10		0.10		0.03		0.12		0.11		0.09		
30	5-0-N	1.00	0°	1.00	+26°	1.00	+130°	1.00	+164°	1.00	+40°	1.00	-30°	1.00	+6°	12A
20	2-90-V	0.16		0.11		0.16		0.11		0.07		0.06		0.08		
30	5-0-N	1.00	-12°	1.00	+162°	1.00	+160°	1.00	0°	1.00	-190°	1.00	-100°	1.00	-60°	12A
30	2-180-V	0.19		0.13		0.13		0.04		0.06		0.14		0.14		
24	2-0-V	0.16 *	+2°	0.10 *	0°	0.11 *	+30°	0.03 *	+32°	0.13 *	-120°	0.14 *	-70°	0.15 *	+30°	12A
30	2-90-V	0.15		0.13		0.15		0.13		0.04		0.07		0.12		
24	2-0-V	0.16 *	+6°	0.10 *	-4°	0.11 *	+118°	0.03 *	0°	0.13 *	0°	0.14 *	-164°	0.15 *	-140°	12A
30	2-180-V	0.17		0.14		0.13		0.03		0.07		0.16		0.14		
30	2-90-V	0.16 *	+8°	0.12 *	0°	0.16 *	-170°	0.12 *	-20°	0.06 *	0°	0.07 *	0°	0.10 *	0°	12A
30	2-180-V	0.18		0.12		0.13		0.04		0.07		0.15		0.11		

* Average Values

Appendix II.

RESPONSE NORMALIZED TO REFERENCE ACCELEROMETER (5-0-N)

PHASE ANGLES BETWEEN LISTED STATIONS

Atten	Station	1.04 hz	0	1.44 hz	0	1.60 hz	0	1.84 hz	0	2.64 hz	0	2.88 hz	0	3.52 hz	0	Test #
24	1-0-N	0.23 *	+2°	0.33 *	-142°	0.21 *	0°	0.09 *	-8°	0.44 *	+64°	0.31 *	+60°	0.50 *	+154°	13A
30	1-90-N	0.37		0.42		0.35		0.43		0.36		0.22		0.57		
24	1-0-N	0.23 *	+4°	0.33 *	0°	0.21 *	-24°	0.09 *	0°	0.44 *	+36°	0.31 *	-20°	0.50 *	-160°	13A
30	1-180-N	0.35		0.58		0.57		0.09		0.42		0.19		0.63		
30	1-90-N	0.37 *	+2°	0.42 *	+178°	0.35 *	0°	0.43 *	0°	0.36 *	-4°	0.22 *	+22°	0.57 *	-120°	13A
30	1-180-N	0.35		0.50		0.57		0.10		0.34		0.11		0.78		
30	5-0-N	1.00	+166°	1.00	0°	1.00	+120°	1.00	0°	1. 00	+180°	1.00	+172°	1.00	0°	14A
30	1-0-N	0.26		0.36		0.28		0.09		0.42		0.25		0.58		
30	1-0-N	0.23 *	+4°	0.33 *	-82°	0.21 *	-78°	0.09 *	-50°	0.44 *	-170°	0.31 *	+12°	0.50 *	0°	14A
30	1-90-T	).@$		0.26		0.26		0.06		0.15		0.19		0.25		
30	1-0-N	0.23 *	-10°	0.33 *	+8°	0.21 *	0°	0.09 *	0°	0.44 *	+40°	0.31 *	0°	0.50 *	-162°	14A
30	1-180-N	0.35		0.57		0.33		0.11		0.42		0.40		0.57		

* Average Values

Appendix II.

RESPONSE NORMALIZED TO REFERENCE ACCELEROMETER (5-0-N)

PHASE ANGLES BETWEEN LISTED STATIONS

Atten	Station	1.04 hz	0	1.44 hz	0	1.60 hz	0	1.84 hz	0	2.64 hz	0	2.88 hz	0	3.52 hz	0	Test #
30	5-0-N	1.00	+46°	1.00	+59°	1.00	0°	1.00	0°	1.00	-10°	1.00	+42°	1.00	+162°	15A
24	1-0-V	0.17		0.19		0.10		0.01		0.11		0.07		0.09		
24	1-0-V	0.13 *	0°	0.13 *	0°	0.07 *	+4°	0.02 *	+142°	0.09 *	+10°	0.09 *	+70°	0.13 *	-140°	15A
30	1-90-V	0.14		0.14		0.08		0.09		0.10		0.18		0.18		
24	1-0-V	0.13 *	0°	0.13 *	0°	0.07 *	0°	0.02 *	+4°	0.09 *	-40°	0.09 *	0°	0.13 *	+144°	15A
24	1-180-V	0.13		0.14		0.08		0.02		0.09		0.09		0.15		
30	1-90-V	0.14 *	+10°	0.14 *	+2°	0.08 *	+28°	0.09 *	-82°	0.10 *	0°	0.18 *	+30°	0.18 *	-60°	15A
24	1-180-V	0.15		0.11		0.06		0.03		0.07		0.10		0.14		
30	5-0-N	1.00	0°	1.00	-120°	1.00	+50°	1.00	+134°	1.00	0°	1.00	0°	1.00	-80°	16A
18	0-0-N	0.10		0.11		0.03		0.01		0.03		0.05		0.05		
18	0-0-N	0.07 *	+6°	0.07 *	0°	0.04 *	0°	0.01 *	+28°	0.03 *	0°	0.06 *	0°	0.08 *	-126°	16A
18	0-90-N	0.08		0.06		0.03		0.01		0.02		0.03		0.04		

* Average Values

Appendix II.

RESPONSE NORMALIZED TO REFERENCE ACCELEROMETER (5-0-N)

PHASE ANGLES BETWEEN LISTED STATIONS

Atten	Station	1.04 hz	0	1.44 hz	0	1.60 hz	0	1.84 hz	0	2.64 hz	0	2.88 hz	0	3.52 hz	0	Test #
18	0-0-N	0.07 *	+6°	0.07 *	-10°	0.04 *	+80°	0.01 *	+40°	0.03 *	0°	0.06 *	0°	0.08 *	+10°	16A
24	0-180-N	0.07		0.07		0.04		0.02		0.03		0.04		0.07		
18	0-90-N	0.07 *	0°	0.06 *	+8°	0.03 *	+8°	0.01 *	+12°	0.02 *	0°	0.03 *	0°	0.04 *	0°	16A
24	0-180-N	0.07		0.08		0.04		0.02		0.03		0.04		0.10		
30	5-0-N	1.00	-40°	1.00	0°	1.00	-44°	1.00	-120°	1.00	0°	1.00	+130°	1.00	0°	17A
12	0-0-V	0.14		0.08		0.05		0.02		0.01		0.03		0.05		
12	0-0-V	0.11 *	0°	0.09 *	-40°	0.05 *	-60°	0.02 *	+30°	0.02 *	-140°	0.05 *	-38°	0.07 *	-110°	17A
12	0-90-V	0.26		0.24		0.19		0.05		0.06		0.10		0.11		
12	0-0-V	0.11 *	0°	0.09 *	+8°	0.05 *	+8°	0.02 *	-8°	0.02 *	+10°	0.05 *	0°	0.07 *	+126°	17A
18	0-180-V	0.10		0.09		0.05		0.02		0.03		0.05		0.09		
12	0-90-V	0.26 *	0°	0.24 *	+54°	0.19 *	+14°	0.05 *	-60°	0.06 *	0°	0.10 *	0°	0.11 *	0°	17A
18	0-180-V	0.11		0.06		0.04		0.02		0.04		0.04		0.06		

* Average Values

Appendix II.

RESPONSE NORMALIZED TO REFERENCE ACCELEROMETER (5-0-N)

PHASE ANGLES BETWEEN LISTE STATIONS

Atten	Station	1.04 hz	0	1.44 hz	0	1.60 hz	0	1.84 hz	0	2.64 hz	0	2.88 hz	0	3.52 hz	0	Test #
30	5-0-N	1.00	+140°	1.00	0°	1.00	-140°	1.00	+16°	1.00	+180°	1.00	-146°	1.00	+ 10°	19A
24	1-0-N	0.17		0.34		0.18		0.07		0.35		0.29		0.33		
30	1-0-N	0.23 *	-40°	0.33 *	+120°	0.21 *	0°	0.09 *	+30°	0.44 *	0°	0.31 *	+154°	0.50 *	+ 10°	19A
24	0.1-0-N	0.06		0.04		0.05		0.02		0.04		0.04		0.10		
24	1-0-N	0.23 *	-20°	0.33 *	0°	0.21 *	0°	0.09 *	-36°	0.44 *	+182°	0.31 *	-150°	0.50 *	+110°	19A
24	0-0-N	0.08		0.07		0.05		0.02		0.03		0.09		0.13		
24	0.1-0-N	0.06 *	0°	0.04 *	+38°	0.05 *	+70°	0.02 *	0°	0.04 *	- 98°	0.04 *	-160°	0.10 *	0°	19A
24	0-0-N	0.04		0.02		0.03		0.01		0.02		0.05		0.07		

* Average Values

Appendix II.

AMBIENT VIBRATION ANALYSIS OF A FULL-SCALE HYPERBOLIC COOLING TOWER

by

Michael Ray Helpingstine

B.S., Kansas State University, 1985

AN ABSTRACT OF A MASTER'S THESIS

submitted in partial fulfillment of the

requirements of the degree

MASTER OF SCIENCE

Department of Civil Engineering

Kansas State University
Manhattan, Kansas
1987

Abstract

A series of ambient vibration tests was conducted on the hyperbolic cooling tower at the Trojan Nuclear Generating Station, near Rainier, Oregon. Acceleration data were collected, and analysed via the Fast Fourier Transform. Seven predominant frequencies were identified, all below five Hertz, and associated mode shapes were plotted. These include vertical, radial, and lateral mode shapes. Collection of data for identification of radial modes was hampered by inaccessibility to various portions of the structure, therefore, accurate representation of the radial modes was not possible. Free-field tests were completed. Modal damping ratios were calculated for three frequencies. This was accomplished using the Half-Power Band Width method.